NAVAL POSTGRADUATE SCHOOL

MONTEREY, CALIFORNIA

THESIS

DUCTED FLOW CONTROL IN A TRANSONIC COMPRESSOR, METHODS AND ANALYSIS

by

Norman J. Spector

June 2023

Thesis Advisor:	Walter C. Smith
Co-Advisor:	Garth V. Hobson
Second Reader:	Anthony J. Gannon

THIS PAGE INTENTIONALLY LEFT BLANK

REPORT DOCUMENTATION PAGE	*Form Approved OMB No. 0704-0188*

1. AGENCY USE ONLY *(Leave blank)*	**2. REPORT DATE** June 2023	**3. REPORT TYPE AND DATES COVERED** Master's thesis

4. TITLE AND SUBTITLE
DUCTED FLOW CONTROL IN A TRANSONIC COMPRESSOR, METHODS AND ANALYSIS

5. FUNDING NUMBERS

6. AUTHOR(S) Norman J. Spector

7. PERFORMING ORGANIZATION NAME(S) AND ADDRESS(ES)
Naval Postgraduate School
Monterey, CA 93943-5000

8. PERFORMING ORGANIZATION REPORT NUMBER

9. SPONSORING / MONITORING AGENCY NAME(S) AND ADDRESS(ES)
N/A

10. SPONSORING / MONITORING AGENCY REPORT NUMBER

11. SUPPLEMENTARY NOTES The views expressed in this thesis are those of the author and do not reflect the official policy or position of the Department of Defense or the U.S. Government.

12a. DISTRIBUTION / AVAILABILITY STATEMENT
Approved for public release. Distribution is unlimited.

12b. DISTRIBUTION CODE
A

13. ABSTRACT (maximum 200 words)

Compressor development is crucial for enhancing gas turbine engine performance. Variations in inlet flow, whirl, and distortion can lead to compressor stall or surge, resulting in flow detachment within blade passages. This study aims to improve the stall margin in the NPS military fan (NPSMF) transonic compressor by incorporating passive flow control devices on the rotor blade tips, housed in casings. Previous thesis students' modeling, manufacturing, and computational analysis methods were utilized to expand upon this research. Experimental tests were conducted on three types of casings: a smooth casing, an internal passage casing, and a novel "NACA" casing. Various engineering plastics like polycarbonate and PEEK were used for casings through fused deposition modeling (FDM) printing. Aluminum casings, capable of withstanding higher temperatures, were created using powderbed and liquid metal jet printing (LMJP). Manufacturing fidelity was measured and experimentally tested for each casing, while computational simulations were obtained for all experimental tests. This project serves as an evaluation of each casing's performance and a review of their creation process, offering valuable insights and recommendations for future manufacturing of passive recirculating casing treatments. The internal passage casing showed minor stall margin improvements of approximately 2%, while further research is needed to establish a comprehensive performance profile for the NACA casing.

14. SUBJECT TERMS transonic, compressor, casing, endwall treatment, casing treatment, NPS military fan, NPSMF, fused deposition modeling, FDM, powderbed and liquid metal jet printing, LMJP	**15. NUMBER OF PAGES** 265
	16. PRICE CODE

17. SECURITY CLASSIFICATION OF REPORT	**18. SECURITY CLASSIFICATION OF THIS PAGE**	**19. SECURITY CLASSIFICATION OF ABSTRACT**	**20. LIMITATION OF ABSTRACT**
Unclassified	Unclassified	Unclassified	UU

NSN 7540-01-280-5500

Standard Form 298 (Rev. 2-89)
Prescribed by ANSI Std. 239-18

THIS PAGE INTENTIONALLY LEFT BLANK

Approved for public release. Distribution is unlimited.

DUCTED FLOW CONTROL IN A TRANSONIC COMPRESSOR, METHODS AND ANALYSIS

Norman J. Spector
Ensign, United States Navy
BS, United States Naval Academy, 2022

Submitted in partial fulfillment of the
requirements for the degree of

MASTER OF SCIENCE IN AEROSPACE ENGINEERING

from the

NAVAL POSTGRADUATE SCHOOL
June 2023

Approved by: Walter C. Smith
Advisor

Garth V. Hobson
Co-Advisor

Anthony J. Gannon
Second Reader

Brian S. Bingham
Chair, Department of Mechanical and Aerospace Engineering

THIS PAGE INTENTIONALLY LEFT BLANK

ABSTRACT

Compressor development is crucial for enhancing gas turbine engine performance. Variations in inlet flow, whirl, and distortion can lead to compressor stall or surge, resulting in flow detachment within blade passages. This study aims to improve the stall margin in the NPS military fan (NPSMF) transonic compressor by incorporating passive flow control devices on the rotor blade tips, housed in casings. Previous thesis students' modeling, manufacturing, and computational analysis methods were utilized to expand upon this research. Experimental tests were conducted on three types of casings: a smooth casing, an internal passage casing, and a novel "NACA" casing. Various engineering plastics like polycarbonate and PEEK were used for casings through fused deposition modeling (FDM) printing. Aluminum casings, capable of withstanding higher temperatures, were created using powderbed and liquid metal jet printing (LMJP). Manufacturing fidelity was measured and experimentally tested for each casing, while computational simulations were obtained for all experimental tests. This project serves as an evaluation of each casing's performance and a review of their creation process, offering valuable insights and recommendations for future manufacturing of passive recirculating casing treatments. The internal passage casing showed minor stall margin improvements of approximately 2%, while further research is needed to establish a comprehensive performance profile for the NACA casing.

THIS PAGE INTENTIONALLY LEFT BLANK

Contents

List of Figures

List of Tables

THIS PAGE INTENTIONALLY LEFT BLANK

List of Acronyms and Abbreviations

AM	Additive Manufacturing
BEP	Best Efficiency Point
Blisk	Bladed-Disk
BPR	Best Pressure Ratio
CFD	Computational Fluid Dynamics
DMLM	Direct Metal Laser Melting
DOD	Department of Defense
FDM	Fused Deposition Modeling
IAWS	In Accordance With Schedule
ID	Inner Diameter
IGV	Inlet Guide Vane
IP	Internal Passages
LMJP	Liquid Metal Jet Printing
NPS	Naval Postgraduate School
NPSMF	NPS Military Fan
OD	Outer Diameter
PS	Pressure Side
RANS	Reynolds-Averaged Navier Stokes
RO	Rotor Only

SLA	Stereolithography
SM	Stall Margin
SS	Suction Side
SST	Shear Stress Transport
TCR	Transonic Compressor Rig
TG	Tip-Gap
TPL	Turbopropulsion Lab
USN	U.S. Navy

Acknowledgments

I would like to thank first and foremost my advisor, Dr. Walter Smith, and my co-advisor and reader Dr. Garth Hobson and Dr. Anthony Gannon. Your guidance has been truly invaluable, and the opportunity to work on something so well-aligned with my career path has been incredible. Many undergraduate engineers feel a sense of 'imposter syndrome' upon the completion of their degree, and I was no exception. Over the course of my year at NPS, I went from stumbling through ANSYS to being able to independently run complex simulations, contribute to discussions, and generate ideas. I didn't feel like an engineer upon graduating college; I can wholeheartedly say I do now. I'm confident what I learned here will not only help me be a better engineer, but a more analytical, and safer pilot. In the words of Edward Richenbacher: "Aviation is proof that given the will, we have the capacity to achieve the impossible."

Thank you to my friends, family and loved ones. Your unwavering support throughout the year made it easy for me, even when I thought I had bitten off more thesis than I could chew.

This thesis reflects my contribution to making Naval Aviation safer for all of our pilots, but it is just the beginning of hopefully much more in the future.

THIS PAGE INTENTIONALLY LEFT BLANK

CHAPTER 1:
Introduction

Compressor development has been a crucial aspect of improvement for performance of gas turbine engines. However, compressors are sensitive components. Large variations in inlet stagnation pressure, flow whirl, or distortion can cause a compressor stage to stall or surge. Stall occurs when a blade passage, or series experiences detachment of flow over the Suction Side (SS) of the compressor blade. Compressor stalls not only damage internal components, but have been the source of numerous aviation mishaps. Thus, efforts to mitigate compressor stalls by increasing Stall Margin (SM) has been a focal point dating back to the 1950's, nearly as old as the inception of the gas turbine itself [1].

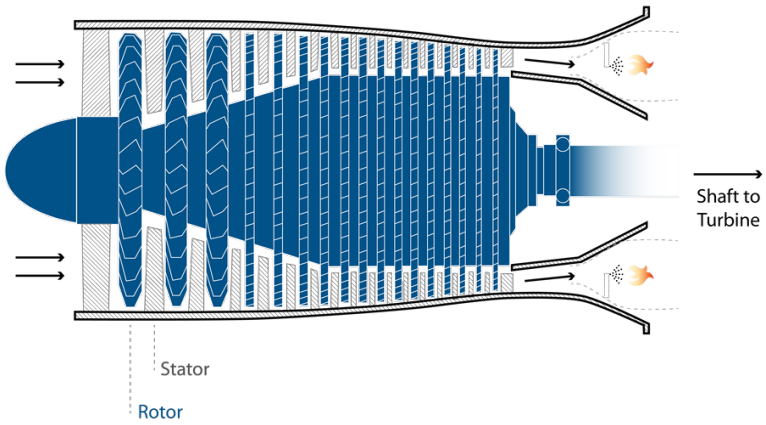

Figure 1.1. Example of an Axial Compressor. Source: [2]

It is well-established that adjustment of the flow-field, whether by passive or active means, can serve to delay the onset of stalling as the compressor face experiences a drop in total pressure. As the stagnation pressure drops, the flow loses momentum. This has most commonly been accomplished through the use of casing treatments; treatments commonly include grooves at the casing wall or recirculating passages. Many of the treatments remedy this either by removing the low-momentum flow that has built up along the casing wall, or by injecting higher total pressure air into the flow (re-energizing). This effect is illustrated in

Fig. 1.2 which showcases one of the experiments described by Hathaway [1]. It is important to note that extending the SM by these methods requires the rotor to be either tip limited, and/or an endwall stall, where the boundary layer inside the test rig expands, resulting low momentum flow, and eventual separation [1]. Additionally, low solidity rotors also seemed less affected by treatments. Low solidity rotors have a small ratio of height to blade chord. Figure 1.3 depicts a typical compressor cascade for reference.

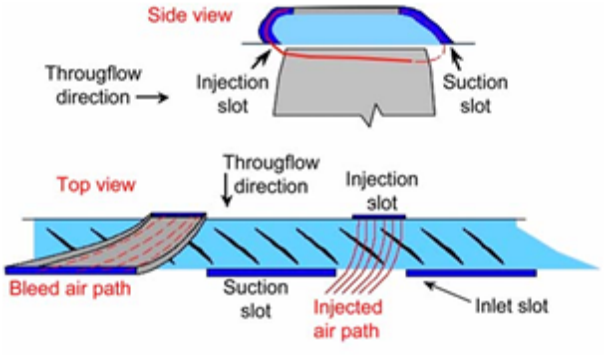

Figure 1.2. Example of a Self-Recirculating Treatment. Source: [1]

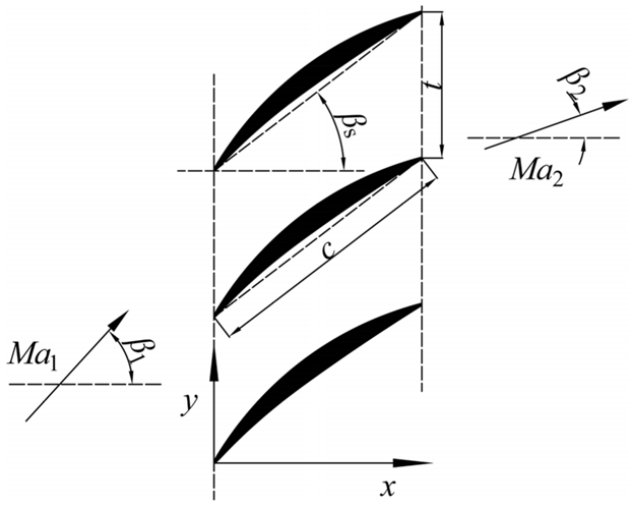

Figure 1.3. Example of a Compressor Cascade. Source: [3]

This project was carried out as part of the ongoing research at the Naval Postgraduate School Turbopropulsion Lab (TPL). The project's objective was to investigate the use of

casing treatments and flow control devices to increase the stall margin of the NPS Military Fan (NPSMF), a 1/4 scale model of a high-performance military compressor section. The NPS Military Fan (NPSMF) is a transonic compressor. In certain operating regimes (85% speed +) the relative mach number at the blade tips surpasses Mach 1. Consequently, this required special consideration for the effective manufacture of the treatments. Grooved treatments, particularly slotted treatments, work very well to extend the stall margin of subsonic compressors [1]. However this effect seems negated when the flow's relative velocity begins to enter the supersonic regime. The objective of this study, therefore, was to create casing treatments to be able to extend stall margin in both subsonic and supersonic regimes. If implemented on an aircraft, these systems would also need to be passive, as otherwise they would necessitate extensive outside plumbing and energy for compressed air injection. The energy that was required for cases such as MIT's active stall control technology [4], would not be able to be implemented in any current gas turbine without massive bleed-air penalties. Many of the past SM improvement techniques, as such, have been active, whereas this study sought to ascertain the effect of passive devices. Furthermore, the casings needed to be rapidly manufactured, owing to the primary use of 3D printing for this project. This allowed for rapid prototyping, as well as design a complex internal geometry. With these constraints in mind, two primary casings were designed in an effort to improve SM while minimizing efficiency and pressure ratio loss.

1.1 Literature Review

1.1.1 External Literature Review

The NASA technical paper on passive treatments for enhancing stability was the most prominent source for this project [1]. Hathaway, in the paper, provides a comprehensive overview of treatments, and explores various theoretical approaches. The central two types being grooves and porous endwalls. As established by previous work, grooved casings were previously explored and yield no benefit to supersonic rotors whereas porous endwalls do [5]. In fact, they served as inspiration for the more modern recirculating flow treatments discussed later in the paper. Hathaway emphasizes that all casing treatments have associated loss mechanisms, and thus, need to be designed meticulously, with careful consideration of their trade-offs. Several examples cited, especially that of Yang, demonstrated a 125%

range extension in a transonic compressor Computational Fluid Dynamics (CFD) simulation when utilizing recirculating casing treatments. Fig. 1.4 illustrates the difference in tip-vortex breakdown with and without the recirculating treatment.

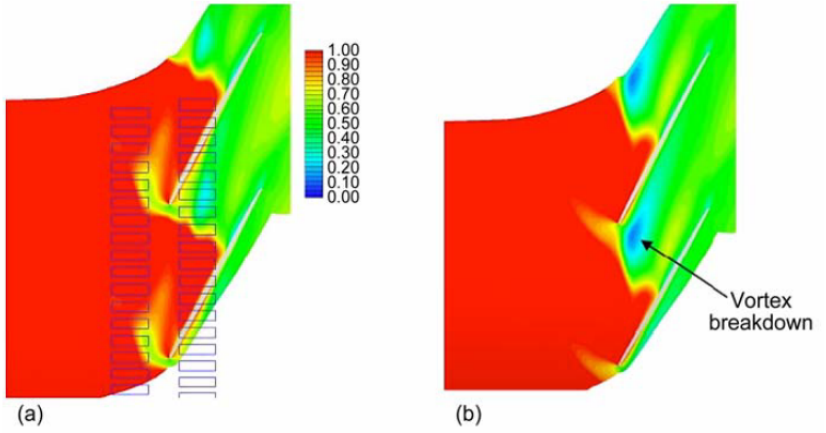

Figure 1.4. Example of Tip Vortex Breakdown Mitigation. Source: [1]

These results were even more encouraging in that there was minimal pressure and efficiency loss. However, due to program constraints, experimental data was unable to be obtained.

Greitzer explores and characterizes the two ways in which a rotor may stall: endwall stall and blade stall [6]. Understanding the difference in these mechanisms is crucial, because of the vast difference in efficacy of the treatment, dependent on the type stall. Endwall stall occurs as a function of boundary layer growth on the case. This robs the flow of momentum. This flow then approaches the rotor and as it has lost momentum, fails to attach over the SS of the blade. On the other hand, blade stall does not depend on boundary layer growth, and largely depends on the compressor geometry. It may also be affected by the relative inlet angle, (α) of the compressor blade tip. This angle is formed by the addition of the inlet velocity angle ($\beta 1$) shown previously in Fig 1.3, added with the rotor rotation speed vector. In the case of blade stall, little can be done to mitigate the stall through methods of blowing or sucking air, as the stall is not dependent on the loss of momentum within the flow.

1.1.2 Internal Literature Review

Previous theses significantly contributed to the manufacturing and computational methods of this paper. Meinster, for example, was able to extend the computational domain of the Transonic Compressor Rig (TCR) according to the following Fig. 1.5 to capture flow farther upstream. Additionally, he employed conforming splines using SOLIDWORKS to create a map of the NPSMF blade [7]. This is depicted in Fig. 1.6. This allowed him to generate a fluid domain that conformed nearly perfectly to the blade of the rotor, resulting in a true periodic surface. This allowed the exchange of information between the periodic surfaces in simulations. His method, along with that of Holmes [8] provided many of the methods used for the construction of those fluid domains in this project.

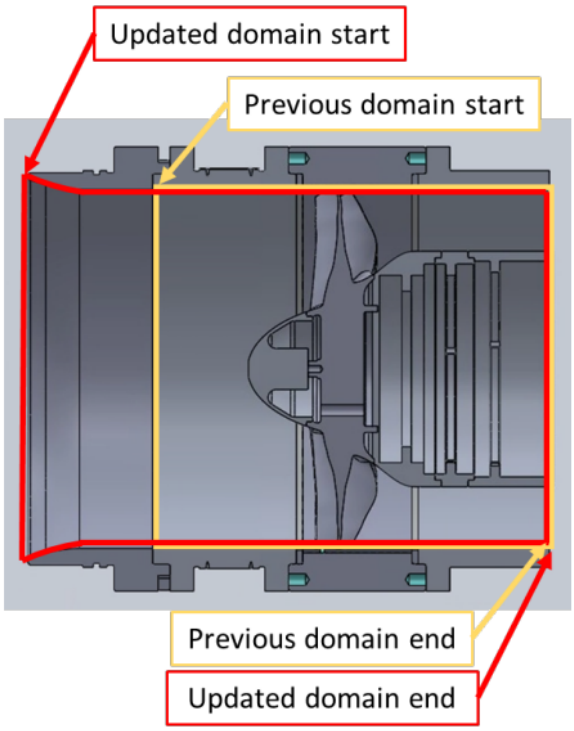

Figure 1.5. Improved Domain Overview.
Source: [7]

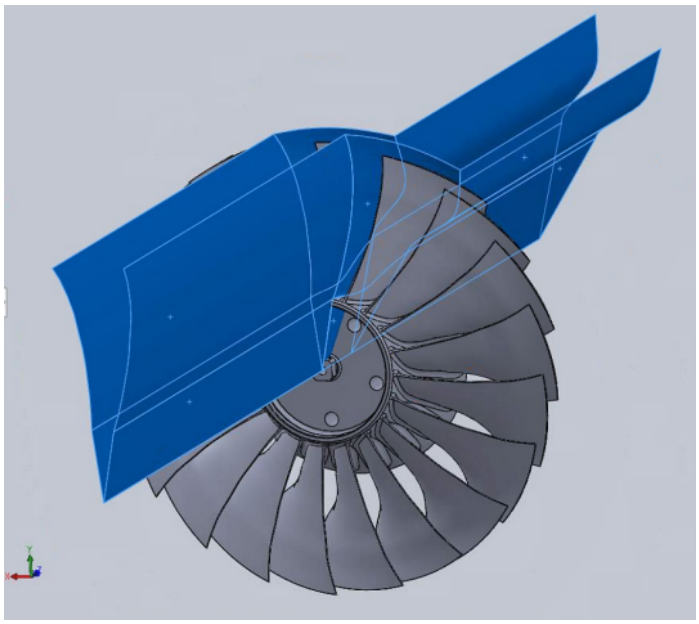

Figure 1.6. Improved Blade Passage Creation.
Source: [7]

Meinster used this improved domain to explore the effects of varying tip-gaps of 0 mm, 0.381 mm (0.0015 in) and 1.27 mm (0.050 in) on rotor stall characteristics. These varying tip-gaps, shown in Fig. 1.7 unearthed drastic effects on rotor performance. The variance of both the leading edge normal shock near the blade tip, and the growth of large Tip-Gap (TG) flow detachment became apparent with his work. The 0.381 mm (0.0015 in) gap exhibited a 1.2% decrease in rotor efficiency, and the 1.27 mm (0.050 in) gap exhibited a nearly 3.3% decrease. This aligned well with available experimental data. As rotor clearance cannot always be specified, Meinster's research allowed corrections to be made for TG differences between casings.

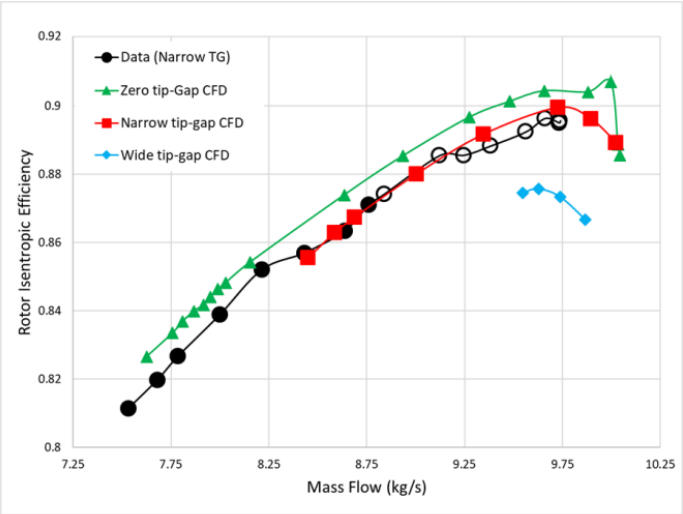

Figure 48. Isentropic efficiency map for the updated CFD model.

Figure 1.7. Tip Gap Performance Effects. Source: [7]

Meinster's thesis also provided the boundary conditions, as well as the turbulent model used in this paper's computational simulations. Specifically, the Gamma-Theta transition model and the SST turbulence model were chosen for their accuracy of regarding experimental flow features. Meinster used a 23 million element mesh, which served as a reference for the comparable mesh used in this paper to gather data for the NPSMF without a casing treatment.

Green's thesis laid the foundation for the design and manufacturing of the flow recirculating casings used in this paper [9]. Although his epoxy manufacturing methods were not specifically used in this project, they inspired the use of Fused Deposition Modeling (FDM) and Direct Metal Laser Melting (DMLM) techniques. Green used plastic inserts in an epoxy layer to create a set of designed casing grooves. The epoxy was secured by an aluminum casing with retaining rings, creating a reservoir in which to imprint a desired casing, (see Fig. 1.11). This method also influenced the creation of an internal passages casing, where the epoxy was used to facilitate the formation of internal passages by filling negative space between the passage tubes and the casing wall.

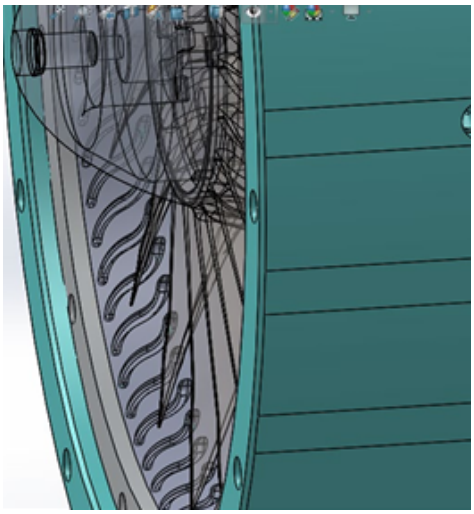

Figure 1.8. Casing S-Groove Design. Source: [9]

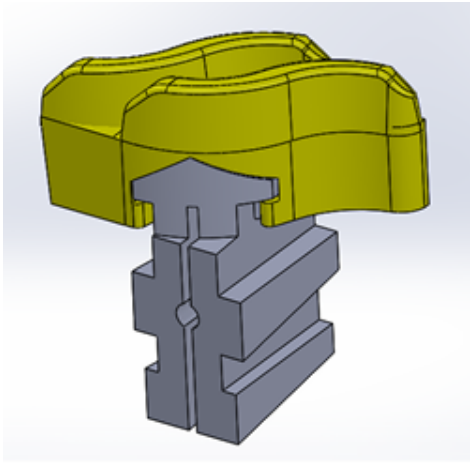

Figure 1.9. S-Groove Imprinting Device. Source: [9]

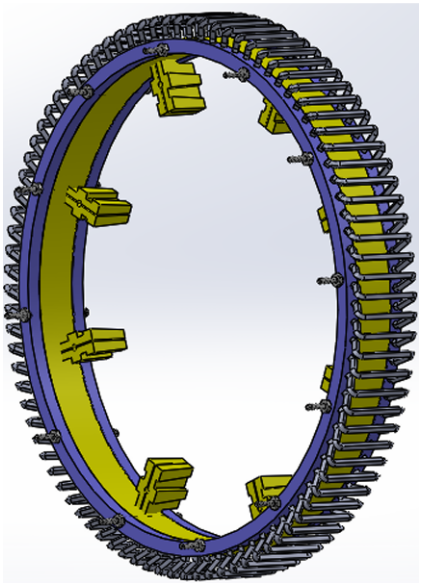

Figure 1.10. Internal Passage Inlet/Outlet Rings, and Passage Inserts. Source: [9]

Figure 1.11. Internal Passage Epoxy Manufacturing. Source: [9]

Holmes conducted research on the Inlet Guide Vane (IGV)s for the TCR [8], and developed models for their passive effects on performance of the NPSMF. This was conducted with and without the IGVs installed and deflected. A separate IGV domain was created using SOLIDWORKS and attached to the previously existing NPSMF rotor domain. Though the

IGVs have variable flaps for different rotor speeds, the IGV domain was constructed for 3 separate IGV flap angles: 0°, ±5°. The aim was to investigate the effects of varying angle of the IGVs, and to model passive effects of the 0° case. Simulations were conducted at 70%, 80%, 85% and 90% rotor speed. In the 90% case, the flaps deflecting positively (rotor-loading) had a strong adverse effect on the stage efficiency of the rotor. On the other hand, the unloading deflection had very minor effects. Notably, unloading the rotor did not result in an expected increase in stage efficiency, but rather a ~0.1-0.2% decrease. Figure 1.12 provides a depiction of the entire computational domain, with the IGV domain indicated as blue/teal.

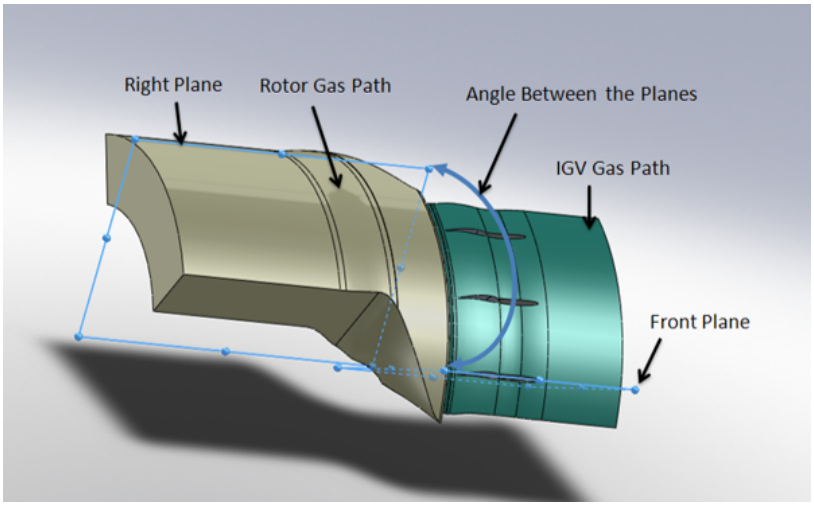

Figure 1.12. IGV Domain Attached to Rotor Domain. Source: [8]

Jones, having also used the above theses in his work, built off of the previous theses to comprehensively develop and test both S-Groove and Internal Passages (IP) casings. The study worked to combine the casing generation method of Green and the computational analysis of Meinster to computationally model the two casing treatments, as well as many simulated deflections of the IGVs. Jones developed a method to obtain the fluid path of the S-Grooves and the internal passages, and mate them to the gas path of the NPSMF in ANSYS CFX. He also developed a pseudo-transient method of analysis that was utilized in the current study, that continuously dropped the inlet pressure at the face of the rotor to move the simulation along a given speedline. This was done until the efficiency diverged from a linear decrease to determine rotor stall. Only the smooth and S-groove casings were

experimentally tested, not allowing a full comparison between treatments, or a validation of the suspected performance of the internal passages. The internal passages design was the first design to rely on passive flow recirculating to improve stall margin. Jones was able to determine that many traditional grooved casing treatments (those that are just cuts in the casing wall) are not effective at increasing stall margin once the rotor tips are supersonic, and so the IP design was put forth as a possible solution.

In computational simulations, Jones found that the recirculating casing treatments (Internal Passages) increased the stall margin by 71.5-82.5% depending on rotor speed. His results also showed an efficiency increase at 90% operating speed, which is not anticipated to reflect real phenomena. Increase in total pressure ratio, π_t, was shown to be possible by Hathaway [1], but not increase in efficiency.

Experimentally, Jones was able to draw conclusions only between the S-groove and smooth casings, but found a large increase in stall margin running the rotor at all speeds, but scheduled for a 70% IGV set angle. Though this increased the SM for all cases, it resulted in large losses of both efficiency and pressure ratio compared to an on-design IGV schedule. Cases where the IGVs were set In Accordance With Schedule (IAWS) resulted in SM losses of 7%, 15%, and 25% respectively for the 80%, 85%, and 90% rotor speed cases. Lastly, inlet guide vane jigs were developed to precisely set the IGV angles of the experimental rig before conducting a run. This allowed the IGV sweep to be completed and additionally allowed the IGV angles to be set much more precisely than previous experiments.

1.1.3 Summary

The below list comprises a summary of key insights from the literature about design of transonic compressor casing treatments. This includes both effective and ineffective methods of design.

- Tip gap of the rotor has a drastic inverse effect on stage efficiency (on order of ~0.066-0.073% per thousandth of an inch added to tip gap)
- Epoxy curing methods are very time consuming, though they allow complex geometry to be made, including recirculating passages
- Recirculating Passages can increase pressure ratio but decrease efficiency
- Casing Treatments are a loss mechanism, and so need be designed precisely and with

the trade-offs in mind

- Casing treatments work best on cases of endwall stall and with high solidity rotors
- Grooved casing treatments are ineffective, and even detrimental top SM above subsonic regimes
- Treatments that actively blow or remove the boundary layer by suction have been shown to improve stall margins greatly (by over 100%) in transonic rotors
- Injecting mass as axially as possible seems to benefit stall margin the most
- The mechanisms for casing treatment effectiveness are still yet to be fully understood

1.2 Overview of the Current Study

This study combines the modeling methods of Meinster, manufacturing considerations of Green, and CFD evaluation methods of Jones. Three types of casings were experimentally tested: A smooth-walled (referred to as 'smooth' or Rotor Only (RO)) casing, an Internal Passage (IP) casing, and finally a novel 'NACA' casing. The IP casing design was based off of Jones's work, but with improvements in the exit section of the passages [5]. The NACA casing was developed novelistically, incorporating the most effective methods of increasing SM from the papers above. Manufacturing of the two treatment casings (NACA and IP) proved to be challenging, but solvable. Casings were made out of various engineering plastics, such as polycarbonate and PEEK, through FDM printing. Aluminum casings were also made to withstand higher temperatures, using DMLM and Liquid Metal Jet Printing (LMJP). Ultimately, the methods of Green served as inspiration and guidance for the manufacture of the current study's casings, but epoxy curing was not pursued.

The casings were each measured and experimentally tested, and a full complement of computational simulations were obtained for each conducted and scheduled experimental test. Additionally, the IGVs were able to be fully modeled for the 90% rotor speed case, and were compared with the IGV estimation method used by adding inlet whirl to the simulations. The paper below serves both as a digestion of the performances of each casing, as well as a review of the process of their creation, hopefully offering helpful insights and recommendations for future manufacture of passive recirculating casing treatments.

THIS PAGE INTENTIONALLY LEFT BLANK

CHAPTER 2:
Methodology and Experimental Setup

2.1 The TCR

The Transonic Compressor Rig was designed to allow the testing of various axial compressor stages, with the ability to quickly exchange test articles. The rig begins with a bell-mouth, a newly updated throttle body, and digital encoder [10] and flow straightening screens [11]. These allow the conditioning of the airflow be as uniform as possible, and dictate the inlet pressure. A 12-stage axial compressor that is electrically powered is used to drive the TCR drive turbines with high-pressure air, these turbines are power limited to 27,000 RPM, or 90% speed designed for the NPSMF, meaning data is only available for 90% speed and below.

The TCR test section consists of Inlet Guide Vanes, each with a straight airfoil section and adjustable flap, shown in Fig. 2.3. Behind this sits the test article, for this study the NPSMF rotor, shown in Fig. 2.2. Finally there are a set of stator blades to remove the whirl imparted to the flow by the NPSMF. This encompasses the test section of the TCR and is where much of the pressure and temperature instrumentation is located. The test section is outlined in Fig. 2.1 with the highlighted IGV, fan, and stator sections. The exhaust from the rig is vented out into the test cell via an annular channel also annotated on Fig. 2.1.

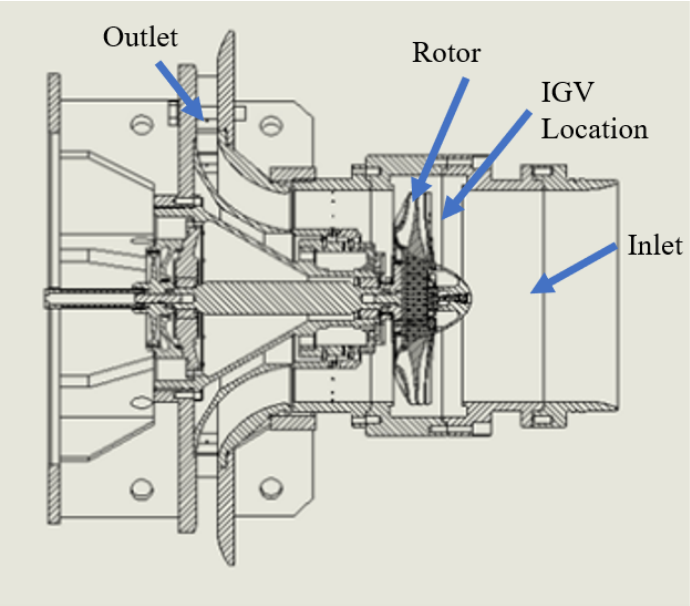

Figure 2.1. TCR Test Section with Rotor Only (No IGVs).
Source: [7]

2.2 NPSMF Rotor

The NPS Military Fan is a 20-blade transonic axial compressor made of a titanium alloy. It is a Bladed-Disk (Blisk) meaning is machined out of a single piece of metal, rather than being assembled from a hub ring and separate blade pieces. The NPSMF was obtained by the Naval Postgraduate School in 2009 and the NPSMF has been the subject of numerous studies since. In addition to the continued work on experimental casing treatments, work by Giambruno and Adams, [10], [12] and their predecessors has helped modernize the instrumentation upstream and downstream, respectively, of the NPSMF to obtain higher fidelity temperature and pressure measurements.

The table from McNab [13] summarizes key parameters of the NPSMF:

Table 2.1. NPSMF Characteristics Source: [13]

Design Speed	30,000 RPM
Rotor Diameter	287.02 mm (11.3 in)
Maximum Mass Flow Rate	10.14 kg/sec (2.23 lbm/sec)
Tip Inlet Relative Mach	1.52
Max Pressure Ratio	1.70

Figure 2.2. The NPS Military Fan Blisk. Source: [7]

2.3 IGVs

The Inlet Guide Vanes (IGV) are a set of 17 stationary blades that provide whirl co-rotational to the rotor. The assembly is shown in Fig. 2.3 and directly precedes the NPSMF.

Each IGV blade is made up of a stationary airfoil section and a movable flap, depicted in Fig. 2.4 and 2.5. The flap has a significant degree of washout along the span, unloading the tip of the rotor and loading the base of the rotor. This has been only approximated in previous year's theses as linear twist (washout) whilst assuming every airfoil section in between root

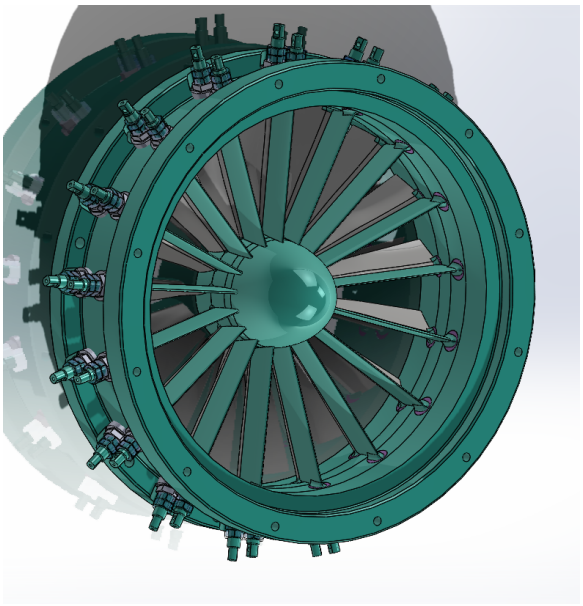

Figure 2.3. The IGV Assembly

and tip is a linear interpolation of the washout based upon position.

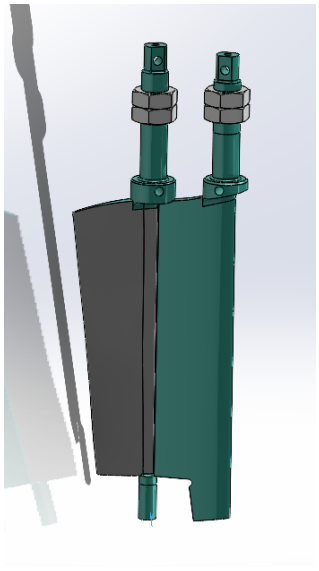

Figure 2.4. Side View of One IGV Flap

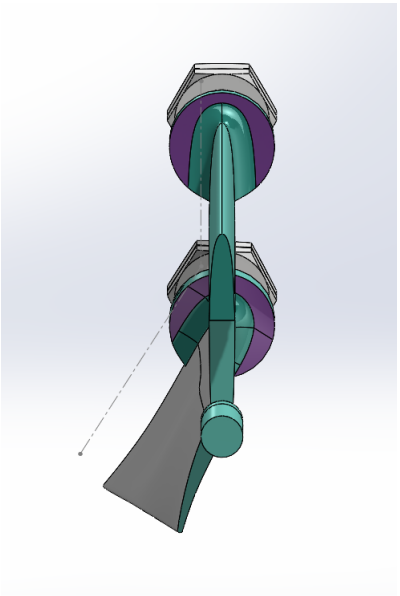

Figure 2.5. IGV Trailing Flap Deflection

The IGVs produce this whirl to significantly unload the rotor at speeds lower than 100%. This serves to intentionally decrease the pressure ratio for the first stage, as is common with high-performance compressors, to allow later stages to operate at a similar pressure ratio (π_t) and prevent choking of later stages. This also works to improve stage efficiency (η_{TT}). These blades need to be set manually prior to each test condition, as outlined by Jones [5] but are computer controlled in in-aircraft operation. A depiction of the velocity triangle adjustment is in Fig. 2.6. Note how the IGV introduction reduces the angle of attack (α) experienced by the rotor blade.

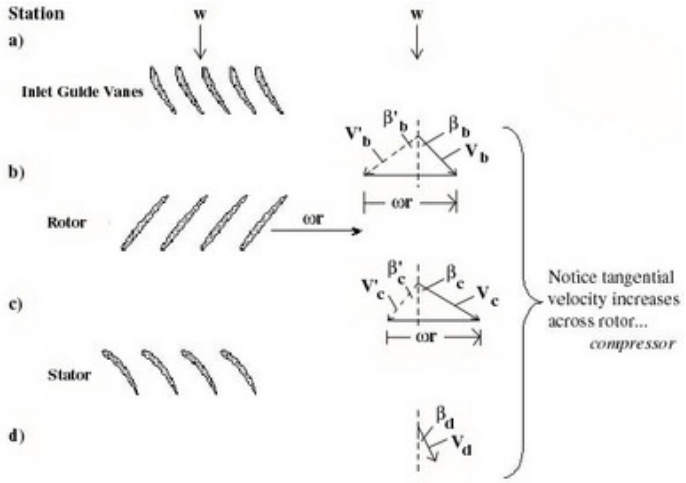

Figure 2.6. Velocity Triangle Example for Axial Compressor with Guide Vanes

2.4 Testing procedure and Data Collection

The TCR operation followed the method outlined by Jones and McNab, [5] and [13] and is summarized below. Each experiment began by taking atmospheric condition data (humidity, temperature and pressure) after which the TCR was brought up to speed by the drive fan. The desired inlet conditions were achieved by a throttle body; previously moved by visual observation and manual adjustment through an electronic switch, the throttle body was updated to use an encoder developed by Giambruno [10] where the desired position can be input digitally. The rig exhaust vented to atmospheric conditions keeping the back-pressure stable, and the inlet throttle was slowly closed to move the TCR along its speedline. Once the TCR was near the expected stall point, a relay was used, as supposed to the throttle encoder,

for precise adjustments of throttle. Throttle movements using this relay were on the order of 0.5% of the total throttle range. The relay allowed the TCR to be rapidly brought out of stall once detected [5]. Throttle positions during the test were recorded, but became unreliable once the TCR entered the near-stall phase being controlled by the relay. Ultimately this did not affect data quality and still allowed for the precise measurement of mass flow and pressure at the stall point.

At each throttle setting, the drive turbine feed pressure needed to be adjusted to maintain the desired rotor RPM. Once stabilized, each point along the speedline was an average of 40 separate measurements collected at a sample rate of 1 Hz.

Outlined by Jones, a 'jog' method was used to establish the mass flow at which compressor stall occurred [5]. As the TCR approached the previous known stall-point, the throttle was moved in small increments, and the rig was allowed to stabilize. Stall was easily audibly detected by a rapid, loud, pulsating buzz. Stall onset was also reflected in the experimental data with a sharp drop in the stage pressure ratio and efficiency. The recorded stall point was the most closed throttle position that still resulted in stable rig performance.

2.5 Test Cases

Table 2.2 highlights all computational test cases performed in this study, in the order in which they were performed. To complement this is the experimental test table (table 2.3 which details the various TCR runs completed. Note that in each experimental test run, all 4 rotor speeds were tested (70-90%). For nomenclature clarification, the CFD test case with no casing treatment, just the NPSMF, will be referred to as the 'Rotor Only' Case. The internal passages and NACA casings will be 'IP' and 'NACA' respectively, and the computational case with the modeled IGVs as the 'IGV' case. The experimental cases will be referred to as the 'smooth' case (no treatment), IP and NACA cases.

The experimental cases were completed with the rotor, IGVs, and stator all installed. The computational cases simulated either the rotor alone (no Whirl), or the rotor with IGVs installed (Whirl). Effects of the lack of a stator in ANSYS simulations are discussed in chapter 6, and complimented with Adams's [12] comprehensive overview of the stator exit temperature and pressure profiles.

Table 2.2. Computational Tests, all @ 0.0381mm (0.015in) TG

Casing Type	Whirl (Y/N)	Rotor Speed	Mesh Count
Rotor Only (smooth)	N	90%	800,000
Rotor Only (smooth)	N	90%	6 million
Rotor Only (smooth)	N	90%	21 million
Rotor Only (smooth)	N	90%	32 million
Rotor Only (smooth)	Y	90%	38 million
Rotor Only (smooth)	Y	85%	38 million
Rotor Only (smooth)	Y	80%	38 million
Rotor Only (smooth)	Y	70%	38 million
Rotor Only (smooth)	N	90%	38 million
Rotor Only (smooth)	N	85%	38 million
Rotor Only (smooth)	N	80%	38 million
Rotor Only (smooth)	N	70%	38 million
Internal Passages	Y	90%	39 million
Internal Passages	Y	85%	39 million
Internal Passages	Y	80%	39 million
Internal Passages	Y	70%	39 million
Internal Passages	N	90%	39 million
Internal Passages	N	85%	39 million
Internal Passages	N	80%	39 million
Internal Passages	N	70%	39 million
NACA	Y	90%	38 million
NACA	Y	85%	38 million
NACA	Y	80%	38 million
NACA	Y	70%	38 million
NACA	N	90%	38 million
NACA	N	85%	38 million
NACA	N	80%	38 million
NACA	N	70%	38 million
IGV	N/A	90%	34 million
IGV	N/A	90%	41 million
IGV+NACA	N/A	90%	61 million

Table 2.3. Experimental Test Table

Casing Speed & Type	IGV IAWS/0°	Casing Material	Tip Gap (mm)
90% Smooth	IAWS	Aluminum Alloy	0.0381
85% Smooth	IAWS	Aluminum Alloy	0.0381
80% Smooth	IAWS	Aluminum Alloy	0.0381
70% Smooth	IAWS	Aluminum Alloy	0.0381
85% Internal Passages	IAWS	Polycarbonate	0.0381
80% Internal Passages	IAWS	Polycarbonate	0.0381
70% Internal Passages	IAWS	Polycarbonate	0.0381
85% NACA	0°	Polycarbonate	0.03556
85% NACA	IAWS	Polycarbonate	0.03556
90% NACA	IAWS	AlSi10Mg	0.0381

CHAPTER 3:
Casing Design and Manufacture

3.1 Physical Geometry Creation

The NPSMF sits inside of a rotor casing, shown in blue (Fig. 3.1). The outer casing has 32 tapped holes at increasing axial distances down the casing. This allows a pressure tap to be placed anywhere axially along the rotor. The outer casing had 12, 12.7 mm (0.5 in) diameter lobes cut out of it to hold an inner casing. As supposed to Green's method, with retaining rings on either side of the epoxy inner-casing, the lobes allow an inner casing to be press-fit and held. A depiction of a smooth-walled inner casing is shown in orange (Fig. 3.2).

This 'orange' inner casing is what will be referred to as simply 'the casing' for the remainder of this study. This was the part of the casing carrying all casing treatments or flow control devices. Being done in this manner, multiple inner casings could be made and fit or switched-out from a single outer casing. The exits of the casings were made to be as-axial as possible, but due to construction fidelity and material strength considerations, an exit angle of 45° relative to the axial direction was settled upon. Any significantly lower exit angle than this (more axial) created a very weak lip, particularly for the NACA casing and those constructed with polycarbonate plastic.

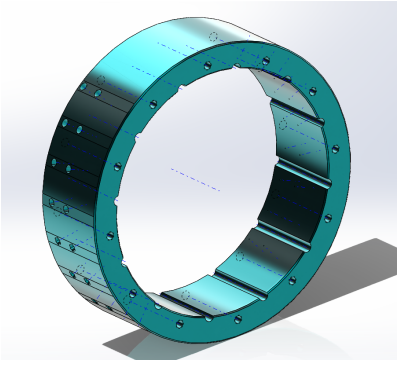

Figure 3.1. Outer Casing (blue)

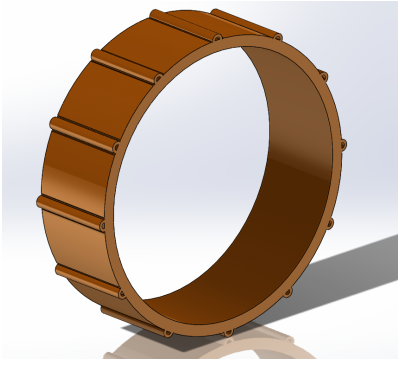

Figure 3.2. Inner Casing (Orange) (Test Article)

The inner and outer casings were fit together, and housed the NPSMF such as in Fig. 3.3

and 3.4.

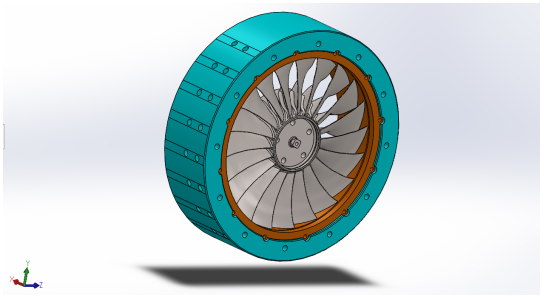

Figure 3.3. NPSMF Rotor Inside Casing Treatment (Orange) and Outer Casing (Blue)

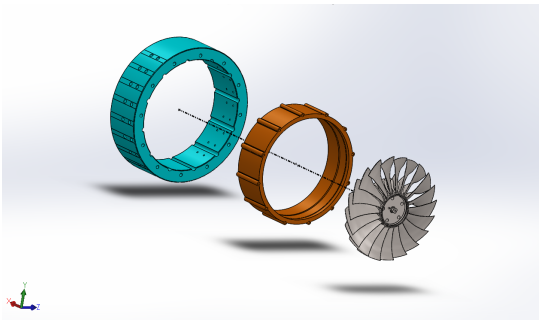

Figure 3.4. Exploded View of Casing Stack

Below is an outline of the two types of casing treatments modeled for this study, the IP casing and the NACA casing. These sections cover the models used for manufacturing and initial design of the casings, while later chapters delve into specific computational modeling.

3.1.1 Internal Passage Casing

The design of the Internal Passages casing, though adapted from Green, was sized differently [9]. Green's casing had 181 separate recirculating passages around the annulus of the casing for an estimated 5.74% masssflow recirculation. He sized 89 passages to target a 2.5% mass flow recirculation, with the passages having a cross-sectional area of $6.435e^{-6}\ m^2$ (0.009975 in^2). Green used a series of the Fanno flow calculations to iteratively solve for the mass flow rate through each passage. The number of passages was kept to a prime number to mitigate any potential resonance effects.

For this study, the passages were sized up to be 4x the area of those created by Green, necking down to 2x the area at each passage exit. Due to the complex geometry of these passages, an accurate Fanno flow estimation could not be completed for the IP casing in study. The design change that resulted in the exit area of the duct being halved was done in accordance with data from Hathaway [1], to mechanically accelerate flow exiting from the passage. Each inlet was $1.290e^{-4}\ m^2$ (0.2 in^2) and each exit $6.452e^{-5}\ m^2$ (0.1 in^2). The theory behind sizing down the exit was to translate more of the fluid pressure from inside the passage into velocity, thereby imparting more momentum into the exiting flow and thus

the boundary layer at the tip of the rotor. The sketch locations were also parameterized so subsequent studies can axially move the inlet and exit ports of the casing treatment with ease. However, Hathaway makes clear the best known locations of exit nozzles for increasing stall margin are directly ahead of the rotor tip [1].

Due to program constraints, a casing with a radial exit was unable to be made to compare effectiveness to the axial-angled exit. This is an encouraged area of further research. Similarly the inlet to the passages was angled upstream at 45° to capture flow. The passages were otherwise rectangular ducts, with the inlets and exits offset radially as to accept more flow, given the whirl imparted by the rotor. Fig. 3.5 depicts a cross section of the IP casing, detailing the path of each of the internal passages.

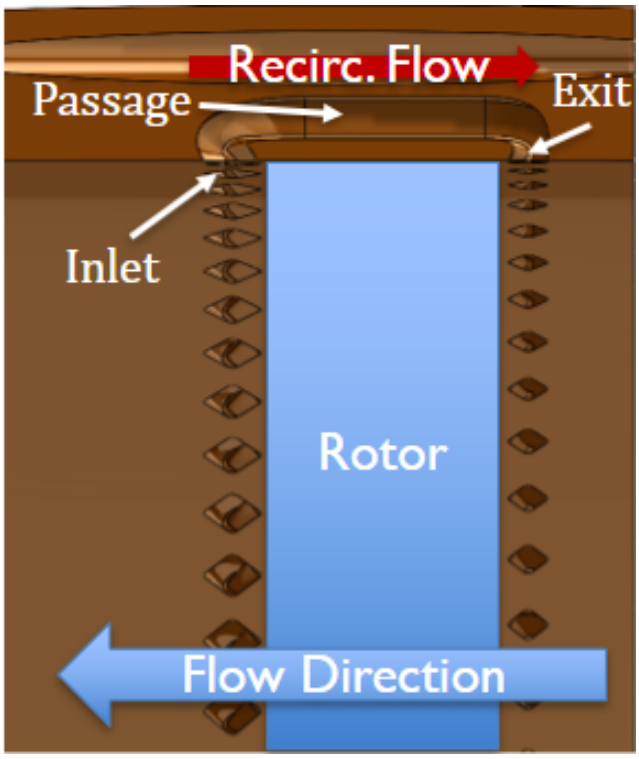

Figure 3.5. Internal Path of IP Casing

3.1.2 NACA

As the NACA casing was a novel design, many development iterations were undertaken with the casing before finalization. The theory behind the NACA casing was to recirculate

as much mass flow as possible. This was predicted to result in large efficiency losses. If the treatment had massive improvement effects for SM though, especially at supersonic operating speeds, the channels could subsequently be narrower. This would allow the sizing of the channels to be upper-limit bounded, and subsequently smaller treatments could be made in attempt to find a balance of SM improvement and retaining stage efficiency ratio, η_{TT}.

While the initial concept of the casing is shown in Fig. 3.6, the final design is shown alongside in Fig. 3.7. This casing began with an 'open channel' design concept, where instead of small individual passages, large sections of the casing would be cavitied out, with only ~5° sections of the casing un-treated to maintain structural integrity. As annotated in Fig. 3.6, however, this led to large portions of the casing wall above the rotor to be inadequately supported.

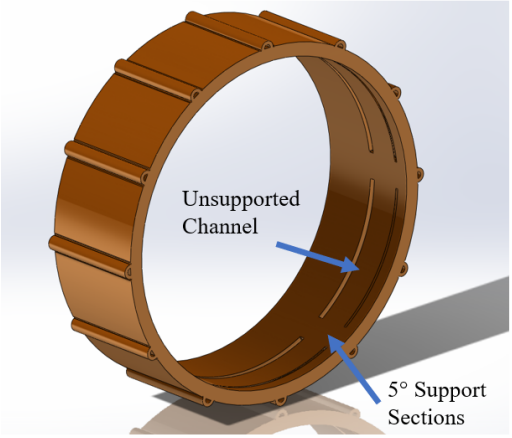

Figure 3.6. Initial 'Open Channel' Casing Design

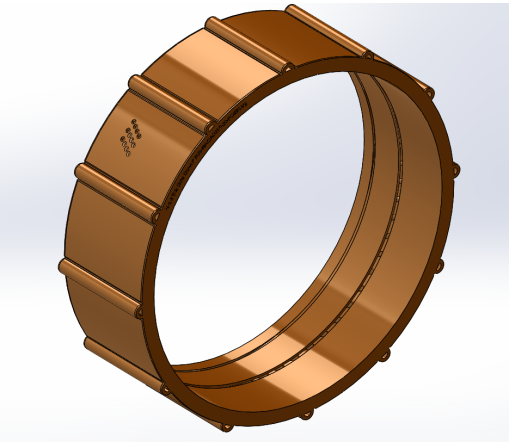

Figure 3.7. Final NACA Casing Design

The best way to support the inner wall of the casing was decided to be creating struts from the outer channel surface to the unsupported inner channel surface. To minimize disruption to the flow-field, airfoil profiles were chosen for the struts (specifically NACA 0015, hence the name of the casing). These struts can be seen in the final casing iteration cutaway in Fig. 3.9. These supporting struts also meant the 5° untreated sections of the casing could be removed, and so the casing could have a completely open annular inlet and exit. This greatly simplified the setup for CFD detailed in section 4.1.3 by allowing the use of periodic

boundary surfaces.

A cutaway of the initial NACA casing design is shown in Fig. 3.8. Note the annotated inlet and exit locations, as the flow through the compressor is depicted as right-to-left, and so the recirculating channel flow is left-to-right. Of these supports, 61 were patterned around the annulus to support the casing inner wall.

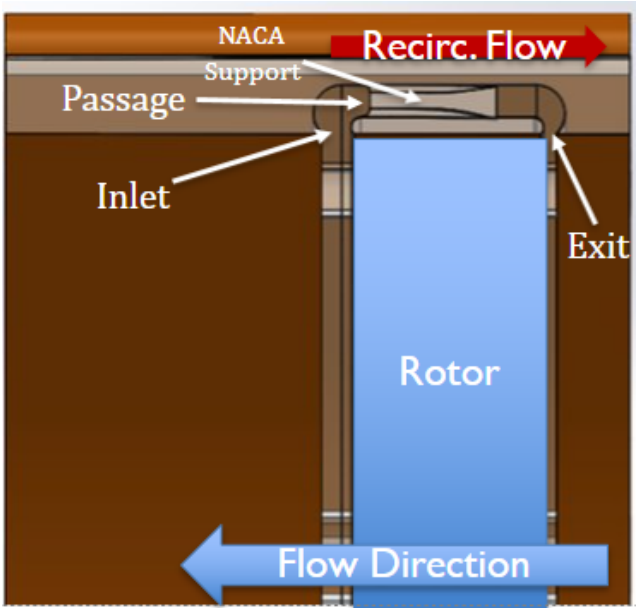

Figure 3.8. Initial NACA Casing with Straight Supports

Manufacturing considerations introduced challenges for the casing's creation. The airfoils needed to be swept to be able to be manufactured with Additive Manufacturing (AM) methods without generating support material within the passages of the casing. The airfoil supports were chosen to have a 45° sweep for ease of manufacture. Additionally, the channel shape near the treatment exit needed to be changed to a sharp corner rather than a radius. This was done to allow AM printing without having an unsupported radius, so again, the part could be made with minimal support material. These features can be seen in Fig. 3.9.

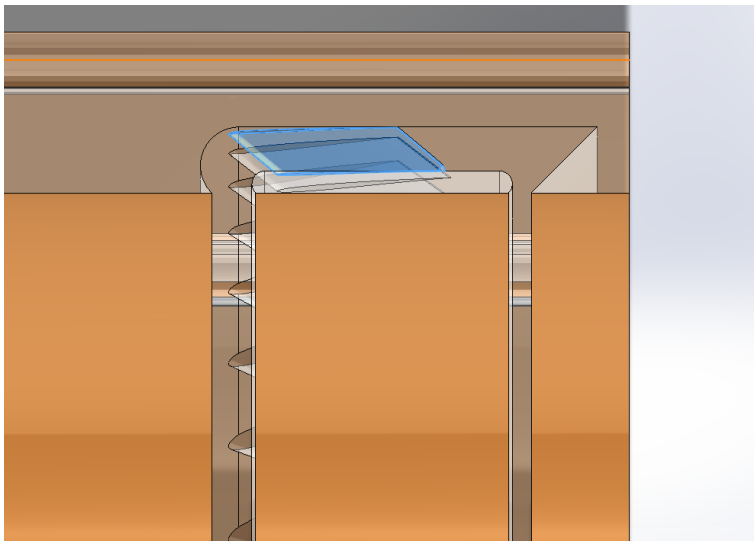

Figure 3.9. Final NACA Casing
Blade Passage Depiction

Finally, the blades were angled 30° from the axial direction, as shown in Fig. 3.10. This roughly matched the inflow angle of air to the treatment inlet, allowing the blades to ideally unload the flow. Straight blades would simply be at too large of an α to the incoming flow, causing separation over the airfoil struts, likely resulting in undue efficiency penalties. Even as such, in computational simulations the 30° angle was still not enough to prevent separation. An area of encouraged further study is the optimization of the blade angle for unloading the incoming flow to the channel. The blade profile could be changed as well to a cambered airfoil instead of a symmetrical NACA 0015 allowing the casing treatment take a shape much like a traditional stator.

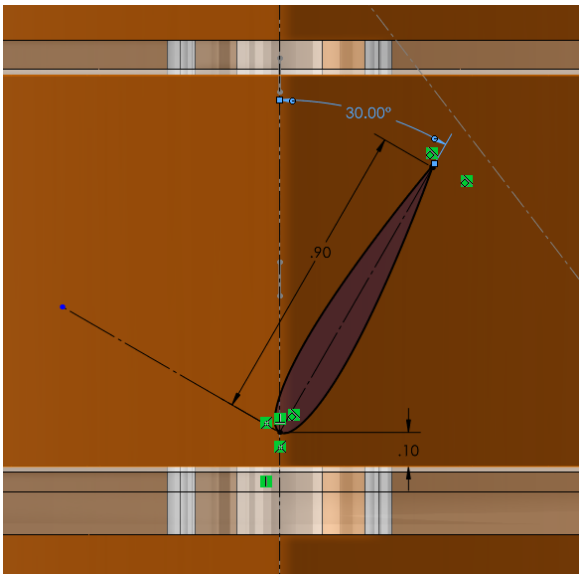

Figure 3.10. Final NACA Casing 30° Blade Angle

Finally, a desire for pressure monitoring inside the treatment was accomplished through a series of access ports. Unlike the IP casing, Fanno flow could not be used to estimate the mass flow travelling through the treatment. This is due to the complex shape the airfoil struts create, narrowing the passage width as the airfoil increases in thickness, and then widening the passage after. Monitoring the pressure at varying axial distances inside the passage would allow calibration of mass flow through the treatment. There were 4 static pressure ports placed along 2 separate channels, as well as 3 stagnation pressure ports placed into the nose of one of the airfoil struts. While not put into use for this study, these access ports could be used in the future as a means to size the passages for a certain mass flow, or to compare flow with CFD predictions. A depiction of the static and total pressure ports is in Fig. 3.11.

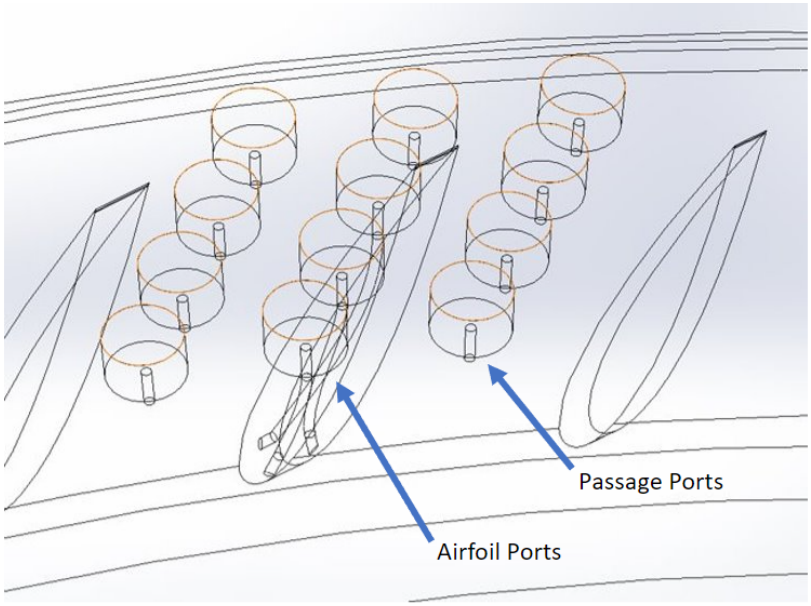

Figure 3.11. NACA Casing Instrumentation Ports

3.2 Casing Manufacture and Sensitivity Study

3.2.1 FDM Polycarbonate Casings

Manufacturing of the polycarbonate casings was done using a Stratasys Fortus 450mc Industrial FDM 3D Printer [14]. FDM is the process of constructing a part by selectively depositing material in layers using an extruder. This is done in a predetermined path, created by a process called slicing. In addition to being much more inexpensive to construct, the polycarbonate casings were able to be manufactured in one print, unlike other in-house manufacturing methods explored in appendix A. The print resolution, however, was much higher along with the print quality. As can be seen from the sensitivity study at the conclusion of the chapter in table 3.2, the polycarbonate casings had acceptable tolerances, though not as high as the aluminum casing.

Minor manufacturing problems were experienced with the polycarbonate prints. As a result of the slicing software, some support structure was deposited inside the passageways of the NACA casing, requiring design iterations before successful manufacture with minimal structure. This casing particularly necessitated a change in geometry of the exit area of the passage, as detailed above in section 3.1.2.

Table 3.1. Polycarbonate Material Properties
Source: [15]

Property	Value
Glass Transition Temperature	141-150°C
Maximum Service Temperature (Air)	115-135°C
Melt Temperature	250-343°C
Specific Heat Capacity	1.17-1.70 J/g-°C

As seen in table 3.1, the polycarbonate casings had undesirable thermal properties for testing in the TCR [15]. With a glass transition temperature of 141-150°C (302°F) and a melting temperature of 265°C (510°F), the casings proved unsuitable to run above 85% rotor speed. A predictive analysis was done using the CFD simulations to judge the average and maximum predicted wall temperature over the various runs. Since the TCR was operated mostly near stall for the experiments, the temperatures were taken from a stall condition. This is shown in Fig. 3.12, highlighting the fact that the average casing temperature rapidly approaches polycarbonate's glass transition temperature even at 85% rotor speed, and surpasses it at 90% speed. In previous experiments, the polycarbonate casings experienced permanent deformation even at 85% speeds. The maximum spot temperature surpasses polycarbonate's glass transition temperature easily by 80% rotor speed. This possibly explains the phenomenon of the slight deformations found on the polycarbonate casings after low-speed runs. Future studies are encouraged to develop an accurate and reliable way of experimentally measuring the casing temperature whilst conducting a run. This is likely achievable through a J-type thermocouple inserted into the casing. Once could even use the method described above in section 3.1.2 of the pressure port construction to also create a thermocouple slot.

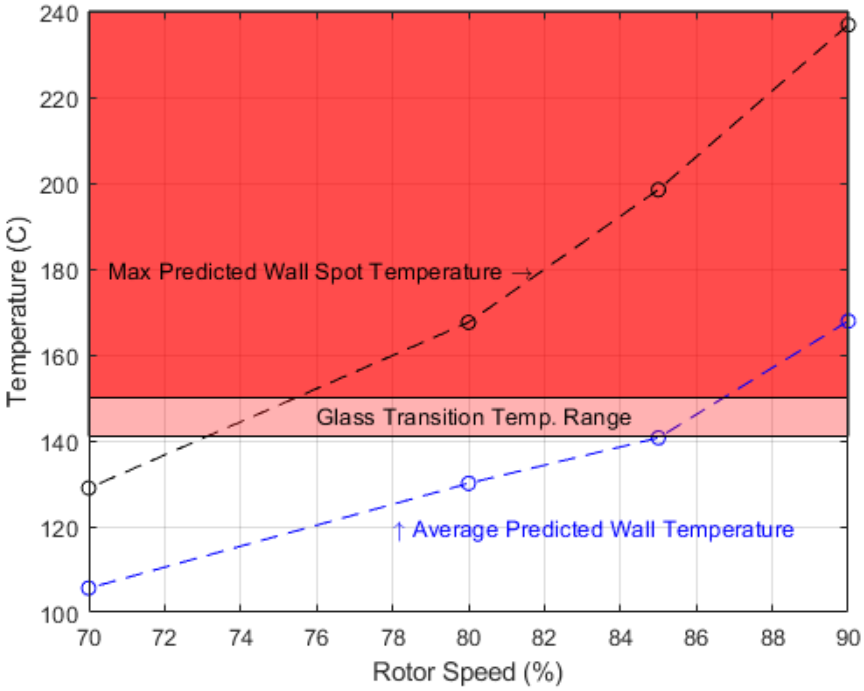

Figure 3.12. Polycarbonate Failure Prediction Plot

The completed IP and NACA polycarbonate casings can be seen in Fig. 3.13 and 3.14. These were the two experimentally tested polycarbonate casings. A depiction of the inlet and exit profiles is also in Fig. 3.15 to give context for the how the inlet/ exit design manifested in contraction using polycarbonate. Overall the features of the design had remarkable visual quality considering their low construction time and cost.

Figure 3.13. IP Polycarbonate Casing

Figure 3.14. NACA Polycarbonate Casing

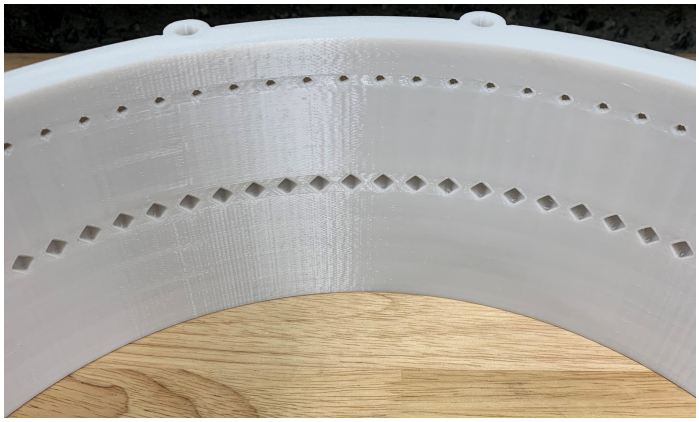

Figure 3.15. Polycarbonate Passage Inlet and Exit Manufacturing Quality

3.2.2 DMLM Aluminum Casings

DMLM is process by which a metal powder is melted into a solid by way of a high powered laser. This is done in layers until the final desired part is created. This manufacturing method allowed the casings, produced by Protolabs, to conform to tight tolerances and have above a 90% infill [16]. The minimum feature size specified for this print method was 0.762 mm (0.0300 in), which, although excellent by industry standard, was not the 0.0254 mm (0.001 in) precision desired for the casings. The specific metal used for these prints was AlSi10Mg, an aluminum alloy similar to most 3000 series Al alloys, with a 186 MPa (27 ksi) yield stress, and the ability to easily withstand the maximum compressor wall temperatures of 167°C. Though no specific glass transition temperature was listed, typical 3000 series aluminum

alloys have a melting temperature above 625°C [17], and have no concerns operating below ~170°C (332.6°F) for prolonged periods.

Two casings were manufactured with this method; the first casing, shown in Fig. 3.16 was manufactured with the Outer Diameter (OD) slightly larger than the specified tolerance and so would not fit into the outer casing. The second casing made was the only one experimentally tested, and it was post-machined immediately after production to be exactly 0.287782 m (11.330 in) in Inner Diameter (ID), thus it was excluded from the sensitivity study.

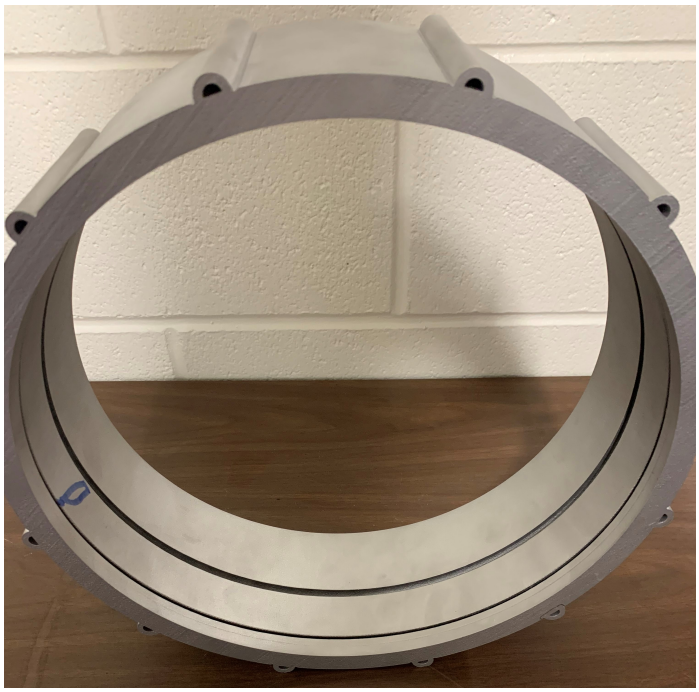

Figure 3.16. Aluminum DMLM Casing

Again, a close view of the inlet is shown in Fig. 3.17, this time for the DMLM casing. Comparing to the print quality of the polycarbonate inlets in Fig. 3.15, the aluminum casings were smoother, and did not contain small extraneous extrusions such as the polycarbonate inlets. Overall the print quality of the aluminum casing was higher than the polycarbonate casings, but not vastly so.

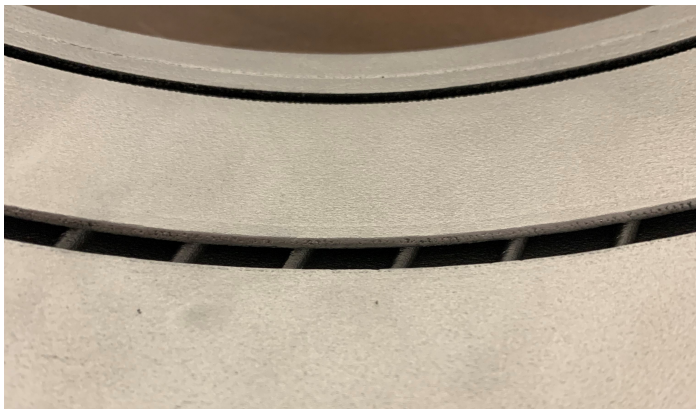

Figure 3.17. Aluminum Casing Inlet Depiction

3.2.3 Sensitivity Study

A sensitivity study was completed to assess the printing fidelity of each of the casings. ID, and OD measurements were taken around the casings to provide insight into manufacturing tolerances. Table 3.2 summarized this below, showing both the ID and OD casing measurements, and providing the standard deviation of the diameters based on manufacturing method. The diameter averages were comprised of 4 separate measurements of each casing (ID and OD each). The casings were also each subject to the average of two roughness tests, carried out with a Mitutoyo Portable Surface Roughness Tester.

Table 3.2. Casing Sensitivity Study Table

Casing type	Spec. ID (m)	Measured ID (m)	σ (mm)	Error (%)	Ra (μm)
Polycarb. IP	0.287782	0.287856	0.6452	$5.45e^{-4}$	16.74
Polycarb. NACA	0.287782	0.287734	0.4191	$1.13e^{-3}$	16.91
DMLM NACA	0.287020	0.287035	0.1397	$1.55e^{-3}$	13.52

3.3 Summary

There was ultimately an unsolvable deficiency with the polycarbonate casing with its inability to withstand elevated temperatures, preventing running with the polycarbonate casing at 90% rotor speed. Apart from that, the polycarbonate casing was satisfactory in all other

aspects. They were easily manufactured, inexpensive, and were produced with acceptable tolerance and roughness. Each print took 24-30 hours but an entire casing could be made at once.

The aluminum casing, in addition to having slightly better manufacturing tolerances than polycarbonate, could easily withstand the elevated compressor temperatures, making it the ideal case for testing. The one drawback of the casing was the long lead time. From design submission to completion, the aluminum DMLM casing took upwards of 8 weeks. This method for manufacture was preferred, but only recommended for future test if the test group allows sufficient manufacture time.

Below is a list of key summary points from the design and manufacture of the casings:

- The exit angle of the treatments were made to meet the casing at a 45° angle from axial for construction integrity, this should look to be minimized in the future with aluminum casings
- Differing inlet angles of treatments should be explored, the current study used a forward-angling inlet to capture more flow, but other studies have used directly radial or even downstream-angled passage inlets
- The NACA casing blades were offset 30° from the axial direction, however this proved to be too little and the blades still experienced large separation bubbles in computational simulation. As steeper angles are used, the manufacturing considerations of maintaining casing integrity must be integrated
- The internal passages were intentionally sized as large as possible. Future studies should seek to refine the passage size (almost certainly smaller) to optimize the trade-off between efficiency retention and SM improvement

CHAPTER 4:
Computational Modeling

The computational geometry creation involved 4 separate undertakings: The Rotor Only RO domain, the IP domain, the **NACA!** (**NACA!**) domain, and the IGV domain. The objective was to create a fluid volume representative of the flowpath of air through the TCR for each casing tested (Smooth, IP, and NACA). This was accomplished through the use of periodic surfaces to model only a section of the TCR but obtain computational results for the entire rig. The same process was done for each of the treatments, as well as the IGV domain, in accordance with the method laid out by Jones and Holmes [5], [8]. The NACA and IP cases were created by attaching the treatment fluid path to the rotor fluid path, and carving out contact surfaces between the two volumes. This is detailed further for each individual fluid domain.

4.1 Computational Geometry Creation

4.1.1 Rotor

The rotor gas path geometry was directly taken from Meinster [7], and represents the domain covered in Fig. 1.5. The geometry used can be seen in Fig. 4.1, which is the path of air around one blade of the NPSMF, or one 18° slice of the full rotor. This model used a 0.381 mm (0.0015 in) rotor tip gap for the space between the tip of the blade in the domain and the highlighted outer surface of the casing in Fig. 4.1. The casing treatments sat atop the rotor gas path in Fig. 4.1.

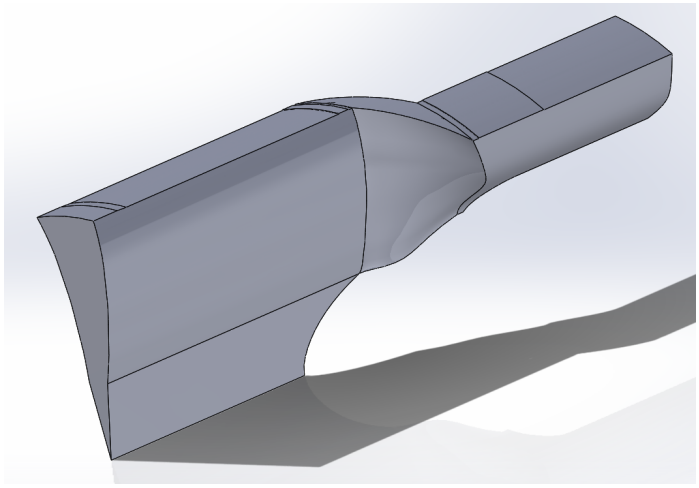

Figure 4.1. Rotor Only Domain

4.1.2 Internal Passage Fluid Domain

The IP fluid domain was created by largely the same method as Jones [5], whereby first, a large extrusion was mated with the IP casing in SOLIDWORKS. The cavity tool was then used to obtain just the geometry of the individual passages. The passages are shown in Fig. 4.3. Following this, a thin annulus then needed to be created as an interface. This annulus served as a sliding layer between the rotating domain of the rotor, and the stationary domain of the treatment. The passages with the attached annuli are shown in Fig. 4.4, as well as their profile in Fig. 4.5. In keeping with Jones's method, the sliding layer was sized to be less than 50% the thickness of the distance between the rotor tip and the casing wall 0.0381 mm (0.015 in). The thickness of the annulus was set at 0.0254 mm (0.001 in).

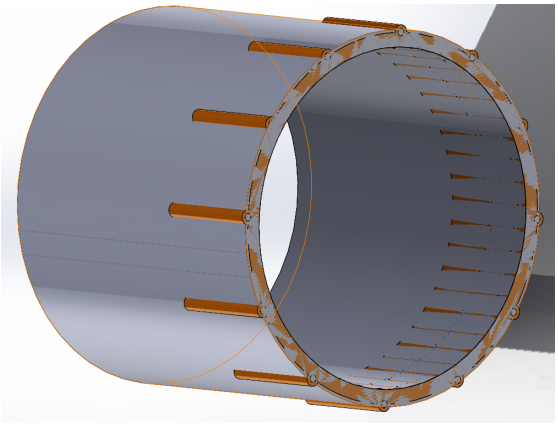

Figure 4.2. IP Casing Passage Geometry Extraction

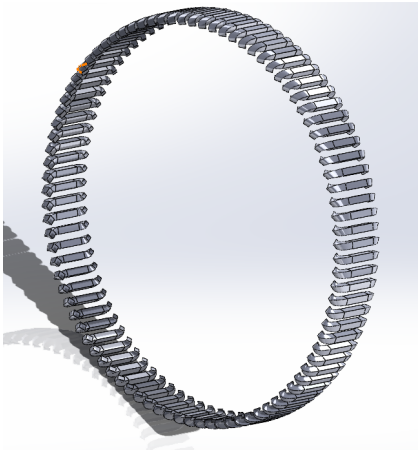

Figure 4.3. 89 Extracted Internal Passages

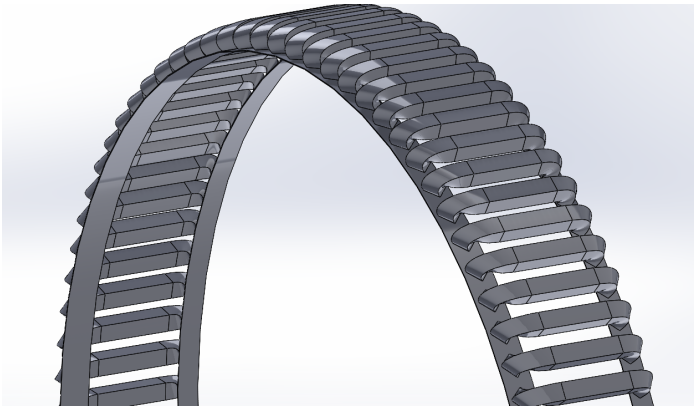

Figure 4.4. IP Passages with Annulus

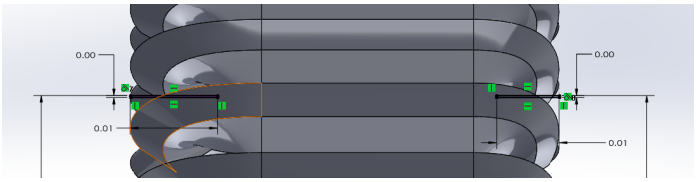

Figure 4.5. IP Annulus Profiles

Since there was no radial overlap between treatment passages, a straight cut was used to section off 13 of 89 passages in an 52.74° slice, shown in Fig. 4.6. This allowed the creation of a periodic surface on either side of the annulus, and for the entire casing treatment ring to be modeled with just the 52.74° section.

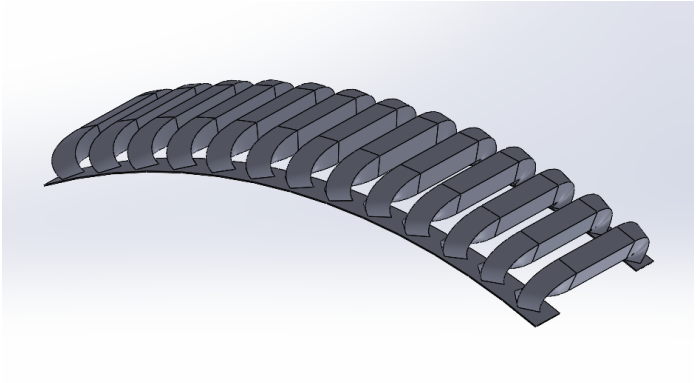

Figure 4.6. IP Treatment Slice

The IP passage then needed to be mated to the rotor domain, and again the cavity tool was used to carve out the annulus from the rotor domain after mating the two together. The full domain is shown in Fig. 4.7, with the rotor and the treatment kept as two separate solids. This was crucial for each case as it allowed the treatment to remain stationary but the rotor domain to be rotating.

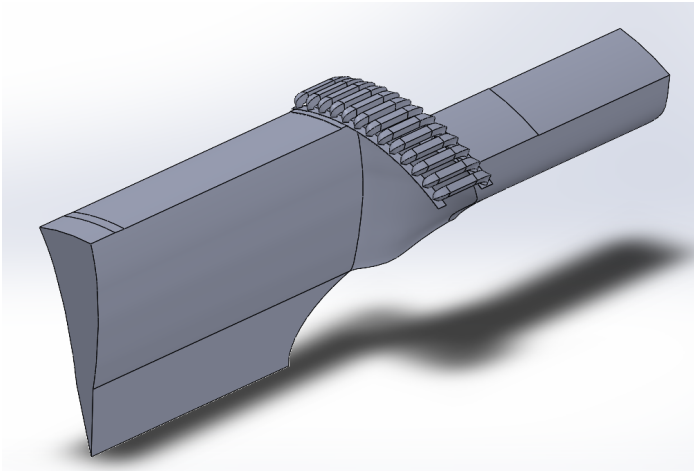

Figure 4.7. IP Domain

4.1.3 NACA Fluid Domain

The same method as above was used to extract the treatment fluid volume for the NACA casing. The entire treatment ring can be seen in Fig. 4.8. However, importantly, the NACA

casing was not radially symmetric (or very close like the IP casing) and so a simple straight slice of the treatment fluid volume would not suffice for the CFD geometry. To remedy this, a helix was used, using the lead angle equation

$$\tan(\alpha) = \frac{P}{\pi D} \tag{4.1}$$

to calculate the helix pitch. Equation 4.1 was used specifically to match the 30° airfoil deflection, with α_h being the helix pitch angle, D the casing diameter and P the pitch of the helix, in inches. This yielded a 1.651 m (65 in) pitch for the helix, allowing the cut to be made exactly between the airfoil supports and a perfectly periodic surface to be created. This resulted in the geometry in Fig. 4.9.

Figure 4.8. NACA Treatment Fluid Volume

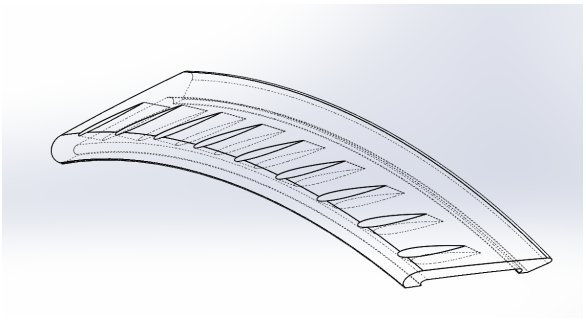

Figure 4.9. NACA Treatment Fluid Volume 54°Slice

The annuluses were added, and as in the IP case, the NACA treatment was mated to the rotor domain. The interface was then created by using the cavity tool. A depiction of the final NACA geometry is shown in Fig. 4.10.

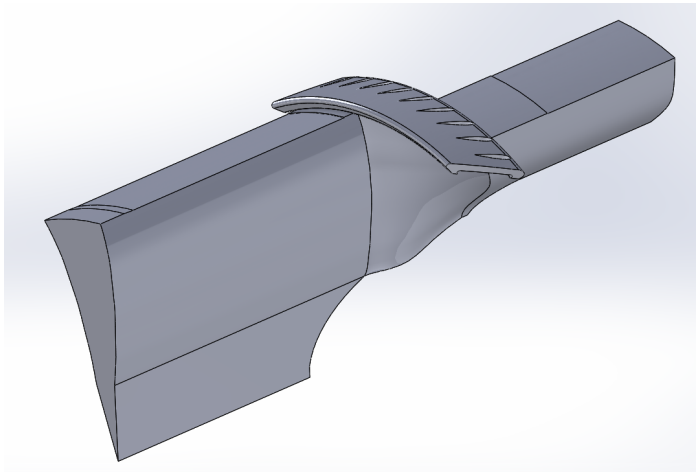

Figure 4.10. NACA Fluid Domain

4.1.4 IGV Fluid Domain

The IGV domain creation was inspired by the methods of Holmes and Meinster [7], [8]. The impetus behind its creation was to more accurately model and predict the effects of casing treatments on the NPSMF. Without the IGV modeled, a simple linear estimation was used to induce pre-whirl into the flow of the rotor, based on the measured exit angle of the IGVs at different rotor speeds [5]. Fully modeling the IGVs in ANSYS CFX would allow comparison with the whirl estimation method. Specifically this would allow the measurement of the effect of stagnation pressure drop created by the IGVs. This could not be modeled with the pre-whirl method, and ideally the fully modeled IGV would yield results more similar to that of the observed results in the TCR.

As Holmes had previously created an IGV domain for a 100% rotor speed case, his method was primarily used, with Meinster's providing a reliable way to extract a fluid volume that sat neatly between two of the IGV blades, thus creating as perfect of a periodic boundary as possible. This was used to help create the IGV domain for the 90% case. It should be noted that unlike the treatments above, a boundary with the exact shape of the IGV blades was unable to be created, but was rather closely approximated by the steps below:

The first step for the creation of the domain was to obtain an IGV blade model and copy both of the airfoil sections 1/17 (~21.18°) of the way around the central axis of the TCR. Next, five lines were drawn between the same spots on the airfoils, both on top and bottom;

splines were then drawn to connect the midpoints of these lines. These steps are represented in Fig. 4.11 as the first part of the IGV creation.

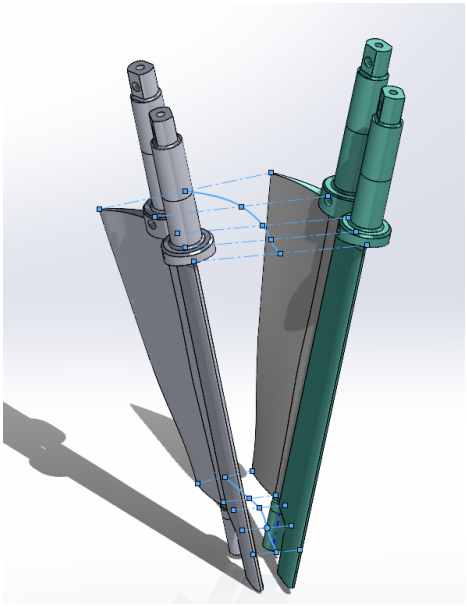

Figure 4.11. IGV Flow Domain Creation Step 1

The second step in the creation process created a lofted surface from the two splines, this created a surface that was nearly radially mid-plane (i.e. perfectly) between the two IGV blades. This surface is shown in Fig. 4.12.

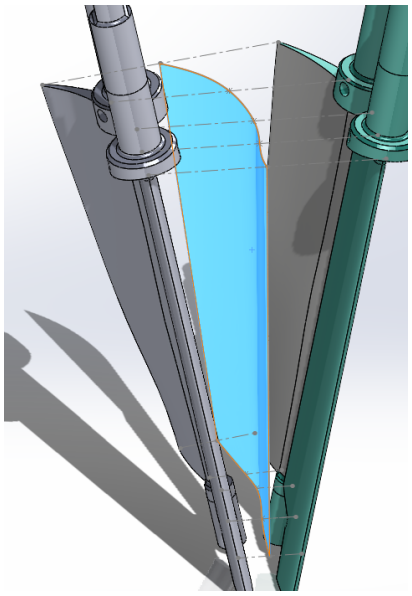

Figure 4.12. IGV Flow Domain Creation Step 2

To create the entire IGV domain, the surface created above in Fig. 4.13 needed to be extended both upstream, downstream to the rotor, and both radially inwards and outwards to the hub and the IGV casing wall. The first extrusion was completed between one corner of the previously lofted surface and the centerline of the TCR, shown in Fig. 4.13. This surface, and its extrusion to meet the centerline of the rig, was the seed surface for creating a periodic boundary which would successfully mesh in ANSYS CFX.

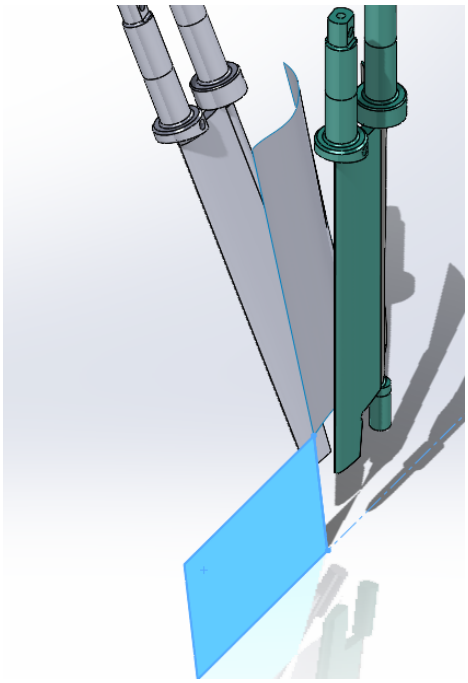

Figure 4.13. IGV Flow Domain Creation Step 3

The fourth step in the IGV domain construction was to extend the previous surface radially outwards, and downstream, using the edges of the first lofted surface as the extrusion path. A vertical extruded section was then added to ensure the surface had enough height to intersect the outer IGV casing, allowing a proper cavity of the casing housing of the IGV to be cut into the domain. The full amalgamation of these surfaces is shown in Fig. 4.14. These surfaces were then stitched together to form one surface; the stitched surface was then copied over 1/17 of a full circle in angle, creating the two surfaces shown in Fig. 4.15. These two surfaces bounded one of the IGV blades.

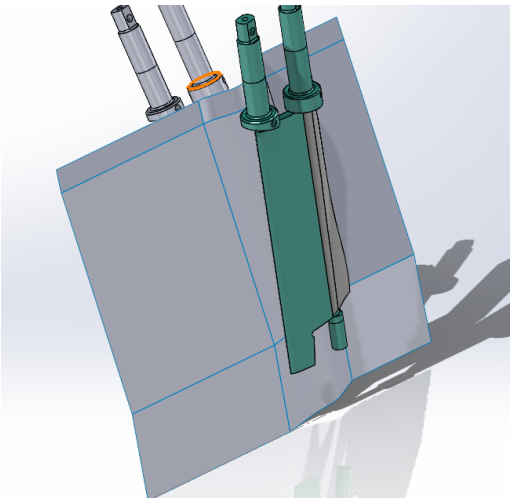

Figure 4.14. IGV Flow Domain Creation Step 4

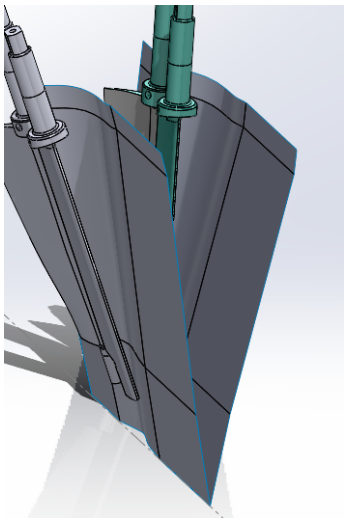

Figure 4.15. IGV Flow Domain Creation Step 5

These surfaces were then trimmed to create vertical upstream and downstream faces. This was completed using a separate extruded surface, seen in Fig. 4.16. With this complete, a lofted volume was then created using the two surfaces. Guide curves concentric with the central axis were created between the surfaces as shown in Fig. 4.17. The volume created is directly beside in Fig. 4.18.

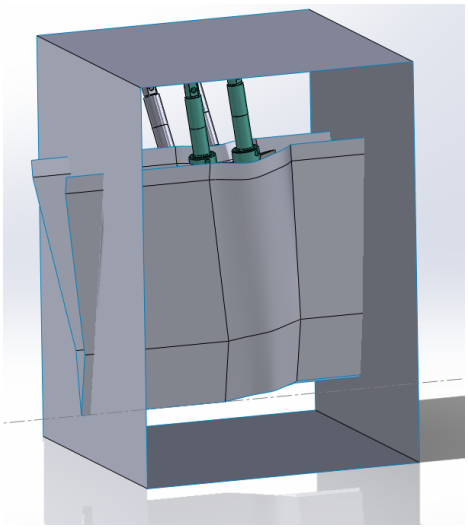

Figure 4.16. IGV Flow Domain Creation Step 6

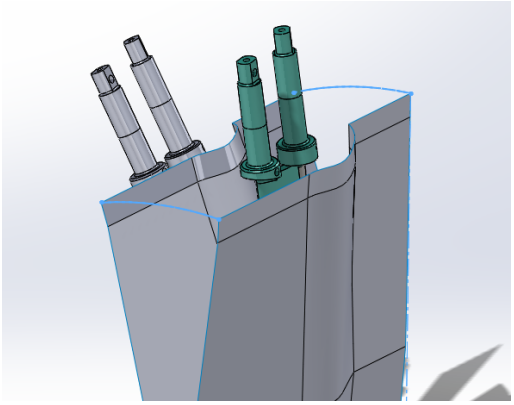

Figure 4.17. IGV Flow Domain Creation Step 7

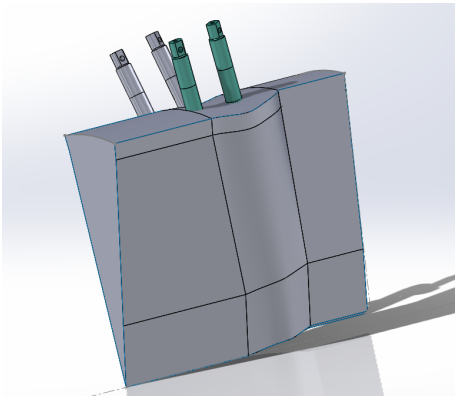

Figure 4.18. IGV Creation Step 8

To obtain the IGV blade shape within the volume, the created loft needed to be mated to the IGV assembly, this is shown in Fig. 2.3. Once again, the cavity tool was used to extract the blade shape and casing wall shape from the IGV fluid volume. After this tool was used, the volume in Fig. 4.20 was yielded.

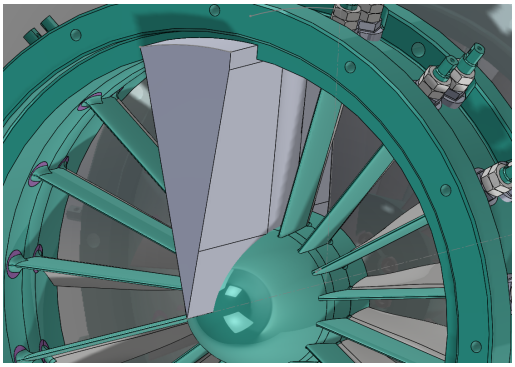

Figure 4.19. IGV Flow Domain Creation Step 9

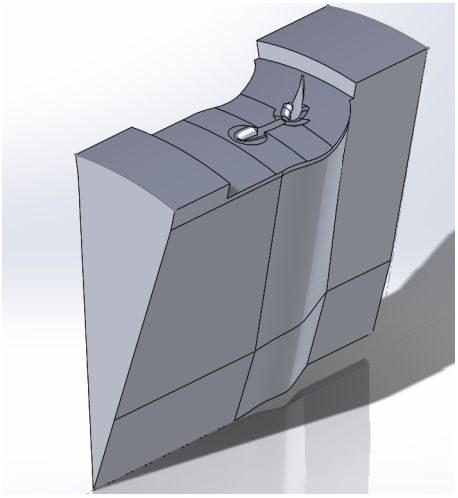

Figure 4.20. IGV Flow Domain Creation Step 10

The final step was to clean the extraneous extrusions from the IGV domain, including cutting an ellipse to approximate the central hub. Additionally, the downstream end of the domain was cut to yield an inner radius to match that of the rotor domain, so a contact

surface between the two could be created without issue. The outer radii of the rotor and IGV domain were already equivalent due to the IGV assembly casing wall being included in the cavity feature for the domain. The final IGV domain is shown in Fig. 4.21 for the 90% rotor speed schedule.

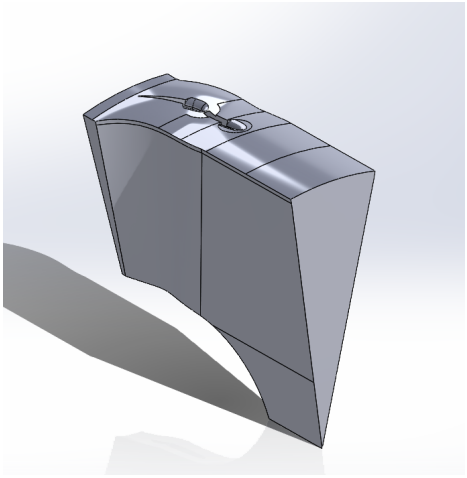

Figure 4.21. IGV Flow Domain Creation Step 11

The IGV and rotor domain were then joined, though still kept as two separate solid bodies, as the rotor necessitated a rotating domain, and the IGV a stationary domain. The final assembly is shown in Fig. 4.22. This full domain will subsequently be referred to as 'the IGV domain' in analysis, indicating that it was the only computational simulation to directly model the IGV blade geometry. The simulations which used whirl to approximate the effect of the IGVs will be referred to as the 'Whirl' simulations.

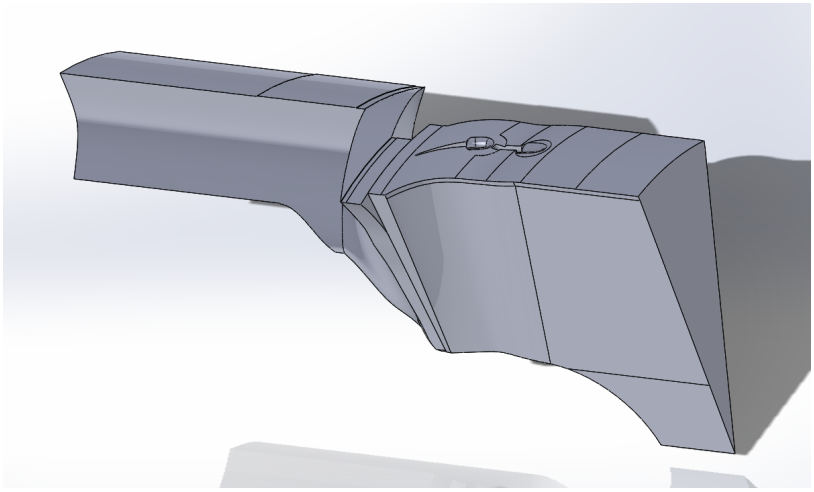

Figure 4.22. Full IGV Flow Domain (With Rotor)

4.2 Mesh Generation

The meshes were generated similarly using the ANSYS CFX commercial meshing software. The goal of the mesh generation process was to create a structure of elements which would provide accurate results, free from effects dependent on specific mesh elements. This is commonly called mesh independence, and was the focus of chapter 5. The figures following represent the final meshes used for the study, ranging between 21 million elements for the rotor only case, to 53 million elements for the IGV with NACA treatment case. All of these domains were meshed using a tetrahedron patch conforming method, and all cases used the same rotor only mesh for the specific rotor domain. Most of the bulk mesh was comprised of tetrahedral elements, and most of the inflation layers used to capture boundary layers used wedge, rectangular or pyramidal elements. There are many ways to evaluate the quality of a given mesh, and these parameters are evaluated further in the chapter 5 refinement study. The definitions of the main parameters are summarized below from ANSYS's meshing guide [18]:

1. Mesh Element Quality: A General measure of the quality of the elements based on the ratio of volume to the sum of the squares of the ledge lengths. It ranges between 0-1, with elements under 0.25 being considered poor
2. Mesh Skewness: The difference between the shape of a mesh cell and that of an equilateral triangle of equivalent volume. The Skewness becomes very high when

vertex angles of elements vastly differ from 60°

3. Mesh Aspect Ratio: A measure of the stretching of a mesh cell, generally > 5:1 ratios are avoided for non-inflation cells (bulk flow)
4. Mesh Edge Length Ratio: Length of the longest element edge to the shortest in the mesh, preferable to not exceed 5 for non-inflation elements
5. Mesh Element Volume Ratio: Volume of smallest element over that of the largest element
6. y+: A non dimensional measure of the grid height adjacent to a wall (to the center of the first cell). This number must be kept near or below 1 if using a wall-resolved turbulence setting ($k - \omega$) to ensure capture of the laminar sublayer

All of these parameters except for y+ can be evaluated immediately after the creation of the mesh. However, the y+ value needs information such as the freestream velocity (u_∞), and as such cannot be calculated until after a simulation is run. Thus the satisfaction of y+<1 also depends on the flow conditions in addition to the mesh itself.

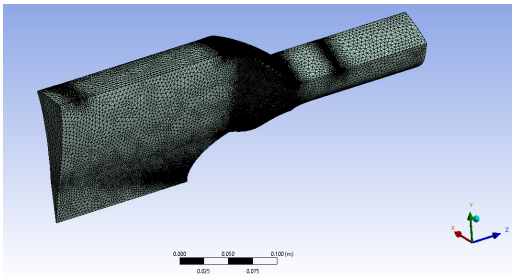

Figure 4.23. Rotor Only Mesh

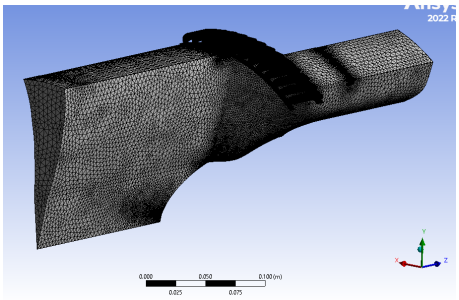

Figure 4.24. IP Case Mesh

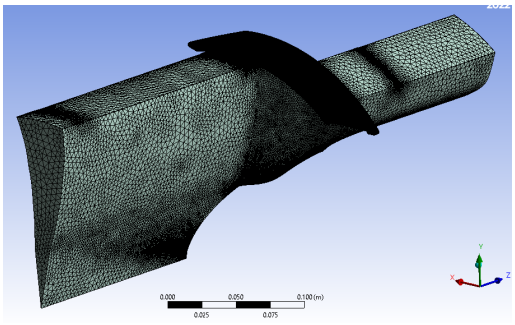

Figure 4.25. NACA Case

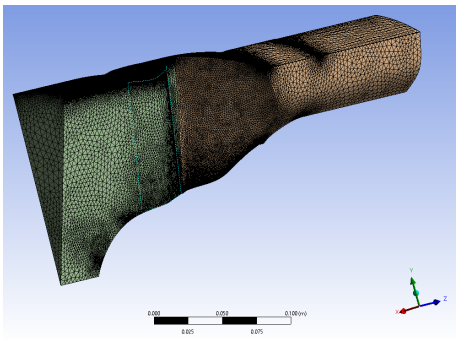

Figure 4.26. IGV Case

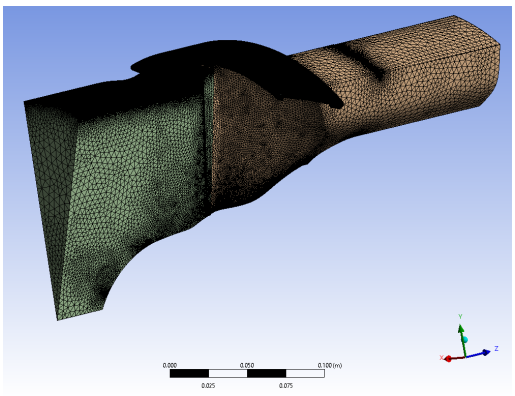

Figure 4.27. IGV+NACA Case

4.2.1 Areas of Importance

There were a few key areas of importance in the mesh for resolving flow features. These areas are simply a listing of locations of importance within the domain. The mesh methods used to capture the flow behavior, and the intended flow features being captured are further detailed in chapter 5.

- The rotor tip, and the area radially outwards to the wall of the casing
- The rotor blade leading and trailing edges (also IGV leading and trailing edges)
- Rotor-treatment domain contact surfaces (3 faces for inlet and 3 for exit)
- Any no-slip wall. This includes the casing outer walls, inner walls, and the blade itself
- Periodic boundaries. They must have the same mesh, (though not a mesh of any specific resolution) to allow proper simulation execution
- The treatment passage walls both in the NACA and IP treatments
- The IGV straight blade and flap in the IGV case

Depictions of these locations are below for visual reference. Fig. 4.28 contains an image of the blade tip, and the 0.0381 mm (0.0015 in) gap between the tip and the casing wall. Inflation layers can be seen bridging radially up from the blade and down from the wall, both of which were no-slip surfaces.

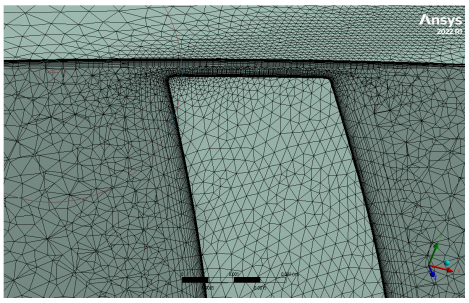

Figure 4.28. Blade tip mesh

A cross section of the blade in Figs. 4.29 and 4.30, allowing the inflation layers on the blade to be seen. These elements begin on the blade's surface with heights of $1e^{-6}$ m ($3.94e^{-5}$ in) and radiate outwards, increasing in height until reaching the size of the surrounding bulk mesh.

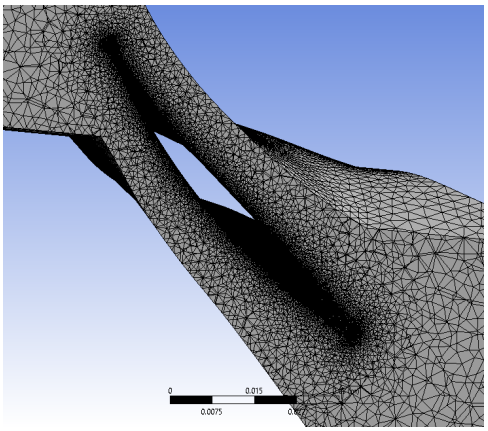

Figure 4.29. NPSMF Blade Profile Mesh

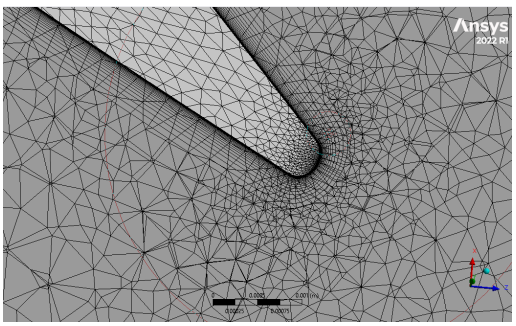

Figure 4.30. Trailing Edge of NPSMF Mesh

The outer wall of the casing needed the same inflation layers as the blade to be able to capture boundary layer growth. As mentioned, the growth of the boundary layer contributes significantly to compressor endwall stall situations, and so this was a key area of consideration. A cutaway from upstream of the rotor is shown in Fig. 4.31, showing the inflation layers.

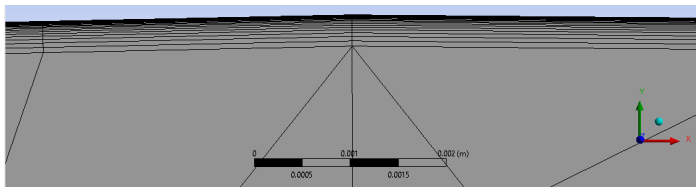

Figure 4.31. Outer Wall Mesh

Below is a comparison of the high and low periodic boundary meshes in Figs. 4.32 and 4.33. These were set as periodic surfaces using match controls, ensuring the meshes matched on either side.

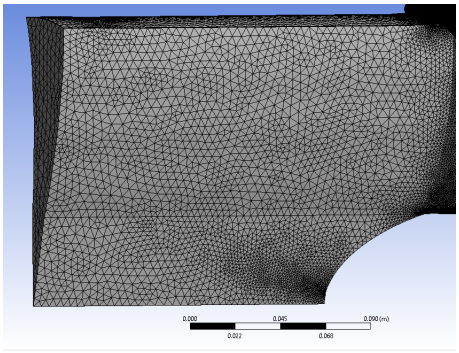

Figure 4.32. High Periodic Side Mesh

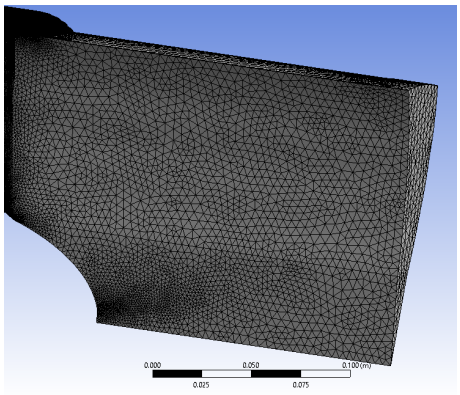

Figure 4.33. Low Periodic Side Mesh

The treatment passages themselves were a key area for the mesh, both for the inflation layers on the walls of the treatments, as well as the bulk mesh inside the passages. This area can be seen in the Fig. 4.34 as a cross section of both the IP treatment section of the IP mesh, as well as the NACA treatment section of the NACA mesh.

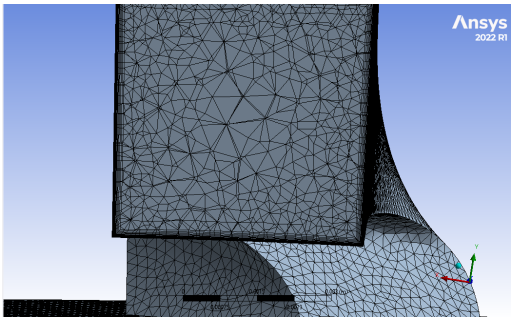

Figure 4.34. IP Passage Mesh

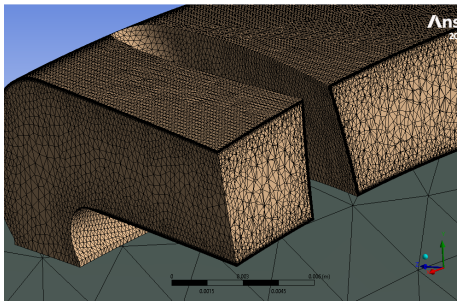

Figure 4.35. NACA Passage Mesh

Similar to the rotor blade profile inflation layers, there was a need for the same inflation layers on the IGV domain to capture both the effects of the IGVs on turning the flow, but more importantly the losses that came from their use. The boundary layer was key to accurately capturing the stagnation pressure loss cause by the IGVs, and in Fig. 4.37, the mesh surrounding the profile of the IGV blades is shown. The IGVs spanned the entire test section, so there was no need for any meshing in the blade tip-gap.

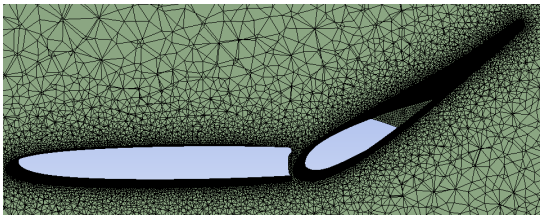

Figure 4.36. IGV Blade Profile Mesh

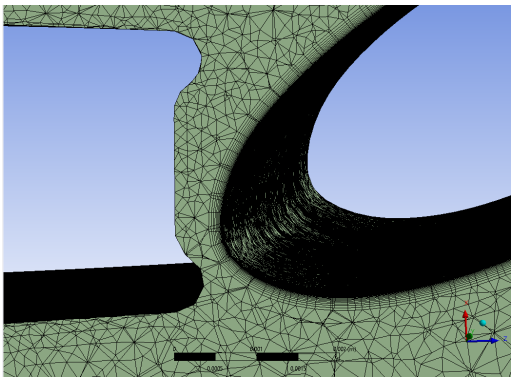

Figure 4.37. IGV Flap Leading Edge

4.3 Computational Setup

A depiction of the overall setup is outlined in Fig. 4.38 for the IGV+NACA, case it was the most complex and all-encompassing setup.

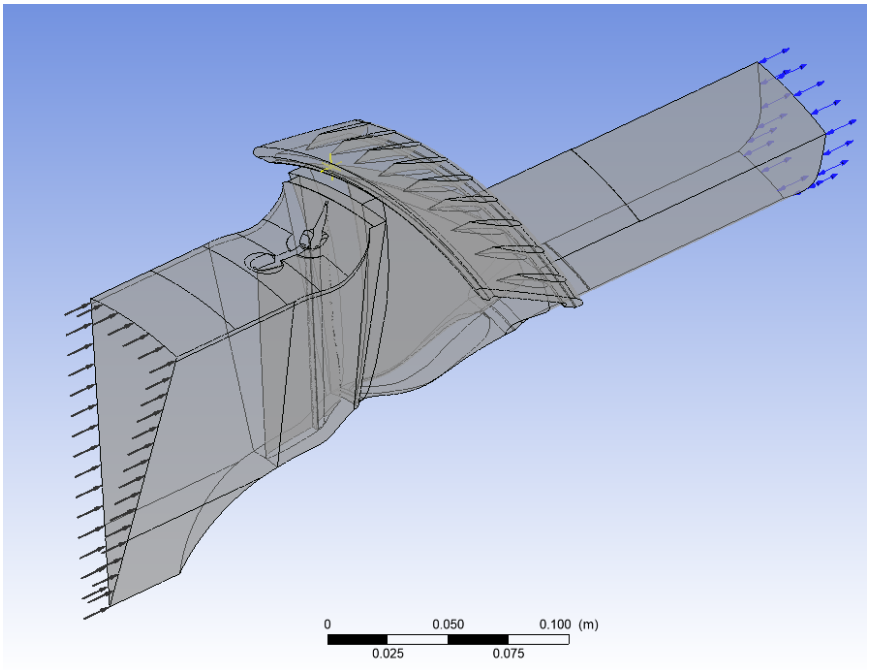

Figure 4.38. Full IGV Domain Setup

4.3.1 Physics

All of the simulations in this study used a steady-state analysis solver, however as described in subsection 4.3.3 this was used to vary parameters over iterations to obtain a pseudo-transient result, where an entire compressor speedline was able to be created.

The rotor domain was set to be a rotating fluid domain (rotating at the given case rotor speed), and the treatment domains and IGV domain were set as stationary. The Shear Stress Transport turbulence model was used with $\gamma - Re_\theta$ transitional turbulence also selected. The $\gamma - Re_\theta$ model has been specifically tuned to best capture flows around airfoils and turbomachinery blades.

The model was run for 300 iterations to obtain a steady-state solution at choke before the pseudo-transient program took effect. This number of iterations was determined by visually determining convergence of the residuals for a choke condition, and the agreement of those flow results with a solution taken to many thousands of iterations. Thus, convergence criteria were set to be extremely restrictive such that the program would run to the conclusion of the speedline, rather than being stopped by satisfied convergence criterion.

Lastly, one expert parameter was used. The number of maximum continuity loops used was 3 under convergence control. This allowed the momentum equation to be re-run thrice within each iteration along the speedline. This aided in making sure there were no transient effects of the speed at which the inlet pressure to the domain was changed (the metric used to move the simulation along a speedline).

These aspects of the simulation were coupled with adjusting the compressor back-pressure and inlet stagnation pressure. The back-pressure was held constant and the inlet pressure was adjusted as described in Section 4.3.3 to drive the compressor along a speedline. The rotor was deemed to be in stall when a disagreement of inlet and exit mass flows appeared.

4.3.2 Test Conditions

A concatenated version of the computational test table, Table 2.2, in Ch. 1, is shown below. Table 4.1 shows the 4 types of simulations conducted, each requiring its own mesh. Though the range of rotor speeds and whirl addition varied for each of these cases below, the meshes remained the same between computational runs.

Table 4.1. Final Mesh Sizes

Run Type	Final Mesh Size
Rotor Only	21 Million
IP	37 Million
NACA	39 Million
IGV	40 Million
NACA+IGV	53 Million

4.3.3 Boundary Conditions and Expressions

The Rotor Only, IP and NACA cases from Table 4.1 were all each run with and without inlet whirl applied. As the IGV actually physically modeled the inlet whirl, it was simply run with a 'no whirl' inlet condition. All outlets were specified as openings with a static pressure equal to 1 atm and set to be stationary.

The simulations encompassed both rotating and non-rotating domains. The fluid volume of the Rotor domain was set to rotating. A parameterized variable of `RevPerMin` was used to set the rotor speed. Thus, the NPSMF blade and Blisk were set to be rotating walls. To obtain the proper boundary layer, the outer and inner walls of the TCR were set to be counter-rotating walls with angular velocity equal to that of the rotor speed. The fluid volumes of the IGV domain and the treatment (IP & NACA) domains were set to be stationary. The outer and inner walls, as well as the IGV blades and treatment walls could be set as no-slip walls without issue.

Contact surfaces were applied to connect the treatment domain to the Rotor domain. The inlet and exit to the treatment had 3 faces each, labeled 1,2,3 and corresponding faces were labeled for the matching surfaces in the Rotor domain. The treatment inlet contact surfaces were downstream, and were labeled 'Aft' while the treatment exit surfaces were labeled 'Forward.' The surfaces are highlighted in Fig. 4.39.

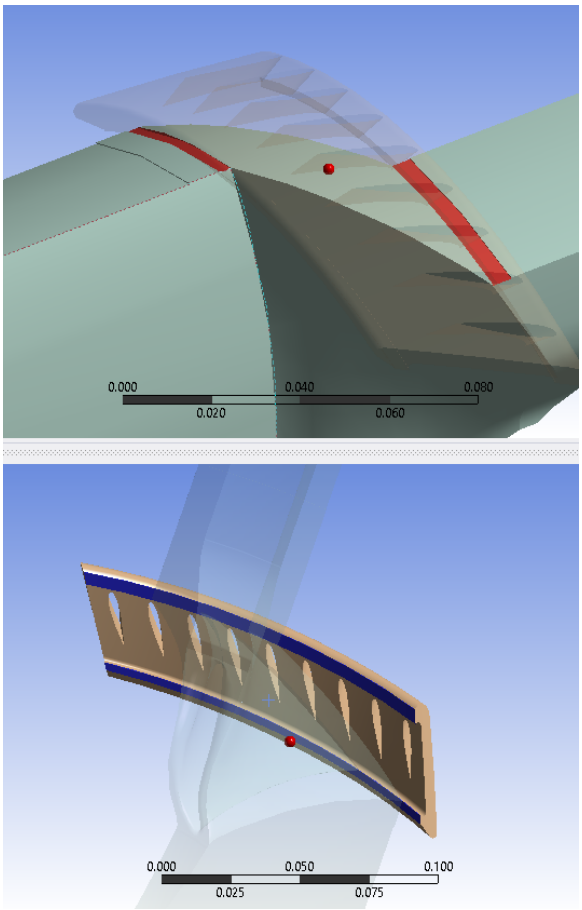

Figure 4.39. NACA/Rotor Domain Contact Surfaces

The expressions used for this study relied upon those developed by Jones [5] for use in his IP treatment study. This was expanded to be used both in the IP case for this study, the NACA case as well as the IGV case. The accomplishment of the pseudo-transient simulation relied upon the use of variable inlet pressures. The inlet stagnation pressure was controlled with the variable `RelPStagIn`, varying between the parameters `RelPStagInInitial`, and `RelPStagInFinal` to control the start and endpoints respectively along the compressor speedline. The desired iteration number was set by `nfinal` with n as the current iteration number. The length of the initial steady-state simulation was dictated by the variable `SteadyIteration`, set to 300. To depress the inlet stagnation pressure linearly during the simulation run, the logic governed by

$$\texttt{if}(n > \texttt{SteadyIteration}), \texttt{RelPStagIn} = \texttt{RelPStagInitial} + \frac{n - \texttt{SteadyIteration}}{\texttt{nfinal} - \texttt{SteadyIteration}} * (\texttt{RelPStagInFinal} - \texttt{RelPStagInInitial})$$
$$\texttt{else}, (\texttt{RelPStagIn}) = \texttt{RelPStagInInitial} \quad (4.2)$$

was used to calculate RelPStagIn. This logic expression allowed the total Δ of inlet pressures to be equally subdivided over $nfinal$ iterations. With nfinal−SteadyIteration => $3300 - 300$ => 3000 and ΔP = RelPStagInInitial − RelpStagInFinal = 30000 Pa, the inlet pressure variation was $30,000/3000 = 10$ Pa per time-step. Near stall, this proved to be a very large pressure jump per iteration and it is recommended that subsequent work be done to vary the pressure drop between iterations so as to provide higher resolution (smaller jumps) closer to stall.

The inlet boundary conditions varied depending on if the simulation was run as 'whirl' or 'no-whirl,' simulating the IGVs or not. The 'no-whirl' case was straightforward, simply setting the inlet velocity to 0 and the inlet pressure to the aforementioned RelPStagIn. The velocity for the 'whirl cases, however, was more complex. The ability to simulate whirl was governed by the expression

$$\sin(\texttt{MinFlapAngle} + \texttt{UnitRadius} * (\texttt{MaxFlapAngle} - \texttt{MinFlapAngle}))$$
$$\cos(\texttt{MinFlapAngle} + \texttt{UnitRadius} * (\texttt{MaxFlapAngle} - \texttt{MinFlapAngle})) \quad (4.3)$$

which linearly estimated the velocity of the flow coming from the trailing edge of the IGV. This method was developed by Jones [5], who estimated the whirl imparted by the IGVs by using the physical trailing edge angle of the IGV flaps. Since the IGV flaps only twisted radially, a linear estimation sufficed. SetAngle was used to set the angle of the simulated IGVs relative to the incoming flow. The rotor radius was non-dimentionalized into a unit length (UnitRadius) with MaxFlapAngle and MinFlapAngle serving as the tip and hub IGV flap angles respectively.

There were 6 key parameters monitored throughout the run, which are outlined in Table 4.2. Many of these monitors could be calculated directly from existing expressions, or taken as measurements from surfaces inside the casing, i.e. total pressure ratio π_t was simply the fraction $\frac{P_{T,Out}}{P_{T,In}}$. The mass flows were taken directly from their respective inlets/outlets. The stage efficiency η_{TT}, however, was calculated according to Eq. 4.4,

$$\eta_{TT} = \frac{\left(1 - \left(\frac{P_{T,Out}}{P_{T,In}}\right)^{\frac{\gamma-1}{\gamma}}\right)}{\left(1 - \frac{T_{T,Out}}{T_{T,In}}\right)} \tag{4.4}$$

following the laws of compressible aerodynamics.

Table 4.2. CFD Monitors

Monitor	Symbol
Pressure Ratio	π_t
Inlet Mass flow	$\dot{m}_{in}$
Exit Mass flow	$\dot{m}_{out}$
Treatment Inlet Mass flow	$\dot{m}_{tr,in}$
Treatment Exit Mass flow	$\dot{m}_{tr,out}$
Efficiency	η_{TT}

CHAPTER 5:
Mesh Refinement

5.1 Objectives

A mesh refinement study was conducted to assure the obtained computational results were mesh independent, and to pinpoint an ideal mesh size. A successful mesh refinement was defined by the largest mesh where subsequent refinement brought about minimal (~1%) changes in obtained pressure ratios and efficiencies. Further refinement of the mesh beyond the goal would lead only to diminishing returns of computational accuracy at the expense of vast computational time.

The case chosen for the refinement was the rotor only case with no whirl at 90% speed. The rotor only case was chosen as results could be compared with previous theses' mesh refinements. From Jones and Meinster [5], [7], an estimated best mesh size of ~20 million elements was targeted. Once the mesh parameters were finalized, the same parameters were used to mesh the treatment and IGV volumes. Table 5.1 illustrates the test matrix of meshes.

Table 5.1. Mesh Refinement Test Table

Mesh Size	Inflation Layers (Y/N)
800,000	N
7 Million	N
21 Million	Y
38 Million	Y

5.2 Method

A mesh was generated for the rotor-only case, and then refined until there was minimal change in the monitors (π_t, η_{TT}). This process began by varying the sizing parameters and inflation layers on faces of the computational domain to create 4 different meshes. Like Meinster, a mesh refinement goal table was created to show the varied mesh parameters.

Table 5.2 outlines the mesh parameters used and the aspect of mesh refinement for which they were used. As can be seen from the table, inflation layers were mainly used to capture boundary layer information, sizing was used to cleanly capture geometrical features and small radii, such as the blade leading and trailing edges. Patch conforming methods were also used to control the type of bulk mesh elements.

Table 5.2. Mesh Feature Table

Mesh Feature	Location(s)	Purpose(s)
Bulk Sizing	Rotor Domain Treatment Domain IGV Domain	General Flow Resolution
Match Control	Rotor Periodic Boundaries Treatment Periodic Boundaries IGV Periodic Boundaries	Computational Efficiency
Proximity Sizing Face Sizing	Rotor Blade Base Rotor Tip Rotor LE/TE Rotor Base Rotor Blisk/Hub IGV Blades Treatment Walls Rotor Base	Geometry Capture
Contact Surfaces	IGV to Rotor Domain Treatment Inlet to Rotor Domain Treatment Exit to Rotor Domain	Contact Mesh Generation
Inflation	IGV Blades Rotor Blades Rotor Domain Outer Wall IGV Domain Outer Wall Treatment Wall	Boundary Layer Resolution

A rotor speed of 90% was used, the maximum rotor speed case. This was done to put the most strain on satisfying having a y+ value under 1. As can be seen from equation 5.1,

$$y+ = y_p \frac{u_*}{\nu} \tag{5.1}$$

the freestream velocity grows, so does the associated wall shear stress, with it the friction velocity. As the freestream velocity grows, then, so too does the y+ value, thus the fastest rotor speed would create the 'worst case' y+. y_p is the distance from the wall to the centroid of the first cell, u_* is the friction velocity, and ν is the kinematic viscosity of the fluid [18]. Keeping the y+ value under 1 for all simulations in this study was key to resolving the laminar sublayer on the rotor blade and the outer wall of the TCR. The used Shear Stress Transport (SST) turbulence model combines $k-\epsilon$ for far field turbulence and $k-\omega$ for wall resolution. The SST model eliminates common sensitivity issues of the $k-\omega$ model in freestream conditions [18]. Though the program can operate with high y+ values (using $k-\epsilon$ at the wall as well) the model needs sufficient grid points within the laminar sublayer of the boundary layer on a surface to properly resolve the boundary layer, and associated wall shear stress forces. It does not necessitate a y+ value under 1, but results will not be representative of real phenomenon if this occurs.

These meshes were all run with no inlet whirl, and their π_t and η_{TT} were evaluated and plotted. A bracket of 1% variance was over-plotted with each run to determine whether it was sufficiently close to the next smallest mesh used. In addition, the y+ values were evaluated and a selection was made of the best rotor-only mesh for the study.

5.3 Results

Upon creation of the meshes in table 5.1, the quality of the mesh had to be evaluated and deemed satisfactory. The most common metric by which this was judged was element quality, along with the aspect ratio and orthogonality, as listed in section 4.2. An example is given below of the final mesh quality histograms in Figs. 5.1 and 5.2. These two plots depict the same thing, though Fig. 5.1 depicts categorization by element volume whereas Fig. 5.2 categorizes by element number. While the number of elements with poor quality is significant, their relative volume is extremely small. Nearly all of these poor-quality elements are also inflation layer elements, shown in green, which necessitate extremely small height rectangular elements. This vastly skews the average mesh quality down to ~0.35 for all the meshes containing inflation layers. Importantly, though, the vast majority of the volume of the fluid domain contains high-quality mesh elements (above 0.5) which satisfied criterion for a usable mesh.

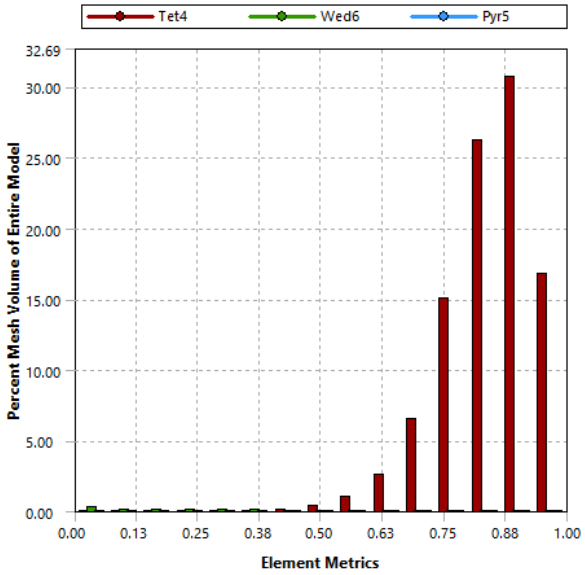

Figure 5.1. Mesh Quality Example, by Volume

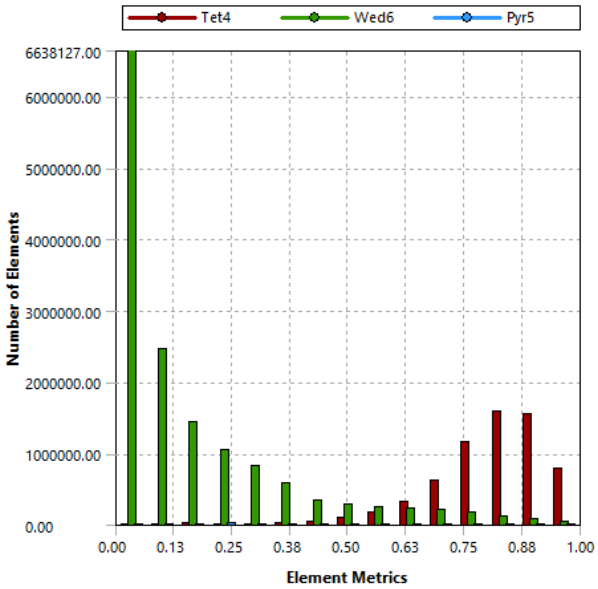

Figure 5.2. Mesh Quality Example, by Element Number

Table 5.3 illustrates the resultant parameters for this refinement. The most significant number was the y+ value, which was satisfactory for the 21 million element mesh and above. Lastly, the mesh data for one of the NACA runs is also shown for comparison. A check was done to make sure the y+ value for the flow through the casing treatment also satisfied the y+<1 criteria. The meshes that satisfied the criteria were the 7M, 21M, and 38M element meshes, and as such the 800,000 element mesh was discarded from consideration.

Table 5.3. Mesh Refinement Data

Mesh Count	Nodes	Edge Length Ratio	Vol. Ratio	Average y+ (Blade)
888,591	171,913	1/9.38451	1/158.338	185.7
7,190,314	1,340,563	1/170.29	1/4718.61	36.37
21,000,809	8,577,123	1/6715.63	1/423.23	0.4431
38,656,361	16,803,438	1/8165.46	1/577.401	0.4267
39,351,848	16,204,883	1/6723.33	1/12407.5	0.4547 @Blade, 0.5925 @Treatment

Finally, stall detection criteria had to be implemented to determine where along the speedline the rotor had stalled. Previous methods from Meinster [7] included observing a divergence from a linear decrease in efficiency. A newer method was developed since, to monitor the inlet and outlet mass flows, and when there was disagreement of the mass flows beyond 10% of the normal value for the run, the rotor was deemed to have stalled. An illustration of the mass flow divergence is shown in Fig. 5.3. The mass flows remained extremely steady through the majority of the run but became chaotic quickly, making stall point discernment relatively easy. The first significant rise above the nominal level was used to terminate the simulation, shown by the solid red line in Fig.5.3.

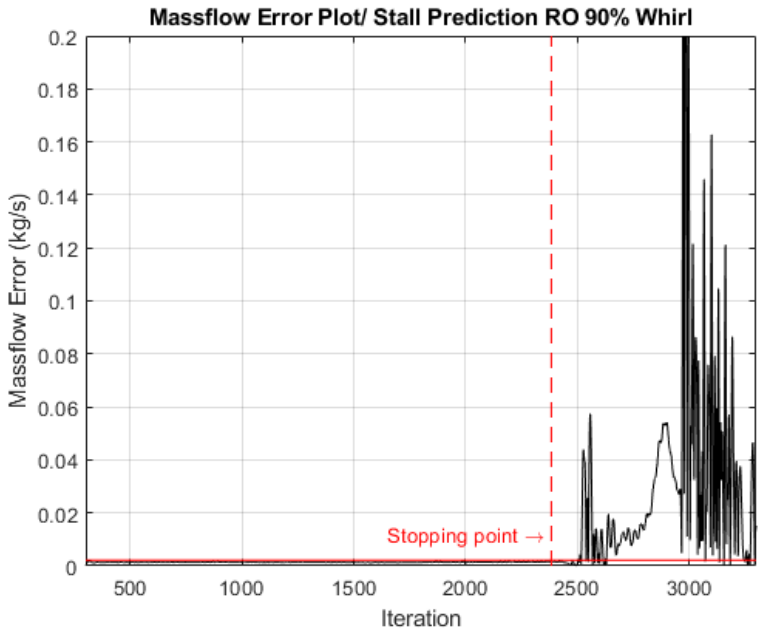

Figure 5.3. Mass flow Divergence Stall Prediction

This process was a significant improvement over the linear efficiency method, but still not foolproof. Since the simulation used inlet stagnation pressure to drive mass flow, the relationship between the iteration number and the mass flow was highly nonlinear. This meant that over 3000 used timesteps, each with a 10 Pa decrease, the final range of 2 kg/s (4.4 lbm/s) of mass flow near stall was covered by less than 100 iterations. Future work should look to incorporate a nonlinear scaling of the pressure step to reduce the inlet pressure jump between iterations the closer the compressor gets to stall.

A final method of determining stall was briefly evaluated after the completion of the study. This involved taking the rotational torque experienced by the blade and looking for sharp torque drops at the onset of stall. Fig. 5.4 depicts the torque monitoring for the 90% Whirl case of the rotor only, with points every 100 iterations. The resolution of the plot is thus compromised, being 100x coarser compared to the other speedlines. Still, the drop in torque is much more discernible than the divergence in mass flow of Fig. 5.3. This is the recommended method for stall prediction for future studies, and should be implemented into the setup with an expression calculating $torque\_z()@Blade$ and using the variable as a monitor point.

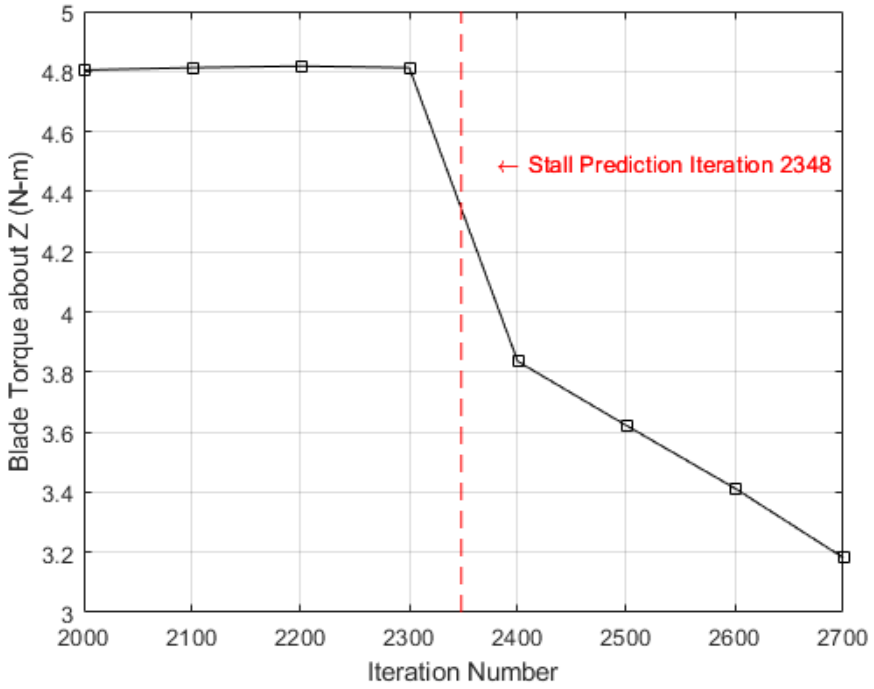

Figure 5.4. Torque Drop stall prediction

As can be seen in Figs. 5.5 and 5.6, the four rotor only meshes showed comparable values for their respective π_t and η_{TT}. The error-bar plotted for the 21M element (green) run shows a 1% deviation from its value, the goal being for the next-finer mesh to be within the error bars. The 38M (blue) line is within the acceptable error deviation, unlike the previous meshes when compared to their next-finer mesh. The 21 million element mesh was deemed acceptably refined, and used as the mesh for the rotor volume for all computational runs. The mesh sizing and parameters that were used for its creation were also used for respective features on both the IGV fluid volume and the treatment volumes.

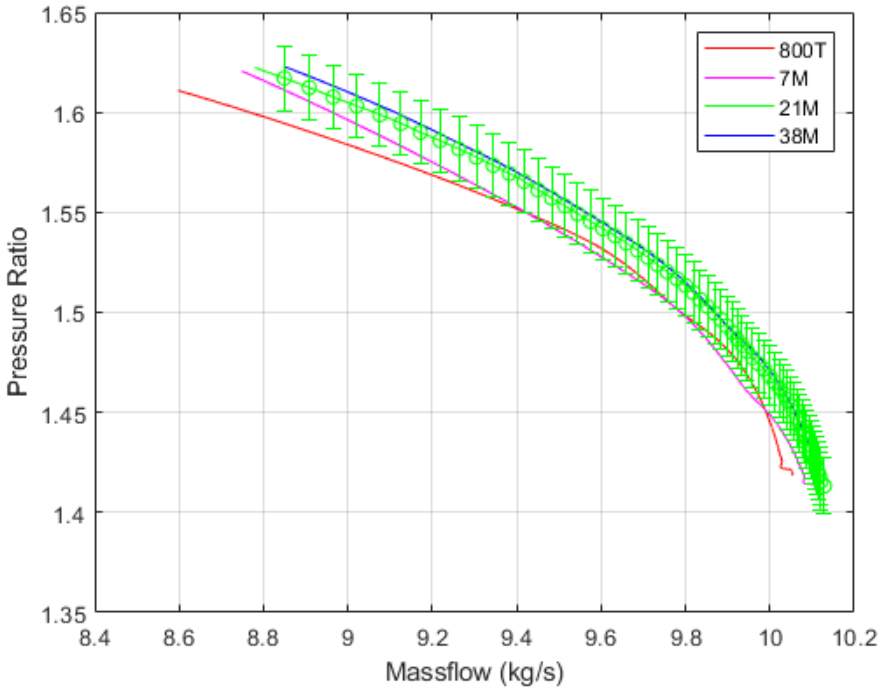

Figure 5.5. Mesh Refinement
Pressure Ratio

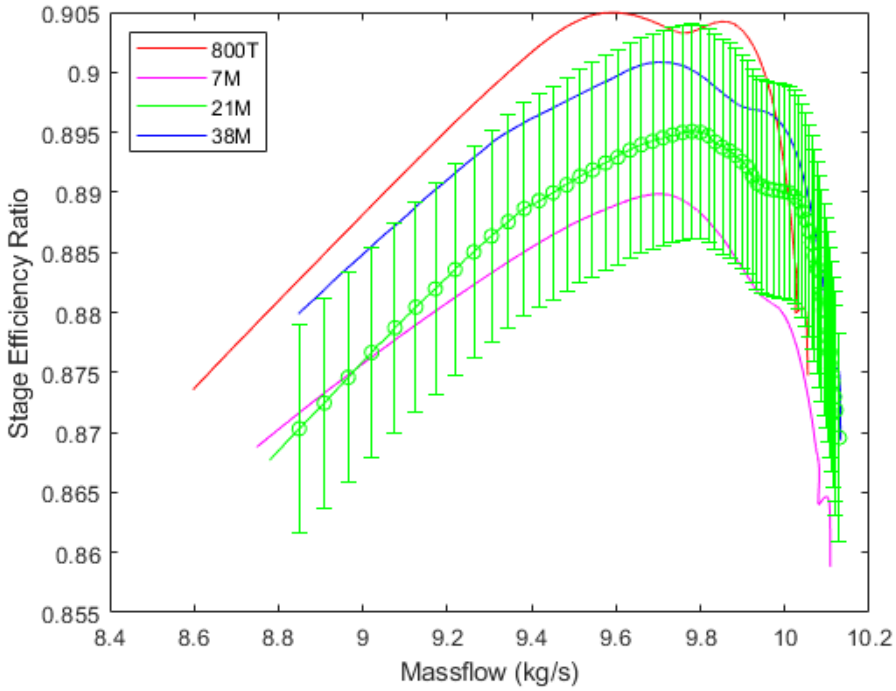

Figure 5.6. Mesh Refinement Efficiency

THIS PAGE INTENTIONALLY LEFT BLANK

CHAPTER 6:
Results

6.1 Computational Results

In total, there were 27 unique compressor speedlines computed for this study. These are broken into cases with inlet whirl, and those without. Those simulations with inlet whirl are shown in Figs. 6.2 and 6.1, below, and also include the IGV and NACA+IGV runs. Later figures highlight the specific differences caused by modeling the IGVs rather than using inlet whirl. Figures 6.4 and 6.3 show the speedlines computed for cases without inlet whirl. The main information sought from these speedlines is listed below:

- The effect of simulating whirl on the Pressure Ratio and Efficiency curves
- The predicted SM of each case
- The losses in π_t and η_{TT} incurred from each of the treatments
- The losses incurred from the IGV case when compared to the whirl approximation. (how unrepresentative of reality is simulating the whirl)
- Ensuring that the NACA+IGV case simulates a similar pressure drop to the NACA case, as the IGV case does to the Rotor Only case

Additionally, contours were collected of various regions aided in the analysis of the treatment flow effects. Contours were only obtained for the 90% rotor speed case as this was deemed the most important rotor speed to increase SM. The regions outlined below:

- A Mach contour of the blade profile at 95% blade span
- A pressure map of the suction side of the NPSMF blade at important points along the speedline
- A velocity vector plot near the inlets and outlets of the casing treatments to monitor the inlet/exit direction and speed of the recirculating flow
- A velocity vector plot throughout the entirety of the treatment to monitor amount and speed of the total recirculating mass flow

The Mach contour at 95% blade span was used to monitor where the normal shocks occurred

on the blade, and the flow characteristics near stall. The suction side of the blade plot was crucial in attempt to detect separated flow over the blade, and gain knowledge over the location of the shocks chord-wise on the blade. The treatment vector plots were both used to gain insight into the directional of the incoming and exiting flow, to help reshape the ducts for future endeavors. The duct re-shaping is both in the interest of efficiency (turning and separating the flow as little as possible) as well as controlling the direction of the exit flow to have a relative incidence angle of 0° to the rotor.

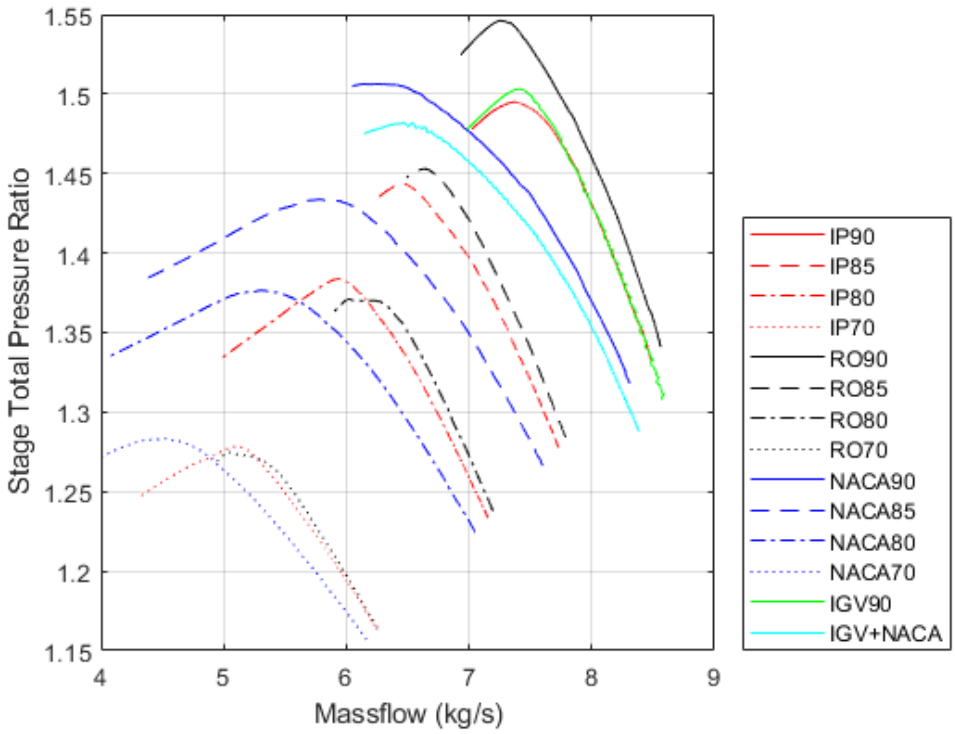

Figure 6.1. All Pressure Ratio Curves with Whirl (or modelled IGV)

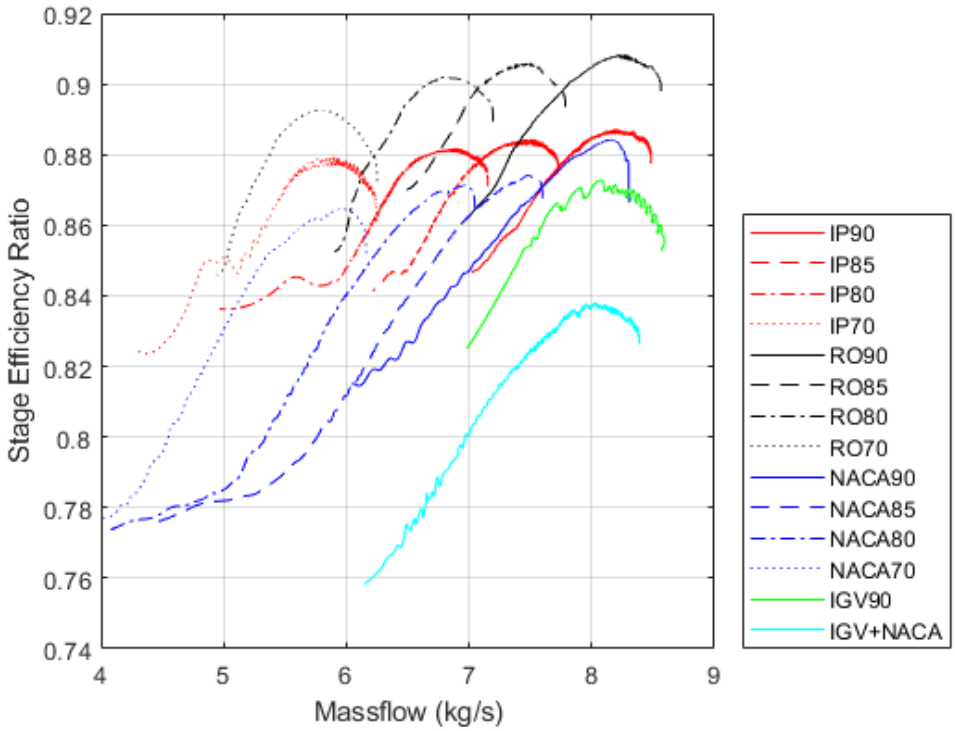

Figure 6.2. All Efficiency Curves with Whirl (or modelled IGV)

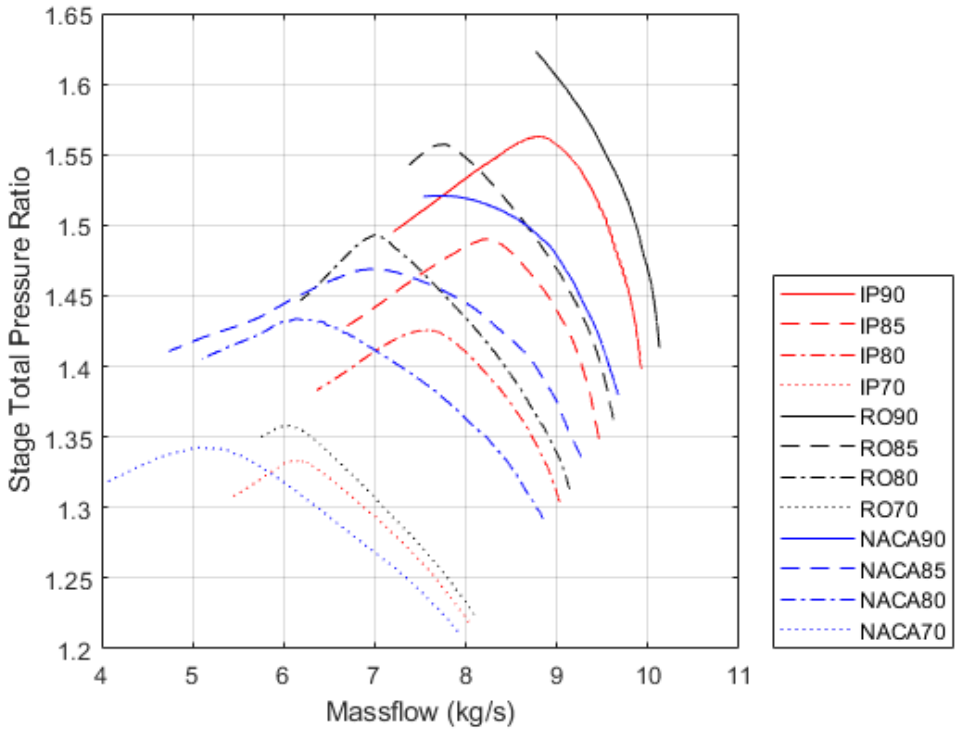

Figure 6.3. All Pressure Ratio Curves without Whirl

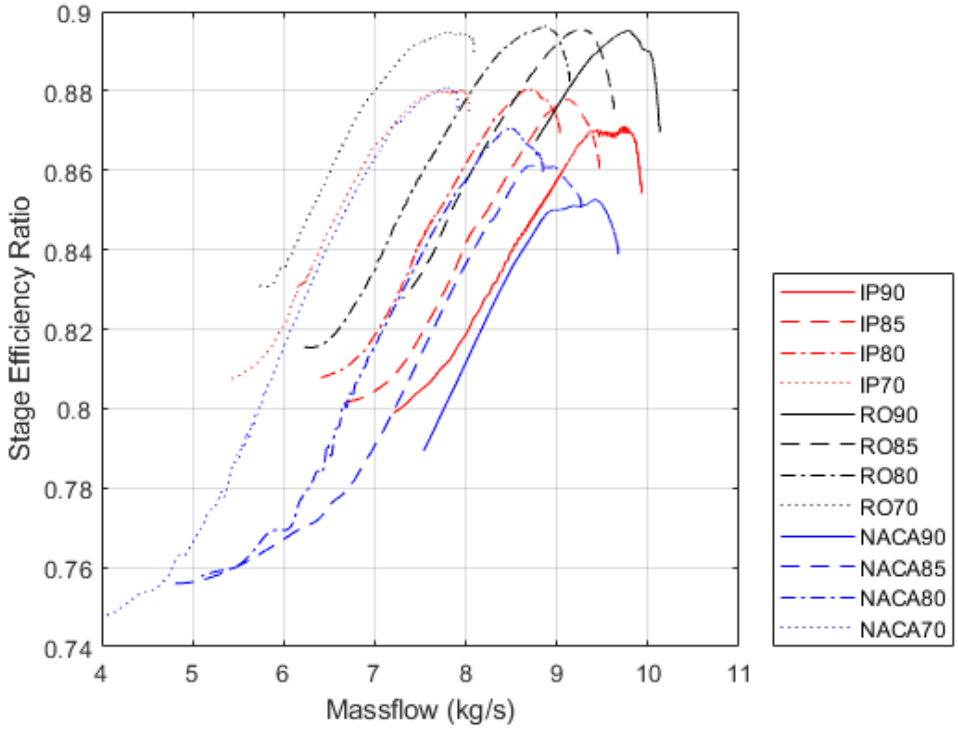

Figure 6.4. All Efficiency Curves without Whirl

Table 6.1 serves to illustrate the markers, line colors and their associated meanings for the results to follow. A test/ simulation having the IGV angles set, or having Whirl or No whirl is directly annotated for each plot.

Table 6.1. Plot Guide Table

Marker	Meaning
Smooth line (-)	90% Speed
Dashed line (–)	85% Speed
Dash/Dot line (-.)	80% Speed
Dotted line (..)	70% Speed
Black	Rotor Only/ Smooth
Red	Internal Passage
Blue	NACA
Green	IGV
Cyan	IGV+NACA
Circular Data Marker	Best Efficiency Point
Square Marker	Rotor Only/ Smooth Experimental Data
Triangular Marker	IP Experimental Data
Inverted Triangular Marker	NACA Experimental Data

6.1.1 Whirl Effect

The first effect to compare in the analysis of the computational results is the effect of adding whirl to the simulations. Figures 6.6 and 6.5 below detail the effect of whirl on the Rotor Only case. Regarding the compressor efficiency, adding whirl moves the efficiency curves up for the 90%, 85% and 80% rotor speed cases, and nearly uniformly shifts the lines to a lower mass flow. It also serves to increase the peak efficiency of the stages in addition to those peaks occurring at lower mass flows. This aligns with what the IGVs are intended to produce, which is a whirl that unloads the rotor (specifically the tip), and this unloading allows later compressor stages to not be choked by excessive mass flow when the compressor operates at less than 100% rotor speed. The peak efficiency jumps for no-whirl to whirl cases are shown in table 6.2.

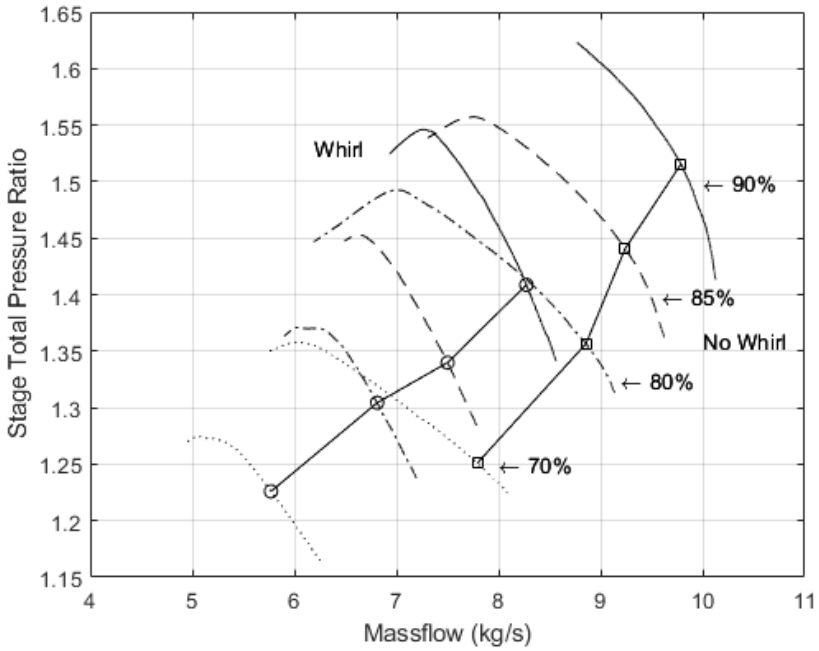

Figure 6.5. Comparison of Whirl/ No Whirl for Rotor Only, Pressure Ratio

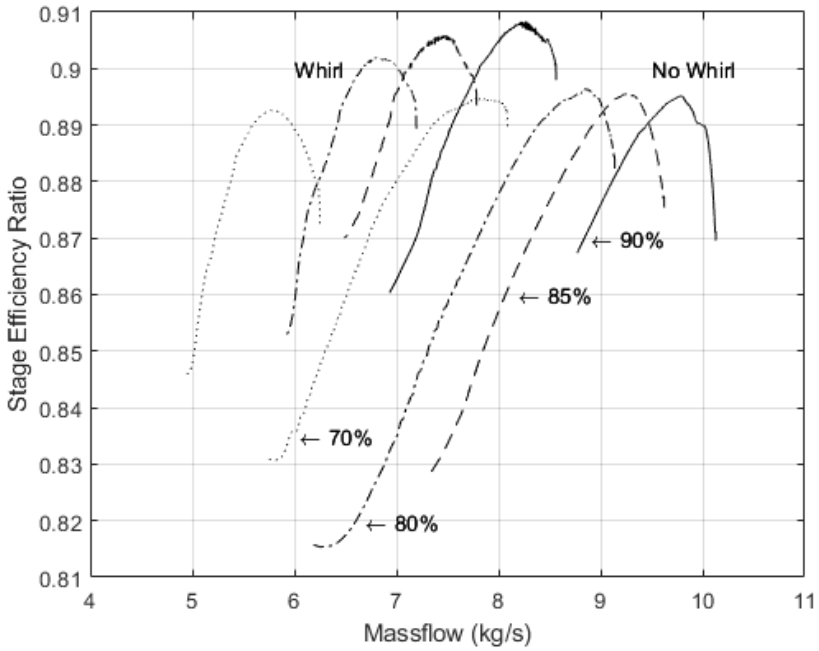

Figure 6.6. Comparison of Whirl/ No Whirl for Rotor Only, Efficiency

Table 6.2. Rotor Only No Whirl to Whirl Comparison

Case	$\Delta\pi_t$ (%)	$\Delta\eta_{TT}$ (%)	Δ SM (%)
90%	-4.74	1.47	55.9
85%	-6.70	1.17	-35.7
80%	-8.17	0.613	-55.7
70%	-4.41	-0.268	-46.1

As can be seen in the table, moderate efficiency increases of up to 1.47% were seen with the addition of whirl to the inlet flow. This though came with pressure losses on the order of single-digit percentage, as well as large double-digit stall margin decreases, other than the 90% case, which saw a large stall margin increase. Due to the simulation sensitivity, it is likely that the SM increase with the 90% Whirl case was likely an overproduction of real phenomena. These efficiency gains, while seemingly minor, are very important to the overall compressor efficiency if compounded over many stages, thus why most modern compressors do use IGVs to generate inlet whirl.

The pressure ratio plot shows the distinct decrease in peak pressure ratio for the Whirl cases. It also depicts the Best Efficiency Points (Best Efficiency Point (BEP)s), where the compressor would operate at an on-design condition, once again showing that the whirl cases have the compressor reach peak efficiency at much lower mass flows.

In Figs. 6.8 and 6.7 the effect of whirl on the NACA casings can be seen. These curves were used as a validation of the phenomenon seen in the Rotor Only case. Like 6.6, the NACA cases experienced an efficiency bump when adding whirl, and a pressure ratio loss, as well as operating at a lower mass flow.

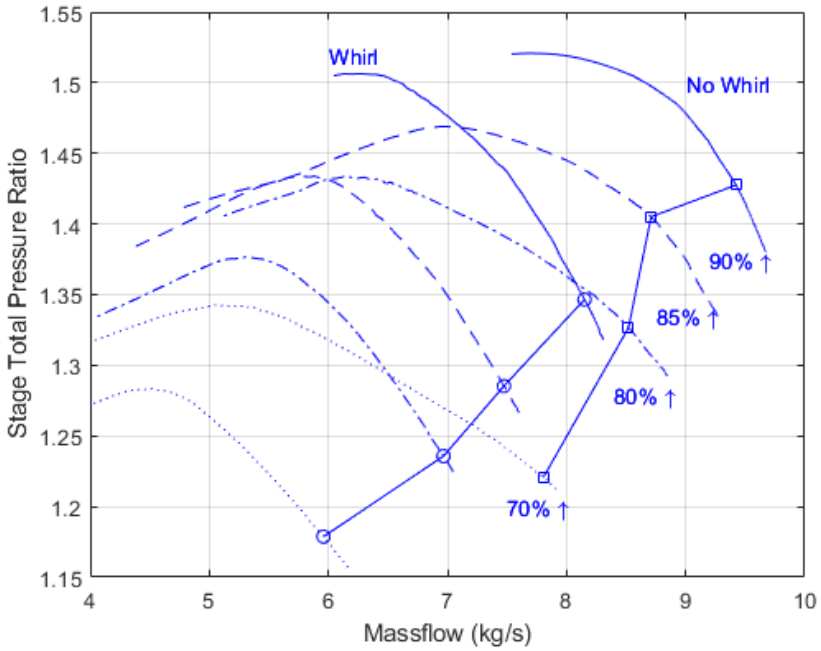

Figure 6.7. Comparison of Whirl/ No Whirl for NACA, Pressure Ratio

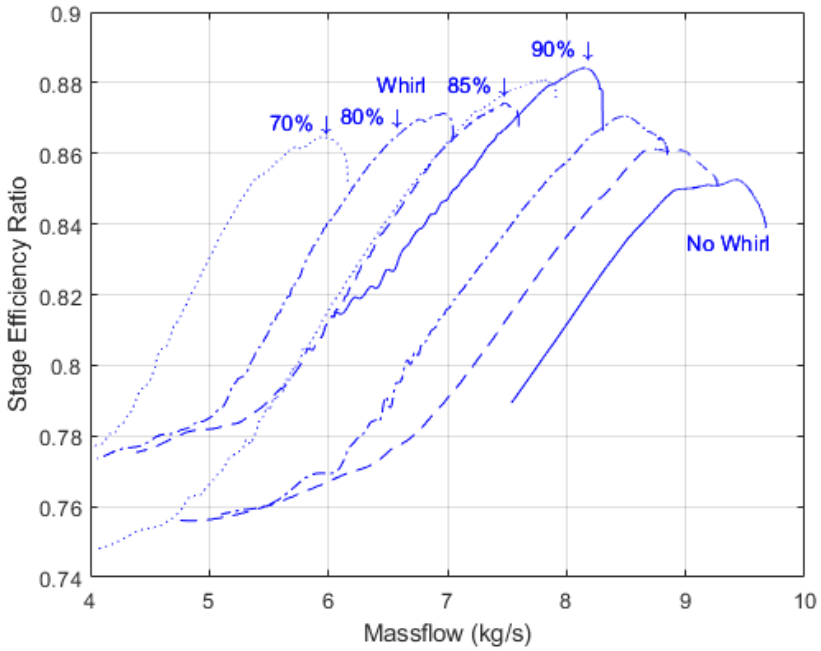

Figure 6.8. Comparison of Whirl/ No Whirl for NACA, Efficiency

Specific details of the SM, π_t, and η_{TT} changes are shown in table 6.3.

Table 6.3. Rotor Only Whirl Comparison

Case	$\Delta\pi_t$ (%)	$\Delta\eta_{TT}$ (%)	ΔSM (%)
90%	-4.74	1.47	55.9
85%	-6.70	1.17	-35.7
80%	-8.17	0.613	-55.7
70%	-4.41	-0.268	-46.1

6.1.2 Treatment Effectiveness

The treatment effectiveness was evaluated by comparing the previously outlined parameters between the Rotor only with Whirl and IP with Whirl cases, as well as the NACA with Whirl cases. Since the compressor operates with IGVs in the field, only the Whirl cases were compared against each other in this study. The first Figs. 6.10 and 6.9 show the difference in performance of the IP casing compared to the Rotor Only simulation. The IP case shows a distinct, nearly uniform drop in efficiency across all rotor speeds. The efficiency drop was on the order of 2-2.4%, as shown in table 6.4.

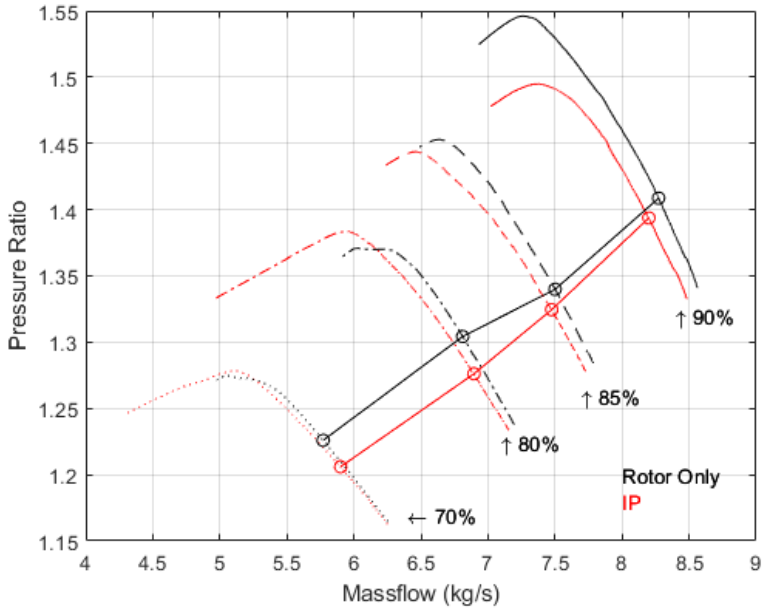

Figure 6.9. IP Treatment Evaluation Pressure Ratio Plot, Whirl Cases

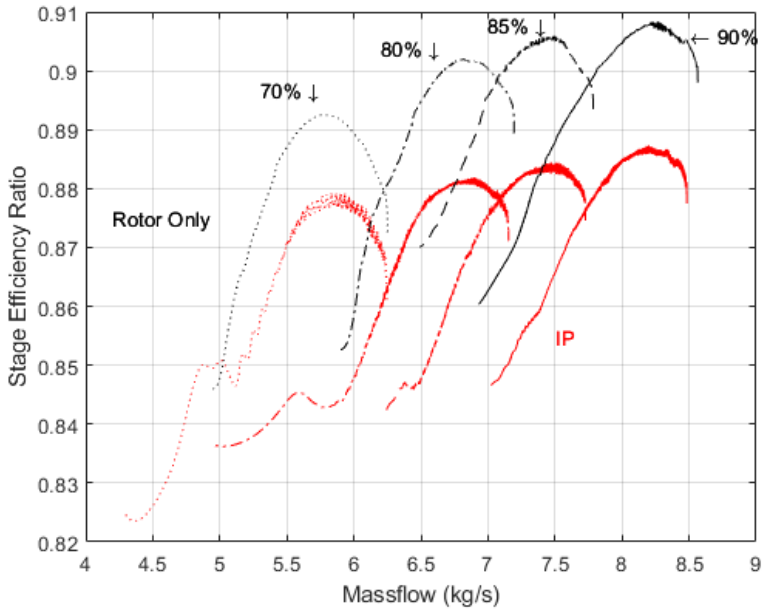

Figure 6.10. IP Treatment Evaluation Efficiency Plot, Whirl Cases

Although the IP cases reduced the stage pressure ratio for the 90% and 85% cases it increased the peak pressure ratio for the 80% and 70% cases. This resulted in the BEP remaining at a higher mass flow than the Rotor Only case for 70% and 80% speeds. The 85% and 90% speeds resulted in an operating point with slightly lower mass flow. With similar BEPs (within 0.3 kg/s), though, most of the stall margin increase/decrease was observed by how far down in mass flow each of the cases could go before stalling. As detailed in table 6.4, the predicted SM actually decreased for the IP casing for the 90% rotor speed by 11%. All other cases showed an increase, and an especially large increase for the 80% speed case.

Table 6.4. RO-IP Data Comparison

Case	$\Delta\pi_t$ (%)	$\Delta\eta_{TT}$ (%)	ΔSM (%)
90%	-3.29	-2.32	-11.3
85%	-0.62	-2.38	25.0
80%	0.941	-2.23	109
70%	0.298	-1.49	91.0

The NACA cases are detailed in Figs. 6.12 and 6.11. The efficiency drop for the NACA case was more severe than for the IP case, up to 3.5% for the 90% speed case. This efficiency drop is likely too large to offset any stall margin gains, however the objective of this study intended to over-size the ducts to place an upper bound on the size of a recirculating casing treatment for the NPSMF. The stall margin gains for the NACA casing were quite large, shown in table 6.5, and reflected by the long tails of the efficiency curves (blue) in Fig. 6.12. The pressure ratio drops were much more severe than the IP casing, though still there was not much difference in the mass flows for the BEPs.

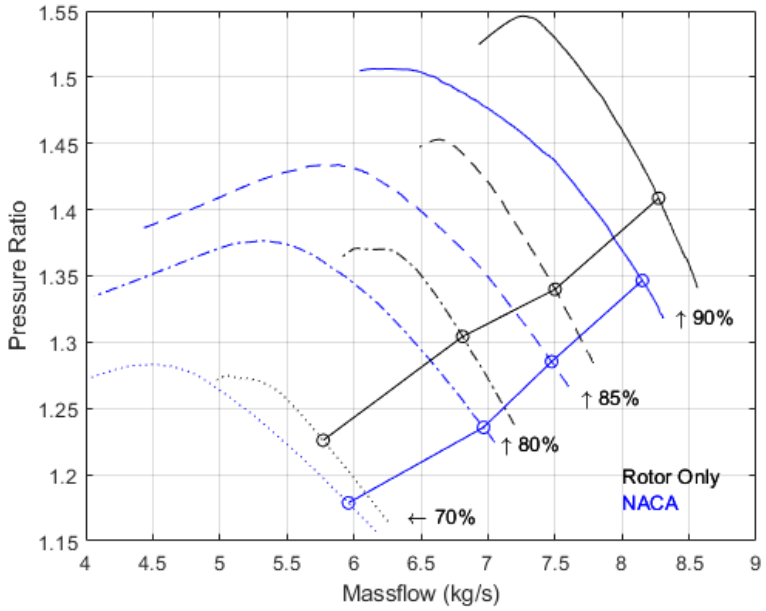

Figure 6.11. Rotor Only and NACA Pressure Ratio Plot, Whirl Cases

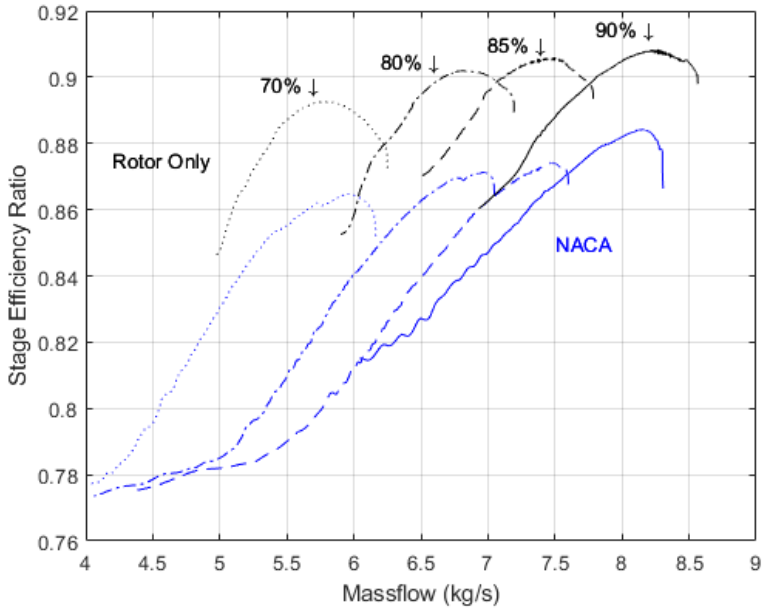

Figure 6.12. Rotor Only and NACA Efficiency Plot, Whirl Cases

Table 6.5. RO-NACA Data Comparison

Case	$\Delta\pi_t$ (%)	$\Delta\eta_{TT}$ (%)	ΔSM (%)
90%	-2.57	-2.66	59.6
85%	-1.31	-3.50	207
80%	0.408	-3.40	212
70%	0.675	-3.11	122

The bar plots below serve as a summary of the stall margin data from the computational runs, as they are more easily digestible than table data. The first figure, 6.13 shows a summary of the stall margin data from the section. It is starkly apparent how well the NACA casing performs across all rotor speeds with respect to increasing SM. The largest gains were seen for 80% and 85% speed, and the smallest gain for 90%.

Future research should seek to understand why the SM varies so much with rotor speed for these casings and seek to further increase the SM in higher rotor speed regimes. The IP casing greatly increased SM in the subsonic cases (70% and 80%) though there was only a slight increase and even a decrease for the higher speed cases. Candidate causes for this include insufficient amount of recirculating mass flow, non-optimized duct shape, or non-optimized duct inlet and exit geometry.

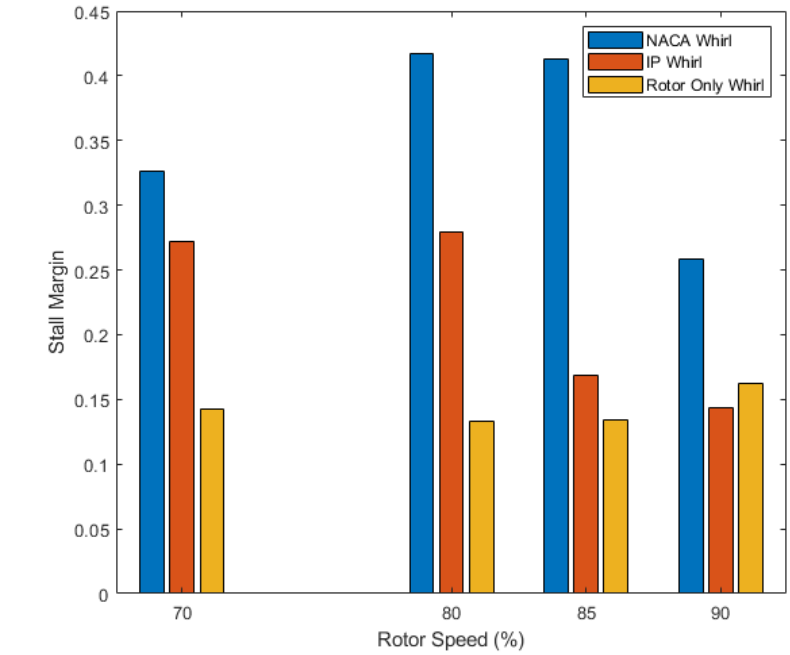

Figure 6.13. Stall Margin Bar Plot
for Treatments, Whirl Cases

Figure 6.14 depicts the SM changes for the no-whirl cases. The speedlines for these were not depicted earlier, but the SM 'story' is much the same as the whirl cases. The NACA casing shows a large increase in SM across all speed ranges, though the IP shows mixed improvement and detriment across all speed ranges apart from the 90% case. The IP casing still shows large a SM increase at 90%.

The analysis of the treatments was not limited to just plotting. Specific areas were targeted for analysis to obtain information about how the casing treatments changed the flow around the NPSMF. The first contour sought was of the suction-side (SS) of the blade. This was chosen in an effort to see what stall appeared as on the blade in terms of pressure, and to see if there was a noticeable change upon stall. Each of the contour plots consists of a photo, along with the commensurate place along the speedline the photo is from, the four points are compressor Choke, the BEP, the Peak pressure ratio (Best Pressure Ratio (BPR)), and at Stall. A star denotes the exact place along the speedline to the right of each photo. It should also be noted that since files were available only every 100 iterations, the stall points

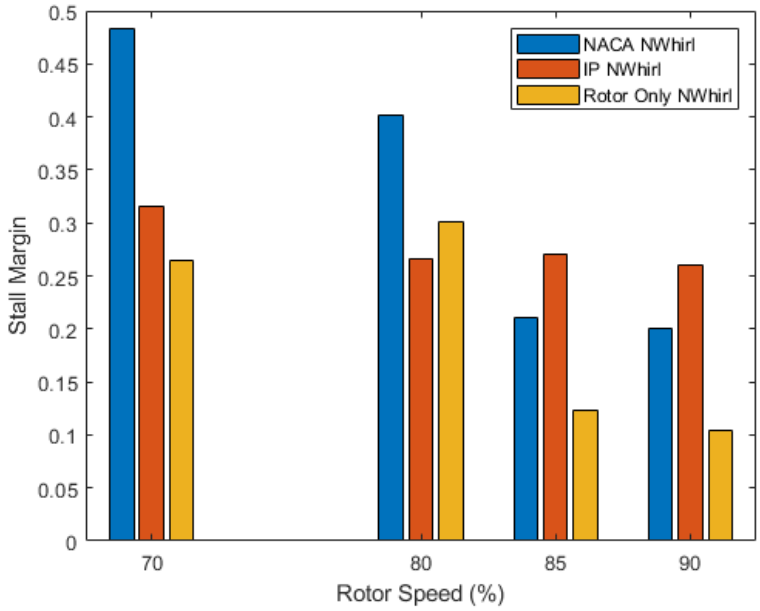

Figure 6.14. Stall Margin Bar Plot
for Treatments, No-Whirl Cases

were rounded to the nearest file available, and so are not necessarily perfectly representative comparisons between cases. Figure 6.15 shows the Rotor Only case SS. As the rotor moves along the speedline, a thick low pressure zone can be seen to from the midspan of the blade to the tip, however this zone is no longer there at stall. This is also reflected in theIP and NACA contours in Figs. 6.16 and 6.17, where a large low-pressure zone forms, but actually disappears at stall. This may either be an error of the simulation (the CFD predicted stall too late) or could be a real flow effect. Possible mechanisms that would cause this include a complete detachment of the shockwaves from the blade. If in stall, the flow shocks down to subsonic before being encountered by the rotor, there would no longer be distinct attached shockwaves to the rotor to cause the pressure drop. Insight into why this may be the case is reflected in all 3 figure's choke and BEP contours, where distinct pressure jumps can be seen (yellow-green) along the blade span. This is likely the location of a shock that becomes unapparent when the blade approaches stall.

The differences between the IP and Rotor Only contours are minimal, aside from a less pronounced shock delineation on the IP casing. The NACA casing, however, shows an

additional low pressure region at the blade tip at both the BPR and Stall points. This is the opposite effect of what was predicted, as the treatment was supposed to reduce the low-pressure area at the blade tip. This is further discussed below with vector plots of the outlet flow, but this was the first indication that the outlet angle and direction of the NACA casing may be sub-optimal.

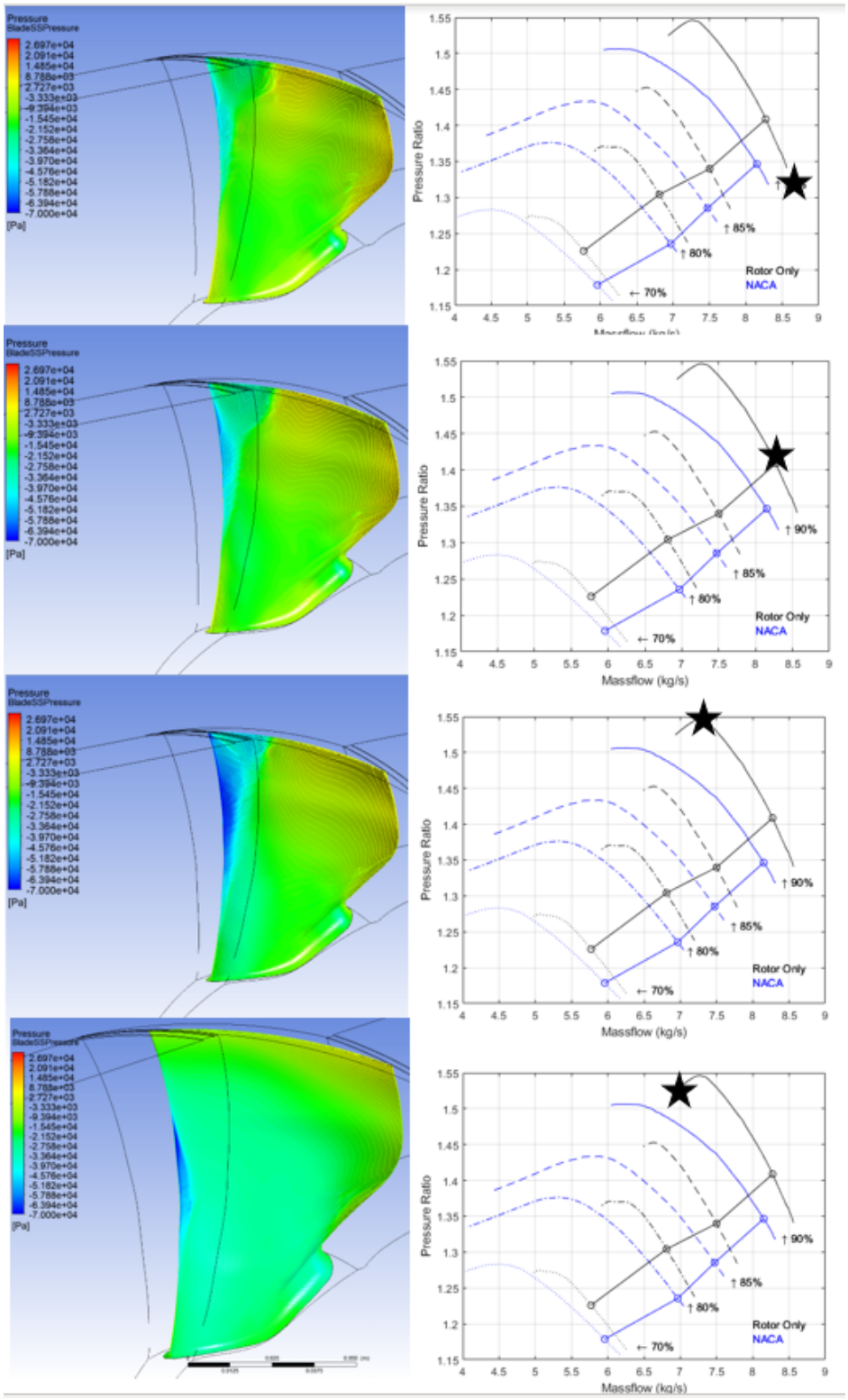

Figure 6.15. Rotor Only Blade Suction Side Along Speedline, 90% Whirl

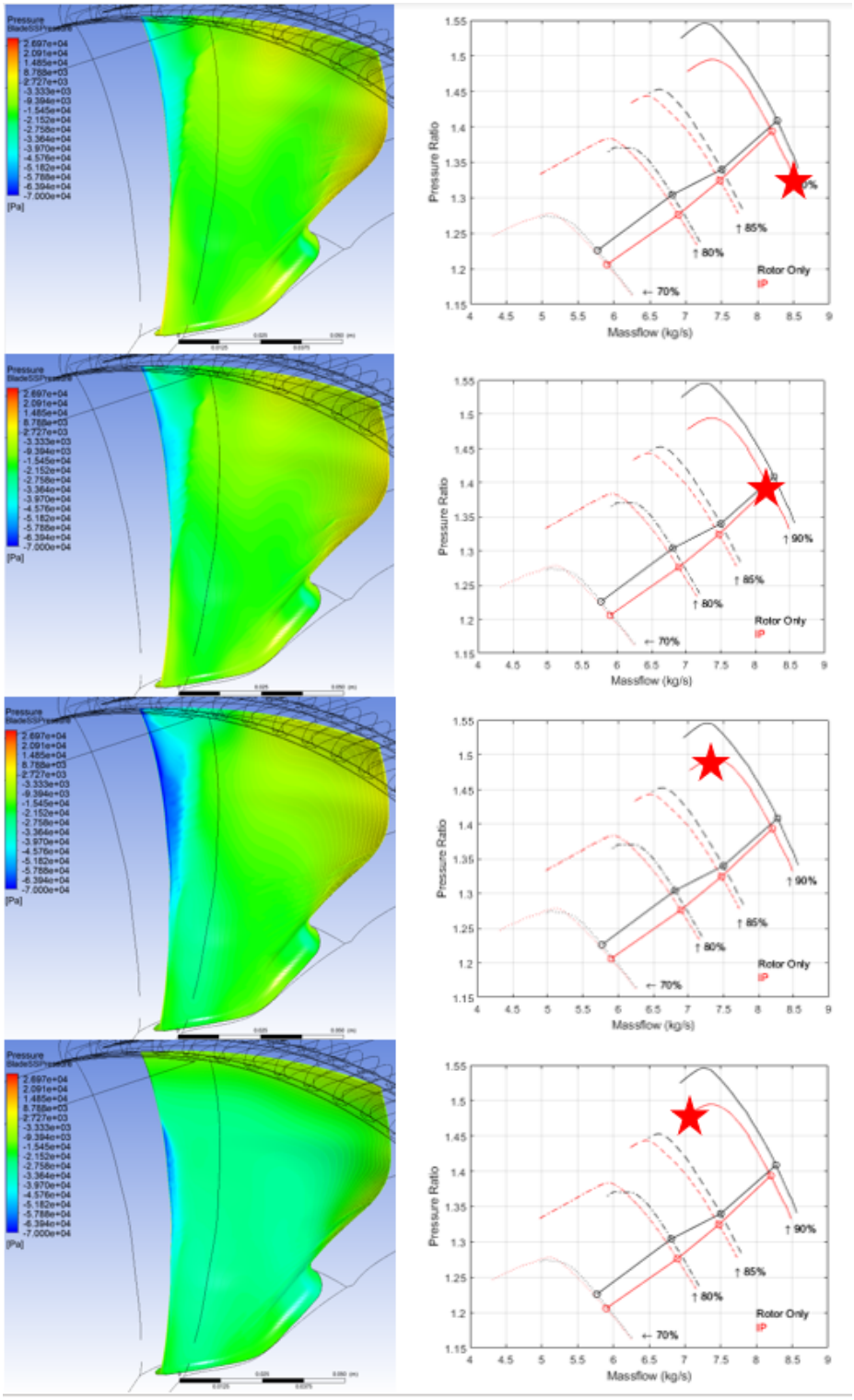

Figure 6.16. Internal Passages Blade Suction Side Along Speedline, 90% Whirl

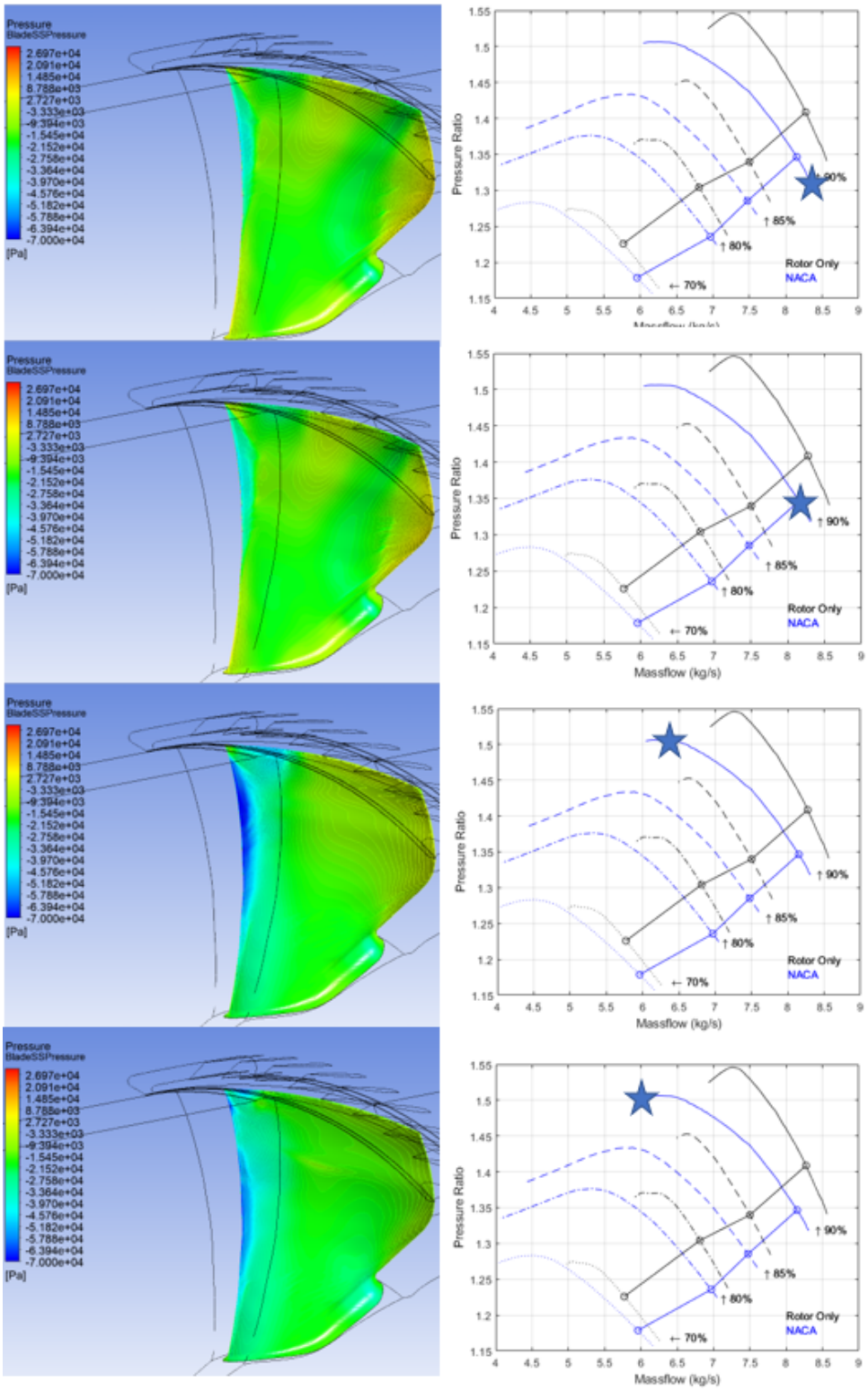

Figure 6.17. NACA Blade Suction Side Along Speedline, 90% Whirl

Below, in Fig. 6.18, compares the Rotor Only, IP, and NACA cases all at stall. The low pressure zone on the NACA blade tip at stall is readily apparent, though the midspan pressure zone is higher than that of the Rotor Only case.

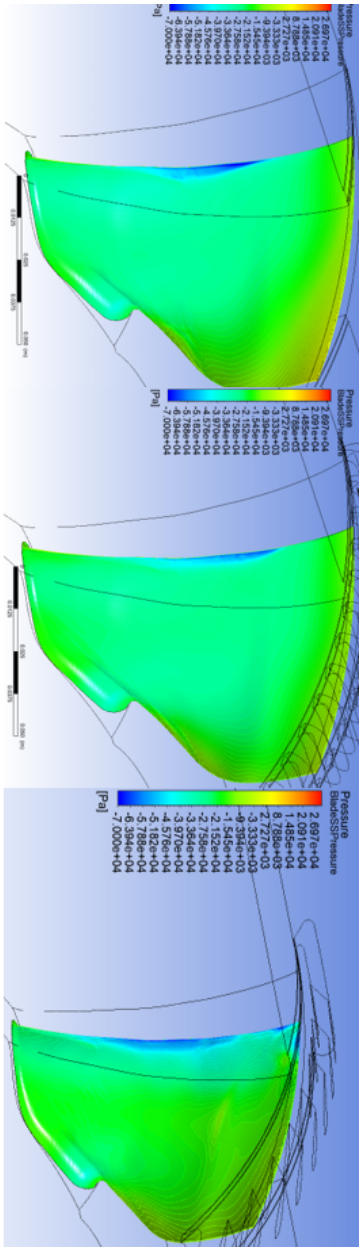

Figure 6.18. Comparison of Blades at Stall for RO, IP, NACA, all Whirl Cases

The second contour taken was of the Mach number at 95% blade span (near tip). This was done to better compare the shock locations along the blade chord between each case and within each speedline. Figure 6.19 shows the Mach contour for the Rotor Only case. The shocks on the leading edge of the blade can clearly be seen, as well as the shock on the SS of the blade at the midspan. This then develops into a very low speed area near stall, until massive recirculation bubbles form at stall on the Pressure Side (PS), and the flow appears 'smeared' on the SS. The IP and NACA cases in Figs. 6.20 and 6.21 appear similar, though with less distinct. Especially with the NACA case, the 'smearing' of the Mach number on the SS appears earlier on the speedline, and is much more severe at stall than on either of the other cases. This is encouraging if reflecting real phenomena, that the rotor can sustain these kinds of adverse pressure gradients without a torque loss, though it may indicate the simulation predicting stall later than it really occurs.

Importantly, as can be seen from the BPR point in each of the figures, initial separation of the flow seems to begin on the pressure side, not the suction side of the blade. This was seen in Meinster's work, though without inlet whirl [7]. It was thought that inlet whirl would unload the rotor tip enough so as to stall on the SS; this looks not to be the case. Further work should thus also incorporate PS contours of the blade if possible in stall prediction.

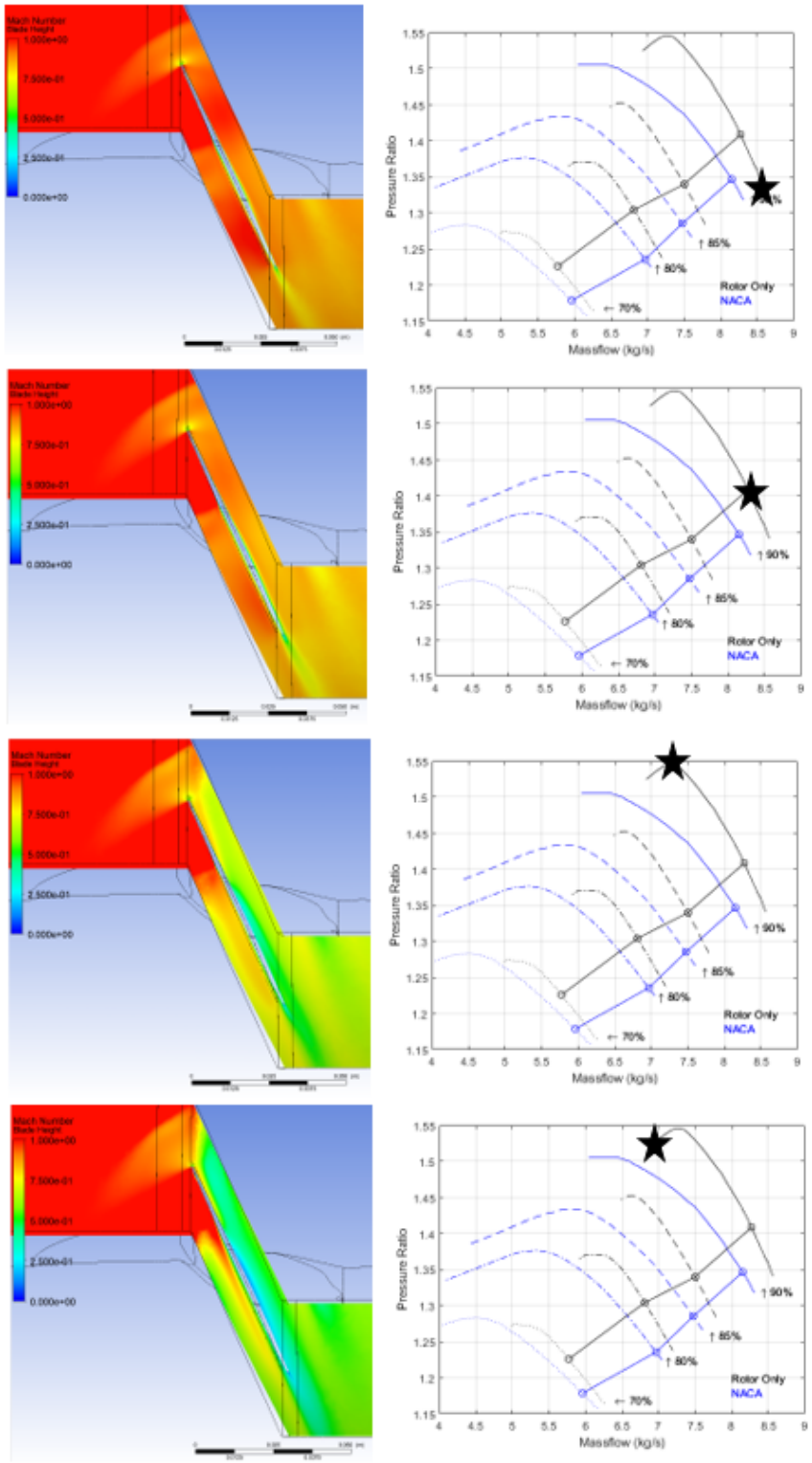

Figure 6.19. Rotor Only 95% Blade Span Mach Contour, 90% Speed, Whirl

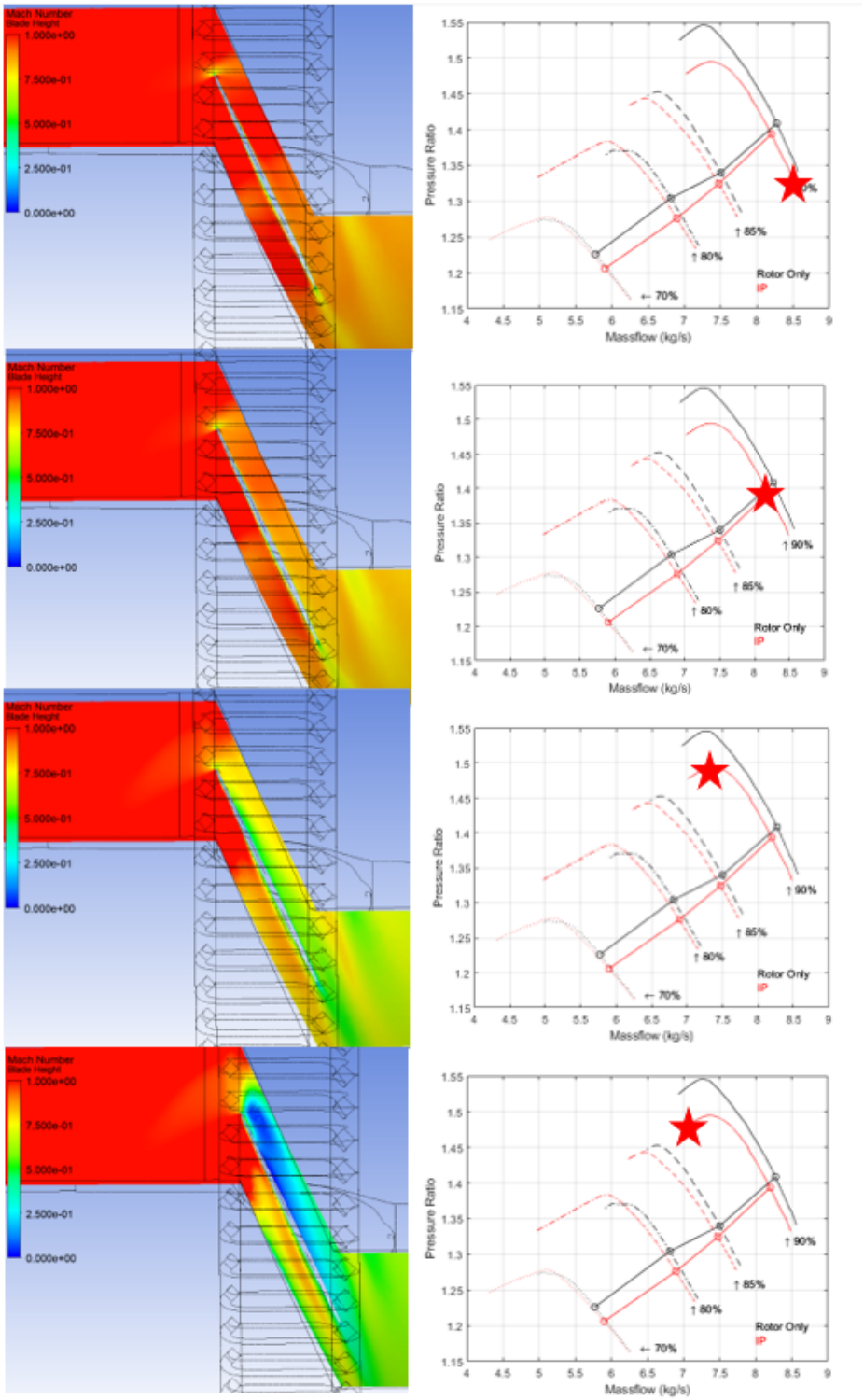

Figure 6.20. Internal Passages 95% Blade Span Mach Contour, 90% Speed, Whirl

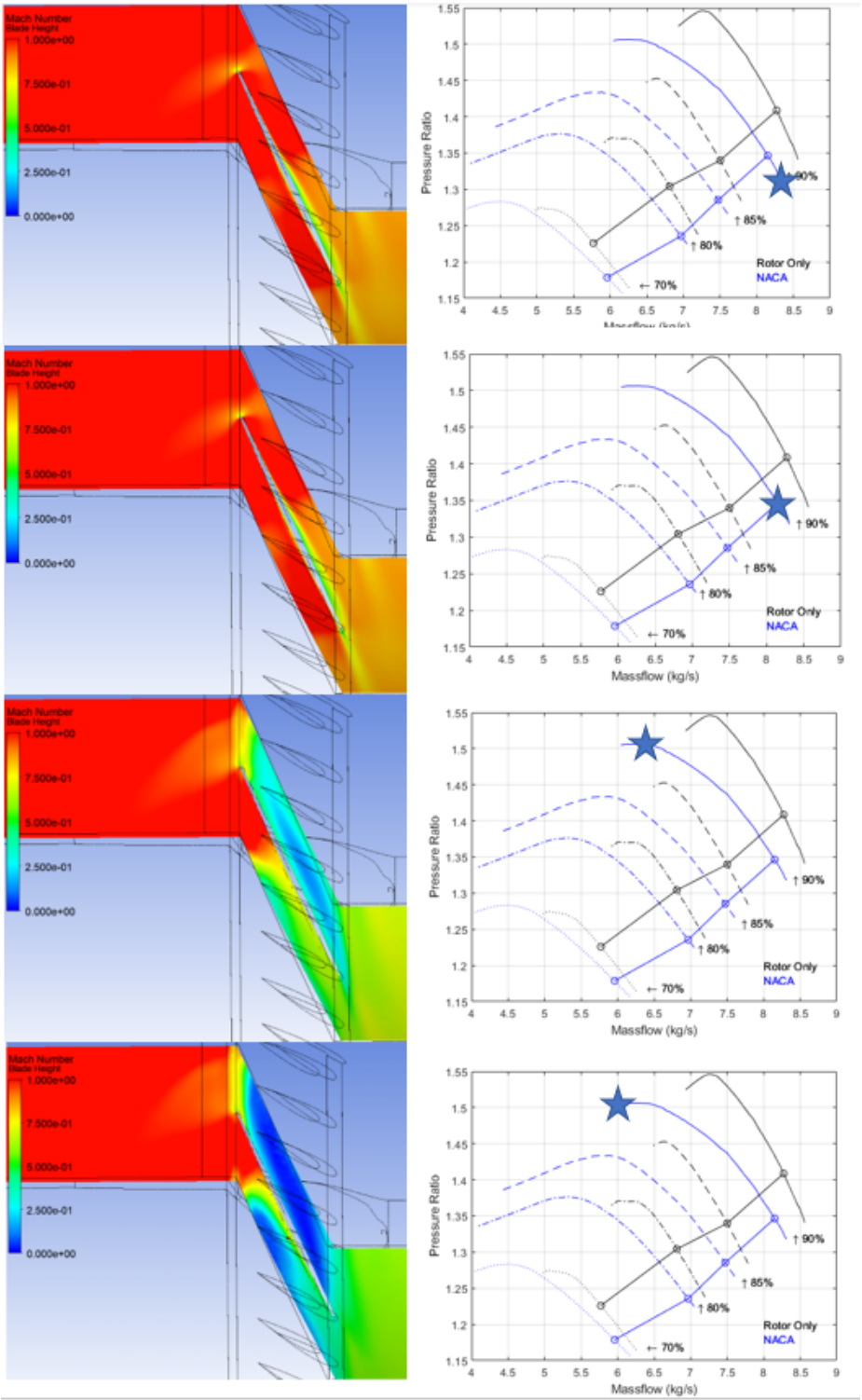

Figure 6.21. NACA 95% Blade Span Mach Contour,90% Speed, Whirl

6.1.3 Flow Recirculation

One of the objectives of this study was to obtain as much mass flow recirculation with the NACA casing as possible, when compared to previous work. Figure 6.22 highlights the percentage of mass flow recirculated for the IP case and the NACA case. As can be seen in the plot, the NACA case recirculated much more (2-3x) flow than the IP case. This is almost certainly due to the increased inlet area of having an annular channel. Having discrete passages necessitates a maximum density such that the passages overlap, capping the amount of mass flow that can recirculate. Additionally, the NACA casing increases its mass flow recirculation as it moves down the speedline, which is encouraging. Ideally, a treatment could be created that did not recirculate any mass flow at choke, BEP and BPR to preserve operating efficiency, and only take effect once the compressor approached stall. This is very difficult to do with a passive treatment, but this simulation indicates it is possible to design treatments that have scalable affect in the desired direction. The IP does not show this effect, showing a peak and a decrease in mass flow towards stall.

The mass flow of the IP casing remained constant between rotor speeds, whereas the NACA casing increased in mass flow with decreasing rotor speed. This is not intrinsically bad for the NACA casing, though the optimal effect would have the most mass flow recirculating at the highest rotor speeds. The likely effect of this is the angle with respect to axial of the NACA airfoil supports in the NACA casing. A 30°angle is likely too low, such that the incidence grows at higher rotor speeds, (more whirl) and further separates flow from the NACA airfoils, thus effectively blocking the flow of air through the treatment.

Figure 6.23 depicts the mass flow recirculation for the no-whirl cases. The increasing effect of mass flow recirculation with decreasing rotor speed is even more pronounced for these cases than Fig. 6.22. Even for the IP case, the mass flow increases with rotor speed reduction. This further strengthens the hypothesis that the effect is whirl-driven, and that further work should be done with varying NACA airfoil angles.

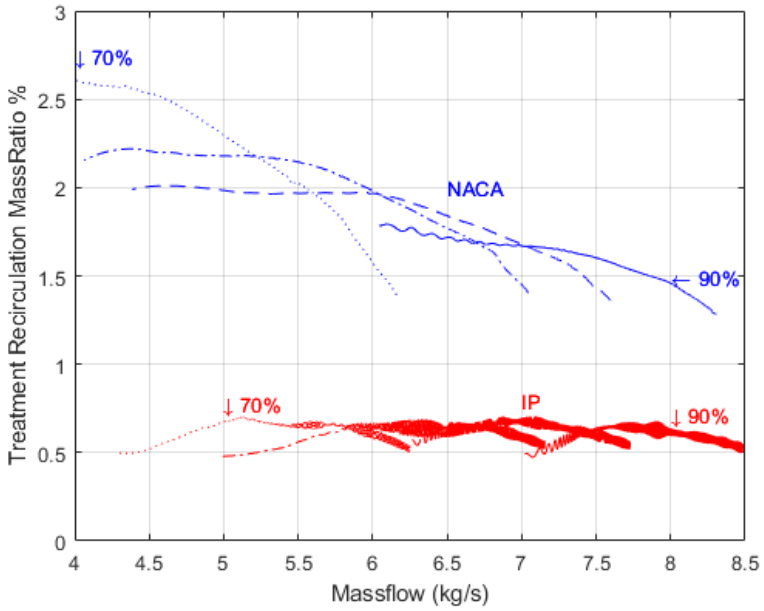

Figure 6.22. Treatment Recirculation Mass flow, Whirl Cases

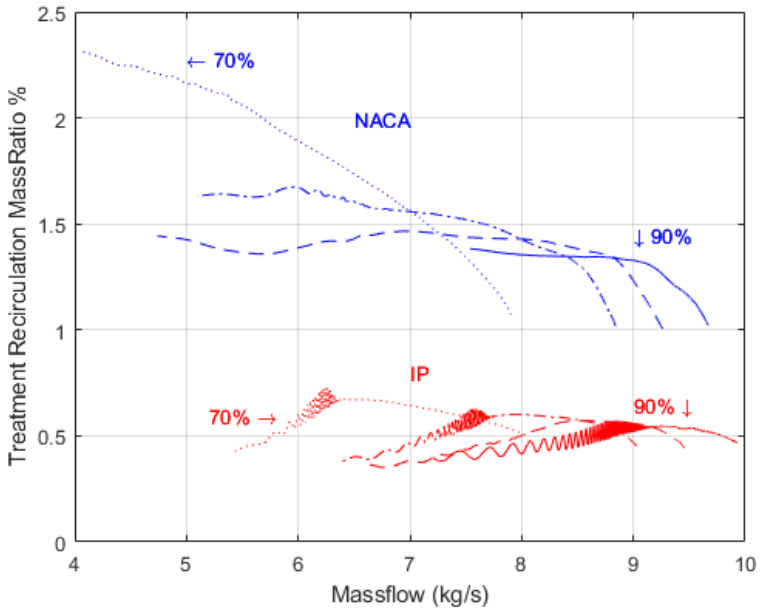

Figure 6.23. Treatment Recirculation Mass flow, No-Whirl Cases

The phenomena sought to be understood from the treatments included the effectiveness of the inlet and exit angles (both axial and θ) as well as the overall flowpath of air through the treatment.

The first of these cases involves the Inlet/Exit flow analysis, shown in Figs. 6.24 and 6.25. Highlighted in red circles are the inlet and exit of each treatment (exit on left). The velocity vectors distinctly show how much more flow is being directed into the treatment in the NACA case as supposed to the IP case. In both cases, however, the flow seems to come in from both the upstream and downstream side, meaning there is likely a recirculation bubble downstream of the treatment inlet and a drop in efficiency. This suggests that the 'scoop' shape to the inlet, i.e. the inlet being angled upstream, may not help direct flow into the treatment and may actually create a substantial efficiency drop.

Regarding the outlet velocities, both of the treatments are very similar to one another. An undesirable effect at the outlets, though, is the friction of the exit flow. At choke and BEP, the exit flow of the treatment is very axial, but further towards stall the flow becomes more radial, and even slightly jetting upstream. This is not desirable, as nearly the entire literature concurs that axial jetting is the best for stall mitigation [1], [6]. This is likely due to the relatively steep angle (45°) of the exit duct; it is recommended for future work to incorporate a section in the treatment where the duct makes a full downstream turn before re-introducing the flow to maximize the axial velocity component of the jet. Not shown in the figures as well is the θ component to the velocity, which is much lower than the incoming flow at stall. This means the flow is loading the tip of the blade rather than unloading it. This comes back to the internal angle of the NACA airfoils and the exit θ angle of the IP casing. Future casings should further angle the airfoil in attempt to have the treatment exit flow be co-rotational with the rotor.

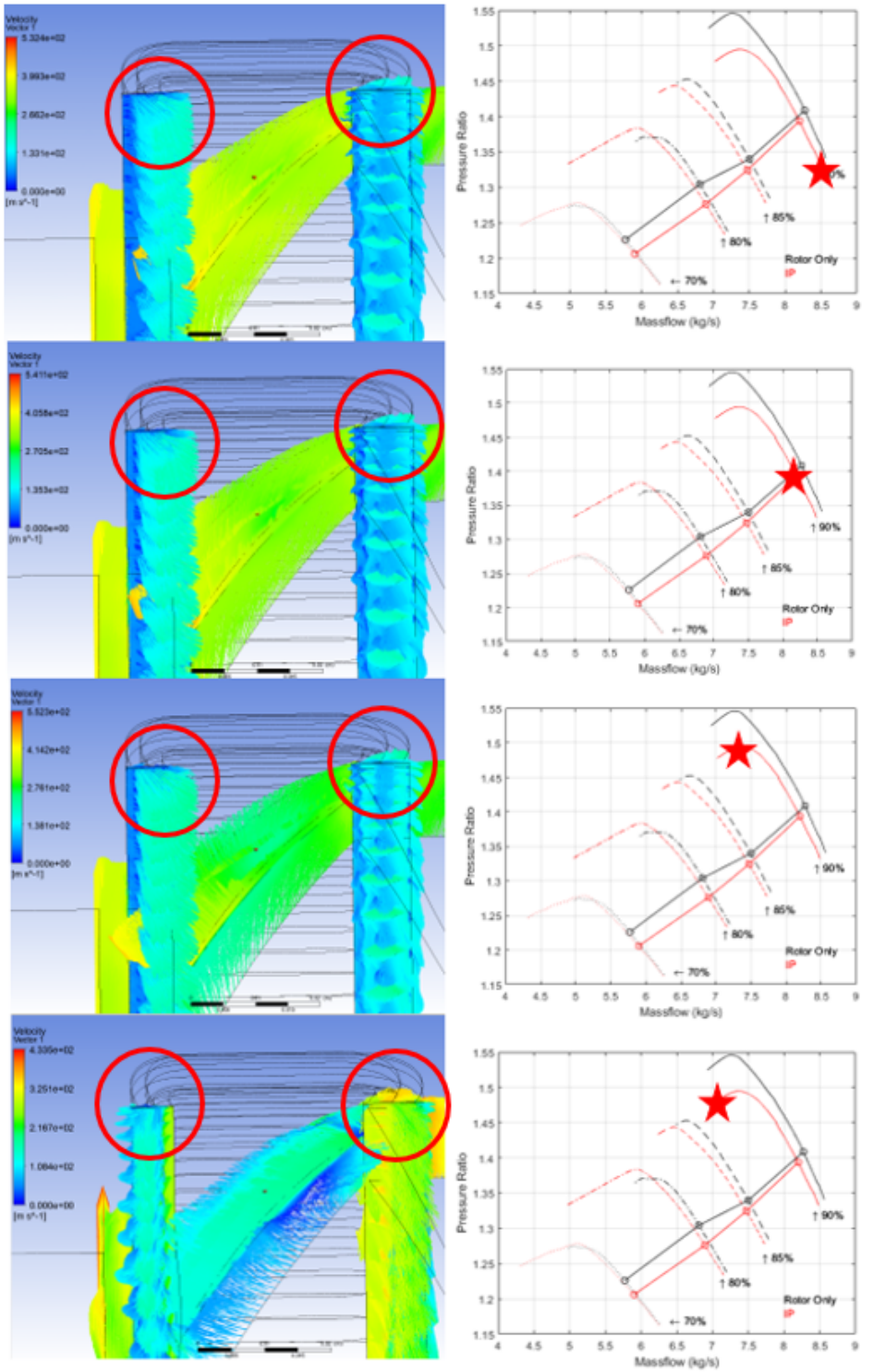

Figure 6.24. IP Treatment Inlet/Exit Velocity Vectors

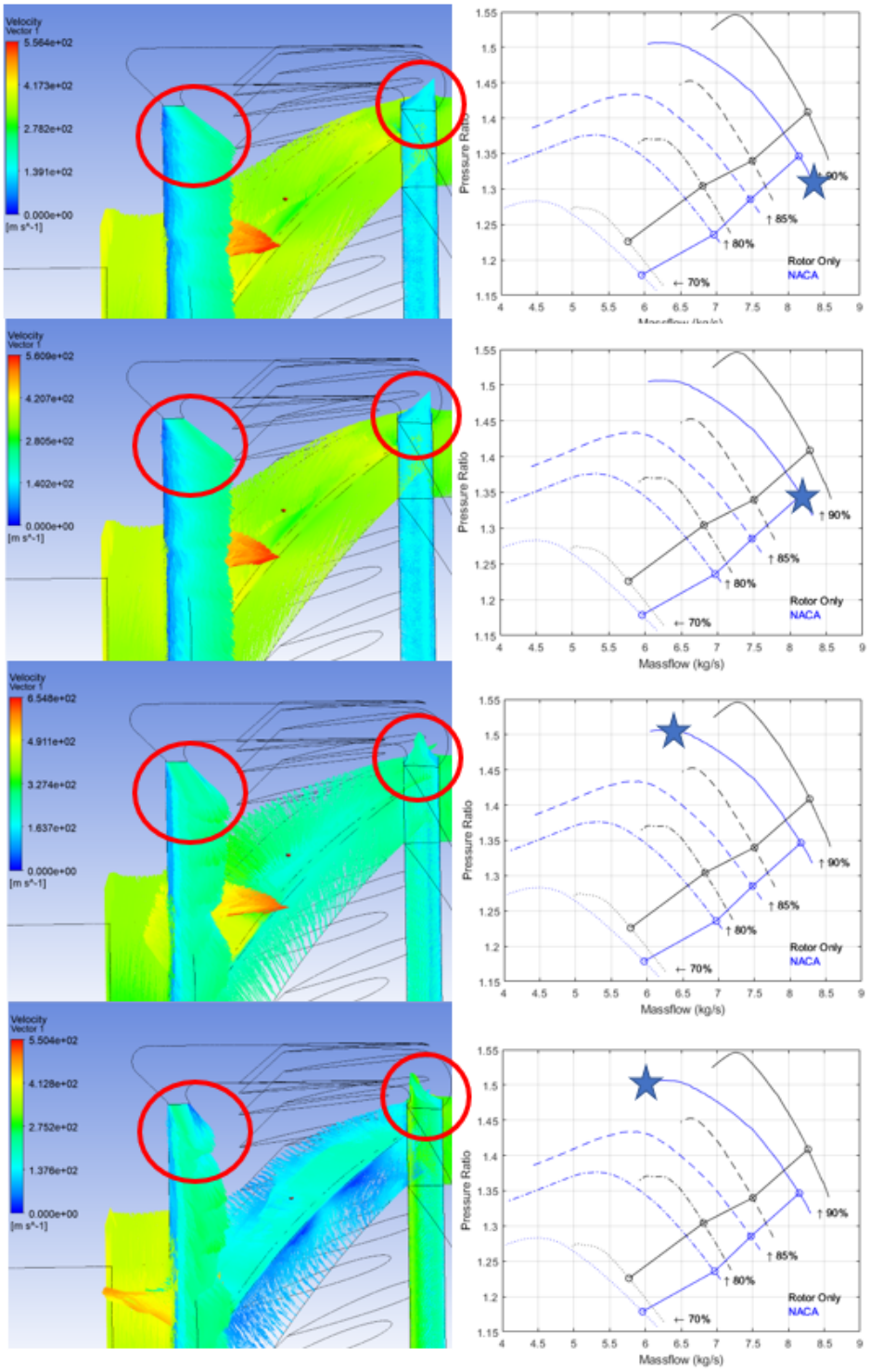

Figure 6.25. NACA Treatment Inlet/Exit Velocity Vectors

Velocity vectors were also used to characterize the flow within the passages of the IP casing and the channel of the NACA casing. Figure 6.26 shows the vectors within each of the passages in the IP casing. The inlet flow is very fast, and large Fanno effects appear to take over, slowing the flow before the exit. The constriction of each passage causes a velocity increase, but the passages do not seem to be choked. The passages are recommended to be kept at the same inlet area for further analysis, but the passage cross-section may be reduced to promote increase in the flow speed.

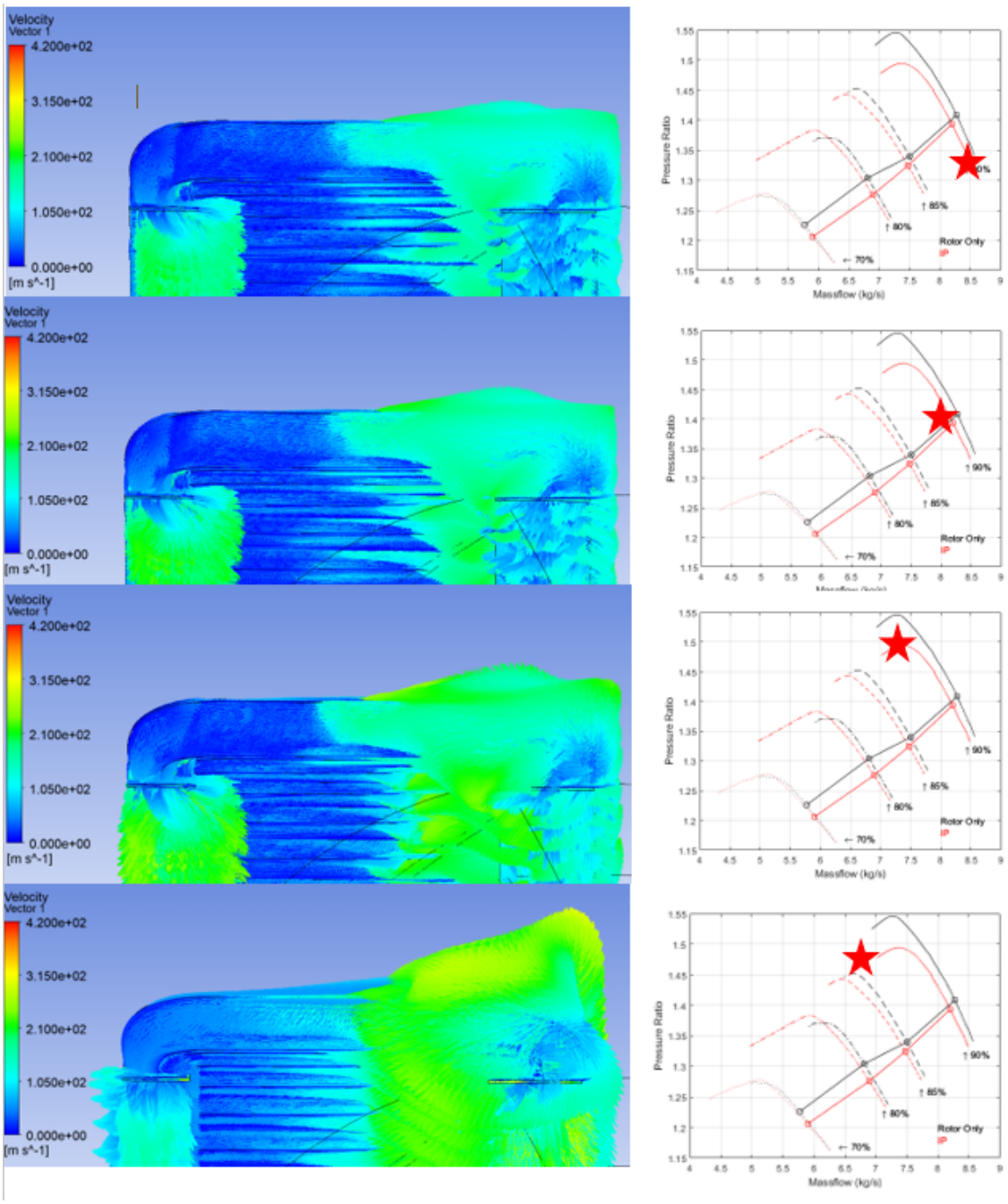

Figure 6.26. IP Treatment Velocity Vectors, 90% Speed, Whirl

The NACA case provides a clearer view than the IP case of the flow within the recirculating channel. The flow within the NACA passage is shown in Fig. 6.27. Near stall and BEP,

the flow appears to attach well to the outer wall of the treatment and ‘turn the corner’ of the inlet, but as the pressure rises it detaches, leaving a quite large low pressure bubble on the downstream side of the inlet, and a low speed zone on the radially) inner surface of the passage. This, like the inlet/exit analysis, suggests non-optimal design of the geometry. Further work should look to incorporate a downstream angled inlet, as opposed to the ‘scoop’ design of the upstream angled inlet. The inlet meeting the inner casing surface at a shallower angle would also allow the flow to not detach from the inner surface of the passage. These changes, in combination with a treatment outlet that is much more axial, would likely result in greater improvements in SM with less efficiency penalty than the tested casings in this study.

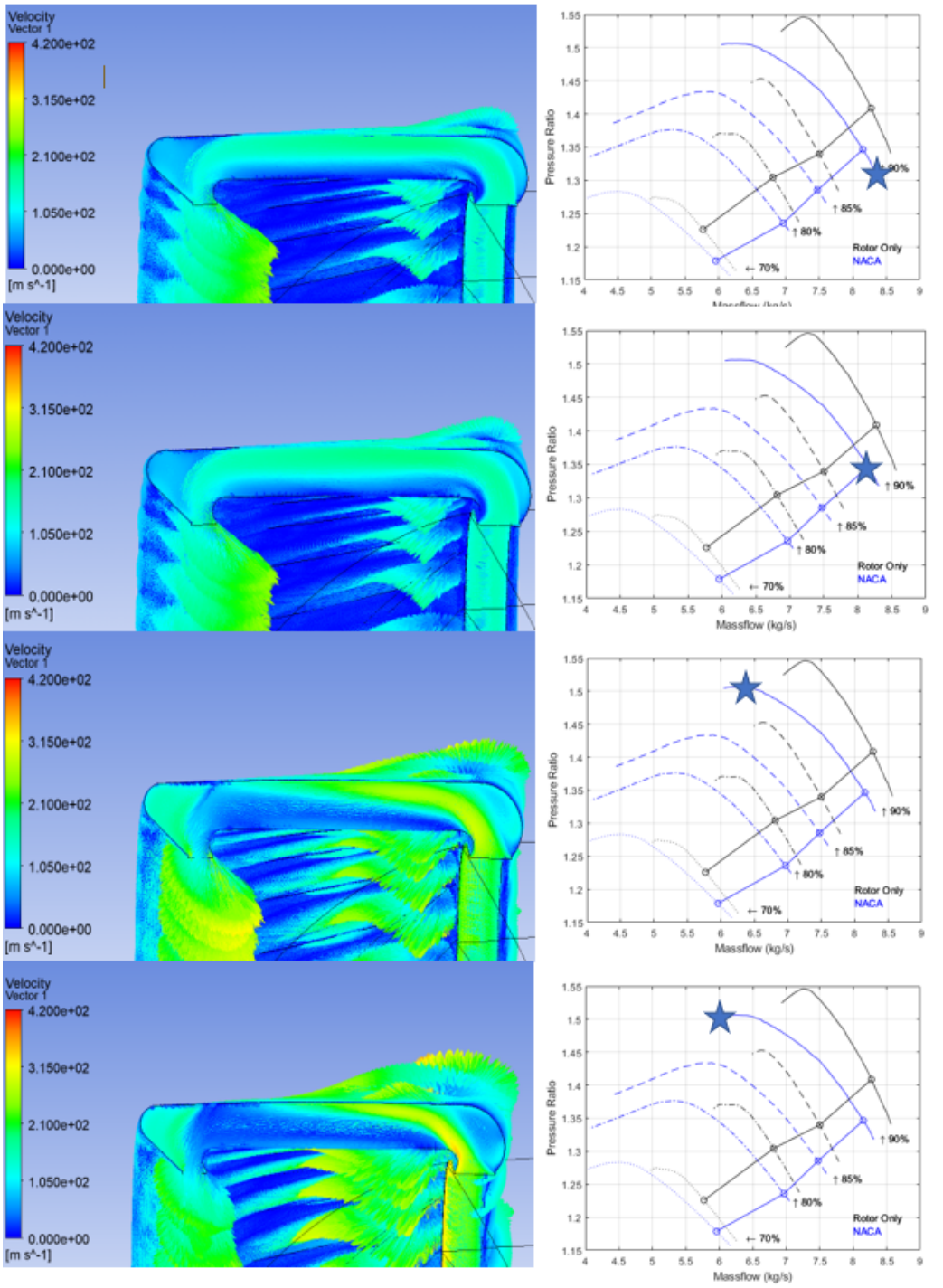

Figure 6.27. NACA Treatment Velocity Vectors, 90% Speed, Whirl

6.1.4 IGV Domain Comparison

The final aspect of this study was to fully model the IGVs and evaluate the quality of the whirl approximation used for much of the previous work on the NPSMF. Figures 6.29 and 6.28 show the efficiency and pressure ratio of the Rotor Only 90% Whirl simulation compared to the 90% IGV simulation. This served as an analysis of how well the whirl approximation performed. It is readily apparent from the plots that the Rotor Only with Whirl simulation over-predicts the stage efficiency by a large margin, seen in table 6.6. The IGVs impart nearly a 4% loss in stage efficiency. Encouragingly, the shape of both curves is visually extremely similar. The oscillations seen in the IGV simulation is almost certainly a mesh problem and not representative of reality. Otherwise, the whirl approximation serves very well to predict the overall shape of the pressure and efficiency curves. Unfortunately, only the 90% rotor speed case was able to be run for this study, and more work should be done to see if the whirl approximation is consistent over the other rotor speeds tested.

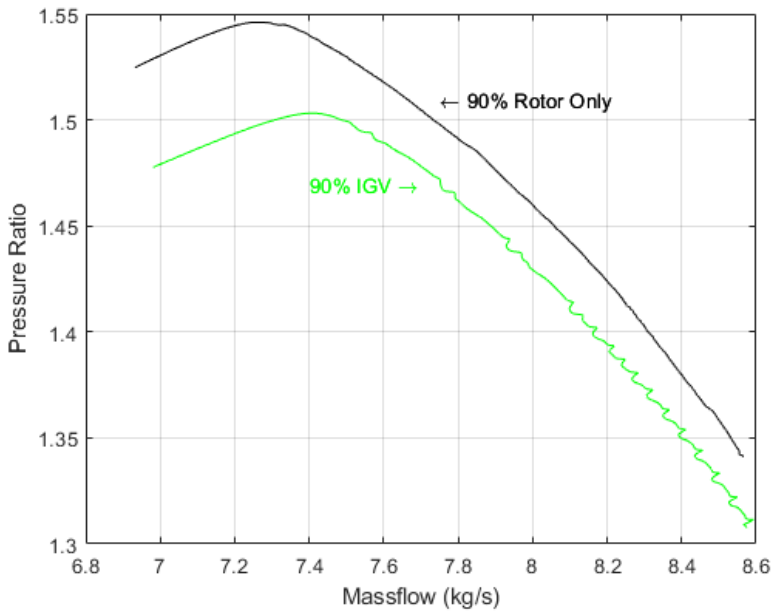

Figure 6.28. IGV to RO
Pressure Ratio Comparison, with Whirl

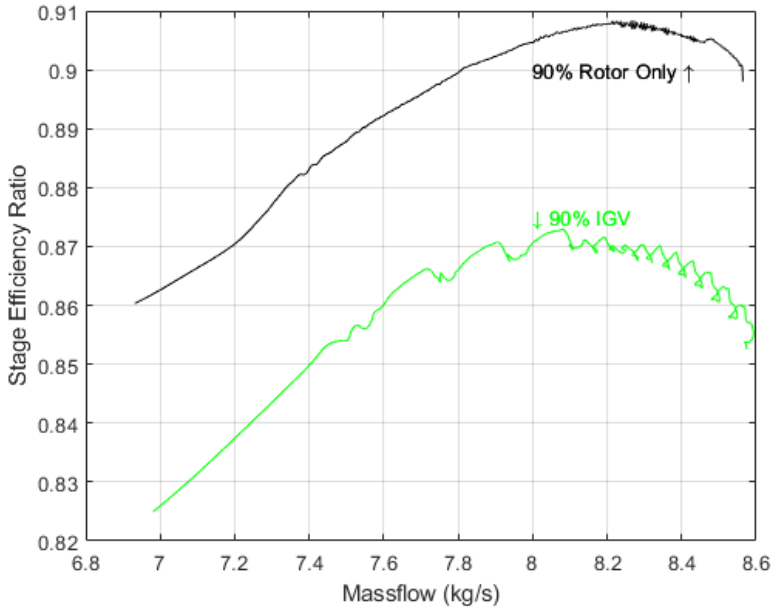

Figure 6.29. IGV to RO Efficiency Comparison, with Whirl

Additionally, the NACA case was compared to the NACA+IGV case, seeking to determine if the effects of the RO-IGV comparison were shared when the NACA treatment was added. Again, this simulation was conducted only at 90%, as different geometries need to be individually created for each IGV set angle at each rotor speed. Figures 6.31 and 6.30 show the efficiencies and pressure ratios of these simulations. While the shapes of the curves were very similar, an even larger 5.2% efficiency loss was observed between the NACA Whirl case and the NACA+IGV case. A smaller SM difference was observed, as well as a smaller pressure ratio difference. All relevant data is presented in table 6.6.

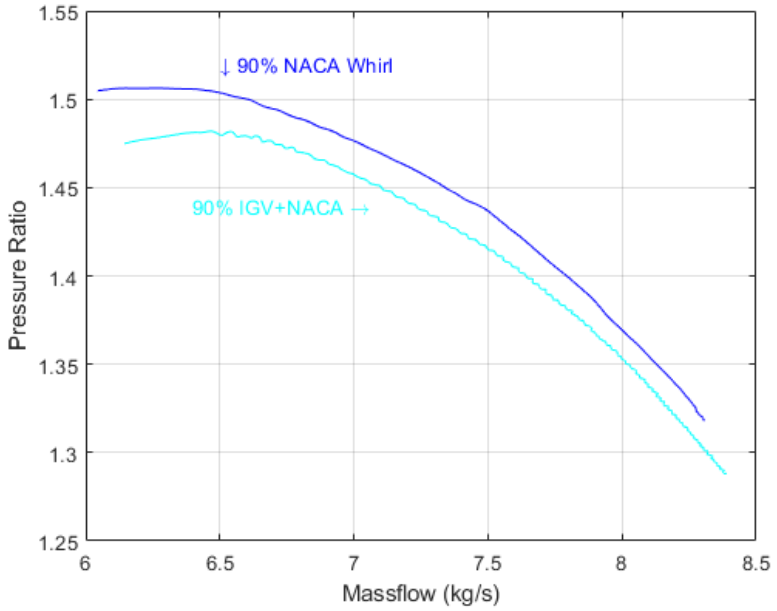

Figure 6.30. IGV+NACA to NACA Pressure Ratio Comparison with Whirl

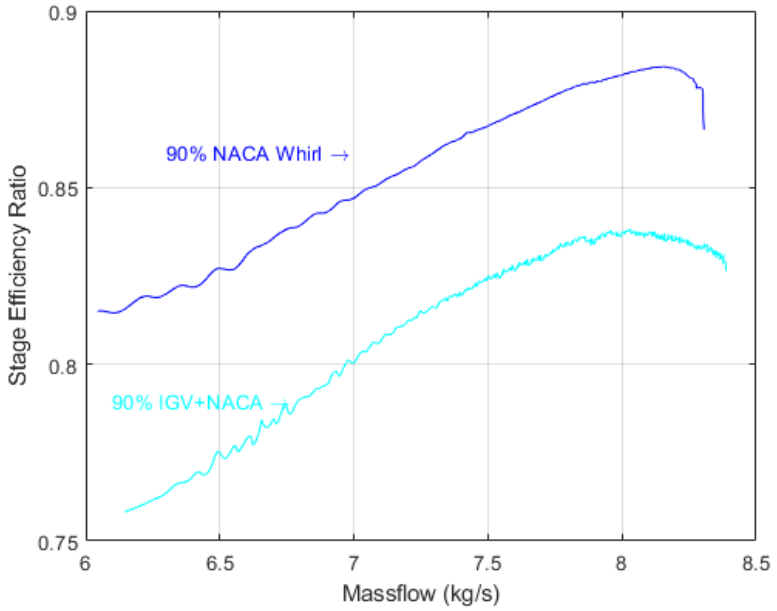

Figure 6.31. IGV+NACA to NACA Efficiency Comparison with Whirl

Table 6.6. RO-IGV and NACA-IGV+NACA Data Comparison

Case	$\Delta\pi_t$ (%)	$\Delta\eta_{TT}$ (%)	ΔSM (%)
RO-IGV (90%)	-2.77	-3.91	-16.0
NACA-IGV+NACA (90%)	-1.62	-5.20	-9.21

A visual representation of the SM for the IGV cases is shown in Fig. 6.32. ANSYS indicates that the whirl approximation slightly over-predicts the stall margin, when compared to modeling the IGVs. Both for the Rotor Only and NACA cases, the difference is relatively minor, ~10-15%. This indicated that the whirl approximation can continue to be used if necessary and does not seem to have an invalidating effect on when the rotor will stall. The whirl simulations should not, however, be used to reliable predict stage efficiency calculations without a correction factor added for the stagnation pressure drop of the IGVs, on the order of 3.5-5%.

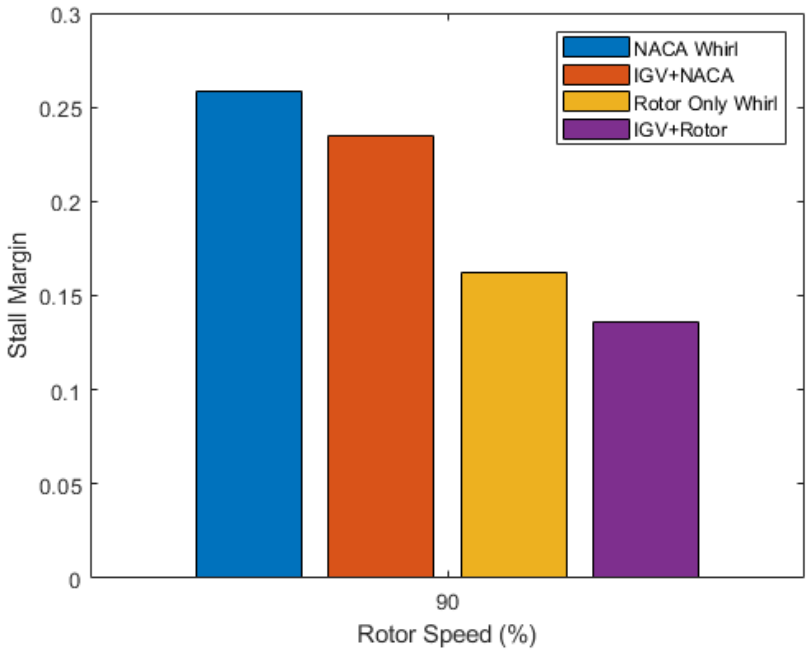

Figure 6.32. SM Comparison between IGV Modeling and Whirl Approximation

6.2 Experimental Results

Unfortunately, a 1:1 match of each computational case could not be completed with the TCR due to program constraints, so the experimental data collected was compared to its respective simulation counterpart. Research continuing after the completion of this study, so future work will be able to incorporate the relevant experimental counterparts to this study's simulations.

6.2.1 Internal Passage Casing

The IP casing was able to be run at 70%, 80% and 85% speeds to be able to compare to a smooth casing. The comparison between the IP experimental casing and the smooth experimental casing is detailed in Figs. 6.34 and 6.33. The efficiency plot shows a close match of the IP casing to the smooth casing for the 85% case, and has a commensurately small, 2.46% efficiency penalty, just resulting in a 2.16% SM increase. The efficiency penalties for the lower speeds were much greater, and the efficiency plot shows a distinct dip where the point of peak efficiency should be. Despite this, the pressure ratios for all 3 cases remained quite close to the smooth casing pressure ratios. The fact that the efficiency curve dip only occurs on select casings indicates it is not a fundamental problem to the treatment, but rather likely a problem regarding flow phenomenon than is rotor speed dependent. Possibly, with the lower whirl of the 70% and 80% cases, the there is a separation bubble near the inlet exit of the treatment, degrading efficiency, or the treatment is improperly jetting.

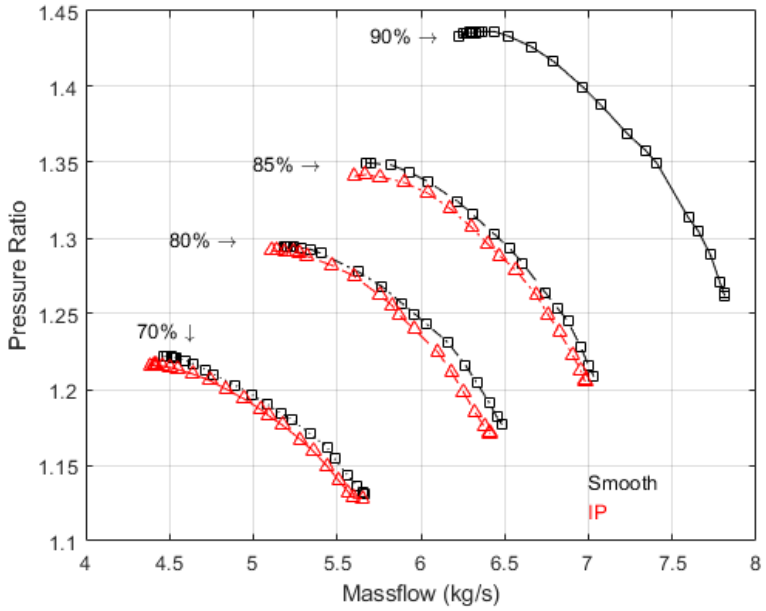

Figure 6.33. RO to IP Experimental Data Pressure Ratio Plot
IGV set IAWS

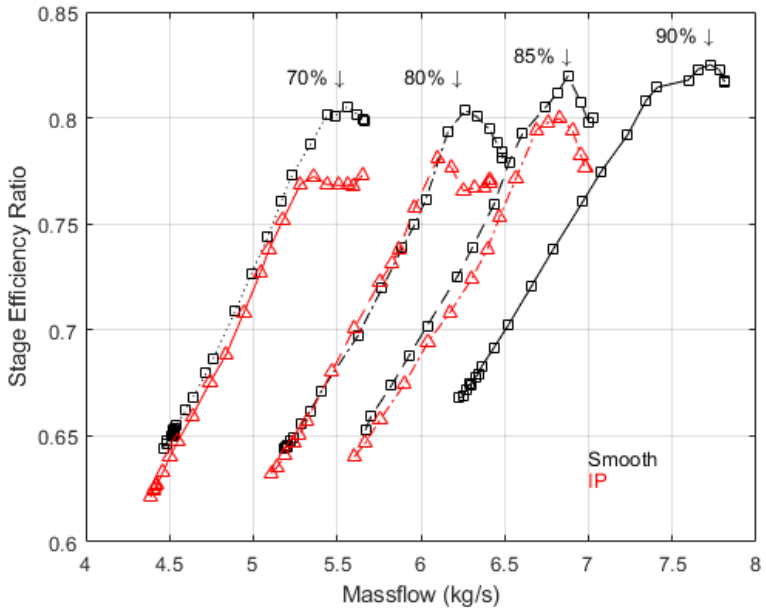

Figure 6.34. RO to IP Experimental Data Efficiency Plot
IGV set IAWS

Table 6.7. Rotor Only to IP, Parameter Comparison

Case	$\Delta\pi_t$ (%)	$\Delta\eta_{TT}$ (%)	ΔSM (%)
85%	-0.585	-2.46	2.16
80%	-.232	-2.81	-5.52
70%	-0.491	-4.04	13.21

The stall margin bars, shown in Fig. 6.35 indicate only slight differences between the IP and Smooth Casings experimentally. The IP casing did improve the stall margin, most in the 70% case, but the efficiency penalty is certainly too large with the current passage sizing. The changes to be made to the IP are likely in line with those proposed for the NACA casing, those being adjustment of the inlet and exit duct to face downstream.

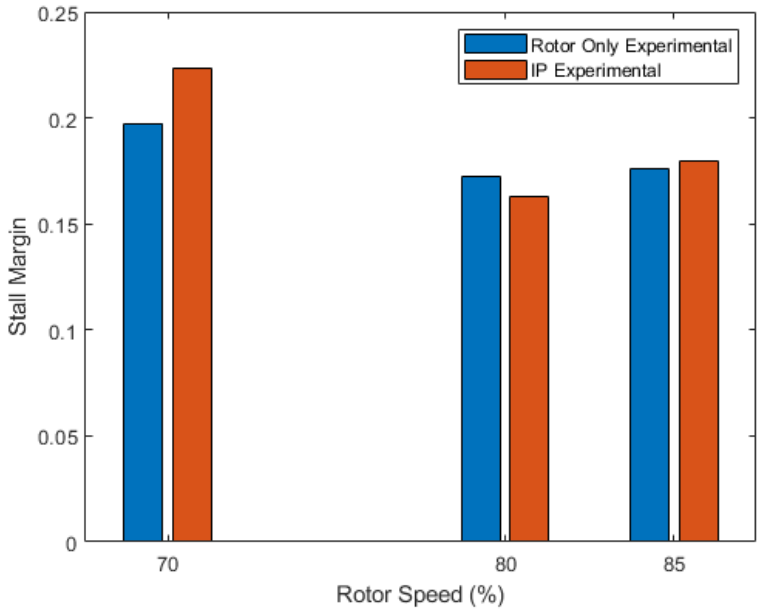

Figure 6.35. RO to IP Experimental SM Comparison

6.2.2 NACA Casing

The only experimental test conducted for the NACA casing was at 85% rotor speed. The test was conducted with the IGVs at 0°, or a 'no-whirl' test run. Figure 6.37 and 6.36 show

the results for this test. The depressed peak of the efficiency curve, seen for the two speeds in the IP casing test run are reflected even more severely for the NACA casing in Fig. 6.37. As the NACA casing has a much larger aggregate inlet and exit area of the passages, this aligns with the presumption that the ducts were oversized. Crucially, the NACA casing in this no-whirl run was not able to operate at a lower mass flow than the smooth casing.

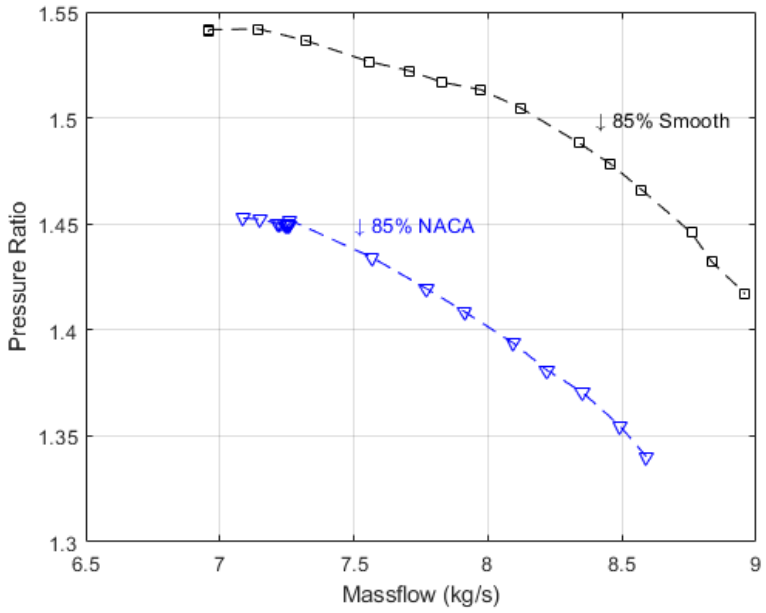

Figure 6.36. RO to NACA Experimental Data Pressure Ratio Plot

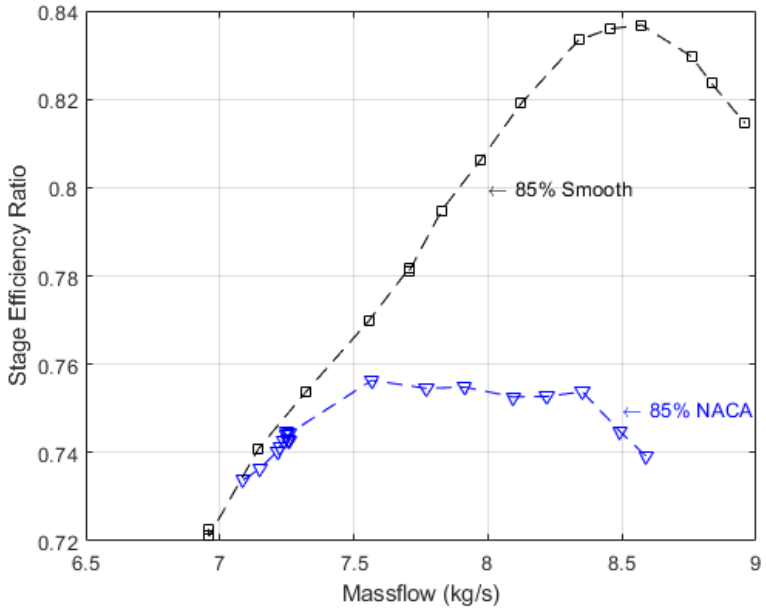

Figure 6.37. RO to NACA Experimental Data Efficiency Plot

Table 6.8. RO to NACA, Experimental Data Comparison

Case	$\Delta\pi_t$ (%)	$\Delta\eta_{TT}$ (%)	ΔSM (%)
85%	-5.79	-9.61	-19.60

One experimental test is not enough data to form a comprehensive conclusion, and so further tests are recommended, with the IGVs in accordance with their schedule, to be able to fully analyze the effectiveness of the NACA casing. For the 85% speed, no whirl case, the NACA casing did not perform as expected, having a massive reduction on stall margin, as well as efficiency and pressure ratio. More promisingly, testes were completed, though not digested fully, where the NACA casing did have a SM increasing effect with the IGVs set IAWS.

6.3 Overlay and Comparison of Results

Even with limited experimental data, each successful experimental run was compared with its corresponding CFD counterpart. This was done in an effort to see where the CFD predic-

tions succeed, and fall short, as well as to provide insight into possible improvements for the simulations. Importantly, all experimental cases were run as a 'Full Stage' configuration, with a stator. As the stator unloads the flow, as well as imparting a pressure and efficiency penalty, the experimental data necessarily carries lower π_t and η_{TT} values than the CFD counterparts. With this discrepancy in mind, the results for the IP casing are shown in Figs. 6.39 and 6.38.

The shape of the pressure ratio curves predicted by CFD in Fig. 6.38 is much closer to the actual experimental speedlines. In all cases, there is a higher π_t and mass flow, but linearly so. It is very encouraging that the pressure ratios from CFD are 'in-line' with the experimental data, i.e. the 70% CFD lines are shifted up and to the right of the 70% experimental data, but they are shifted directly towards the 80% speed pressure line, and so too with the other CFD predictions. This means the fundamental simulation physics is correct, but simply over-predictive of real performance (as an 'ideal' CFD case should be).

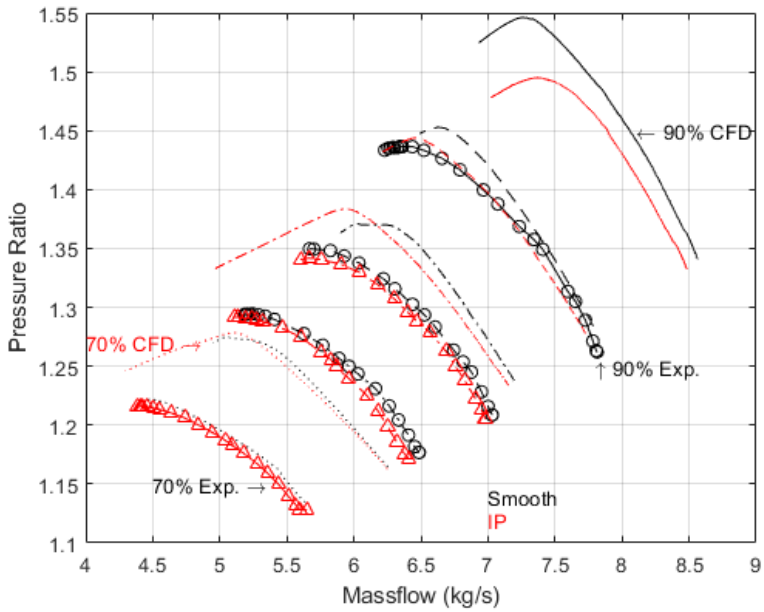

Figure 6.38. RO to IP Experimental Data Pressure Ratio Plot

Like Jones, a large difference in efficiencies is apparent between the computational and experimental results. The experimental runs had a much steeper line of decreasing efficiency before stall as well. This is in part due to all of the uncontrollable of the physical TCR but

mainly due to the lack of a modeled stator in the CFD. The mass flow range (choke to stall) of each of the cases is well predicted, with the CFD over-predicting peak mass flow by ~1kg/s (2.2 lbm/s).

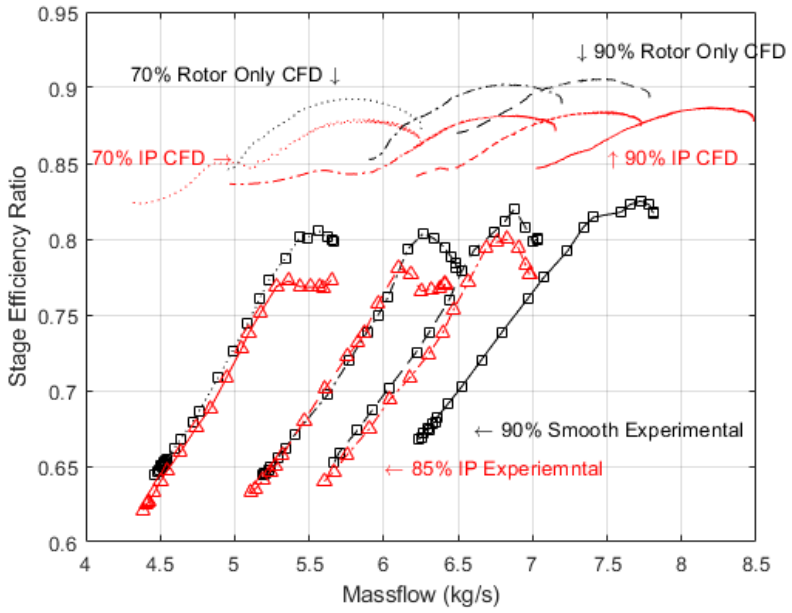

Figure 6.39. RO to IP Experimental Data Efficiency Plot

The story for the NACA casing is much the same. The efficiency curves in Fig 6.41 portray a large drop between the CFD predicted lines and the experimental lines, but retaining the same shape. The NACA casing efficiency line is much flatter, with a wider range of peak efficiencies than the smooth casing. The smooth casing SM was under-predicted from the CFD and the NACA casing was over-predicted. This could reflect a possible difference in experimental test conditions from the CFD case, or could add to the presumption that there needs to be a more robust method for stall prediction for the computational runs. Regarding the pressure ratio Fig. 6.40, the computational lines are further right, having higher mass flow than the experimental runs, but do not have predictably higher pressure ratios. Again, without a modeled stator there is no ways to easily pinpoint the mechanism of difference between the runs.

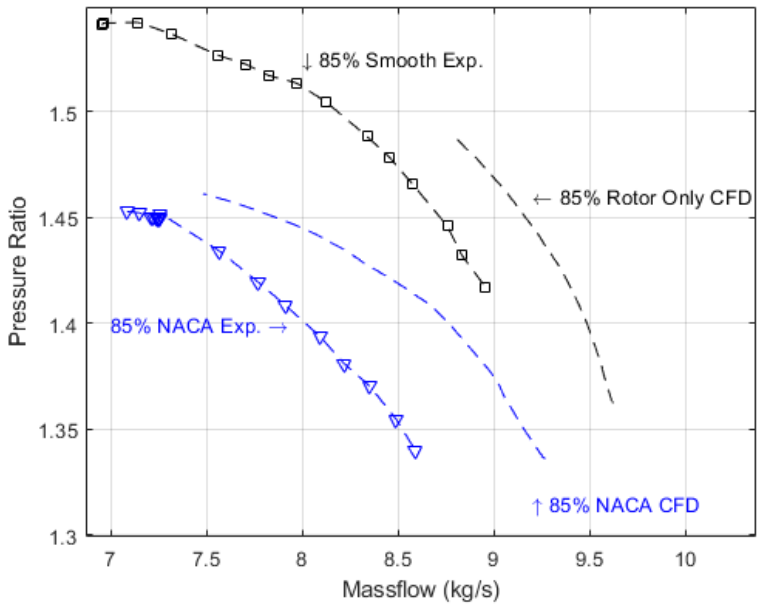

Figure 6.40. RO to NACA, Exp. to CFD,
Data Pressure Comparison

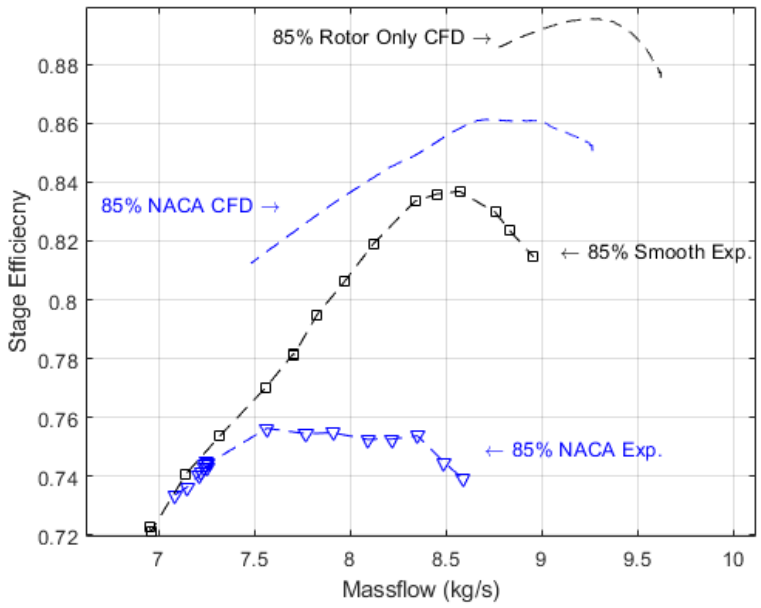

Figure 6.41. RO to NACA, Exp. to CFD
Data Efficiency Comparison

The stall margins, shown in Fig. 6.42 show a 19.6% decrease for the tested NACA casing when compared to the smooth casing.

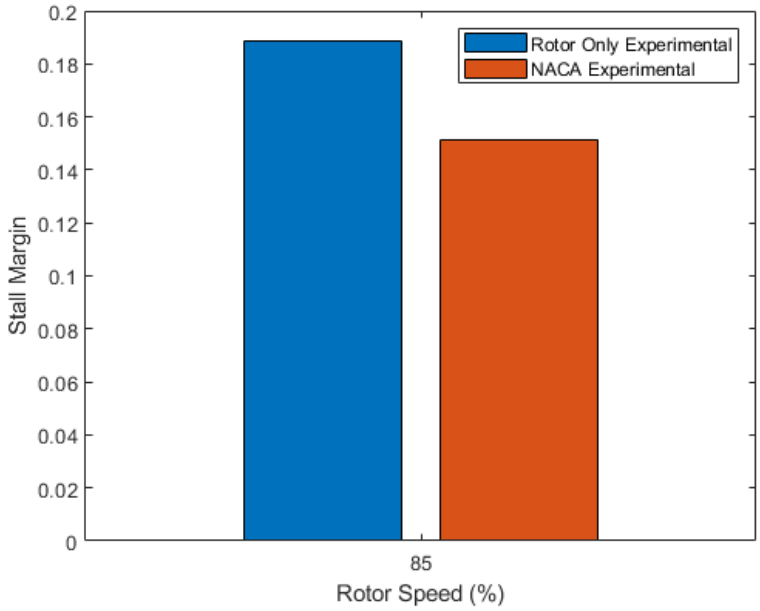

Figure 6.42. RO-NACA Exp.-CFD Data SM Plot

Lastly, the 90% speed, with Whirl case was used to ascertain how close the CFD predictions of the smooth casing were to the experimental data. As can be seen from Fig. 6.44, there was still a large gap in efficiencies (nearly 10%) between the CFD prediction using Whirl, and the realized data. In green is the IGV case, which nearly halves the distance between the smooth experimental and CFD cases. With the addition of the stator, the CFD prediction will likely become even more representative of the experimental results, reducing the predicted efficiency and lowering the mass flow.

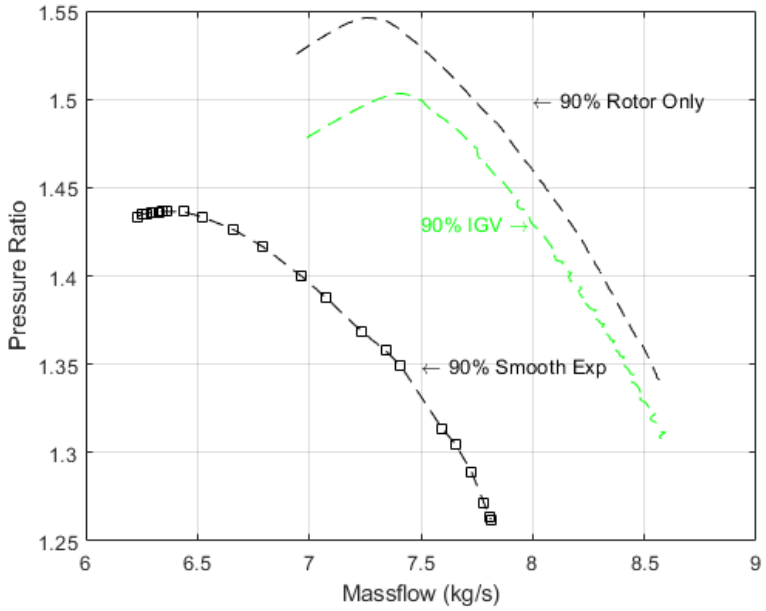

Figure 6.43. ROIP Experimental Data Pressure Ratio Plot

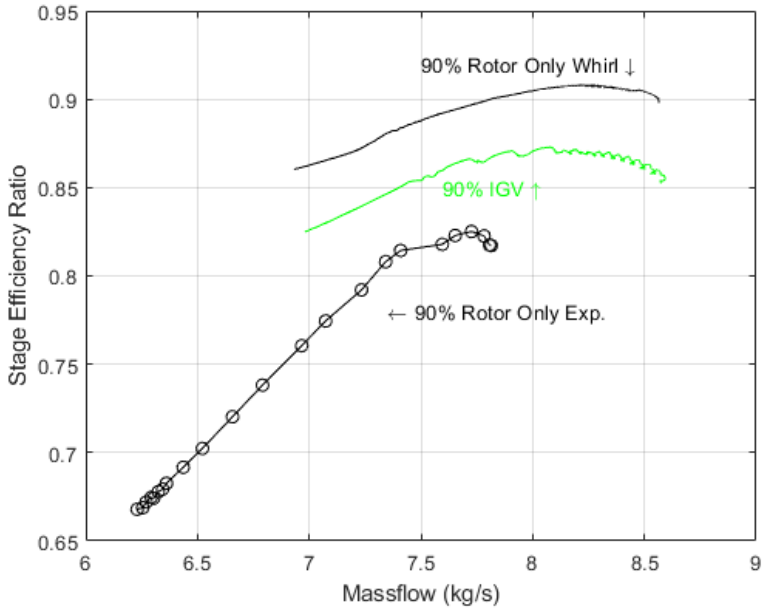

Figure 6.44. RO-IGV Experimental Data SM Plot

CHAPTER 7:
Conclusions and Recommendations

This study encompassed four distinct avenues of research, all of which were vital to further improvement of the NPSMF and flow control devices. These areas were the conceptual casing designs and their modeling in SOLIDWORKS, the manufacture and post-processing of the physical casings, the computational modeling of the casings, and the experimental testing of the casings.

The IP casing design allowed for simple and variable small passages, though not as much mass flow recirculation as the NACA casing. Both of the concepts should continue to be explored thought he recommended geometrical changes will be easier to implement for the NACA casing, specifically having a passage outlet that fully turns downstream before re-introducing the recirculating flow.

The manufacturing methods used in this study were both very efficient when compared to previous work. Much of this came in the reduced need of post-processing time to near-zero, even for a plastic polycarbonate casing. The only post processing needed was the removal of support structure from the passage inlets/ exits. Future work should continue to design casings with this constraint in mind, support material deposited within a passage will be difficult to extract, and will affect results.

In immediate continuation of this study, the IP and NACA casings should be run at all rotor speeds, and in accordance with the IGV schedule, to build a comprehensive picture of current casing performance. Additionally, garnering information from the CFD simulations allows recommendations to be made for immediate changes to future casings, which are listed below:

- Treatment inlets should be angled downstream
- Treatment passages need to be made to turn downstream before their exit, and have an exit angled as far downstream as possible
- NACA airfoil angles with respect to axial direction should be explored. Higher angles are likely to not take out whirl from the flow, helping to unload the rotor tip and fill in the SS low pressure zone. If possible a sweep should be done with many casings at many angles

Information from the results of this study also help to shape the picture of future work to be accomplished on treatment design, and on the TCR overall. The main areas for further research are outlined below:

- Implementing recommended geometrical changes to flow control devices/ casing treatments
- Exploring other NACA support airfoils, highly cambered airfoils may prevent separation over a wider operating range
- Additions to CFD domain to build a more comprehensive simulation (stator)
- Addition of variable control pressure step in CFD simulations
- Refinement of a stall prediction method (e.x. blade torque)
- Incorporation of the instrumented casings to monitor pressures within the treatment
- Upon implementation of effective casings, shifting the inlet air to post-stator, or more aft compressor stages for higher treatment inlet pressures
- Seeking a way to implement treatment air to be directed to not only injected at the blade-tip, but also midspan for non-tip-limited rotors. Options include possibly ducting air out of later compressor stages, to the trailing edges of the IGVs

With these changes in mind, future work will hopefully be able to create casing which provide substantial supersonic SM improvement without as drastic penalties on compressor performance. If successfully and implemented in aircraft, this could aid in the mitigation of compressor stall and the safety of pilots. These gains could be realized not only in aggressive maneuvering, but also routine operations with large throttle transients, such as on approach to carrier recovery, helping to create an overall safer environment for aviation.

APPENDIX A:
ElemX Casing Creation

The sensitivity study confirmed the quality issues with the ElemX manufacturing method. The casing diameter was very inconsistent, with standard deviations over 10x that of the other manufacturing methods used. Roughness measurements were above the limit of measurement of the instrumentation used. Additionally, the ElemX was the only printer where multiple sections of the casings needed to be separately printed, greatly adding to the manufacturing time. Use of the ElemX for casing manufacturing is not recommended. The manufacturing process, and an overview of the machine is outlined below for those interested:

A.0.1 ElemX Aluminum Droplet Casings

The Xerox ElemX is an LMJP printer, melting Aluminum wire in a ceramic reservoir and dispensing it in droplets to fabricate a desired part [19]. The most constraining factor for using the ElemeX 3D printing machine, shown in figure A.4 was the build plate size. With a square build plate the maximum manufacturing dimensions were 300mm x 300mm (11.81 in^2), necessitating 4 flat surfaces be cut onto the casing ring to fit within the build dimensions. These flat faces are all viewable in the three figures below, and reduced the distance from the casing edge to the internal passages.

Additionally, the print fidelity and surface roughness of the ElemX parts rapidly deteriorated after 1kg of material was expended, likely due to the wearing of the argon nozzle coating. This meant that each casing needed to be segmented into 5 separate rings, that would need to be stacked, aligned and post-machined to the 11.330 in internal diameter. The segmented rings can be seen in figure A.3. Each of these rings required 8 hours of print time, though 2-3X print time in setup and post-processing.

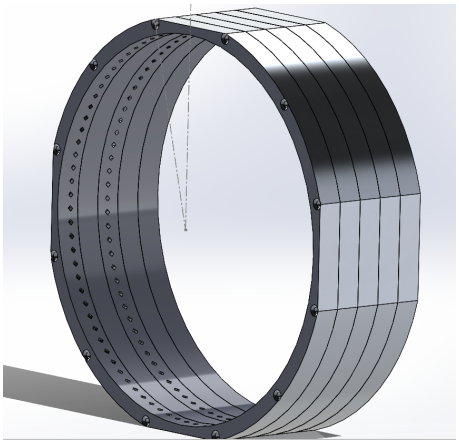

Figure A.1. ElemX Casing Treatment Assembly

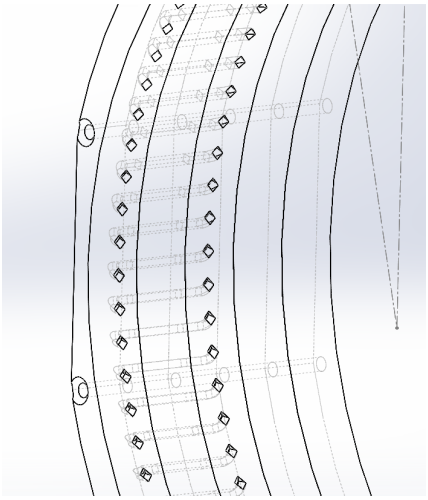

Figure A.2. View of the Passages in ElemX Casing Rings

Figure A.3. Separated ElemX Casing Rings

Figure A.4. ElemX 3D Printer Source: [19]

APPENDIX B:
A Comprehensive Guide to Hamming HPC

ENS N. Jack Spector

03/29/2023

A Comprehensive Guide to Getting Started on Hamming using ANSYS CFX

Hamming is one of the local high-performance supercomputers at NPS, which students can utilize to perform a variety of computationally intensive projects. In the case of Flow Control for the TCR, Hamming was used to run ANSYS CFX with large meshes on the order of 39 million elements over several 3300 iterations. Hamming operates by tasking jobs submitted to it with nodes, and one node contains either 32 or 64 processors (mostly 64). Allowing simulations to be run in parallel, using multiple cores, can greatly reduce the computation time needed for completion. Additionally, individual processors do take time to communicate information between each other, and the optimum number of processors given a certain mesh size can vary greatly; this is to say that more processors is not always better. Running multiple of the same simulation, but using different numbers of processors is often a good idea initially, and monitoring the CPU time between iterations can provide insight into how many CPUs is optimal for each computation case.

Below are a series of steps which outline how to download the necessary resources, and guidance on utilizing those resources, in order to submit a desired CFX job to be completed on Hamming.

Step 1: Read through the hamming WIKI

This will provide general guidance on what hamming is capable of and will go hand-in-hand with this gouge sheet. Many of the references and links below can also be found on this website, and the 'Gentle introduction to Hamming' page is very useful.

https://wiki.nps.edu/display/HPC/Getting+Started

Step 2: Go to the link below to set up an hpc account. (also accessible from link above)

An account is needed to obtain a working folder, and have access to hamming.

https://hamming.uc.nps.edu/ssar

The account request form should look like this:

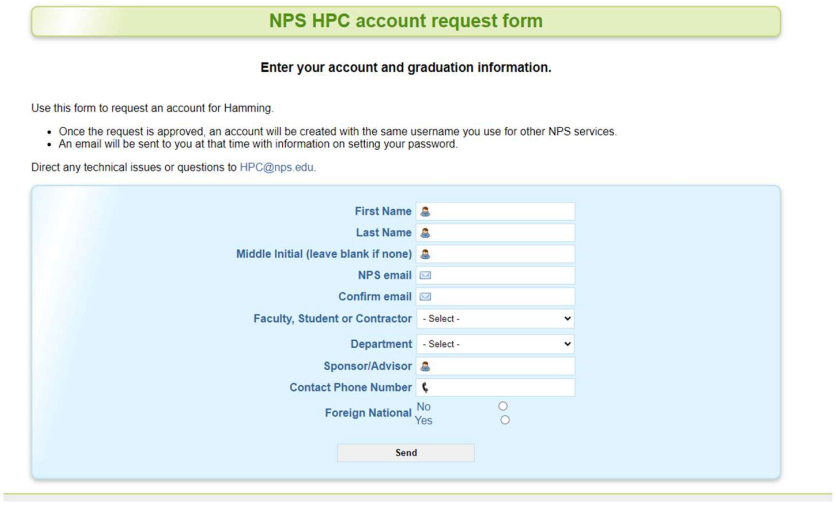

After which you should get this email either the day of submission, or the 1-2 days following:

Welcome to the hpc-hamming@lists.nps.edu mailing list!

To post to this list, send your email to:

hpc-hamming@lists.nps.edu

General information about the mailing list is at:

https://lists.nps.edu/mailman/listinfo/hpc-hamming

If you ever want to unsubscribe or change your options (eg, switch to or from digest mode, change your password, etc.), visit your subscription page at:

https://lists.nps.edu/mailman/options/hpc-hamming/norman.spector%40nps.edu

You can also make such adjustments via email by sending a message to:

hpc-hamming-request@lists.nps.edu

with the word `help' in the subject or body (don't include the quotes), and you will get back a message with instructions.

You must know your password to change your options (including changing the password, itself) or to unsubscribe. It is:

ohabummu

Step 3: Download MobaXTerm and WINSCP

https://mobaxterm.mobatek.net/

https://winscp.net/eng/download.php

These are also downloadable from just googling the names “winscp” and “mobaxterm” and should be the top results. Ensure for MobaXterm you download the free version. Each should be setup at a chosen location (most common is to simply setup on one’s desktop). These applications serve to allow commands to be sent and for file transfer between devices. MobaXterm allows one to change directories, convert .txt files from DOS to UNIX, and execute the commands for running jobs as well as monitor the contents of files. WINSCP allows you to transfer files between your dedicated folder on the hamming server, and your personal/work machine.

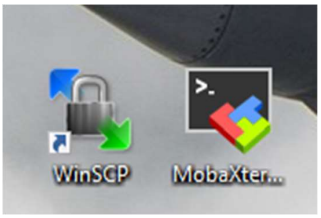

Step 4: Setup MobaXTerm and WINSCP

Once you have a hamming account from step 2, you will be able to login using both of these applications. Start MobaXterm and go to the “Sessions” tab in the top lefthand corner and make a “New Session.” You will then be prompted with the window below:

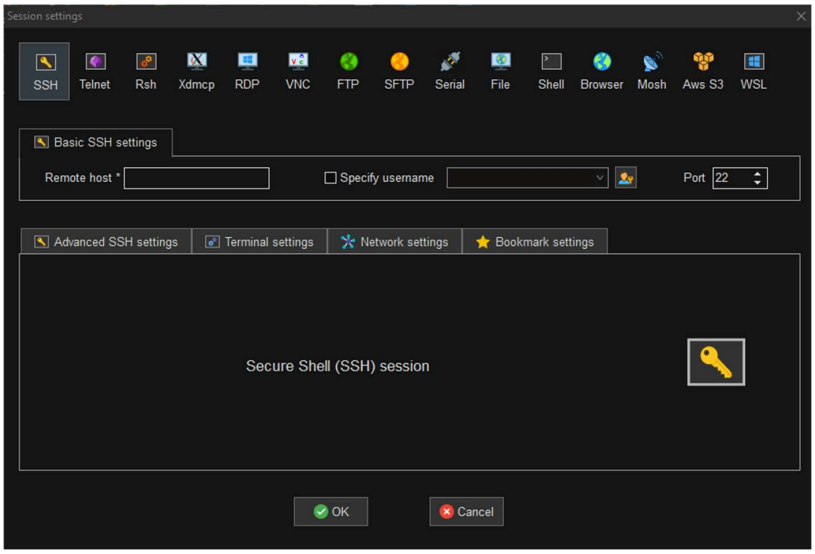

For Remote host, type in: hamming-sub1.uc.nps.edu

This is what tells the client what server you are looking to connect to, in this case the hamming server. You may then specify a username or click the icon to the right to specify a login that will autofill your name and password every time, or just type them in once prompted whenever you login to the server.

You may then click “OK” type your username when prompted by “login as” which will be you hamming account username, most likely your email without the “@NPS.edu” i.e. **norman.spector**

You will then be prompted for your password.

Note, when prompted for a password upon connecting you will not see anything whilst typing but it does work

Note, if off campus you must have a VPN connection to campus to login to the hamming server, info found at https://wiki.nps.edu/pages/viewpage.action?pageId=1192100676

If you are unable to login consider resetting your hpc account password with the link below, or email the help desk personnel at hpc-hamming-owner@lists.nps.edu

https://hamming.uc.nps.edu/ssp/

WINSCP

Similar to MobaXterm, WINSCP is used to access folders on one’s hamming account. It is mainly used, though for file transfer but is also extremely helpful for continuously monitoring runs as well as editing files. To login using WINSCP, open the application and click on “New Session” then enter the same information as above:

Host name: hamming-sub1.uc.nps.edu

User name: (Your username)

Password: (Your password)

And for convenience, the login can be saved so as to not require entering it each time one wants to connect. Again, one needs to be on the NPS local network or have a VPN.

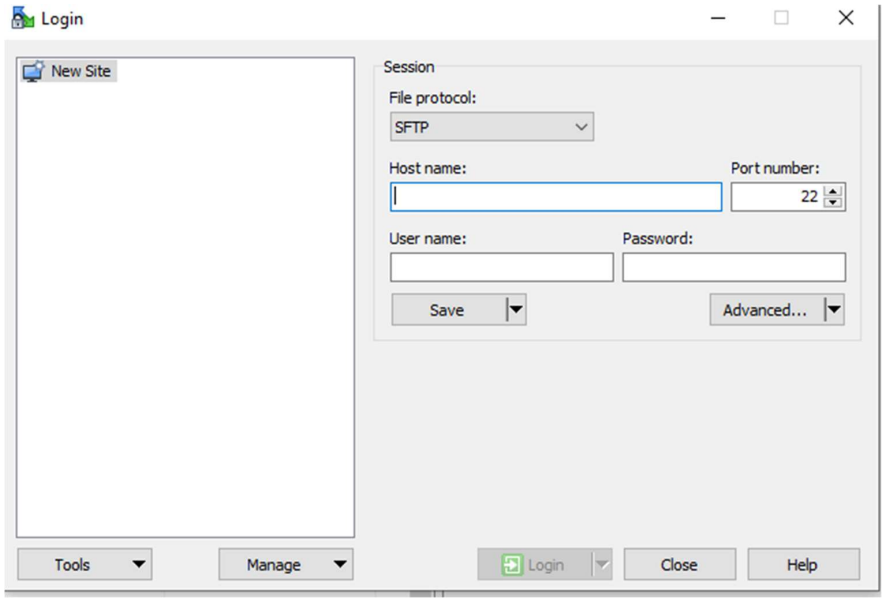

Step 5: Directory Navigation

There are three folders in every main account's directory, labeled 'archive', 'data', and 'smallwork'. For the purposes of running NASYS CFX jobs, all work should be done in the 'data' folder. Now one should familiarize oneself with some basic UNIX commands in order to be able to navigate the folders within MobaXterm. Navigation in WINSCP is much more intuitive, only requiring point-and-click. Some basic commands are outlined below:

Appendix: Essential Unix file commands

Name	Description	DOS equivalent
`ls`	List files in the current working directory	DIR
`mv`	Move or rename files	REN
`cp`	Copy files	COPY
`cd`	Change the current working directory	CD
`pwd`	Show the current working directory	CD (w/o arguments)
`cat`	Dump (concatenate) files to the screen	TYPE
`#`	A comment. Tells the shell to stop evaluating until the next line.	REM
`| less` or `| more`	(Placed after a command) Display the output of the program one page at a time, scroll with arrow keys or the space bar.	**MORE**
`rm`	Remove a file	DEL
`mkdir`	Make a new directory (folder)	MKDIR
`man (command name)`	Show the manual for (command name)	HELP
`nano`	A simple text-based file editor. (Usage: `^X` means Ctrl-x, `^O` means Ctrl-o, etc.)	EDIT

cd (desired directory name)	% changes directory to the one specified
squeue	% lists all of the jobs running and queued
squeue -u (your username)	% lists your jobs, their Job ID, status, and current runtime
q	% quits a window/ escape
less (filename)	% allows viewing of the contents of a file
dos2unix (filename)	% converts a .txt file from DOS to UNIX to be able to execute it
sbatch (filename)	% executes a batch file, used to actually submit a job
scancel (Job ID number)	% cancels job

Step 6: Submitting a Job

The final step covers exactly how to submit a job on Hamming. First, both a .def file and a batch file (.sh) will be needed.

Creating the .def file is straightforward. One needs to open the desired project in CFX Pre and go to the tools menu, and subsequently . This must be done in 'standalone' pre and not as part of a workbench file or the option will not be available. On any machine with ANSYS loaded simply hit the windows key, type 'CFX' and the application should pop up. From there click CFX-pre and open the desired project (even if it is in a workbench file, navigate to the source of that file wherever the workbench file is saved). Once ready to create the .def file, go to 'tools' → 'solve' → 'Write Solver input file'.

The batch file is a text file which sets up and opens the cfx solver and directs it to run the .def file. A sample batch file is presented below, inside of the two lines and with all necessary manual inputs specified with parentheses, i.e. (your input file name) would be something like: Casing_Treatment_90

```
#!/usr/bin/csh
#SBATCH --job-name=(Name for your job)
#SBATCH --error=(Name for your job).err.%j
#SBATCH --output=(Name for your job).out.%j
#SBATCH --time=500:10:00
#SBATCH --nodes=1
#SBATCH --ntasks=(Number of cores, usually put 64)
#SBATCH --tasks-per-node=(equal to number above)
#SBATCH --mem-per-cpu=1024M
#SBATCH --mail-type=END
#SBATCH --no-requeue

###. /etc/profile
module purge
module load app/ansys/20.2

set MYFILEHOSTS="hosts.$SLURM_JOB_ID"
srun hostname | sort > $MYFILEHOSTS
###echo $MYFILEHOSTS > test.hostlist.txt
###echo $MYFILEHOSTS
###set PARLIST=`cat $MYFILEHOSTS`
###echo $PARLIST
wait
```

```
foreach i (`scontrol show hostname "$SLURM_NODELIST" | tr "\n" " "`)
    set compnode=`grep "^${i}.hamming.cluster" ~/.ssh/known_hosts`
    if ("$compnode" == "" ) then
      ssh-keyscan -t ecdsa "${i}.hamming.cluster" | tee -a ~/.ssh/known_hosts;
    endif
end
sed -z 's/\n/,/g;s/,$/\n/' $MYFILEHOSTS > tmp.hosts
wait
set PARLIST=`cat tmp.hosts`
echo $PARLIST
wait
cfx5solve -size 2 -def (Your def file name).def -parallel -par-dist $PARLIST -start-method "Intel MPI Distributed Parallel"
```

Copying the text above and replacing the desired names with ones of your own (obviously for the .def file name it needs to match what you actually name your .def file) consists of making your batch file. Each .def file will need its own batch file to be run. This should be saved as a .txt file using a desired application (usually notepad). The next step for submission is transferring over the files to your hamming data directory. To do this, use WINSCP, find your saved files on the lefthand side and drag your .def and .txt file to your 'data' folder.

Next, your batch (.txt) file likely had DOS linebreaks, and as the workload manager, SLURM uses UNIX, you will need to convert your batch file from DOS to UNIX using the aforementioned command. This will be done using MobaXterm and this might look something like:

```
dos2unix Casing_Treatment_90.txt
```

Finally, the batch file needs the correct file extension, and so change the extension on your batch file from .txt to .sh and now you are ready to run! The only thing left to do is submit the job using the sbatch command, and use the queue viewing commands to ensure that the job is actually running. The submission command will look something like:

```
sbatch Casing_Treatment_90.sh
```

Step 7: Viewing Results

Viewing results is an integral part of hamming submissions, to be able to monitor the tail of the CFX output file to ensure the simulation is running, and to view any error codes. The batch script will generate three files, two immediately and one upon completion of the job (along with any intermediate results). A .out file will be created which contains the CFX tail and can be monitored using the 'less' or 'more' command inside of MobaXterm, and a .err file will contain any errors encountered. One can also view the contents of the .out file by double clicking it in WINSCP and hitting refresh, this is the preferred method of the author. Once complete the simulation will terminate and a .res file will be generated which can be copied back over to one's personal or work computer and loaded into Post.

THIS PAGE INTENTIONALLY LEFT BLANK

APPENDIX C:
Sensitivity Study Full Data Table

Casing Type	Specified ID	Actual ID 1	Actual ID 2	Actual ID 3	Actual ID 4	Average ID
ElemX 1	11.3	11.34	11.264	11.323	11.249	11.294
ElemX 2	11.3	11.285	11.26	11.249	11.36	11.2885
ElemX 3	11.3	11.286	11.282	11.267	11.324	11.28975
ElemX 4	11.3	11.307	11.272	11.338	11.242	11.28975
IP PC	11.33	11.333	11.333	11.332	11.3335	11.332875
NACAPC	11.33	11.327	11.328	11.3275	11.33	11.328125
NACA Alum	11.3	11.298	11.3015	11.301	11.302	11.300625

Once Mounted In TCR

NACA Polycarb Mounting Data	aft measure	t measure post tighten
	0.5075	0.528
	0.508	0.515

Error	Sigma ID	Specified OD	Actual OD 1	Actual OD 2	Actual OD 3	Actual OD 4	Average OD
0.05309735	0.0383471	12.8	12.769	12.8	12.812	12.778	12.78975
0.10176991	0.0432926	12.8	12.819	12.778	12.843	12.788	12.807
0.09070796	0.0210045	12.8	12.783	12.81	12.817	12.792	12.8005
0.09070796	0.0361274	12.8	12.824	12.837	12.8	12.83	12.82275
0.02537511	0.0005449	12.29	12.29	12.288	12.29	12.284	12.288
0.01654898	0.0011388	12.3	12.3	12.296	12.196	12.299	12.27275
0.00553097	0.0015562	12.315	12.315	12.313	12.315	12.316	12.31475

Error	Sigma OD	Ra (micro in)
0.01025	0.017093	Too Rough
0.007	0.0257	Too Rough
0.0005	0.013611	Too Rough
0.02275	0.013917	Too Rough
0.002	0.002449	658.85
0.02725	0.044336	665.6
0.00025	0.00109	532.23

THIS PAGE INTENTIONALLY LEFT BLANK

APPENDIX D:
ANSYS Mesh Reports

Ansys

Project

First Saved	Friday, January 13, 2023
Last Saved	Thursday, March 16, 2023
Product Version	2022 R1
Save Project Before Solution	No
Save Project After Solution	No

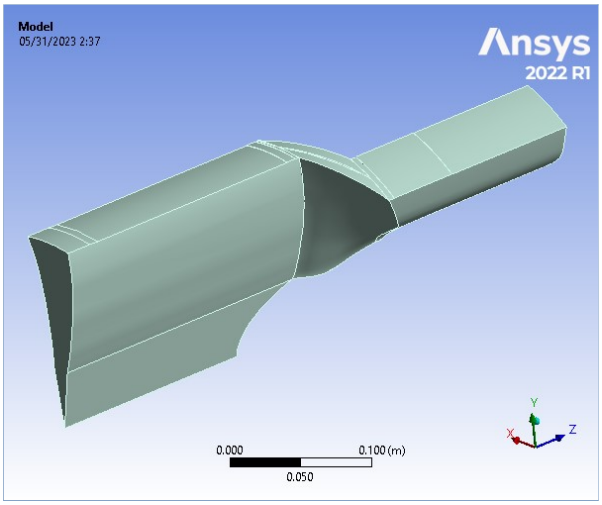

Contents

Units

TABLE 1

Unit System	Metric (m, kg, N, s, V, A) Degrees rad/s Celsius
Angle	Degrees
Rotational Velocity	rad/s
Temperature	Celsius

Model (A3)

TABLE 2
Model (A3) > Geometry Imports

Object Name	*Geometry Imports*
State	Solved

TABLE 3
Model (A3) > Geometry Imports > Geometry Import (A2)

Object Name	*Geometry Import (A2)*
State	Solved
Definition	
Source	C:\Users\garth\Downloads\OneDrive_2023-02-16\Gas Path Creation\Assembly for Blade Slicing.x_t
Type	Parasolid
Basic Geometry Options	
Solid Bodies	Yes
Surface Bodies	Yes
Line Bodies	Yes
Parameters	Independent
Parameter Key	
Attributes	Yes
Attribute Key	
Named Selections	Yes
Named Selection Key	
Material Properties	Yes
Advanced Geometry Options	
Use Associativity	Yes
Coordinate Systems	Yes
Coordinate System Key	
Reader Mode Saves Updated File	No
Use Instances	Yes
Smart CAD Update	Yes
Compare Parts On Update	No
Compare Parts Tolerance	Tight
Analysis Type	3-D
Mixed Import Resolution	None
Import Facet Quality	Source
Clean Bodies On Import	No
Stitch Surfaces On Import	Program Tolerance
Stitch Tolerance	0.0000001

Decompose Disjoint Geometry	Yes
Enclosure and Symmetry Processing	No

Geometry

TABLE 4
Model (A3) > Geometry

Object Name	*Geometry*
State	Fully Defined
Definition	
Source	C:\Users\garth\Downloads\OneDrive_2023-02-16\Gas Path Creation\Assembly for Blade Slicing.x_t
Type	Parasolid
Length Unit	Meters
Bounding Box	
Length X	0.1062 m
Length Y	0.14389 m
Length Z	0.40459 m
Properties	
Volume	1.0614e-003 m³
Scale Factor Value	1.
Statistics	
Bodies	2
Active Bodies	1
Nodes	8577123
Elements	21000809
Mesh Metric	None
Update Options	
Assign Default Material	No
Basic Geometry Options	
Solid Bodies	Yes
Surface Bodies	Yes
Line Bodies	Yes
Parameters	Independent
Parameter Key	
Attributes	Yes
Attribute Key	
Named Selections	Yes
Named Selection Key	
Material Properties	Yes
Advanced Geometry Options	
Use Associativity	Yes
Coordinate Systems	Yes
Coordinate System Key	
Reader Mode Saves Updated File	No
Use Instances	Yes
Smart CAD Update	Yes
Compare Parts On Update	No
Analysis Type	3-D
Mixed Import Resolution	None
Import Facet Quality	Source
Clean Bodies On Import	No
Stitch Surfaces On Import	Program Tolerance
Decompose Disjoint Geometry	Yes
Enclosure and Symmetry Processing	No

TABLE 5
Model (A3) > Geometry > Parts

Object Name	*OG_Blade_ColdShape_15TTG*	*CavityBoss*
State	Meshed	Suppressed
Graphics Properties		
Visible	Yes	
Transparency	1	
Definition		
Suppressed	No	Yes
Coordinate System	Default Coordinate System	
Treatment	None	
Reference Frame	Lagrangian	

Material		
Assignment		
Fluid/Solid	Defined By Geometry (Solid)	
Bounding Box		
Length X	0.1062 m	0. m
Length Y	0.14389 m	0. m
Length Z	0.40459 m	0. m
Properties		
Volume	1.0614e-003 m³	
Centroid X	-2.3283e-002 m	
Centroid Y	9.8485e-002 m	
Centroid Z	-2.853e-002 m	
Statistics		
Nodes	8577123	0
Elements	21000809	0
Mesh Metric	None	
CAD Attributes		
Color:202.209.237		

TABLE 6
Model (A3) > Materials

Object Name	*Materials*
State	Fully Defined
Statistics	
Materials	0
Material Assignments	0

Coordinate Systems

TABLE 7
Model (A3) > Coordinate Systems > Coordinate System

Object Name	*Global Coordinate System*
State	Fully Defined
Definition	
Type	Cartesian
Coordinate System ID	0.
Origin	
Origin X	0. m
Origin Y	0. m
Origin Z	0. m
Directional Vectors	
X Axis Data	[1. 0. 0.]
Y Axis Data	[0. 1. 0.]
Z Axis Data	[0. 0. 1.]

Connections

TABLE 8
Model (A3) > Connections

Object Name	*Connections*
State	Fully Defined
Auto Detection	
Generate Automatic Connection On Refresh	Yes
Transparency	
Enabled	Yes

Mesh

TABLE 9
Model (A3) > Mesh

Object Name	*Mesh*
State	Solved
Display	
Display Style	Use Geometry Setting
Defaults	
Physics Preference	CFD
Solver Preference	CFX

Element Order	Linear
Element Size	5.e-003 m
Sizing	
Use Adaptive Sizing	No
Growth Rate	Default (1.2)
Max Size	5.e-003 m
Mesh Defeaturing	Yes
Defeature Size	1.e-004 m
Capture Curvature	Yes
Curvature Min Size	5.e-004 m
Curvature Normal Angle	Default (18.0°)
Capture Proximity	Yes
Proximity Min Size	5.e-004 m
Proximity Gap Factor	5.0
Proximity Size Sources	Faces and Edges
Bounding Box Diagonal	0.46315 m
Average Surface Area	2.4119e-003 m²
Minimum Edge Length	3.764e-007 m
Quality	
Check Mesh Quality	Yes, Errors
Target Skewness	Default (0.9)
Smoothing	Medium
Mesh Metric	None
Inflation	
Use Automatic Inflation	None
Inflation Option	Smooth Transition
Transition Ratio	0.77
Maximum Layers	5
Growth Rate	1.2
Inflation Algorithm	Pre
View Advanced Options	No
Advanced	
Number of CPUs for Parallel Part Meshing	32
Straight Sided Elements	
Rigid Body Behavior	Dimensionally Reduced
Triangle Surface Mesher	Program Controlled
Topology Checking	Yes
Pinch Tolerance	Default (4.5e-004 m)
Generate Pinch on Refresh	No
Statistics	
Nodes	8577123
Elements	21000809

TABLE 10
Model (A3) > Mesh > Mesh Controls

Object Name	*Gas_Path_Match*	*Patch Conforming Method*	*BladeFace*	*BladeEdge*	*BladeBase*	*BladeBaseOuter*	*Blade_LE_TE*	*Inflation*	*Inflation 2*
State	Fully Defined								
Scope									
Scoping Method	Named Selection		Geometry Selection						
High Boundary	Periodic_High								
Low Boundary	Periodic_Low								
Named Selection		Gas_Path							
Geometry			2 Faces	5 Faces	6 Faces	1 Face	2 Faces	1 Body	
Definition									
Suppressed	No								
Transformation	Cyclic								
Axis of Rotation	Global Coordinate System								
Control Messages	No								
Method		Tetrahedrons							
Algorithm		Patch Conforming							
		Use Global							

Element Order		Setting				
Type			Element Size			
Element Size			2.5e-004 m	5.e-005 m	2.5e-004 m	5.e-005 m
Boundary Scoping Method					Named Selections	Geometry Selection
Boundary					Blade	7 Faces
Inflation Option					First Layer Thickness	
First Layer Height					1.e-006 m	
Maximum Layers					23	20
Growth Rate					1.2	
Inflation Algorithm					Pre	
Advanced						
Defeature Size		1.e-007 m				
Influence Volume		No				
Behavior		Soft				
Growth Rate		Default (1.2)				
Capture Curvature		No				
Capture Proximity		No				

TABLE 11
Model (A3) > Mesh Edit

Object Name	*Mesh Edit*
State	Solved
Auto Detection	
Generate Automatic Mesh Connections On Refresh	No
Transparency	
Enabled	Yes

Named Selections

TABLE 12
Model (A3) > Named Selections > Named Selections

Object Name	*Inlet*	*Outlet*	*Periodic_High*	*Periodic_Low*	*Inner_Wall*	*Gas_Path*	*Outer_Wall*	*Blade*	*Blisk_Minus_Blade*
State	Fully Defined								
Scope									
Scoping Method	Geometry Selection								
Geometry	1 Face		4 Faces		7 Faces	1 Body	15 Faces		5 Faces
Definition									
Send to Solver	Yes								
Protected	Program Controlled								
Visible	Yes								
Program Controlled Inflation	Exclude								
Statistics									
Type	Manual								
Total Selection	1 Face		4 Faces		7 Faces	1 Body	15 Faces		5 Faces
Surface Area	3.2389e-003 m²	1.8353e-003 m²	4.2538e-002 m²	4.2544e-002 m²	4.3381e-003 m²		1.8322e-002 m²	1.1733e-002 m²	8.6746e-004 m²
Suppressed	0								
Used by Mesh Worksheet	No								

Ansys

Project*

First Saved	Friday, January 13, 2023
Last Saved	Thursday, March 16, 2023
Product Version	2022 R1
Save Project Before Solution	No
Save Project After Solution	No

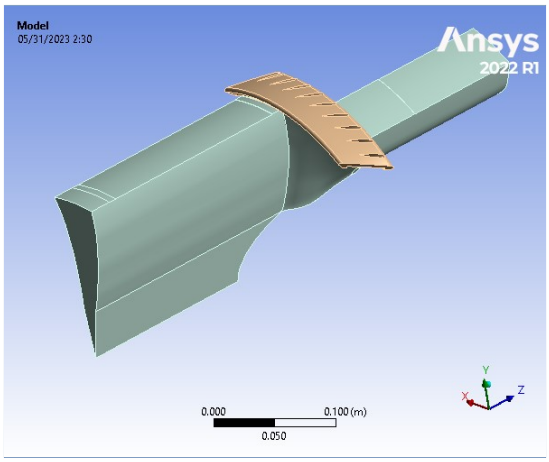

Contents

Report Not Finalized

Not all objects described below are in a finalized state. As a result, data may be incomplete, obsolete or in error. View first state problem. To finalize this report, edit objects as needed and solve the analyses.

Units

TABLE 1

Unit System	Metric (m, kg, N, s, V, A) Degrees rad/s Celsius
Angle	Degrees
Rotational Velocity	rad/s
Temperature	Celsius

Model (A3)

TABLE 2
Model (A3) > Geometry Imports

Object Name	*Geometry Imports*
State	Solved

TABLE 3
Model (A3) > Geometry Imports > Geometry Import (A2)

Object Name	*Geometry Import (A2)*
State	Solved
Definition	
Source	C:\Users\garth\Downloads\OneDrive_2023-02-16\Gas Path Creation\Assembly for Blade Slicing.x_t
Type	Parasolid
Basic Geometry Options	
Solid Bodies	Yes
Surface Bodies	Yes
Line Bodies	Yes
Parameters	Independent
Parameter Key	
Attributes	Yes
Attribute Key	
Named Selections	Yes
Named Selection Key	
Material Properties	Yes
Advanced Geometry Options	
Use Associativity	Yes
Coordinate Systems	Yes
Coordinate System Key	
Reader Mode Saves Updated File	No
Use Instances	Yes
Smart CAD Update	Yes
Compare Parts On Update	No
Compare Parts Tolerance	Tight
Analysis Type	3-D
Mixed Import Resolution	None
Import Facet Quality	Source
Clean Bodies On Import	No
Stitch Surfaces On Import	Program Tolerance
Stitch Tolerance	0.0000001
Decompose Disjoint Geometry	Yes
Enclosure and Symmetry Processing	No

Geometry

TABLE 4
Model (A3) > Geometry

Object Name	*Geometry*
State	Fully Defined
Definition	
Source	C:\Users\garth\Downloads\OneDrive_2023-02-16\Gas Path Creation\Assembly for Blade Slicing.x_t
Type	Parasolid

Length Unit	Meters
Bounding Box	
Length X	0.16 m
Length Y	0.15878 m
Length Z	0.40459 m
Properties	
Volume	1.092e-003 m³
Scale Factor Value	1.
Statistics	
Bodies	2
Active Bodies	2
Nodes	16204883
Elements	39351848
Mesh Metric	Element Quality
Min	2.3351e-005
Max	1.
Average	0.35602
Standard Deviation	0.35195
Update Options	
Assign Default Material	No
Basic Geometry Options	
Solid Bodies	Yes
Surface Bodies	Yes
Line Bodies	Yes
Parameters	Independent
Parameter Key	
Attributes	Yes
Attribute Key	
Named Selections	Yes
Named Selection Key	
Material Properties	Yes
Advanced Geometry Options	
Use Associativity	Yes
Coordinate Systems	Yes
Coordinate System Key	
Reader Mode Saves Updated File	No
Use Instances	Yes
Smart CAD Update	Yes
Compare Parts On Update	No
Analysis Type	3-D
Mixed Import Resolution	None
Import Facet Quality	Source
Clean Bodies On Import	No
Stitch Surfaces On Import	Program Tolerance
Decompose Disjoint Geometry	Yes
Enclosure and Symmetry Processing	No

TABLE 5
Model (A3) > Geometry > Parts

Object Name	*OG_Blade_ColdShape_15TTG*	*CavityBoss*
State	Meshed	
Graphics Properties		
Visible	Yes	
Transparency	1	
Definition		
Suppressed	No	
Coordinate System	Default Coordinate System	
Treatment	None	
Reference Frame	Lagrangian	
Material		
Assignment		
Fluid/Solid	Defined By Geometry (Solid)	
Bounding Box		
Length X	0.1062 m	0.16 m
Length Y	0.14389 m	6.664e-002 m
Length Z	0.40459 m	4.2893e-002 m
Properties		
Volume	1.0614e-003 m³	3.0575e-005 m³
Centroid X	-2.3283e-002 m	-4.4867e-002 m
Centroid Y	9.8485e-002 m	0.1356 m
Centroid Z	-2.853e-002 m	2.0585e-002 m
Statistics		
Nodes	10663859	5541024
Elements	25425136	13926712
Mesh Metric	Element Quality	
Min	2.3351e-005	1.1645e-004
Max	1.	
Average	0.37701	0.31771
Standard Deviation	0.34142	0.36733
CAD Attributes		
Color:202.209.237		
Color:202.209.238		

TABLE 6
Model (A3) > Materials

Object Name	*Materials*
State	Fully Defined
Statistics	

Materials	0
Material Assignments	0

Coordinate Systems

TABLE 7
Model (A3) > Coordinate Systems > Coordinate System

Object Name	*Global Coordinate System*
State	Fully Defined
Definition	
Type	Cartesian
Coordinate System ID	0.
Origin	
Origin X	0. m
Origin Y	0. m
Origin Z	0. m
Directional Vectors	
X Axis Data	[1. 0. 0.]
Y Axis Data	[0. 1. 0.]
Z Axis Data	[0. 0. 1.]

Connections

TABLE 8
Model (A3) > Connections

Object Name	*Connections*
State	Fully Defined
Auto Detection	
Generate Automatic Connection On Refresh	Yes
Transparency	
Enabled	Yes

TABLE 9
Model (A3) > Connections > Contacts

Object Name	*Contacts*
State	Fully Defined
Definition	
Connection Type	Contact
Scope	
Scoping Method	Geometry Selection
Geometry	All Bodies
Auto Detection	
Tolerance Type	Slider
Tolerance Slider	0.
Tolerance Value	1.1579e-003 m
Use Range	No
Face/Face	Yes
Face-Face Angle Tolerance	75. °
Face Overlap Tolerance	Off
Cylindrical Faces	Include
Face/Edge	No
Edge/Edge	No
Priority	Include All
Group By	Bodies
Search Across	Bodies
Statistics	
Connections	1
Active Connections	1

TABLE 10
Model (A3) > Connections > Contacts > Contact Regions

Object Name	*Contact Region 2*
State	Fully Defined
Scope	
Scoping Method	Geometry Selection
Contact	6 Faces
Target	6 Faces
Contact Bodies	OG_Blade_ColdShape_15TTG
Target Bodies	CavityBoss
Protected	No
Advanced	
Small Sliding	Program Controlled

Mesh

TABLE 11
Model (A3) > Mesh

Object Name	*Mesh*
State	Solved
Display	
Display Style	Use Geometry Setting
Defaults	
Physics Preference	CFD
Solver Preference	CFX
Element Order	Linear
Element Size	5.e-003 m
Sizing	
Use Adaptive Sizing	No

Growth Rate	Default (1.2)
Max Size	5.e-003 m
Mesh Defeaturing	Yes
Defeature Size	1.e-004 m
Capture Curvature	Yes
Curvature Min Size	5.e-004 m
Curvature Normal Angle	Default (18.0°)
Capture Proximity	Yes
Proximity Min Size	5.e-004 m
Proximity Gap Factor	5.0
Proximity Size Sources	Faces and Edges
Bounding Box Diagonal	0.46315 m
Average Surface Area	1.4875e-003 m²
Minimum Edge Length	3.764e-007 m
Quality	
Check Mesh Quality	Yes, Errors
Target Skewness	Default (0.9)
Smoothing	Medium
Mesh Metric	Element Quality
Min	2.3351e-005
Max	1.
Average	0.35602
Standard Deviation	0.35195
Inflation	
Use Automatic Inflation	None
Inflation Option	Smooth Transition
Transition Ratio	0.77
Maximum Layers	5
Growth Rate	1.2
Inflation Algorithm	Pre
View Advanced Options	No
Advanced	
Number of CPUs for Parallel Part Meshing	32
Straight Sided Elements	
Rigid Body Behavior	Dimensionally Reduced
Triangle Surface Mesher	Program Controlled
Topology Checking	Yes
Pinch Tolerance	Default (4.5e-004 m)
Generate Pinch on Refresh	No
Statistics	
Nodes	16204883
Elements	39351848

TABLE 12
Model (A3) > Mesh > Mesh Controls

Object Name	*Gas_Path_Match*	*Treatment_Match*	*Patch Conforming Method*	*Blade Faces*	*Blade LE TE*	*Blade Tip*	*Blade Base*	*Blade Base Outer*	*Inflation*	*Treatment*	*Treatment Sizing*
State	Fully Defined										
Scope											
Scoping Method	Named Selection			Geometry Selection							Named Selection
High Boundary	Periodic_High	Treatment_Periodic_High									
Low Boundary	Periodic_Low	Treatment_Periodic_Low									
Named Selection			Gas_Path								Treatment_Wall
Geometry				2 Faces		5 Faces	6 Faces	3 Faces	1 Body		
Definition											
Suppressed	No										
Transformation	Cyclic										
Axis of Rotation	Global Coordinate System										
Control Messages	No										
Method			Tetrahedrons								
Algorithm			Patch Conforming								
Element Order			Use Global Setting								
Type				Element Size							Element Size
Element Size				2.5e-004 m	5.e-005 m	2.5e-005 m	2.5e-004 m				2.5e-004 m
Boundary Scoping Method									Named Selections		
Boundary									Multiple Entities	Treatment_Wall	
Inflation Option									First Layer Thickness		
First Layer Height									1.e-006 m		
Maximum Layers									23	20	
Growth Rate									1.2		
Inflation Algorithm									Pre		
Advanced											
Defeature Size				1.e-007 m							1.e-007 m
Influence Volume				No							No
Behavior				Soft							Soft
Growth Rate				Default (1.2)							Default (1.2)
Capture Curvature				No							No
Capture Proximity				No							No

TABLE 13
Model (A3) > Mesh Edit

Object Name	*Mesh Edit*
State	Solved
Auto Detection	

Generate Automatic Mesh Connections On Refresh	No
Transparency	
Enabled	Yes

TABLE 14
Model (A3) > Mesh Edit > Contact Match Group

Object Name	*Contact Match Group*
State	Not Solved
Scope	
Scoping Method	Geometry Selection
Geometry	All Bodies
Definition	
Suppressed	No
Auto Detection	
Tolerance Type	Slider
Tolerance Slider	0.
Tolerance Value	1.1579e-003 m
Use Range	No
Group By	Bodies
Search Across	Bodies
Statistics	
Connections	0
Active Connections	0

Named Selections

TABLE 15
Model (A3) > Named Selections > Named Selections

Object Name	*Inlet*	*Outlet*	*Periodic_High*	*Periodic_Low*	*Inner_Wall*	*Treatment*	*Gas_Path*	*Forward_Gas_Interface1*	*Aft_Gas_Interface1*	*Outer_Wall*	*Blade*
State	Fully Defined										
Scope											
Scoping Method	Geometry Selection										
Geometry	1 Face		4 Faces		7 Faces	1 Body		1 Face		9 Faces	15 Faces
Definition											
Send to Solver	Yes										
Protected	Program Controlled										
Visible	Yes										
Program Controlled Inflation	Exclude										
Statistics											
Type	Manual										
Total Selection	1 Face		4 Faces		7 Faces	1 Body		1 Face		9 Faces	15 Faces
Surface Area	3.2389e-003 m²	1.8353e-003 m²	4.2538e-002 m²	4.2544e-002 m²	4.3381e-003 m²			1.3009e-004 m²	2.1451e-004 m²	1.7928e-002 m²	1.1733e-002 m²
Suppressed	0										
Used by Mesh Worksheet	No										

TABLE 16
Model (A3) > Named Selections > Named Selections

Object Name	*Blisk_Minus_Blade*	*Forward_Treatment_Interface1*	*Aft_Treatment_Interface1*	*Treatment_Periodic_High*	*Treatment_Periodic_Low*	*Treatment_Wall*	*Forward_Gas_Interfac*
State	Fully Defined						
Scope							
Scoping Method	Geometry Selection						
Geometry	5 Faces	1 Face				35 Faces	
Definition							
Send to Solver	Yes						
Protected	Program Controlled						
Visible	Yes						
Program Controlled Inflation	Exclude						
Statistics							
Type	Manual						
Total Selection	5 Faces	1 Face				35 Faces	
Surface Area	8.6746e-004 m²	3.8923e-004 m²	6.4302e-004 m²	2.6927e-004 m²		1.4162e-002 m²	1.3606e-005 m²
Suppressed	0						
Used by Mesh Worksheet	No						

TABLE 17
Model (A3) > Named Selections > Named Selections

Object Name	*Forward_Treatment_Interface3*	*Aft_Treatment_Interface2*	*Aft_Treatment_Interface3*
State	Fully Defined		
Scope			
Scoping Method	Geometry Selection		
Geometry	1 Face		
Definition			
Send to Solver	Yes		
Protected	Program Controlled		
Visible	Yes		
Program Controlled Inflation	Exclude		
Statistics			

Type	Manual		
Total Selection	1 Face		
Surface Area	3.4245e-005 m²	4.5189e-005 m²	3.4585e-005 m²
Suppressed	0		
Used by Mesh Worksheet	No		

Ansys

Project

First Saved	Friday, January 13, 2023
Last Saved	Monday, April 24, 2023
Product Version	2022 R1
Save Project Before Solution	No
Save Project After Solution	No

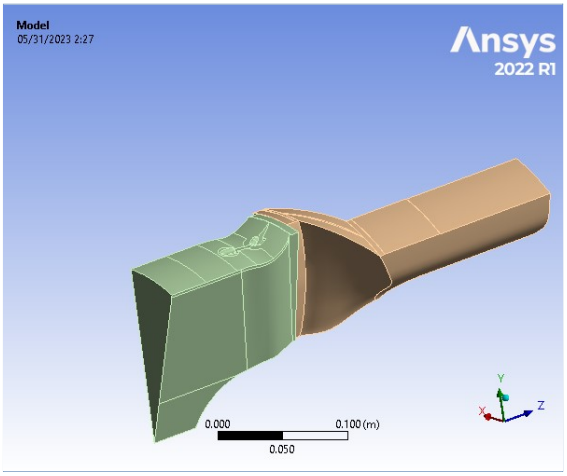

Contents

Report Not Finalized

Not all objects described below are in a finalized state. As a result, data may be incomplete, obsolete or in error. View first state problem. To finalize this report, edit objects as needed and solve the analyses.

Units

TABLE 1

Unit System	Metric (m, kg, N, s, V, A) Degrees rad/s Celsius
Angle	Degrees
Rotational Velocity	rad/s
Temperature	Celsius

Model (A3)

TABLE 2
Model (A3) > Geometry Imports

Object Name	*Geometry Imports*
State	Solved

TABLE 3
Model (A3) > Geometry Imports > Geometry Import (A2)

Object Name	*Geometry Import (A2)*
State	Solved
Definition	
Source	C:\Users\njack\OneDrive\Desktop\IGV Creation\Gas Path Creation\Assembly for Blade SlicingIGV_V14.x_t
Type	Parasolid
Basic Geometry Options	
Solid Bodies	Yes
Surface Bodies	Yes
Line Bodies	No
Parameters	Independent
Parameter Key	ANS;DS
Attributes	No
Attribute Key	SDFEA;DDM
Named Selections	No
Named Selection Key	NS
Material Properties	No
Advanced Geometry Options	
Use Associativity	Yes
Coordinate Systems	No
Coordinate System Key	
Reader Mode Saves Updated File	No
Use Instances	Yes
Smart CAD Update	Yes
Compare Parts On Update	No
Compare Parts Tolerance	Tight
Analysis Type	3-D
Mixed Import Resolution	None
Import Facet Quality	Source
Clean Bodies On Import	No
Stitch Surfaces On Import	None
Stitch Tolerance	0.0000001
Decompose Disjoint Geometry	Yes
Enclosure and Symmetry Processing	No

Geometry

TABLE 4
Model (A3) > Geometry

Object Name	*Geometry*
State	Fully Defined

Definition	
Source	C:\Users\njack\OneDrive\Desktop\IGV Creation\Gas Path Creation\Assembly for Blade SlicingIGV_V14.x_t
Type	Parasolid
Length Unit	Meters
Bounding Box	
Length X	0.12966 m
Length Y	0.15595 m
Length Z	0.33744 m
Properties	
Volume	8.8534e-004 m³
Scale Factor Value	1.
Statistics	
Bodies	2
Active Bodies	2
Nodes	16092228
Elements	40335461
Mesh Metric	None
Update Options	
Assign Default Material	No
Basic Geometry Options	
Solid Bodies	Yes
Surface Bodies	Yes
Line Bodies	No
Parameters	Independent
Parameter Key	ANS;DS
Attributes	No
Named Selections	No
Material Properties	No
Advanced Geometry Options	
Use Associativity	Yes
Coordinate Systems	No
Reader Mode Saves Updated File	No
Use Instances	Yes
Smart CAD Update	Yes
Compare Parts On Update	No
Analysis Type	3-D
Mixed Import Resolution	None
Import Facet Quality	Source
Clean Bodies On Import	No
Stitch Surfaces On Import	None
Decompose Disjoint Geometry	Yes
Enclosure and Symmetry Processing	No

TABLE 5
Model (A3) > Geometry > Parts

Object Name	*IGV_Geom*	*OG_Blade_ColdShape_15TTGIGV*
State	Meshed	
Graphics Properties		
Visible	Yes	
Transparency	1	
Definition		
Suppressed	No	
Coordinate System	Default Coordinate System	
Treatment	None	
Reference Frame	Lagrangian	
Material		
Assignment		
Fluid/Solid	Defined By Geometry (Solid)	
Bounding Box		
Length X	9.9888e-002 m	0.1062 m
Length Y	0.15595 m	9.927e-002 m
Length Z	0.13424 m	0.2032 m
Properties		
Volume	4.6938e-004 m³	4.1597e-004 m³
Centroid X	-2.0069e-002 m	-4.9533e-002 m
Centroid Y	9.6336e-002 m	0.10277 m
Centroid Z	-7.3699e-002 m	9.0843e-002 m
Statistics		
Nodes	7368366	8723862
Elements	19217720	21117741
Mesh Metric	None	

TABLE 6
Model (A3) > Materials

Object Name	*Materials*
State	Fully Defined
Statistics	
Materials	0
Material Assignments	0

Coordinate Systems

TABLE 7
Model (A3) > Coordinate Systems > Coordinate System

Object Name	*Global Coordinate System*

State	Fully Defined
Definition	
Type	Cartesian
Coordinate System ID	0.
Origin	
Origin X	0. m
Origin Y	0. m
Origin Z	0. m
Directional Vectors	
X Axis Data	[1. 0. 0.]
Y Axis Data	[0. 1. 0.]
Z Axis Data	[0. 0. 1.]

Connections

TABLE 8
Model (A3) > Connections

Object Name	*Connections*
State	Fully Defined
Auto Detection	
Generate Automatic Connection On Refresh	Yes
Transparency	
Enabled	Yes

TABLE 9
Model (A3) > Connections > Contacts

Object Name	*Contacts*
State	Fully Defined
Definition	
Connection Type	Contact
Scope	
Scoping Method	Geometry Selection
Geometry	All Bodies
Auto Detection	
Tolerance Type	Slider
Tolerance Slider	0.
Tolerance Value	9.8425e-004 m
Use Range	No
Face/Face	Yes
Face-Face Angle Tolerance	75. °
Face Overlap Tolerance	Off
Cylindrical Faces	Include
Face/Edge	No
Edge/Edge	No
Priority	Include All
Group By	Bodies
Search Across	Bodies
Statistics	
Connections	1
Active Connections	1

TABLE 10
Model (A3) > Connections > Contacts > Contact Regions

Object Name	*Contact Region 3*
State	Fully Defined
Scope	
Scoping Method	Geometry Selection
Contact	1 Face
Target	1 Face
Contact Bodies	IGV_Geom
Target Bodies	OG_Blade_ColdShape_15TTGIGV
Protected	No
Advanced	
Small Sliding	Program Controlled

Mesh

TABLE 11
Model (A3) > Mesh

Object Name	*Mesh*
State	Solved
Display	
Display Style	Use Geometry Setting
Defaults	
Physics Preference	CFD
Solver Preference	CFX
Element Order	Linear
Element Size	5.e-003 m
Sizing	
Use Adaptive Sizing	No
Growth Rate	Default (1.2)
Max Size	5.e-003 m
Mesh Defeaturing	Yes
Defeature Size	1.e-004 m
Capture Curvature	Yes

Curvature Min Size	5.e-004 m
Curvature Normal Angle	Default (18.0°)
Capture Proximity	Yes
Proximity Min Size	5.e-004 m
Proximity Gap Factor	5.0
Proximity Size Sources	Faces and Edges
Bounding Box Diagonal	0.3937 m
Average Surface Area	1.2166e-003 m²
Minimum Edge Length	3.764e-007 m
Quality	
Check Mesh Quality	Yes, Errors
Target Skewness	Default (0.9)
Smoothing	Medium
Mesh Metric	None
Inflation	
Use Automatic Inflation	None
Inflation Option	Smooth Transition
Transition Ratio	0.77
Maximum Layers	5
Growth Rate	1.2
Inflation Algorithm	Pre
View Advanced Options	No
Advanced	
Number of CPUs for Parallel Part Meshing	32
Straight Sided Elements	
Rigid Body Behavior	Dimensionally Reduced
Triangle Surface Mesher	Program Controlled
Topology Checking	Yes
Pinch Tolerance	Default (4.5e-004 m)
Generate Pinch on Refresh	No
Statistics	
Nodes	16092228
Elements	40335461

TABLE 12
Model (A3) > Mesh > Mesh Controls

Object Name	*Gas_Path_Match*	*Patch Conforming Method*	*BladeFace*	*BladeEdge*	*BladeBase*	*BladeBaseOuter*	*Blade_LE_TE*	*Inflation*	*Match Control*	*Inflation 2*	*IGV_OuterWall*
State	Fully Defined										
Scope											
Scoping Method	Named Selection		Geometry Selection						Named Selection	Geometry Selection	Named Selection
High Boundary	Periodic_High								IGV_Periodic_High		
Low Boundary	Periodic_Low								IGV_Periodic_Low		
Named Selection		Gas_Path									IGV_OuterWall
Geometry			2 Faces	5 Faces	6 Faces	3 Faces	2 Faces	1 Body		1 Body	
Definition											
Suppressed	No										
Transformation	Cyclic								Cyclic		
Axis of Rotation	Global Coordinate System								Global Coordinate System		
Control Messages	No								No		
Method		Tetrahedrons									
Algorithm		Patch Conforming									
Element Order		Use Global Setting									
Type			Element Size								Element Size
Element Size			2.5e-004 m	5.e-005 m	2.5e-004 m		5.e-005 m				5.e-004 m
Boundary Scoping Method								Named Selections		Geometry Selection	
Boundary								Multiple Entities		19 Faces	
Inflation Option								First Layer Thickness		First Layer Thickness	
First Layer Height								1.e-006 m		1.e-006 m	
Maximum Layers								23		20	
Growth Rate								1.2		1.2	
Inflation Algorithm								Pre		Pre	
Advanced											
Defeature Size			1.e-007 m								1.e-007 m
Influence Volume			No								No
Behavior			Soft								Soft
Growth Rate			Default (1.2)								Default (1.2)
Capture Curvature			No								No
Capture											

Proximity		No		No

TABLE 13
Model (A3) > Mesh > Mesh Controls

Object Name	*IGV_Blades*
State	Fully Defined
Scope	
Scoping Method	Named Selection
Named Selection	IGV_Blades
Definition	
Suppressed	No
Type	Element Size
Element Size	2.e-004 m
Advanced	
Defeature Size	1.e-007 m
Influence Volume	No
Behavior	Soft
Growth Rate	Default (1.2)
Capture Curvature	No
Capture Proximity	No

TABLE 14
Model (A3) > Mesh Edit

Object Name	*Mesh Edit*
State	Solved
Auto Detection	
Generate Automatic Mesh Connections On Refresh	No
Transparency	
Enabled	Yes

TABLE 15
Model (A3) > Mesh Edit > Contact Match Group

Object Name	*Contact Match Group*
State	Not Solved
Scope	
Scoping Method	Geometry Selection
Geometry	All Bodies
Definition	
Suppressed	No
Auto Detection	
Tolerance Type	Slider
Tolerance Slider	0.
Tolerance Value	9.8425e-004 m
Use Range	No
Group By	Bodies
Search Across	Bodies
Statistics	
Connections	0
Active Connections	0

Named Selections

TABLE 16
Model (A3) > Named Selections > Named Selections

Object Name	*Inlet*	*Outlet*	*Periodic_High*	*Periodic_Low*	*Inner_Wall*	*Gas_Path*	*Outer_Wall*	*Blade*	*Blisk_Minus_Blade*	*IGV*	*IGV_Periodic_High*
State	Fully Defined										
Scope											
Scoping Method	Geometry Selection										
Geometry	1 Face		4 Faces		9 Faces	1 Body	11 Faces	15 Faces	3 Faces	1 Body	6 Faces
Definition											
Send to Solver	Yes										
Protected	Program Controlled										
Visible	Yes										
Program Controlled Inflation	Exclude										
Statistics											
Type	Manual										
Total Selection	1 Face		4 Faces		9 Faces	1 Body	11 Faces	15 Faces	3 Faces	1 Body	6 Faces
Surface Area	2.9124e-003 m²	1.8353e-003 m²	1.4757e-002 m²	1.4759e-002 m²	4.3055e-003 m²		9.2263e-003 m²	1.1729e-002 m²	3.6098e-004 m²		1.6153e-002 m²
Suppressed	0										
Used by Mesh Worksheet	No										

TABLE 17
Model (A3) > Named Selections > Named Selections

Object Name	*IGV_Periodic_Low*	*IGV_Inlet*	*IGV_InnerWall*	*IGV_OuterWall*	*IGV_Outlet*	*IGV_Blades*
State	Fully Defined					
Scope						
Scoping Method	Geometry Selection					
Geometry	6 Faces	1 Face	2 Faces	11 Faces	1 Face	23 Faces
Definition						
Send to Solver	Yes					
Protected	Program Controlled					

Visible	Yes					
Program Controlled Inflation	Exclude					
Statistics						
Type	Manual					
Total Selection	6 Faces	1 Face	2 Faces	11 Faces	1 Face	23 Faces
Surface Area	1.6163e-002 m²	3.8108e-003 m²	1.2498e-003 m²	6.8072e-003 m²	3.4331e-003 m²	1.1725e-002 m²
Suppressed	0					
Used by Mesh Worksheet	No					

Ansys

Project*

First Saved	Friday, January 13, 2023
Last Saved	Sunday, May 14, 2023
Product Version	2022 R1
Save Project Before Solution	No
Save Project After Solution	No

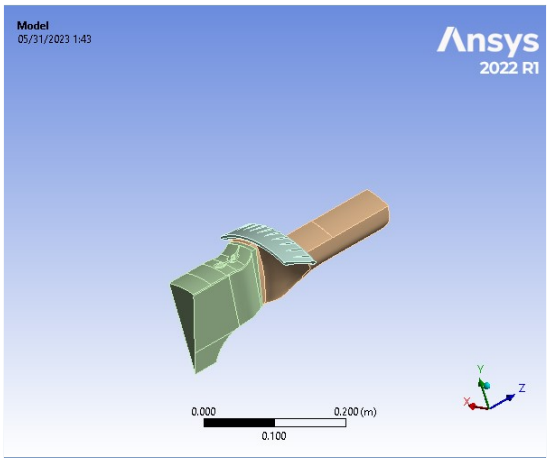

Contents

Report Not Finalized

Not all objects described below are in a finalized state. As a result, data may be incomplete, obsolete or in error. View first state problem. To finalize this report, edit objects as needed and solve the analyses.

Units

TABLE 1

Unit System	Metric (m, kg, N, s, V, A) Degrees rad/s Celsius
Angle	Degrees
Rotational Velocity	rad/s
Temperature	Celsius

Model (A3)

TABLE 2
Model (A3) > Geometry Imports

Object Name	*Geometry Imports*
State	Solved

TABLE 3
Model (A3) > Geometry Imports > Geometry Import (A2)

Object Name	*Geometry Import (A2)*
State	Solved
Definition	
Source	C:\Users\njack\OneDrive\Desktop\IGV Creation\Gas Path Creation\Assembly for Blade SlicingIGV+NACA_V1.x_t
Type	Parasolid
Basic Geometry Options	
Solid Bodies	Yes
Surface Bodies	Yes
Line Bodies	No
Parameters	Independent
Parameter Key	ANS;DS
Attributes	No
Attribute Key	SDFEA;DDM
Named Selections	No
Named Selection Key	NS
Material Properties	No
Advanced Geometry Options	
Use Associativity	Yes
Coordinate Systems	No
Coordinate System Key	
Reader Mode Saves Updated File	No
Use Instances	Yes
Smart CAD Update	Yes
Compare Parts On Update	No
Compare Parts Tolerance	Tight
Analysis Type	3-D
Mixed Import Resolution	None
Import Facet Quality	Source
Clean Bodies On Import	No
Stitch Surfaces On Import	None
Stitch Tolerance	0.0000001
Decompose Disjoint Geometry	Yes
Enclosure and Symmetry Processing	No

Geometry

TABLE 4
Model (A3) > Geometry

Object Name	*Geometry*
State	Fully Defined
Definition	
Source	C:\Users\njack\OneDrive\Desktop\IGV Creation\Gas Path Creation\Assembly for Blade SlicingIGV+NACA_V1.x_t
Type	Parasolid

Length Unit	Meters
Bounding Box	
Length X	0.15852 m
Length Y	0.16201 m
Length Z	0.33744 m
Properties	
Volume	9.1592e-004 m³
Scale Factor Value	1.
Statistics	
Bodies	3
Active Bodies	3
Nodes	20806217
Elements	52596467
Mesh Metric	None
Update Options	
Assign Default Material	No
Basic Geometry Options	
Solid Bodies	Yes
Surface Bodies	Yes
Line Bodies	No
Parameters	Independent
Parameter Key	ANS;DS
Attributes	No
Named Selections	No
Material Properties	No
Advanced Geometry Options	
Use Associativity	Yes
Coordinate Systems	No
Reader Mode Saves Updated File	No
Use Instances	Yes
Smart CAD Update	Yes
Compare Parts On Update	No
Analysis Type	3-D
Mixed Import Resolution	None
Import Facet Quality	Source
Clean Bodies On Import	No
Stitch Surfaces On Import	None
Decompose Disjoint Geometry	Yes
Enclosure and Symmetry Processing	No

TABLE 5
Model (A3) > Geometry > Parts

Object Name	*IGV_Geom*	*OG_Blade_ColdShape_15TTGIGV*	*CavityBoss*
State	Meshed		
Graphics Properties			
Visible	Yes		
Transparency	1		
Definition			
Suppressed	No		
Coordinate System	Default Coordinate System		
Treatment	None		
Reference Frame	Lagrangian		
Material			
Assignment			
Fluid/Solid	Defined By Geometry (Solid)		
Bounding Box			
Length X	9.9888e-002 m	0.1062 m	0.15852 m
Length Y	0.15595 m	9.927e-002 m	5.6729e-002 m
Length Z	0.13424 m	0.2032 m	4.2893e-002 m
Properties			
Volume	4.6938e-004 m³	4.1597e-004 m³	3.0575e-005 m³
Centroid X	-2.0069e-002 m	-4.9533e-002 m	-3.5728e-002 m
Centroid Y	9.6336e-002 m	0.10277 m	0.13829 m
Centroid Z	-7.3699e-002 m	9.0843e-002 m	2.0585e-002 m
Statistics			
Nodes	6670777	8594888	5540552
Elements	17806481	20866516	13923470
Mesh Metric	None		

TABLE 6
Model (A3) > Materials

Object Name	*Materials*
State	Fully Defined
Statistics	
Materials	0
Material Assignments	0

Coordinate Systems

TABLE 7
Model (A3) > Coordinate Systems > Coordinate System

Object Name	*Global Coordinate System*
State	Fully Defined
Definition	
Type	Cartesian
Coordinate System ID	0.
Origin	
Origin X	0. m

Origin Y	0. m
Origin Z	0. m
Directional Vectors	
X Axis Data	[1. 0. 0.]
Y Axis Data	[0. 1. 0.]
Z Axis Data	[0. 0. 1.]

Connections

TABLE 8
Model (A3) > Connections

Object Name	*Connections*
State	Fully Defined
Auto Detection	
Generate Automatic Connection On Refresh	Yes
Transparency	
Enabled	Yes

TABLE 9
Model (A3) > Connections > Contacts

Object Name	*Contacts*
State	Fully Defined
Definition	
Connection Type	Contact
Scope	
Scoping Method	Geometry Selection
Geometry	All Bodies
Auto Detection	
Tolerance Type	Slider
Tolerance Slider	0.
Tolerance Value	1.0163e-003 m
Use Range	No
Face/Face	Yes
Face-Face Angle Tolerance	75. °
Face Overlap Tolerance	Off
Cylindrical Faces	Include
Face/Edge	No
Edge/Edge	No
Priority	Include All
Group By	Bodies
Search Across	Bodies
Statistics	
Connections	2
Active Connections	2

TABLE 10
Model (A3) > Connections > Contacts > Contact Regions

Object Name	*Contact Region*	*Contact Region 2*
State	Fully Defined	
Scope		
Scoping Method	Geometry Selection	
Contact	1 Face	6 Faces
Target	1 Face	6 Faces
Contact Bodies	IGV_Geom	OG_Blade_ColdShape_15TTGIGV
Target Bodies	OG_Blade_ColdShape_15TTGIGV	CavityBoss
Protected	No	
Advanced		
Small Sliding	Program Controlled	

Mesh

TABLE 11
Model (A3) > Mesh

Object Name	*Mesh*
State	Solved
Display	
Display Style	Use Geometry Setting
Defaults	
Physics Preference	CFD
Solver Preference	CFX
Element Order	Linear
Element Size	5.e-003 m
Sizing	
Use Adaptive Sizing	No
Growth Rate	Default (1.2)
Max Size	5.e-003 m
Mesh Defeaturing	Yes
Defeature Size	1.e-004 m
Capture Curvature	Yes
Curvature Min Size	5.e-004 m
Curvature Normal Angle	Default (18.0°)
Capture Proximity	Yes
Proximity Min Size	5.e-004 m
Proximity Gap Factor	5.0
Proximity Size Sources	Faces and Edges
Bounding Box Diagonal	0.4065 m
Average Surface Area	9.5829e-004 m²
Minimum Edge Length	3.764e-007 m

Quality	
Check Mesh Quality	Yes, Errors
Target Skewness	Default (0.9)
Smoothing	Medium
Mesh Metric	None
Inflation	
Use Automatic Inflation	None
Inflation Option	Smooth Transition
Transition Ratio	0.77
Maximum Layers	5
Growth Rate	1.2
Inflation Algorithm	Pre
View Advanced Options	No
Advanced	
Number of CPUs for Parallel Part Meshing	32
Straight Sided Elements	
Rigid Body Behavior	Dimensionally Reduced
Triangle Surface Mesher	Program Controlled
Topology Checking	Yes
Pinch Tolerance	Default (4.5e-004 m)
Generate Pinch on Refresh	No
Statistics	
Nodes	20806217
Elements	52596467

TABLE 12
Model (A3) > Mesh > Mesh Controls

Object Name	*Gas_Path_Match*	*Patch Conforming Method*	*BladeFace*	*BladeEdge*	*BladeBase*	*BladeBaseOuter*	*Blade_LE_TE*	*Inflation*	*IGV_Match*	*IGV_Inflation*	*IGV_OuterWall*
State	Fully Defined										
Scope											
Scoping Method	Named Selection		Geometry Selection						Named Selection	Geometry Selection	Named Selection
High Boundary	Periodic_High								IGV_Periodic_High		
Low Boundary	Periodic_Low								IGV_Periodic_Low		
Named Selection		Gas_Path									IGV_OuterWall
Geometry			2 Faces	5 Faces	6 Faces	2 Faces		1 Body		1 Body	
Definition											
Suppressed	No										
Transformation	Cyclic								Cyclic		
Axis of Rotation	Global Coordinate System								Global Coordinate System		
Control Messages	No								No		
Method		Tetrahedrons									
Algorithm		Patch Conforming									
Element Order		Use Global Setting									
Type	Element Size										Element Size
Element Size			2.5e-004 m	5.e-005 m	2.5e-004 m	5.e-005 m					5.e-004 m
Boundary Scoping Method								Named Selections		Geometry Selection	
Boundary								Blade		4 Faces	
Inflation Option								First Layer Thickness		First Layer Thickness	
First Layer Height								1.e-006 m		1.e-006 m	
Maximum Layers								23		20	
Growth Rate								1.2		1.2	
Inflation Algorithm								Pre		Pre	
Advanced											
Defeature Size	1.e-007 m										1.e-007 m
Influence Volume	No										No
Behavior	Soft										Soft
Growth Rate	Default (1.2)										Default (1.2)
Capture Curvature	No										No
Capture Proximity	No										No

TABLE 13
Model (A3) > Mesh > Mesh Controls

Object Name	*IGV_Blades*	*Match Control*	*Patch Conforming Method 2*	*Treatment_Inflation*	*Treatment_Wal*	*Inflation 2*
State	Fully Defined					
Scope						
Scoping Method	Named Selection		Geometry Selection		Named Selection	Geometry Selection
Named Selection	IGV_Blades				Treatment_Wall	
High Boundary		Treatment_Periodic_High				
Low Boundary		Treatment_Periodic_Low				
Geometry			1 Body			1 Body
Definition						
Suppressed	No					

Type	Element Size				Element Size	
Element Size	2.e-004 m				2.5e-004 m	
Transformation		Cyclic				
Axis of Rotation		Global Coordinate System				
Control Messages		No				
Method			Tetrahedrons			
Algorithm			Patch Conforming			
Element Order			Use Global Setting			
Boundary Scoping Method				Named Selections		Geometry Selection
Boundary				Treatment_Wall		4 Faces
Inflation Option				First Layer Thickness		First Layer Thickness
First Layer Height				1.e-006 m		1.e-006 m
Maximum Layers				20		23
Growth Rate				1.2		1.2
Inflation Algorithm				Pre		Pre
Advanced						
Defeature Size	1.e-007 m				1.e-007 m	
Influence Volume	No				No	
Behavior	Soft				Soft	
Growth Rate	Default (1.2)				Default (1.2)	
Capture Curvature	No				No	
Capture Proximity	No				No	

TABLE 14
Model (A3) > Mesh Edit

Object Name	*Mesh Edit*
State	Solved
Auto Detection	
Generate Automatic Mesh Connections On Refresh	No
Transparency	
Enabled	Yes

TABLE 15
Model (A3) > Mesh Edit > Contact Match Group

Object Name	*Contact Match Group*
State	Not Solved
Scope	
Scoping Method	Geometry Selection
Geometry	All Bodies
Definition	
Suppressed	No
Auto Detection	
Tolerance Type	Slider
Tolerance Slider	0.
Tolerance Value	1.0163e-003 m
Use Range	No
Group By	Bodies
Search Across	Bodies
Statistics	
Connections	0
Active Connections	0

Named Selections

TABLE 16
Model (A3) > Named Selections > Named Selections

Object Name	*Inlet*	*Outlet*	*Periodic_High*	*Periodic_Low*	*Inner_Wall*	*Gas_Path*	*Outer_Wall*	*Blade*	*Blisk_Minus_Blade*	*IGV*	*IGV_Periodic_High*
State	Fully Defined										
Scope											
Scoping Method	Geometry Selection										
Geometry	1 Face		4 Faces		10 Faces	1 Body	5 Faces	15 Faces	2 Faces	1 Body	6 Faces
Definition											
Send to Solver	Yes										
Protected	Program Controlled										
Visible	Yes										
Program Controlled Inflation	Exclude										
Statistics											
Type	Manual										
Total Selection	1 Face		4 Faces		10 Faces	1 Body	5 Faces	15 Faces	2 Faces	1 Body	6 Faces
Surface Area	2.9124e-003 m²	1.8353e-003 m²	1.4757e-002 m²	1.4759e-002 m²	4.4135e-003 m²		8.8362e-003 m²	1.1729e-002 m²	2.5299e-004 m²		1.6153e-002 m²
Suppressed	0										
Used by Mesh Worksheet	No										

TABLE 17
Model (A3) > Named Selections > Named Selections

Object Name	*IGV_Periodic_Low*	*IGV_Inlet*	*IGV_InnerWall*	*IGV_OuterWall*	*IGV_Outlet*	*IGV_Blades*	*Treatment*	*Aft_Gas_Interface1*	*Aft_Gas_Interface2*	*Aft_Gas_Interface3*	*Forward*
State	Fully Defined										
Scope											
Scoping Method	Geometry Selection										
Geometry	6 Faces	1 Face	2 Faces	22 Faces	1 Face	12 Faces	1 Body	1 Face			
Definition											
Send to											

Solver	Yes										
Protected	Program Controlled										
Visible	Yes										
Program Controlled Inflation	Exclude										
Statistics											
Type	Manual										
Total Selection	6 Faces	1 Face	2 Faces	22 Faces	1 Face	12 Faces	1 Body	1 Face			
Surface Area	1.6163e-002 m²	3.8108e-003 m²	1.2498e-003 m²	7.0658e-003 m²	3.4331e-003 m²	1.1467e-002 m²		2.1424e-004 m²	1.1425e-005 m²	1.1424e-005 m²	1.2
Suppressed	0										
Used by Mesh Worksheet	No										

TABLE 18
Model (A3) > Named Selections > Named Selections

Object Name	*Forward_Gas_Interface2*	*Forward_Gas_Interface3*	*Aft_Treatment_Interface1*	*Aft_Treatment_Interface2*	*Aft_Treatment_Interface3*	*Forward_Treatment_Interface1*	*Forwar*
State	Fully Defined						
Scope							
Scoping Method	Geometry Selection						
Geometry	1 Face						
Definition							
Send to Solver	Yes						
Protected	Program Controlled						
Visible	Yes						
Program Controlled Inflation	Exclude						
Statistics							
Type	Manual						
Total Selection	1 Face						
Surface Area	1.1425e-005 m²	1.1885e-005 m²	6.4302e-004 m²	3.4585e-005 m²	4.5189e-005 m²	3.8923e-004 m²	
Suppressed	0						
Used by Mesh Worksheet	No						

THIS PAGE INTENTIONALLY LEFT BLANK

APPENDIX E:
ANSYS CFX Setup Reports

Date

2023/05/31 02:19:07

Contents

1. File Report

Table 1. File Information for RotorOnly_21M_90_W_001

Case	RotorOnly_21M_90_W_001
File Path	E:/ANSYS/Hamming Res Files/Rotor Only RES Files/RotorOnly 21M Final/RotorOnly_21M_90_W_001.res
File Date	13 April 2023
File Time	11:48:46 PM
File Type	CFX5
File Version	20.2

2. Mesh Report

Table 2. Mesh Information for RotorOnly_21M_90_W_001

Domain	Nodes	Elements
Gas_Path	8577123	21000809

3. Physics Report

Table 3. Domain Physics for RotorOnly_21M_90_W_001

Domain - Gas_Path	
Type	Fluid
Location	Gas_Path
Materials	
Air Ideal Gas	
Fluid Definition	Material Library
Morphology	Continuous Fluid
Settings	
Buoyancy Model	Non Buoyant
Domain Motion	Rotating
Angular Velocity	RevPerMin
Axis Definition	Coordinate Axis
Rotation Axis	Coord 0.3
Reference Pressure	1.0000e+0 [atm]
Heat Transfer Model	Total Energy
Include Viscous Work Term	True
Turbulence Model	SST
Transitional Turbulence	Gamma Theta Model
Transition Onset Correlation	Langtry Menter
Turbulent Wall Functions	Automatic
High Speed Model	Off
Domain Interface - Rotor_Periodic	
Boundary List1	Rotor_Periodic Side 1
Boundary List2	Rotor_Periodic Side 2
Interface Type	Fluid Fluid
Settings	
Interface Models	Rotational Periodicity
Axis Definition	Coordinate Axis
Rotation Axis	Coord 0.3
Mesh Connection	GGI

Table 4. Boundary Physics for RotorOnly_21M_90_W_001

Domain	**Boundaries**	
Gas_Path	**Boundary - Inlet**	
	Type	INLET
	Location	Inlet

Settings	
Flow Direction	Cartesian Components
Unit Vector X Component	ThetaWhirl
Unit Vector Y Component	0.0000e+0
Unit Vector Z Component	AxialWhirl
Flow Regime	Subsonic
Heat Transfer	Stationary Frame Total Temperature
Stationary Frame Total Temperature	2.8815e+2 [K]
Mass And Momentum	Stationary Frame Total Pressure
Relative Pressure	RelPStagIn
Turbulence	Medium Intensity and Eddy Viscosity Ratio
Boundary - Rotor_Periodic Side 1	
Type	INTERFACE
Location	Periodic_High
Settings	
Heat Transfer	Conservative Interface Flux
Mass And Momentum	Conservative Interface Flux
Turbulence	Conservative Interface Flux
Boundary - Rotor_Periodic Side 2	
Type	INTERFACE
Location	Periodic_Low
Settings	
Heat Transfer	Conservative Interface Flux
Mass And Momentum	Conservative Interface Flux
Turbulence	Conservative Interface Flux
Boundary - Outlet	
Type	OPENING
Location	Outlet
Settings	
Flow Direction	Normal to Boundary Condition
Flow Regime	Subsonic
Heat Transfer	Opening Temperature
Opening Temperature	2.8815e+2 [K]
Mass And Momentum	Opening Pressure and Direction
Relative Pressure	RelPBack
Turbulence	Medium Intensity and Eddy Viscosity Ratio
Boundary - Blade	
Type	WALL
Location	Blade

Settings	
Heat Transfer	Adiabatic
Mass And Momentum	No Slip Wall
Wall Roughness	Smooth Wall
Boundary - Blisk_Minus_Blade	
Type	WALL
Location	Blisk_Minus_Blade
Settings	
Heat Transfer	Adiabatic
Mass And Momentum	No Slip Wall
Wall Roughness	Smooth Wall
Boundary - InnerWall	
Type	WALL
Location	Inner_Wall
Settings	
Heat Transfer	Adiabatic
Mass And Momentum	No Slip Wall
Wall Velocity	Counter Rotating Wall
Wall Roughness	Smooth Wall
Boundary - OuterWall	
Type	WALL
Location	Outer_Wall
Settings	
Heat Transfer	Adiabatic
Mass And Momentum	No Slip Wall
Wall Velocity	Counter Rotating Wall
Wall Roughness	Smooth Wall

4. User Data

Date

2023/05/31 02:17:17

Contents

1. File Report

Table 1. File Information for IP_37M_90_W_001

Case	IP_37M_90_W_001
File Path	E:/ANSYS/Hamming Res Files/IP Final Files/IP_37M_90_W_001.res
File Date	06 April 2023
File Time	08:59:02 AM
File Type	CFX5
File Version	20.2

2. Mesh Report

Table 2. Mesh Information for IP_37M_90_W_001

Domain	Nodes	Elements
Gas_Path	10629557	25274816
Treatment	5148084	11975601
All Domains	15777641	37250417

3. Physics Report

Table 3. Domain Physics for IP_37M_90_W_001

Domain - Gas_Path	
Type	Fluid
Location	GasPath
Materials	
Air Ideal Gas	
Fluid Definition	Material Library
Morphology	Continuous Fluid
Settings	
Buoyancy Model	Non Buoyant
Domain Motion	Rotating
Angular Velocity	RevPerMin
Axis Definition	Coordinate Axis
Rotation Axis	Coord 0.3
Reference Pressure	1.0000e+0 [atm]
Heat Transfer Model	Total Energy
Include Viscous Work Term	True
Turbulence Model	SST
Transitional Turbulence	Gamma Theta Model
Transition Onset Correlation	Langtry Menter
Turbulent Wall Functions	Automatic
High Speed Model	Off
Domain - Treatment	
Type	Fluid
Location	Treatment
Materials	
Air Ideal Gas	
Fluid Definition	Material Library
Morphology	Continuous Fluid
Settings	
Buoyancy Model	Non Buoyant
Domain Motion	Stationary
Reference Pressure	1.0000e+0 [atm]
Heat Transfer Model	Total Energy
Include Viscous Work Term	True
Turbulence Model	SST

Transitional Turbulence	Gamma Theta Model
Transition Onset Correlation	Langtry Menter
Turbulent Wall Functions	Automatic
High Speed Model	Off
Domain Interface - Aft_Connection_Side1	
Boundary List1	Aft_Connection_Side1 Side 1
Boundary List2	Aft_Connection_Side1 Side 2
Interface Type	Fluid Fluid
Settings	
Interface Models	General Connection
Frame Change	Stage
Frame Type	Rotating
Downstream Velocity Constraint	Constant Total Pressure
Pitch Change	Automatic
Mesh Connection	GGI
Domain Interface - Aft_Connection_Side2	
Boundary List1	Aft_Connection_Side2 Side 1
Boundary List2	Aft_Connection_Side2 Side 2
Interface Type	Fluid Fluid
Settings	
Interface Models	General Connection
Frame Change	Stage
Frame Type	Rotating
Downstream Velocity Constraint	Constant Total Pressure
Pitch Change	Automatic
Mesh Connection	GGI
Domain Interface - Aft_Connection_Side3	
Boundary List1	Aft_Connection_Side3 Side 1
Boundary List2	Aft_Connection_Side3 Side 2
Interface Type	Fluid Fluid
Settings	
Interface Models	General Connection
Frame Change	Stage
Frame Type	Rotating
Downstream Velocity Constraint	Constant Total Pressure
Pitch Change	Automatic
Mesh Connection	GGI
Domain Interface - Aft_Treatment_Periodic	
Boundary List1	Aft_Treatment_Periodic Side 1

Boundary List2	Aft_Treatment_Periodic Side 2
Interface Type	Fluid Fluid
Settings	
Interface Models	Rotational Periodicity
Axis Definition	Coordinate Axis
Rotation Axis	Coord 0.3
Mesh Connection	GGI
Domain Interface - Forward_Connection_Side1	
Boundary List1	Forward_Connection_Side1 Side 1
Boundary List2	Forward_Connection_Side1 Side 2
Interface Type	Fluid Fluid
Settings	
Interface Models	General Connection
Frame Change	Stage
Frame Type	Rotating
Downstream Velocity Constraint	Constant Total Pressure
Pitch Change	Automatic
Mesh Connection	GGI
Domain Interface - Forward_Connection_Side2	
Boundary List1	Forward_Connection_Side2 Side 1
Boundary List2	Forward_Connection_Side2 Side 2
Interface Type	Fluid Fluid
Settings	
Interface Models	General Connection
Frame Change	Stage
Frame Type	Rotating
Downstream Velocity Constraint	Constant Total Pressure
Pitch Change	Automatic
Mesh Connection	GGI
Domain Interface - Forward_Connection_Side3	
Boundary List1	Forward_Connection_Side3 Side 1
Boundary List2	Forward_Connection_Side3 Side 2
Interface Type	Fluid Fluid
Settings	
Interface Models	General Connection
Frame Change	Stage
Frame Type	Rotating
Downstream Velocity Constraint	Constant Total Pressure
Pitch Change	Automatic

Mesh Connection	GGI
Domain Interface - Forward_Treatment_Periodic	
Boundary List1	Forward_Treatment_Periodic Side 1
Boundary List2	Forward_Treatment_Periodic Side 2
Interface Type	Fluid Fluid
Settings	
Interface Models	Rotational Periodicity
Axis Definition	Coordinate Axis
Rotation Axis	Coord 0.3
Mesh Connection	GGI
Domain Interface - Rotor_Periodic	
Boundary List1	Rotor_Periodic Side 1
Boundary List2	Rotor_Periodic Side 2
Interface Type	Fluid Fluid
Settings	
Interface Models	Rotational Periodicity
Axis Definition	Coordinate Axis
Rotation Axis	Coord 0.3
Mesh Connection	GGI

Table 4. Boundary Physics for IP_37M_90_W_001

Domain	**Boundaries**	
Gas_Path	**Boundary - Inlet**	
	Type	INLET
	Location	Inlet
	Settings	
	Flow Direction	Cartesian Components
	Unit Vector X Component	ThetaWhirl
	Unit Vector Y Component	0.0000e+0
	Unit Vector Z Component	AxialWhirl
	Flow Regime	Subsonic
	Heat Transfer	Stationary Frame Total Temperature
	Stationary Frame Total Temperature	2.8815e+2 [K]
	Mass And Momentum	Stationary Frame Total Pressure
	Relative Pressure	RelPStagIn
	Turbulence	Medium Intensity and Eddy Viscosity Ratio
	Boundary - Aft_Connection_Side1 Side 1	
	Type	INTERFACE
	Location	Aft_Gas_Side1

Settings	
Heat Transfer	Conservative Interface Flux
Mass And Momentum	Conservative Interface Flux
Turbulence	Conservative Interface Flux
Boundary - Aft_Connection_Side2 Side 1	
Type	INTERFACE
Location	Aft_Gas_Side2
Settings	
Heat Transfer	Conservative Interface Flux
Mass And Momentum	Conservative Interface Flux
Turbulence	Conservative Interface Flux
Boundary - Aft_Connection_Side3 Side 1	
Type	INTERFACE
Location	Aft_Gas_Side3
Settings	
Heat Transfer	Conservative Interface Flux
Mass And Momentum	Conservative Interface Flux
Turbulence	Conservative Interface Flux
Boundary - Forward_Connection_Side1 Side 1	
Type	INTERFACE
Location	Forward_Gas_Side1
Settings	
Heat Transfer	Conservative Interface Flux
Mass And Momentum	Conservative Interface Flux
Turbulence	Conservative Interface Flux
Boundary - Forward_Connection_Side2 Side 1	
Type	INTERFACE
Location	Forward_Gas_Side2
Settings	
Heat Transfer	Conservative Interface Flux
Mass And Momentum	Conservative Interface Flux
Turbulence	Conservative Interface Flux
Boundary - Forward_Connection_Side3 Side 1	
Type	INTERFACE
Location	Forward_Gas_Side3
Settings	
Heat Transfer	Conservative Interface Flux
Mass And Momentum	Conservative Interface Flux
Turbulence	Conservative Interface Flux

Boundary - Rotor_Periodic Side 1	
Type	INTERFACE
Location	Periodic_High
Settings	
Heat Transfer	Conservative Interface Flux
Mass And Momentum	Conservative Interface Flux
Turbulence	Conservative Interface Flux
Boundary - Rotor_Periodic Side 2	
Type	INTERFACE
Location	Periodic_Low
Settings	
Heat Transfer	Conservative Interface Flux
Mass And Momentum	Conservative Interface Flux
Turbulence	Conservative Interface Flux
Boundary - Outlet	
Type	OPENING
Location	Outlet
Settings	
Flow Direction	Normal to Boundary Condition
Flow Regime	Subsonic
Heat Transfer	Opening Temperature
Opening Temperature	2.8815e+2 [K]
Mass And Momentum	Opening Pressure and Direction
Relative Pressure	RelPBack
Turbulence	Medium Intensity and Eddy Viscosity Ratio
Boundary - Blade	
Type	WALL
Location	Blade
Settings	
Heat Transfer	Adiabatic
Mass And Momentum	No Slip Wall
Wall Roughness	Smooth Wall
Boundary - Blisk_Minus_Blade	
Type	WALL
Location	Blisk_Minus_Blade
Settings	
Heat Transfer	Adiabatic
Mass And Momentum	No Slip Wall
Wall Roughness	Smooth Wall

	Boundary - InnerWall	
	Type	WALL
	Location	InnerWall
	Settings	
	Heat Transfer	Adiabatic
	Mass And Momentum	No Slip Wall
	Wall Velocity	Counter Rotating Wall
	Wall Roughness	Smooth Wall
	Boundary - OuterWall	
	Type	WALL
	Location	OuterWall
	Settings	
	Heat Transfer	Adiabatic
	Mass And Momentum	No Slip Wall
	Wall Velocity	Counter Rotating Wall
	Wall Roughness	Smooth Wall
Treatment	**Boundary - Aft_Connection_Side1 Side 2**	
	Type	INTERFACE
	Location	Aft_Treatment_Side1
	Settings	
	Heat Transfer	Conservative Interface Flux
	Mass And Momentum	Conservative Interface Flux
	Turbulence	Conservative Interface Flux
	Boundary - Aft_Connection_Side2 Side 2	
	Type	INTERFACE
	Location	Aft_Treatment_Side2
	Settings	
	Heat Transfer	Conservative Interface Flux
	Mass And Momentum	Conservative Interface Flux
	Turbulence	Conservative Interface Flux
	Boundary - Aft_Connection_Side3 Side 2	
	Type	INTERFACE
	Location	Aft_Treatment_Side3
	Settings	
	Heat Transfer	Conservative Interface Flux
	Mass And Momentum	Conservative Interface Flux
	Turbulence	Conservative Interface Flux
	Boundary - Aft_Treatment_Periodic Side 1	
	Type	INTERFACE

Location	Aft_Treatment_Periodic_High
Settings	
Heat Transfer	Conservative Interface Flux
Mass And Momentum	Conservative Interface Flux
Turbulence	Conservative Interface Flux
Boundary - Aft_Treatment_Periodic Side 2	
Type	INTERFACE
Location	Aft_Treatment_Periodic_Low
Settings	
Heat Transfer	Conservative Interface Flux
Mass And Momentum	Conservative Interface Flux
Turbulence	Conservative Interface Flux
Boundary - Forward_Connection_Side1 Side 2	
Type	INTERFACE
Location	Forward_Treatment_Side1
Settings	
Heat Transfer	Conservative Interface Flux
Mass And Momentum	Conservative Interface Flux
Turbulence	Conservative Interface Flux
Boundary - Forward_Connection_Side2 Side 2	
Type	INTERFACE
Location	Forward_Treatment_Side2
Settings	
Heat Transfer	Conservative Interface Flux
Mass And Momentum	Conservative Interface Flux
Turbulence	Conservative Interface Flux
Boundary - Forward_Connection_Side3 Side 2	
Type	INTERFACE
Location	Forward_Treatment_Side3
Settings	
Heat Transfer	Conservative Interface Flux
Mass And Momentum	Conservative Interface Flux
Turbulence	Conservative Interface Flux
Boundary - Forward_Treatment_Periodic Side 1	
Type	INTERFACE
Location	Forward_Treatment_Periodic_High
Settings	
Heat Transfer	Conservative Interface Flux
Mass And Momentum	Conservative Interface Flux

Turbulence	Conservative Interface Flux
Boundary - Forward_Treatment_Periodic Side 2	
Type	INTERFACE
Location	Forward_Treatment_Periodic_Low
Settings	
Heat Transfer	Conservative Interface Flux
Mass And Momentum	Conservative Interface Flux
Turbulence	Conservative Interface Flux
Boundary - TreatmetnWall	
Type	WALL
Location	Treatment_Wall
Settings	
Heat Transfer	Adiabatic
Mass And Momentum	No Slip Wall
Wall Roughness	Smooth Wall

4. User Data

Date

2023/05/31 02:21:27

Contents

1. File Report

Table 1. File Information for Treatment_39M_90_W_001

Case	Treatment_39M_90_W_001
File Path	E:/ANSYS/Hamming Res Files/NACA Final Files/Treatment_39M_90_W_001.res
File Date	20 March 2023
File Time	09:45:41 PM
File Type	CFX5
File Version	20.2

2. Mesh Report

Table 2. Mesh Information for Treatment_39M_90_W_001

Domain	Nodes	Elements
Gas_Path	10663859	25425136
Treatment	5541024	13926712
All Domains	16204883	39351848

3. Physics Report

Table 3. Domain Physics for Treatment_39M_90_W_001

Domain - Gas_Path	
Type	Fluid
Location	Gas_Path
Materials	
Air Ideal Gas	
Fluid Definition	Material Library
Morphology	Continuous Fluid
Settings	
Buoyancy Model	Non Buoyant
Domain Motion	Rotating
Angular Velocity	RevPerMin
Axis Definition	Coordinate Axis
Rotation Axis	Coord 0.3
Reference Pressure	1.0000e+0 [atm]
Heat Transfer Model	Total Energy
Include Viscous Work Term	True
Turbulence Model	SST
Transitional Turbulence	Gamma Theta Model
Transition Onset Correlation	Langtry Menter
Turbulent Wall Functions	Automatic
High Speed Model	Off
Domain - Treatment	
Type	Fluid
Location	Treatment
Materials	
Air Ideal Gas	
Fluid Definition	Material Library
Morphology	Continuous Fluid
Settings	
Buoyancy Model	Non Buoyant
Domain Motion	Stationary
Reference Pressure	1.0000e+0 [atm]
Heat Transfer Model	Total Energy
Include Viscous Work Term	True
Turbulence Model	SST

Transitional Turbulence	Gamma Theta Model
Transition Onset Correlation	Langtry Menter
Turbulent Wall Functions	Automatic
High Speed Model	Off
Domain Interface - Aft_ConnectionDownstream	
Boundary List1	Aft_ConnectionDownstream Side 1
Boundary List2	Aft_ConnectionDownstream Side 2
Interface Type	Fluid Fluid
Settings	
Interface Models	General Connection
Frame Change	Stage
Frame Type	Rotating
Downstream Velocity Constraint	Constant Total Pressure
Pitch Change	Automatic
Mesh Connection	GGI
Domain Interface - Aft_ConnectionMain	
Boundary List1	Aft_ConnectionMain Side 1
Boundary List2	Aft_ConnectionMain Side 2
Interface Type	Fluid Fluid
Settings	
Interface Models	General Connection
Frame Change	Stage
Frame Type	Rotating
Downstream Velocity Constraint	Constant Total Pressure
Pitch Change	Automatic
Mesh Connection	GGI
Domain Interface - Aft_ConnectionUpstream	
Boundary List1	Aft_ConnectionUpstream Side 1
Boundary List2	Aft_ConnectionUpstream Side 2
Interface Type	Fluid Fluid
Settings	
Interface Models	General Connection
Frame Change	Stage
Frame Type	Rotating
Downstream Velocity Constraint	Constant Total Pressure
Pitch Change	Automatic
Mesh Connection	GGI
Domain Interface - Forward_ConnectionDownstream	
Boundary List1	Forward_ConnectionDownstream Side 1

Boundary List2	Forward_ConnectionDownstream Side 2
Interface Type	Fluid Fluid
Settings	
Interface Models	General Connection
Frame Change	Stage
Frame Type	Rotating
Downstream Velocity Constraint	Constant Total Pressure
Pitch Change	Automatic
Mesh Connection	GGI
Domain Interface - Forward_ConnectionMain	
Boundary List1	Forward_ConnectionMain Side 1
Boundary List2	Forward_ConnectionMain Side 2
Interface Type	Fluid Fluid
Settings	
Interface Models	General Connection
Frame Change	Stage
Implicit Stage Averaging	Off
Frame Type	Rotating
Downstream Velocity Constraint	Constant Total Pressure
Pitch Change	Automatic
Mesh Connection	GGI
Domain Interface - Forward_ConnectionUpstream	
Boundary List1	Forward_ConnectionUpstream Side 1
Boundary List2	Forward_ConnectionUpstream Side 2
Interface Type	Fluid Fluid
Settings	
Interface Models	General Connection
Frame Change	Stage
Frame Type	Rotating
Downstream Velocity Constraint	Constant Total Pressure
Pitch Change	Automatic
Mesh Connection	GGI
Domain Interface - Rotor_Periodic	
Boundary List1	Rotor_Periodic Side 1
Boundary List2	Rotor_Periodic Side 2
Interface Type	Fluid Fluid
Settings	
Interface Models	Rotational Periodicity
Axis Definition	Coordinate Axis

Rotation Axis	Coord 0.3
Mesh Connection	GGI
Domain Interface - Treatment_Periodic	
Boundary List1	Treatment_Periodic Side 1
Boundary List2	Treatment_Periodic Side 2
Interface Type	Fluid Fluid
Settings	
Interface Models	Rotational Periodicity
Axis Definition	Coordinate Axis
Rotation Axis	Coord 0.3
Mesh Connection	Automatic

Table 4. Boundary Physics for Treatment_39M_90_W_001

Domain	**Boundaries**	
Gas_Path	**Boundary - Inlet**	
	Type	INLET
	Location	Inlet
	Settings	
	Flow Direction	Cartesian Components
	Unit Vector X Component	ThetaWhirl
	Unit Vector Y Component	0.0000e+0
	Unit Vector Z Component	AxialWhirl
	Flow Regime	Subsonic
	Heat Transfer	Stationary Frame Total Temperature
	Stationary Frame Total Temperature	2.8815e+2 [K]
	Mass And Momentum	Stationary Frame Total Pressure
	Relative Pressure	RelPStagIn
	Turbulence	Medium Intensity and Eddy Viscosity Ratio
	Boundary - Aft_ConnectionDownstream Side 1	
	Type	INTERFACE
	Location	Aft_Gas_Interface2
	Settings	
	Heat Transfer	Conservative Interface Flux
	Mass And Momentum	Conservative Interface Flux
	Turbulence	Conservative Interface Flux
	Boundary - Aft_ConnectionMain Side 1	
	Type	INTERFACE
	Location	Aft_Gas_Interface1
	Settings	

Heat Transfer	Conservative Interface Flux
Mass And Momentum	Conservative Interface Flux
Turbulence	Conservative Interface Flux
Boundary - Aft_ConnectionUpstream Side 1	
Type	INTERFACE
Location	Aft_Gas_Interface3
Settings	
Heat Transfer	Conservative Interface Flux
Mass And Momentum	Conservative Interface Flux
Turbulence	Conservative Interface Flux
Boundary - Forward_ConnectionDownstream Side 1	
Type	INTERFACE
Location	Forward_Gas_Interface3
Settings	
Heat Transfer	Conservative Interface Flux
Mass And Momentum	Conservative Interface Flux
Turbulence	Conservative Interface Flux
Boundary - Forward_ConnectionMain Side 1	
Type	INTERFACE
Location	Forward_Gas_Interface1
Settings	
Heat Transfer	Conservative Interface Flux
Mass And Momentum	Conservative Interface Flux
Turbulence	Conservative Interface Flux
Boundary - Forward_ConnectionUpstream Side 1	
Type	INTERFACE
Location	Forward_Gas_Interface2
Settings	
Heat Transfer	Conservative Interface Flux
Mass And Momentum	Conservative Interface Flux
Turbulence	Conservative Interface Flux
Boundary - Rotor_Periodic Side 1	
Type	INTERFACE
Location	Periodic_High
Settings	
Heat Transfer	Conservative Interface Flux
Mass And Momentum	Conservative Interface Flux
Turbulence	Conservative Interface Flux
Boundary - Rotor_Periodic Side 2	

Type	INTERFACE
Location	Periodic_Low
Settings	
Heat Transfer	Conservative Interface Flux
Mass And Momentum	Conservative Interface Flux
Turbulence	Conservative Interface Flux
Boundary - Outlet	
Type	OPENING
Location	Outlet
Settings	
Flow Direction	Normal to Boundary Condition
Flow Regime	Subsonic
Heat Transfer	Opening Temperature
Opening Temperature	2.8815e+2 [K]
Mass And Momentum	Opening Pressure and Direction
Relative Pressure	RelPBack
Turbulence	Medium Intensity and Eddy Viscosity Ratio
Boundary - Blade	
Type	WALL
Location	Blade
Settings	
Heat Transfer	Adiabatic
Mass And Momentum	No Slip Wall
Wall Roughness	Smooth Wall
Boundary - Blisk_Minus_Blade	
Type	WALL
Location	Blisk_Minus_Blade
Settings	
Heat Transfer	Adiabatic
Mass And Momentum	No Slip Wall
Wall Roughness	Smooth Wall
Boundary - InnerWall	
Type	WALL
Location	Inner_Wall
Settings	
Heat Transfer	Adiabatic
Mass And Momentum	No Slip Wall
Wall Velocity	Counter Rotating Wall
Wall Roughness	Smooth Wall

	Boundary - OuterWall	
	Type	WALL
	Location	Outer_Wall
	Settings	
	Heat Transfer	Adiabatic
	Mass And Momentum	No Slip Wall
	Wall Velocity	Counter Rotating Wall
	Wall Roughness	Smooth Wall
Treatment	**Boundary - Aft_ConnectionDownstream Side 2**	
	Type	INTERFACE
	Location	Aft_Treatment_Interface2
	Settings	
	Heat Transfer	Conservative Interface Flux
	Mass And Momentum	Conservative Interface Flux
	Turbulence	Conservative Interface Flux
	Boundary - Aft_ConnectionMain Side 2	
	Type	INTERFACE
	Location	Aft_Treatment_Interface1
	Settings	
	Heat Transfer	Conservative Interface Flux
	Mass And Momentum	Conservative Interface Flux
	Turbulence	Conservative Interface Flux
	Boundary - Aft_ConnectionUpstream Side 2	
	Type	INTERFACE
	Location	Aft_Treatment_Interface3
	Settings	
	Heat Transfer	Conservative Interface Flux
	Mass And Momentum	Conservative Interface Flux
	Turbulence	Conservative Interface Flux
	Boundary - Forward_ConnectionDownstream Side 2	
	Type	INTERFACE
	Location	Forward_Treatment_Interface3
	Settings	
	Heat Transfer	Conservative Interface Flux
	Mass And Momentum	Conservative Interface Flux
	Turbulence	Conservative Interface Flux
	Boundary - Forward_ConnectionMain Side 2	
	Type	INTERFACE
	Location	Forward_Treatment_Interface1

Settings	
Heat Transfer	Conservative Interface Flux
Mass And Momentum	Conservative Interface Flux
Turbulence	Conservative Interface Flux
Boundary - Forward_ConnectionUpstream Side 2	
Type	INTERFACE
Location	Forward_Treatment_Interface2
Settings	
Heat Transfer	Conservative Interface Flux
Mass And Momentum	Conservative Interface Flux
Turbulence	Conservative Interface Flux
Boundary - Treatment_Periodic Side 1	
Type	INTERFACE
Location	Treatment_Periodic_High
Settings	
Heat Transfer	Conservative Interface Flux
Mass And Momentum	Conservative Interface Flux
Turbulence	Conservative Interface Flux
Boundary - Treatment_Periodic Side 2	
Type	INTERFACE
Location	Treatment_Periodic_Low
Settings	
Heat Transfer	Conservative Interface Flux
Mass And Momentum	Conservative Interface Flux
Turbulence	Conservative Interface Flux
Boundary - TreatmentWall	
Type	WALL
Location	Treatment_Wall
Settings	
Heat Transfer	Adiabatic
Mass And Momentum	No Slip Wall
Wall Roughness	Smooth Wall

4. User Data

Date

2023/05/31 02:22:47

Contents

1. File Report

Table 1. File Information for IGVRO_40M_90_003

Case	IGVRO_40M_90_003
File Path	E:/ANSYS/Hamming Res Files/IGVFiles/IGVRO_40M_90_003.res
File Date	19 May 2023
File Time	02:25:45 PM
File Type	CFX5
File Version	20.2

2. Mesh Report

Table 2. Mesh Information for IGVRO_40M_90_003

Domain	Nodes	Elements
Gas_Path	8723862	21117741
IGV	7368366	19217720
All Domains	16092228	40335461

3. Physics Report

Table 3. Domain Physics for IGVRO_40M_90_003

Domain - Gas_Path	
Type	Fluid
Location	Gas_Path
Materials	
Air Ideal Gas	
Fluid Definition	Material Library
Morphology	Continuous Fluid
Settings	
Buoyancy Model	Non Buoyant
Domain Motion	Rotating
Angular Velocity	RevPerMin
Axis Definition	Coordinate Axis
Rotation Axis	Coord 0.3
Reference Pressure	1.0000e+0 [atm]
Heat Transfer Model	Total Energy
Include Viscous Work Term	True
Turbulence Model	SST
Transitional Turbulence	Gamma Theta Model
Transition Onset Correlation	Langtry Menter
Turbulent Wall Functions	Automatic
High Speed Model	Off
Domain - IGV	
Type	Fluid
Location	IGV
Materials	
Air Ideal Gas	
Fluid Definition	Material Library
Morphology	Continuous Fluid
Settings	
Buoyancy Model	Non Buoyant
Domain Motion	Stationary
Reference Pressure	1.0000e+0 [atm]
Heat Transfer Model	Total Energy
Include Viscous Work Term	True
Turbulence Model	SST

Transitional Turbulence	Gamma Theta Model
Transition Onset Correlation	Langtry Menter
Turbulent Wall Functions	Automatic
High Speed Model	Off
Domain Interface - GasPeriodic	
Boundary List1	GasPeriodic Side 1
Boundary List2	GasPeriodic Side 2
Interface Type	Fluid Fluid
Settings	
Interface Models	Rotational Periodicity
Axis Definition	Coordinate Axis
Rotation Axis	Coord 0.3
Mesh Connection	GGI
Domain Interface - IGV Interface	
Boundary List1	IGV Interface Side 1
Boundary List2	IGV Interface Side 2
Interface Type	Fluid Fluid
Settings	
Interface Models	General Connection
Frame Change	Stage
Frame Type	Rotating
Downstream Velocity Constraint	Constant Total Pressure
Pitch Change	Automatic
Mesh Connection	GGI
Domain Interface - IGVPeriodic	
Boundary List1	IGVPeriodic Side 1
Boundary List2	IGVPeriodic Side 2
Interface Type	Fluid Fluid
Settings	
Interface Models	Rotational Periodicity
Axis Definition	Coordinate Axis
Rotation Axis	Coord 0.3
Mesh Connection	GGI

Table 4. Boundary Physics for IGVRO_40M_90_003

Domain	**Boundaries**	
Gas_Path	**Boundary - GasPeriodic Side 1**	
	Type	INTERFACE
	Location	Periodic_High

	Settings
Heat Transfer	Conservative Interface Flux
Mass And Momentum	Conservative Interface Flux
Turbulence	Conservative Interface Flux
Boundary - GasPeriodic Side 2	
Type	INTERFACE
Location	Periodic_Low
	Settings
Heat Transfer	Conservative Interface Flux
Mass And Momentum	Conservative Interface Flux
Turbulence	Conservative Interface Flux
Boundary - IGV Interface Side 1	
Type	INTERFACE
Location	Inlet
	Settings
Heat Transfer	Conservative Interface Flux
Mass And Momentum	Conservative Interface Flux
Turbulence	Conservative Interface Flux
Boundary - Outlet	
Type	OPENING
Location	Outlet
	Settings
Flow Direction	Normal to Boundary Condition
Flow Regime	Subsonic
Heat Transfer	Opening Temperature
Opening Temperature	2.8815e+2 [K]
Mass And Momentum	Opening Pressure and Direction
Relative Pressure	RelPBack
Turbulence	Medium Intensity and Eddy Viscosity Ratio
Boundary - Blade	
Type	WALL
Location	Blade
	Settings
Heat Transfer	Adiabatic
Mass And Momentum	No Slip Wall
Wall Roughness	Smooth Wall
Boundary - Blisk_Minus_Blade	
Type	WALL
Location	Blisk_Minus_Blade

	Settings	
	Heat Transfer	Adiabatic
	Mass And Momentum	No Slip Wall
	Wall Roughness	Smooth Wall
	Boundary - InnerWall	
	Type	WALL
	Location	Inner_Wall
	Settings	
	Heat Transfer	Adiabatic
	Mass And Momentum	No Slip Wall
	Wall Velocity	Counter Rotating Wall
	Wall Roughness	Smooth Wall
	Boundary - OuterWall	
	Type	WALL
	Location	Outer_Wall
	Settings	
	Heat Transfer	Adiabatic
	Mass And Momentum	No Slip Wall
	Wall Velocity	Counter Rotating Wall
	Wall Roughness	Smooth Wall
IGV	**Boundary - Inlet**	
	Type	INLET
	Location	IGV_Inlet
	Settings	
	Flow Direction	Normal to Boundary Condition
	Flow Regime	Subsonic
	Heat Transfer	Static Temperature
	Static Temperature	2.8815e+2 [K]
	Mass And Momentum	Total Pressure
	Relative Pressure	RelPStagIn
	Turbulence	Medium Intensity and Eddy Viscosity Ratio
	Boundary - IGV Interface Side 2	
	Type	INTERFACE
	Location	IGV_Outlet
	Settings	
	Heat Transfer	Conservative Interface Flux
	Mass And Momentum	Conservative Interface Flux
	Turbulence	Conservative Interface Flux
	Boundary - IGVPeriodic Side 1	

Type	INTERFACE
Location	IGV_Periodic_High
Settings	
Heat Transfer	Conservative Interface Flux
Mass And Momentum	Conservative Interface Flux
Turbulence	Conservative Interface Flux
Boundary - IGVPeriodic Side 2	
Type	INTERFACE
Location	IGV_Periodic_Low
	Settings
Heat Transfer	Conservative Interface Flux
Mass And Momentum	Conservative Interface Flux
Turbulence	Conservative Interface Flux
Boundary - IGV_Blade	
Type	WALL
Location	IGV_Blades
	Settings
Heat Transfer	Adiabatic
Mass And Momentum	No Slip Wall
Wall Roughness	Smooth Wall
Boundary - IGV_OuterWall	
Type	WALL
Location	IGV_OuterWall
	Settings
Heat Transfer	Adiabatic
Mass And Momentum	No Slip Wall
Wall Roughness	Smooth Wall
Boundary - IGV_Walls	
Type	WALL
Location	IGV_InnerWall
	Settings
Heat Transfer	Adiabatic
Mass And Momentum	No Slip Wall
Wall Roughness	Smooth Wall

4. User Data

Date

2023/05/31 02:15:13

Contents

1. File Report

Table 1. File Information for IGVNACA_53M_90_001

Case	IGVNACA_53M_90_001
File Path	E:/ANSYS/Hamming Res Files/IGVFiles/IGVNACA_53M_90_001.res
File Date	19 May 2023
File Time	09:15:46 AM
File Type	CFX5
File Version	20.2

2. Mesh Report

Table 2. Mesh Information for IGVNACA_53M_90_001

Domain	Nodes	Elements
Gas_Path	8594888	20866516
IGV	6670777	17806481
Treatment	5540552	13923470
All Domains	20806217	52596467

3. Physics Report

Table 3. Domain Physics for IGVNACA_53M_90_001

Domain - Gas_Path	
Type	Fluid
Location	Gas_Path
Materials	
Air Ideal Gas	
Fluid Definition	Material Library
Morphology	Continuous Fluid
Settings	
Buoyancy Model	Non Buoyant
Domain Motion	Rotating
Angular Velocity	RevPerMin
Axis Definition	Coordinate Axis
Rotation Axis	Coord 0.3
Reference Pressure	1.0000e+0 [atm]
Heat Transfer Model	Total Energy
Include Viscous Work Term	True
Turbulence Model	SST
Transitional Turbulence	Gamma Theta Model
Transition Onset Correlation	Langtry Menter
Turbulent Wall Functions	Automatic
High Speed Model	Off
Domain - IGV	
Type	Fluid
Location	IGV
Materials	
Air Ideal Gas	
Fluid Definition	Material Library
Morphology	Continuous Fluid
Settings	
Buoyancy Model	Non Buoyant
Domain Motion	Stationary
Reference Pressure	1.0000e+0 [atm]
Heat Transfer Model	Total Energy
Include Viscous Work Term	True
Turbulence Model	SST

Transitional Turbulence	Gamma Theta Model
Transition Onset Correlation	Langtry Menter
Turbulent Wall Functions	Automatic
High Speed Model	Off
Domain - Treatment	
Type	Fluid
Location	Treatment
Materials	
Air Ideal Gas	
Fluid Definition	Material Library
Morphology	Continuous Fluid
Settings	
Buoyancy Model	Non Buoyant
Domain Motion	Stationary
Reference Pressure	1.0000e+0 [atm]
Heat Transfer Model	Total Energy
Include Viscous Work Term	True
Turbulence Model	SST
Transitional Turbulence	Gamma Theta Model
Transition Onset Correlation	Langtry Menter
Turbulent Wall Functions	Automatic
High Speed Model	Off
Domain Interface - Aft_Interface1	
Boundary List1	Aft_Interface1 Side 1
Boundary List2	Aft_Interface1 Side 2
Interface Type	Fluid Fluid
Settings	
Interface Models	General Connection
Frame Change	Stage
Frame Type	Rotating
Downstream Velocity Constraint	Constant Total Pressure
Pitch Change	Automatic
Mesh Connection	GGI
Domain Interface - Aft_Interface2	
Boundary List1	Aft_Interface2 Side 1
Boundary List2	Aft_Interface2 Side 2
Interface Type	Fluid Fluid
Settings	
Interface Models	General Connection

Frame Change	Stage
Frame Type	Rotating
Downstream Velocity Constraint	Constant Total Pressure
Pitch Change	Automatic
Mesh Connection	GGI
Domain Interface - Aft_Interface3	
Boundary List1	Aft_Interface3 Side 1
Boundary List2	Aft_Interface3 Side 2
Interface Type	Fluid Fluid
Settings	
Interface Models	General Connection
Frame Change	Stage
Frame Type	Rotating
Downstream Velocity Constraint	Constant Total Pressure
Pitch Change	Automatic
Mesh Connection	GGI
Domain Interface - Forward_Interface1	
Boundary List1	Forward_Interface1 Side 1
Boundary List2	Forward_Interface1 Side 2
Interface Type	Fluid Fluid
Settings	
Interface Models	General Connection
Frame Change	Stage
Frame Type	Rotating
Downstream Velocity Constraint	Constant Total Pressure
Pitch Change	Automatic
Mesh Connection	GGI
Domain Interface - Forward_Interface2	
Boundary List1	Forward_Interface2 Side 1
Boundary List2	Forward_Interface2 Side 2
Interface Type	Fluid Fluid
Settings	
Interface Models	General Connection
Frame Change	Stage
Frame Type	Rotating
Downstream Velocity Constraint	Constant Total Pressure
Pitch Change	Automatic
Mesh Connection	GGI
Domain Interface - Forward_Interface3	

Boundary List1	Forward_Interface3 Side 1
Boundary List2	Forward_Interface3 Side 2
Interface Type	Fluid Fluid
Settings	
Interface Models	General Connection
Frame Change	Stage
Frame Type	Rotating
Downstream Velocity Constraint	Constant Total Pressure
Pitch Change	Automatic
Mesh Connection	GGI
Domain Interface - GasPeriodic	
Boundary List1	GasPeriodic Side 1
Boundary List2	GasPeriodic Side 2
Interface Type	Fluid Fluid
Settings	
Interface Models	Rotational Periodicity
Axis Definition	Coordinate Axis
Rotation Axis	Coord 0.3
Mesh Connection	GGI
Domain Interface - IGV Interface	
Boundary List1	IGV Interface Side 1
Boundary List2	IGV Interface Side 2
Interface Type	Fluid Fluid
Settings	
Interface Models	General Connection
Frame Change	Stage
Frame Type	Rotating
Downstream Velocity Constraint	Constant Total Pressure
Pitch Change	Automatic
Mesh Connection	GGI
Domain Interface - IGVPeriodic	
Boundary List1	IGVPeriodic Side 1
Boundary List2	IGVPeriodic Side 2
Interface Type	Fluid Fluid
Settings	
Interface Models	Rotational Periodicity
Axis Definition	Coordinate Axis
Rotation Axis	Coord 0.3
Mesh Connection	GGI

Domain Interface - TreatmentPeriodic	
Boundary List1	TreatmentPeriodic Side 1
Boundary List2	TreatmentPeriodic Side 2
Interface Type	Fluid Fluid
Settings	
Interface Models	Rotational Periodicity
Axis Definition	Coordinate Axis
Rotation Axis	Coord 0.3
Mesh Connection	Automatic

Table 4. Boundary Physics for IGVNACA_53M_90_001

Domain	Boundaries	
Gas_Path	**Boundary - Aft_Interface1 Side 1**	
	Type	INTERFACE
	Location	Aft_Gas_Interface1
	Settings	
	Heat Transfer	Conservative Interface Flux
	Mass And Momentum	Conservative Interface Flux
	Turbulence	Conservative Interface Flux
	Boundary - Aft_Interface2 Side 1	
	Type	INTERFACE
	Location	Aft_Gas_Interface2
	Settings	
	Heat Transfer	Conservative Interface Flux
	Mass And Momentum	Conservative Interface Flux
	Turbulence	Conservative Interface Flux
	Boundary - Aft_Interface3 Side 1	
	Type	INTERFACE
	Location	Aft_Gas_Interface3
	Settings	
	Heat Transfer	Conservative Interface Flux
	Mass And Momentum	Conservative Interface Flux
	Turbulence	Conservative Interface Flux
	Boundary - Forward_Interface1 Side 1	
	Type	INTERFACE
	Location	Forward_Gas_Interface1
	Settings	
	Heat Transfer	Conservative Interface Flux
	Mass And Momentum	Conservative Interface Flux

Turbulence	Conservative Interface Flux
Boundary - Forward_Interface2 Side 1	
Type	INTERFACE
Location	Forward_Gas_Interface2
	Settings
Heat Transfer	Conservative Interface Flux
Mass And Momentum	Conservative Interface Flux
Turbulence	Conservative Interface Flux
Boundary - Forward_Interface3 Side 1	
Type	INTERFACE
Location	Forward_Gas_Interface3
	Settings
Heat Transfer	Conservative Interface Flux
Mass And Momentum	Conservative Interface Flux
Turbulence	Conservative Interface Flux
Boundary - GasPeriodic Side 1	
Type	INTERFACE
Location	Periodic_High
	Settings
Heat Transfer	Conservative Interface Flux
Mass And Momentum	Conservative Interface Flux
Turbulence	Conservative Interface Flux
Boundary - GasPeriodic Side 2	
Type	INTERFACE
Location	Periodic_Low
	Settings
Heat Transfer	Conservative Interface Flux
Mass And Momentum	Conservative Interface Flux
Turbulence	Conservative Interface Flux
Boundary - IGV Interface Side 1	
Type	INTERFACE
Location	Inlet
	Settings
Heat Transfer	Conservative Interface Flux
Mass And Momentum	Conservative Interface Flux
Turbulence	Conservative Interface Flux
Boundary - Outlet	
Type	OPENING
Location	Outlet

	Settings	
	Flow Direction	Normal to Boundary Condition
	Flow Regime	Subsonic
	Heat Transfer	Opening Temperature
	Opening Temperature	2.8815e+2 [K]
	Mass And Momentum	Opening Pressure and Direction
	Relative Pressure	RelPBack
	Turbulence	Medium Intensity and Eddy Viscosity Ratio
	Boundary - Blade	
	Type	WALL
	Location	Blade
	Settings	
	Heat Transfer	Adiabatic
	Mass And Momentum	No Slip Wall
	Wall Roughness	Smooth Wall
	Boundary - Blisk_Minus_Blade	
	Type	WALL
	Location	Blisk_Minus_Blade
	Settings	
	Heat Transfer	Adiabatic
	Mass And Momentum	No Slip Wall
	Wall Roughness	Smooth Wall
	Boundary - InnerWall	
	Type	WALL
	Location	Inner_Wall
	Settings	
	Heat Transfer	Adiabatic
	Mass And Momentum	No Slip Wall
	Wall Velocity	Counter Rotating Wall
	Wall Roughness	Smooth Wall
	Boundary - OuterWall	
	Type	WALL
	Location	Outer_Wall
	Settings	
	Heat Transfer	Adiabatic
	Mass And Momentum	No Slip Wall
	Wall Velocity	Counter Rotating Wall
	Wall Roughness	Smooth Wall
IGV	**Boundary - Inlet**	

Type	INLET
Location	IGV_Inlet
Settings	
Flow Direction	Normal to Boundary Condition
Flow Regime	Subsonic
Heat Transfer	Static Temperature
Static Temperature	2.8815e+2 [K]
Mass And Momentum	Total Pressure
Relative Pressure	RelPStagIn
Turbulence	Medium Intensity and Eddy Viscosity Ratio
Boundary - IGV Interface Side 2	
Type	INTERFACE
Location	IGV_Outlet
Settings	
Heat Transfer	Conservative Interface Flux
Mass And Momentum	Conservative Interface Flux
Turbulence	Conservative Interface Flux
Boundary - IGVPeriodic Side 1	
Type	INTERFACE
Location	IGV_Periodic_High
Settings	
Heat Transfer	Conservative Interface Flux
Mass And Momentum	Conservative Interface Flux
Turbulence	Conservative Interface Flux
Boundary - IGVPeriodic Side 2	
Type	INTERFACE
Location	IGV_Periodic_Low
Settings	
Heat Transfer	Conservative Interface Flux
Mass And Momentum	Conservative Interface Flux
Turbulence	Conservative Interface Flux
Boundary - IGV_Blade	
Type	WALL
Location	IGV_Blades
Settings	
Heat Transfer	Adiabatic
Mass And Momentum	No Slip Wall
Wall Roughness	Smooth Wall
Boundary - IGV_OuterWall	

	Type	WALL
	Location	IGV_OuterWall
	Settings	
	Heat Transfer	Adiabatic
	Mass And Momentum	No Slip Wall
	Wall Roughness	Smooth Wall
	Boundary - IGV_Walls	
	Type	WALL
	Location	IGV_InnerWall
	Settings	
	Heat Transfer	Adiabatic
	Mass And Momentum	No Slip Wall
	Wall Roughness	Smooth Wall
Treatment	**Boundary - Aft_Interface1 Side 2**	
	Type	INTERFACE
	Location	Aft_Treatment_Interface1
	Settings	
	Heat Transfer	Conservative Interface Flux
	Mass And Momentum	Conservative Interface Flux
	Turbulence	Conservative Interface Flux
	Boundary - Aft_Interface2 Side 2	
	Type	INTERFACE
	Location	Aft_Treatment_Interface2
	Settings	
	Heat Transfer	Conservative Interface Flux
	Mass And Momentum	Conservative Interface Flux
	Turbulence	Conservative Interface Flux
	Boundary - Aft_Interface3 Side 2	
	Type	INTERFACE
	Location	Aft_Treatment_Interface3
	Settings	
	Heat Transfer	Conservative Interface Flux
	Mass And Momentum	Conservative Interface Flux
	Turbulence	Conservative Interface Flux
	Boundary - Forward_Interface1 Side 2	
	Type	INTERFACE
	Location	Forward_Treatment_Interface1
	Settings	
	Heat Transfer	Conservative Interface Flux

Mass And Momentum	Conservative Interface Flux
Turbulence	Conservative Interface Flux
Boundary - Forward_Interface2 Side 2	
Type	INTERFACE
Location	Forward_Treatment_Interface2
	Settings
Heat Transfer	Conservative Interface Flux
Mass And Momentum	Conservative Interface Flux
Turbulence	Conservative Interface Flux
Boundary - Forward_Interface3 Side 2	
Type	INTERFACE
Location	Forward_Treatment_Interface3
	Settings
Heat Transfer	Conservative Interface Flux
Mass And Momentum	Conservative Interface Flux
Turbulence	Conservative Interface Flux
Boundary - TreatmentPeriodic Side 1	
Type	INTERFACE
Location	Treatment_Periodic_High
	Settings
Heat Transfer	Conservative Interface Flux
Mass And Momentum	Conservative Interface Flux
Turbulence	Conservative Interface Flux
Boundary - TreatmentPeriodic Side 2	
Type	INTERFACE
Location	Treatment_Periodic_Low
	Settings
Heat Transfer	Conservative Interface Flux
Mass And Momentum	Conservative Interface Flux
Turbulence	Conservative Interface Flux
Boundary - Treatment_Wall	
Type	WALL
Location	Treatment_Wall
	Settings
Heat Transfer	Adiabatic
Mass And Momentum	No Slip Wall
Wall Roughness	Smooth Wall

4. User Data

THIS PAGE INTENTIONALLY LEFT BLANK

APPENDIX F:
MATLAB Data Processing Script

Thesis Data Reduction Processing Script

ENS N. Jack Spector 01 JUN 2023

Contents

Frontmatter

```
clear
clc
%close all
format compact
```

Data Reading

```
NACAData=xlsread('Master NACA Data.xlsx','A306:BD3305');
IPData=xlsread('Master IP Data.xlsx','A306:BD3305');
ROData=xlsread('Rotor Only Data.xlsx', 'A306:AN3305');
Smoothexp=xlsread('SmoothData.xlsx','A3:AO40');
IGVData=xlsread('Master IGV Data.xlsx','A306:N3305');
RefinementData=xlsread('Master Refinement Data.xlsx','A306:T2750');
```

Experimental Data Parsing

```
%Experimental data, all experimental data has moniker 'ex' in prefix,
%therefore the 'Rex' cases are the Rotor Only, experimental cases. The
%number following each case delineates rotor speed, and the suffix dictates
%the specific parameter parsed. Putting it all together, 'Rex90_E' is the
%Rotor Only, experimental data, 90% speed, efficiency values
% Finally, CFD cases will have an attached 'W' or 'NW' for 'Whirl' or 'No-
% Whirl'

%***PRO TIP*** if re-naming plots or copying figures for large parts of
%data, its often helful to copy into a word doc and use the ;replace'
%command. MATLAB's native form of replacement is good for some applications
%but is lacking

Rex90_E=Smoothexp(1:23,3);
Rex90_Massflow=Smoothexp(1:23,1);
Rex90_Pratio=Smoothexp(1:23,2);

Rex85_E=Smoothexp(1:17,8);
Rex85_Massflow=Smoothexp(1:17,6);
Rex85_Pratio=Smoothexp(1:17,7);

Rex80_E=Smoothexp(1:24,13);
Rex80_Massflow=Smoothexp(1:24,11);
Rex80_Pratio=Smoothexp(1:24,12);

Rex70_E=Smoothexp(1:38,18);
Rex70_Massflow=Smoothexp(1:38,16);
Rex70_Pratio=Smoothexp(1:38,17);

IPex85_E=Smoothexp(1:17,23);
IPex85_Massflow=Smoothexp(1:17,21);
IPex85_Pratio=Smoothexp(1:17,22);
```

```
IPex80_E=Smoothexp(1:19,28);
IPex80_Massflow=Smoothexp(1:19,26);
IPex80_Pratio=Smoothexp(1:19,27);

IPex70_E=Smoothexp(1:23,33);
IPex70_Massflow=Smoothexp(1:23,31);
IPex70_Pratio=Smoothexp(1:23,32);

NACAex85NW_E=Smoothexp(1:18,38);
NACAex85NW_Pratio=Smoothexp(1:18,37);
NACAex85NW_Massflow=Smoothexp(1:18,36);

ROex85NW_E=Smoothexp(1:18,41);
ROex85NW_Pratio=Smoothexp(1:18,40);
ROex85NW_Massflow=Smoothexp(1:18,39);
```

Refinement Data Parsing

```
% Ref prefix is short for 'refinement'... for the mesh refinement cases.
% Number delineates mesh size for this group, as they were all 90% speed,
% no whirl
Ref800T_Time=RefinementData(:,1);
Ref800T_E=RefinementData(:,2);
Ref800T_MassErr=RefinementData(:,3);
Ref800T_Massflow=RefinementData(:,4);
Ref800T_Pratio=RefinementData(:,5);

Ref7M_Time=RefinementData(:,6);
Ref7M_E=RefinementData(:,7);
Ref7M_MassErr=RefinementData(:,8);
Ref7M_Massflow=RefinementData(:,9);
Ref7M_Pratio=RefinementData(:,10);

Ref21M_Time=RefinementData(:,11);
Ref21M_E=RefinementData(:,12);
Ref21M_MassErr=RefinementData(:,13);
Ref21M_Massflow=RefinementData(:,14);
Ref21M_Pratio=RefinementData(:,15);

Ref38M_Time=RefinementData(:,16);
Ref38M_E=RefinementData(:,17);
Ref38M_MassErr=RefinementData(:,18);
Ref38M_Massflow=RefinementData(:,19);
Ref38M_Pratio=RefinementData(:,20);
```

Torque data Parsing

```
% This is a special section for trying out stall prediction with torque.
% Had to use backup files here but CFX post has native variables for torque
% on the blade, I just ran out of time

TorqueIter=[2000 2100 2200 2300 2400 2500 2600 2700];
TorqueZ=[4.80474 4.81245 4.81766 4.81234 3.83517 3.62195 3.41317 3.1818];

figure(1)
plot(TorqueIter,TorqueZ,'-sk')
xlabel('Iteration Number')
ylabel('Blade Torque about Z (N-m)')
title('Blade Torque Stall Pediction')
hold on
grid on
plot([2348 2348],[3 5],'--r')
text(2380,4.5,'\leftarrow Stall Prediction Iteration 2348','color','red')
```

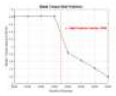

90% Speed CFD Parsing

```
% All of these are the CFD Case data parsing. First section is for 90%
% speed. T is for 'Treatment'... its used in this script for the NACA
% casings. Not great in hindisght, if you dear reader would like to change
% them all to NACA in every instance they appear please do so.

% Time is timestep, E is efficiecny, MassErr is massflow error, Massflow is
%... self expalnatory, Pratio is pressure ratio, treatment In/Out are the
%massflows in and out of the treatment, scaled up to the whole 360 degree
%ring

T90W_Time=NACAData(:,1);
T90W_E=NACAData(:,2);
T90W_MassErr=NACAData(:,3);
T90W_Massflow=NACAData(:,4);
```

```
T90W_Pratio=NACAData(:,5);
T90W_TreatmentIn=NACAData(:,6)*(360/54);
T90W_TreatmentOut=NACAData(:,7)*(360/54);

T90NW_Time=NACAData(:,8);
T90NW_E=NACAData(:,9);
T90NW_MassErr=NACAData(:,10);
T90NW_Massflow=NACAData(:,11);
T90NW_Pratio=NACAData(:,12);
T90NW_TreatmentIn=NACAData(:,13)*(360/54);
T90NW_TreatmentOut=NACAData(:,14)*(360/54);

IP90W_Time=IPData(:,1);
IP90W_E=IPData(:,2);
IP90W_MassErr=IPData(:,3);
IP90W_Massflow=IPData(:,4);
IP90W_Pratio=IPData(:,5);
IP90W_TreatmentIn=IPData(:,6)*(360/54);
IP90W_TreatmentOut=IPData(:,7)*(360/54);

IP90NW_Time=IPData(:,8);
IP90NW_E=IPData(:,9);
IP90NW_MassErr=IPData(:,10);
IP90NW_Massflow=IPData(:,11);
IP90NW_Pratio=IPData(:,12);
IP90NW_TreatmentIn=IPData(:,13)*(360/54);
IP90NW_TreatmentOut=IPData(:,14)*(360/54);

RO90W_Time=RIData(:,1);
RO90W_E=RIData(:,2);
RO90W_MassErr=RIData(:,3);
RO90W_Massflow=RIData(:,4);
RO90W_Pratio=RIData(:,5);

RO90NW_Time=RIData(:,6);
RO90NW_E=RIData(:,7);
RO90NW_MassErr=RIData(:,8);
RO90NW_Massflow=RIData(:,9);
RO90NW_Pratio=RIData(:,10);

IGVRO90_Time=IGVData(:,1);
IGVRO90_E=IGVData(:,2);
IGVRO90_MassErr=IGVData(:,3);
IGVRO90_Massflow=IGVData(:,4);
IGVRO90_Pratio=IGVData(:,5);
IGVRO90_Torque=IGVData(:,6);


IGVNACA90_Time=IGVData(:,7);
IGVNACA90_E=IGVData(:,8);
IGVNACA90_MassErr=IGVData(:,9);
IGVNACA90_Massflow=IGVData(:,10);
IGVNACA90_Pratio=IGVData(:,11);
IGVNACA90_TreatmentIn=IGVData(:,12);
IGVNACA90_TreatmentOut=IGVData(:,13);
IGVNACA90_Torque=IGVData(:,14);
```

85% Speed CFD Parsing

```
T85W_Time=NACAData(:,15);
T85W_E=NACAData(:,16);
T85W_MassErr=NACAData(:,17);
T85W_Massflow=NACAData(:,18);
T85W_Pratio=NACAData(:,19);
T85W_TreatmentIn=NACAData(:,20)*(360/54);
T85W_TreatmentOut=NACAData(:,21)*(360/54);

T85NW_Time=NACAData(:,22);
T85NW_E=NACAData(:,23);
T85NW_MassErr=NACAData(:,24);
T85NW_Massflow=NACAData(:,25);
T85NW_Pratio=NACAData(:,26);
T85NW_TreatmentIn=NACAData(:,27)*(360/54);
T85NW_TreatmentOut=NACAData(:,28)*(360/54);

IP85W_Time=IPData(:,15);
IP85W_E=IPData(:,16);
IP85W_MassErr=IPData(:,17);
IP85W_Massflow=IPData(:,18);
IP85W_Pratio=IPData(:,19);
IP85W_TreatmentIn=IPData(:,20)*(360/54);
IP85W_TreatmentOut=IPData(:,21)*(360/54);

IP85NW_Time=IPData(:,22);
IP85NW_E=IPData(:,23);
IP85NW_MassErr=IPData(:,24);
IP85NW_Massflow=IPData(:,25);
IP85NW_Pratio=IPData(:,26);
IP85NW_TreatmentIn=IPData(:,27)*(360/54);
IP85NW_TreatmentOut=IPData(:,28)*(360/54);
```

```
RO85W_Time=ROData(:,11);
RO85W_E=ROData(:,12);
RO85W_MassErr=ROData(:,13);
RO85W_Massflow=ROData(:,14);
RO85W_Pratio=ROData(:,15);

RO85NW_Time=ROData(:,16);
RO85NW_E=ROData(:,17);
RO85NW_MassErr=ROData(:,18);
RO85NW_Massflow=ROData(:,19);
RO85NW_Pratio=ROData(:,20);
```

80% CFD Parsing

```
T80W_Time=NACAData(:,29);
T80W_E=NACAData(:,30);
T80W_MassErr=NACAData(:,31);
T80W_Massflow=NACAData(:,32);
T80W_Pratio=NACAData(:,33);
T80W_TreatmentIn=NACAData(:,34)*(360/54);
T80W_TreatmentOut=NACAData(:,35)*(360/54);

T80NW_Time=NACAData(:,36);
T80NW_E=NACAData(:,37);
T80NW_MassErr=NACAData(:,38);
T80NW_Massflow=NACAData(:,39);
T80NW_Pratio=NACAData(:,40);
T80NW_TreatmentIn=NACAData(:,41)*(360/54);
T80NW_TreatmentOut=NACAData(:,42)*(360/54);

IP80W_Time=IPData(:,29);
IP80W_E=IPData(:,30);
IP80W_MassErr=IPData(:,31);
IP80W_Massflow=IPData(:,32);
IP80W_Pratio=IPData(:,33);
IP80W_TreatmentIn=IPData(:,34)*(360/54);
IP80W_TreatmentOut=IPData(:,35)*(360/54);

IP80NW_Time=IPData(:,36);
IP80NW_E=IPData(:,37);
IP80NW_MassErr=IPData(:,38);
IP80NW_Massflow=IPData(:,39);
IP80NW_Pratio=IPData(:,40);
IP80NW_TreatmentIn=IPData(:,41)*(360/54);
IP80NW_TreatmentOut=IPData(:,42)*(360/54);

RO80W_Time=ROData(:,21);
RO80W_E=ROData(:,22);
RO80W_MassErr=ROData(:,23);
RO80W_Massflow=ROData(:,24);
RO80W_Pratio=ROData(:,25);

RO80NW_Time=ROData(:,26);
RO80NW_E=ROData(:,27);
RO80NW_MassErr=ROData(:,28);
RO80NW_Massflow=ROData(:,29);
RO80NW_Pratio=ROData(:,30);
```

70% CFD Parsing

```
T70W_Time=NACAData(:,43);
T70W_E=NACAData(:,44);
T70W_MassErr=NACAData(:,45);
T70W_Massflow=NACAData(:,46);
T70W_Pratio=NACAData(:,47);
T70W_TreatmentIn=NACAData(:,48)*(360/54);
T70W_TreatmentOut=NACAData(:,49)*(360/54);

T70NW_Time=NACAData(:,50);
T70NW_E=NACAData(:,51);
T70NW_MassErr=NACAData(:,52);
T70NW_Massflow=NACAData(:,53);
T70NW_Pratio=NACAData(:,54);
T70NW_TreatmentIn=NACAData(:,55)*(360/54);
T70NW_TreatmentOut=NACAData(:,56)*(360/54);

IP70W_Time=IPData(:,43);
IP70W_E=IPData(:,44);
IP70W_MassErr=IPData(:,45);
IP70W_Massflow=IPData(:,46);
IP70W_Pratio=IPData(:,47);
IP70W_TreatmentIn=IPData(:,48)*(360/54);
IP70W_TreatmentOut=IPData(:,49)*(360/54);

IP70NW_Time=IPData(:,50);
IP70NW_E=IPData(:,51);
IP70NW_MassErr=IPData(:,52);
IP70NW_Massflow=IPData(:,53);
```

```
IP70NW_Pratio=IPData(:,54);
IP70NW_TreatmentIn=IPData(:,55)*(360/54);
IP70NW_TreatmentOut=IPData(:,56)*(360/54);

RO70W_Time=ROData(:,31);
RO70W_E=ROData(:,32);
RO70W_MassErr=ROData(:,33);
RO70W_Massflow=ROData(:,34);
RO70W_Pratio=ROData(:,35);

RO70NW_Time=ROData(:,36);
RO70NW_E=ROData(:,37);
RO70NW_MassErr=ROData(:,38);
RO70NW_Massflow=ROData(:,39);
RO70NW_Pratio=RODData(:,40);
```

Mass Error Calculations

```
% This is what was used to predic stall. Fill in the desired timestep and
% MassErr in the plot below, and visually determine the stall iteration,
% then inset that breakpoint into the 'Breakpoints for data' section below

figure(2)
plot(T85NW_Time,T85NW_MassErr, '-k')
hold on
%plot([300 3300], [.00144 0.00144]*1.5,'-r')
%plot([2383 2383], [0 .2],'--r')
%plot([2633 2633],[0 0.15],'-r')
axis([300 3300 0 .2])
xlabel('Iteration')
ylabel('Massflow Error (kg/s)')
title('Massflow Error Plot/ Stall Prediction RO 90% Whirl')
text(1650,.012,'Stopping point \rightarrow','color','red')
%legend('No Whirl')
grid on
```

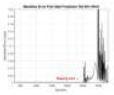

Breakpoints for data (excluding stall)

```
% This is where the breakpoint is set for each run, it is based on the
% iteration at which the simulation stalls. Enter the iteration and keep
% the '-300' This is necessary to cutout the first 300 iterations of the
% data where the simulation is still settling

T90WBreak=2548-300;
T90NWBreak=2548-300;

T85WBreak=2340-300;
T85NWBreak=2449-300;

T80WBreak=2169-300;
T80NWBreak=2491-300;

T70WBreak=1869-300;
T70NWBreak=2292-300;

IP90WBreak=2156-300;
IP90NWBreak=2583-300;

IP85WBreak=2104-300;
IP85NWBreak=2389-300;

IP80WBreak=1965-300;
IP80NWBreak=2238-300;

IP70WBreak=1663-300;
IP70NWBreak=2052-300;

RO90WBreak=2381-300;
RO90NWBreak=2750-300;

RO85WBreak=2053-300;
RO85NWBreak=2550-300;

RO80WBreak=1793-300;
RO80NWBreak=2612-300;

RO70WBreak=1578-300;
RO70NWBreak=2181-300;


IGVRO90Break=2181-300;
IGVNACA90Break=2422-300;
```

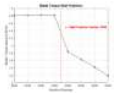

Beest Efficiecny and Peak Pressure Ratio Calcs

```
[BE_T90W,BEP_T90W]=max(T90W_E(1:T90WBreak));
[BE_T90NW,BEP_T90NW]=max(T90NW_E(1:T90NWBreak));
[BE_T85W,BEP_T85W]=max(T85W_E(1:T85WBreak));
[BE_T85NW,BEP_T85NW]=max(T85NW_E(1:T85NWBreak));
[BE_T80W,BEP_T80W]=max(T80W_E(1:T80WBreak));
[BE_T80NW,BEP_T80NW]=max(T80NW_E(1:T80NWBreak));
[BE_T70W,BEP_T70W]=max(T70W_E(1:T70WBreak));
[BE_T70NW,BEP_T70NW]=max(T70NW_E(1:T70NWBreak)) ;

[BE_IP90W,BEP_IP90W]=max(IP90W_E(1:IP90WBreak));
[BE_IP90NW,BEP_IP90NW]=max(IP90NW_E(1:IP90NWBreak));
[BE_IP85W,BEP_IP85W]=max(IP85W_E(1:IP85WBreak));
[BE_IP85NW,BEP_IP85NW]=max(IP85NW_E(1:IP85NWBreak));
[BE_IP80W,BEP_IP80W]=max(IP80W_E(1:IP80WBreak));
[BE_IP80NW,BEP_IP80NW]=max(IP80NW_E(1:IP80NWBreak));
[BE_IP70W,BEP_IP70W]=max(IP70W_E(1:IP70WBreak));
[BE_IP70NW,BEP_IP70NW]=max(IP70NW_E(1:IP70NWBreak));

[BE_RO90W,BEP_RO90W]=max(RO90W_E(1:RO90WBreak));
[BE_RO90NW,BEP_RO90NW]=max(RO90NW_E(1:RO90NWBreak));
[BE_RO85W,BEP_RO85W]=max(RO85W_E(1:RO85WBreak));
[BE_RO85NW,BEP_RO85NW]=max(RO85NW_E(1:RO85NWBreak));
[BE_RO80W,BEP_RO80W]=max(RO80W_E(1:RO80WBreak));
[BE_RO80NW,BEP_RO80NW]=max(RO80NW_E(1:RO80NWBreak));
[BE_RO70W,BEP_RO70W]=max(RO70W_E(1:RO70WBreak));
[BE_RO70NW,BEP_RO70NW]=max(RO70NW_E(1:RO70NWBreak));

[BE_Rex90,BEP_Rex90]=max(Rex90_E);
[BE_Rex85,BEP_Rex85]=max(Rex85_E);
[BE_Rex80,BEP_Rex80]=max(Rex80_E);
[BE_Rex70,BEP_Rex70]=max(Rex70_E);
%[BE_IPex90,BEP_IPex90]=max(IPex90_E);
[BE_IPex85,BEP_IPex85]=max(IPex85_E);
[BE_IPex80,BEP_IPex80]=max(IPex80_E);
[BE_IPex70,BEP_IPex70]=max(IPex70_E);

[BE_ROex85NW,BEP_ROex85NW]=max(ROex85NW_E);
[BE_NACAex85NW,BEP_NACAex85NW]=max(NACAex85NW_E);
BEP_NACAex85NW=16;
BE_NACAex85NW=NACAex85NW_E(BEP_NACAex85NW);


[BE_IGVRO90,BEP_IGVRO90]=max(IGVRO90_E(1:IGVRO90Break));
[BE_IGVNACA90,BEP_IGVNACA90]=max(IGVNACA90_E(1:IGVNACA90Break));


[BP_T90W,BPR_T90W]=max(T90W_Pratio(1:T90WBreak));
[BP_T90NW,BPR_T90NW]=max(T90NW_Pratio(1:T90NWBreak));
[BP_T85W,BPR_T85W]=max(T85W_Pratio(1:T85WBreak));
[BP_T85NW,BPR_T85NW]=max(T85NW_Pratio(1:T85NWBreak));
[BP_T80W,BPR_T80W]=max(T80W_Pratio(1:T80WBreak));
[BP_T80NW,BPR_T80NW]=max(T80NW_Pratio(1:T80NWBreak));
[BP_T70W,BPR_T70W]=max(T70W_Pratio(1:T70WBreak));
[BP_T70NW,BPR_T70NW]=max(T70NW_Pratio(1:T70NWBreak)) ;

[BP_IP90W,BPR_IP90W]=max(IP90W_Pratio(1:IP90WBreak));
[BP_IP90NW,BPR_IP90NW]=max(IP90NW_Pratio(1:IP90NWBreak));
[BP_IP85W,BPR_IP85W]=max(IP85W_Pratio(1:IP85WBreak));
[BP_IP85NW,BPR_IP85NW]=max(IP85NW_Pratio(1:IP85NWBreak));
[BP_IP80W,BPR_IP80W]=max(IP80W_Pratio(1:IP80WBreak));
[BP_IP80NW,BPR_IP80NW]=max(IP80NW_Pratio(1:IP80NWBreak));
[BP_IP70W,BPR_IP70W]=max(IP70W_Pratio(1:IP70WBreak));
[BP_IP70NW,BPR_IP70NW]=max(IP70NW_Pratio(1:IP70NWBreak));

[BP_RO90W,BPR_RO90W]=max(RO90W_Pratio(1:RO90WBreak));
[BP_RO90NW,BPR_RO90NW]=max(RO90NW_Pratio(1:RO90NWBreak));
[BP_RO85W,BPR_RO85W]=max(RO85W_Pratio(1:RO85WBreak));
[BP_RO85NW,BPR_RO85NW]=max(RO85NW_Pratio(1:RO85NWBreak));
[BP_RO80W,BPR_RO80W]=max(RO80W_Pratio(1:RO80WBreak));
[BP_RO80NW,BPR_RO80NW]=max(RO80NW_Pratio(1:RO80NWBreak));
[BP_RO70W,BPR_RO70W]=max(RO70W_Pratio(1:RO70WBreak));
[BP_RO70NW,BPR_RO70NW]=max(RO70NW_Pratio(1:RO70NWBreak));

[BP_Rex90,BPR_Rex90]=max(Rex90_Pratio);
[BP_Rex85,BPR_Rex85]=max(Rex85_Pratio);
[BP_Rex80,BPR_Rex80]=max(Rex80_Pratio);
[BP_Rex70,BPR_Rex70]=max(Rex70_Pratio);
%[BP_IPex90,BPR_IPex90]=max(IPex90_Pratio);
[BP_IPex85,BPR_IPex85]=max(IPex85_Pratio);
[BP_IPex80,BPR_IPex80]=max(IPex80_Pratio);
[BP_IPex70,BPR_IPex70]=max(IPex70_Pratio);

[BP_ROex85NW,BPR_ROex85NW]=max(ROex85NW_Pratio);
```

```
[BP_NACAex85NW,BPR_NACAex85NW]=max(NACAex85NW_Pratio);

[BP_IGVRO90,BPR_IGVRO90]=max(IGVRO90_Pratio(1:IGVRO90Break));
[BP_IGVNACA90,BPR_IGVNACA90]=max(IGVNACA90_Pratio(1:IGVNACA90Break));
```

Stall margin calculation

```
SM_T_90W=(T90W_Massflow(BEP_T90W)-T90W_Massflow(T90WBreak))/T90W_Massflow(BEP_T90W);
SM_T_85W=(T85W_Massflow(BEP_T85W)-T85W_Massflow(T85WBreak))/T85W_Massflow(BEP_T85W);
SM_T_80W=(T80W_Massflow(BEP_T80W)-T80W_Massflow(T80WBreak))/T80W_Massflow(BEP_T80W);
SM_T_70W=(T70W_Massflow(BEP_T70W)-T70W_Massflow(T70WBreak))/T70W_Massflow(BEP_T70W);
SM_T_90NW=(T90NW_Massflow(BEP_T90NW)-T90NW_Massflow(T90NWBreak))/T90NW_Massflow(BEP_T90NW);
SM_T_85NW=(T85NW_Massflow(BEP_T85NW)-T85NW_Massflow(T85NWBreak))/T85NW_Massflow(BEP_T85NW);
SM_T_80NW=(T80NW_Massflow(BEP_T80NW)-T80NW_Massflow(T80NWBreak))/T80NW_Massflow(BEP_T80NW);
SM_T_70NW=(T70NW_Massflow(BEP_T70NW)-T70NW_Massflow(T70NWBreak))/T70NW_Massflow(BEP_T70NW);

SM_IP_90W=(IP90W_Massflow(BEP_IP90W)-IP90W_Massflow(IP90WBreak))/IP90W_Massflow(BEP_IP90W);
SM_IP_85W=(IP85W_Massflow(BEP_IP85W)-IP85W_Massflow(IP85WBreak))/IP85W_Massflow(BEP_IP85W);
SM_IP_80W=(IP80W_Massflow(BEP_IP80W)-IP80W_Massflow(IP80WBreak))/IP80W_Massflow(BEP_IP80W);
SM_IP_70W=(IP70W_Massflow(BEP_IP70W)-IP70W_Massflow(IP70WBreak))/IP70W_Massflow(BEP_IP70W);
SM_IP_90NW=(IP90NW_Massflow(BEP_IP90NW)-IP90NW_Massflow(IP90NWBreak))/IP90NW_Massflow(BEP_IP90NW);
SM_IP_85NW=(IP85NW_Massflow(BEP_IP85NW)-IP85NW_Massflow(IP85NWBreak))/IP85NW_Massflow(BEP_IP85NW);
SM_IP_80NW=(IP80NW_Massflow(BEP_IP80NW)-IP80NW_Massflow(IP80NWBreak))/IP80NW_Massflow(BEP_IP80NW);
SM_IP_70NW=(IP70NW_Massflow(BEP_IP70NW)-IP70NW_Massflow(IP70NWBreak))/IP70NW_Massflow(BEP_IP70NW);

SM_RO_90W=(RO90W_Massflow(BEP_RO90W)-RO90W_Massflow(RO90WBreak))/RO90W_Massflow(BEP_RO90W);
SM_RO_85W=(RO85W_Massflow(BEP_RO85W)-RO85W_Massflow(RO85WBreak))/RO85W_Massflow(BEP_RO85W);
SM_RO_80W=(RO80W_Massflow(BEP_RO80W)-RO80W_Massflow(RO80WBreak))/RO80W_Massflow(BEP_RO80W);
SM_RO_70W=(RO70W_Massflow(BEP_RO70W)-RO70W_Massflow(RO70WBreak))/RO70W_Massflow(BEP_RO70W);
SM_RO_90NW=(RO90NW_Massflow(BEP_RO90NW)-RO90NW_Massflow(RO90NWBreak))/RO90NW_Massflow(BEP_RO90NW);
SM_RO_85NW=(RO85NW_Massflow(BEP_RO85NW)-RO85NW_Massflow(RO85NWBreak))/RO85NW_Massflow(BEP_RO85NW);
SM_RO_80NW=(RO80NW_Massflow(BEP_RO80NW)-RO80NW_Massflow(RO80NWBreak))/RO80NW_Massflow(BEP_RO80NW);
SM_RO_70NW=(RO70NW_Massflow(BEP_RO70NW)-RO70NW_Massflow(RO70NWBreak))/RO70NW_Massflow(BEP_RO70NW);

SM_Rexp_90=(Rex90_Massflow(BEP_Rex90)-min(Rex90_Massflow))/Rex90_Massflow(BEP_Rex90);
SM_Rexp_85=(Rex85_Massflow(BEP_Rex85)-min(Rex85_Massflow))/Rex85_Massflow(BEP_Rex85);
SM_Rexp_80=(Rex80_Massflow(BEP_Rex80)-min(Rex80_Massflow))/Rex80_Massflow(BEP_Rex80);
SM_Rexp_70=(Rex70_Massflow(BEP_Rex70)-min(Rex70_Massflow))/Rex70_Massflow(BEP_Rex70);
%SM_IPexp_90=(IPex90_Massflow(BEP_IPex90)-min(IPex90_Massflow))/IPex90_Massflow(BEP_IPex90);
SM_IPexp_85=(IPex85_Massflow(BEP_IPex85)-min(IPex85_Massflow))/IPex85_Massflow(BEP_IPex85);
SM_IPexp_80=(IPex80_Massflow(BEP_IPex80)-min(IPex80_Massflow))/IPex80_Massflow(BEP_IPex80);
SM_IPexp_70=(IPex70_Massflow(BEP_IPex70)-min(IPex70_Massflow))/IPex70_Massflow(BEP_IPex70);

SM_Rexp85NW=(ROex85NW_Massflow(BEP_ROex85NW)-min(ROex85NW_Massflow))/ROex85NW_Massflow(BEP_ROex85NW);
SM_NACAexp85NW=(NACAex85NW_Massflow(BEP_NACAex85NW)-min(NACAex85NW_Massflow))/NACAex85NW_Massflow(BEP_NACAex85NW);


SM_IGVRO_90=(IGVRO90_Massflow(BEP_IGVRO90)-IGVRO90_Massflow(IGVRO90Break))/IGVRO90_Massflow(BEP_IGVRO90);
SM_IGVNACA_90=(IGVNACA90_Massflow(BEP_IGVNACA90)-IGVNACA90_Massflow(IGVNACA90Break))/IGVNACA90_Massflow(BEP_IGVNACA90);
```

Stall Margin Plot

```
SMplotx=[70 80 85 90];
SMploty=[SM_T_70W,SM_IP_70W,SM_RO_70W,SM_T_70NW,SM_IP_70NW,SM_RO_70NW,SM_Rexp_70,0;
    SM_T_80W,SM_IP_80W,SM_RO_80W,SM_T_80NW,SM_IP_80NW,SM_RO_80NW,SM_Rexp_80,0;
    SM_T_85W,SM_IP_85W,SM_RO_85W,SM_T_85NW,SM_IP_85NW,SM_RO_85NW,SM_Rexp_85,0;
    SM_T_90W,SM_IP_90W,SM_RO_90W,SM_T_90NW,SM_IP_90NW,SM_RO_90NW,SM_Rexp_90,SM_IGVRO_90;];

figure(3)
bar(SMplotx,SMploty)
xlabel('Rotor Speed (%)')
ylabel('Stall Margin')
legend('NACA Whirl','IP Whirl','Rotor Only Whirl','NACA No Whirl','IP No Whirl','Rotor Only No Whirl','Smooth Casing Experimental','IGV Rotor', 'Location','northeas
title('Stall Margin Improvement Comparison')
```

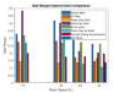

Traditional/ Working Plots

```
% Pressure Ratio NACA
figure(4)
plot(T90W_Massflow(1:T90WBreak),T90W_Pratio(1:T90WBreak), '-r')
hold on
plot(T90NW_Massflow(1:T90NWBreak),T90NW_Pratio(1:T90NWBreak),'-b')

plot(T85W_Massflow(1:T85WBreak),T85W_Pratio(1:T85WBreak), '--r')
plot(T85NW_Massflow(1:T85NWBreak),T85NW_Pratio(1:T85NWBreak),'--b')

plot(T80W_Massflow(1:T80WBreak),T80W_Pratio(1:T80WBreak), '-.r')
plot(T80NW_Massflow(1:T80NWBreak),T80NW_Pratio(1:T80NWBreak),'-.b')

plot(T70W_Massflow(1:T70WBreak),T70W_Pratio(1:T70WBreak), ':r')
plot(T70NW_Massflow(1:T70NWBreak),T70NW_Pratio(1:T70NWBreak),':b')
```

```
%legend('90% Whirl','90% No Whirl','85% Whirl','85% No Whirl','80% Whirl','80% No Whirl','70% Whirl','70% No Whirl')
xlabel('Massflow (kg/s)')
ylabel('Pressure Ratio')
title('Pressure Ratio Plot for NACA Casing')
text(7.6,1.53,'90% NW \downarrow','Color','blue')
text(6,1.52,'90% W \downarrow','Color','red')
text(7,1.48,'\downarrow 85% NW','Color','blue')
text(5.4,1.445,'85% W \downarrow','Color','red')
text(6.9,1.425,'\leftarrow 80% NW ','Color','blue')
text(6,1.35,'\leftarrow 80% W','Color','red')
text(5,1.32,'\uparrow 70% NW','Color','blue')
text(4.5,1.29,'\downarrow 70% NW ','Color','red')
grid on



% Efficiency NACA
figure(5)
plot(T90W_Massflow(1:T90WBreak),T90W_E(1:T90WBreak), '-r')
hold on
plot(T90NW_Massflow(1:T90NWBreak),T90NW_E(1:T90NWBreak),'-b')

plot(T85W_Massflow(1:T85WBreak),T85W_E(1:T85WBreak), '--r')
plot(T85NW_Massflow(1:T85NWBreak),T85NW_E(1:T85NWBreak),'--b')

plot(T80W_Massflow(1:T80WBreak),T80W_E(1:T80WBreak), '-.r')
plot(T80NW_Massflow(1:T80NWBreak),T80NW_E(1:T80NWBreak),'-.b')

plot(T70W_Massflow(1:T70WBreak),T70W_E(1:T70WBreak), ':r')
plot(T70NW_Massflow(1:T70NWBreak),T70NW_E(1:T70NWBreak),':b')

%legend('90% Whirl','90% No Whirl','85% Whirl','85% No Whirl','80% Whirl','80% No Whirl','70% Whirl','70% No Whirl')
xlabel('Massflow (kg/s)')
ylabel('Stage Efficiency Ratio')
%title('Isentropic Efficiency Plot')
grid on
text(4.7,.86,'70% W \rightarrow','Color','red')
text(5.7,.874,'80% W \downarrow','Color','red')
text(6.6,.88,'85% W \downarrow','Color','red')
text(7.5,.89,'90% W \downarrow','Color','red')
text(8.1,.88,'\leftarrow 70% NW','Color','blue')
text(8.8,.87,'\leftarrow 80% NW','Color','blue')
text(9.1,.86,'\leftarrow 85% NW','Color','blue')
text(9,.835,'\uparrow 90% NW','Color','blue')

% Treatment flow NACA and IP 90%
figure(6)
plot(T90W_Massflow(1:T90WBreak),100*T90W_TreatmentIn(1:T90WBreak)./T90W_Massflow(1:T90WBreak),'--r')
hold on
plot(T90NW_Massflow(1:T90NWBreak),100*T90NW_TreatmentOut(1:T90NWBreak)./T90NW_Massflow(1:T90NWBreak),'-.r')
plot(IP90W_Massflow(1:IP90WBreak),100*IP90W_TreatmentIn(1:IP90WBreak)./IP90W_Massflow(1:IP90WBreak),'--b')
plot(IP90NW_Massflow(1:IP90NWBreak),100*IP90NW_TreatmentOut(1:IP90NWBreak)./IP90NW_Massflow(1:IP90NWBreak),'-.b')
legend('NACA Whirl','NACA No Whirl','IP Whirl','IP No Whirl')
xlabel('Massflow (kg/s)')
ylabel('Treatment Recirculation MassRatio %')
%title('Mass Recirculation')
grid on

figure(7)
plot(T90W_Massflow(1:T90WBreak),T90W_Pratio(1:T90WBreak), '--r')
hold on
plot(T90NW_Massflow(1:T90NWBreak),T90NW_Pratio(1:T90NWBreak),'-.r')
plot(IP90W_Massflow(1:IP90WBreak),IP90W_Pratio(1:IP90WBreak), '--b')
plot(IP90NW_Massflow(1:IP90NWBreak),IP90NW_Pratio(1:IP90NWBreak),'-.b')

plot(T70W_Massflow(1:T70WBreak),T70W_Pratio(1:T70WBreak), '--r')
hold on
plot(T70NW_Massflow(1:T70NWBreak),T70NW_Pratio(1:T70NWBreak),'-.r')
plot(IP70W_Massflow(1:IP70WBreak),IP70W_Pratio(1:IP70WBreak), '--b')
plot(IP70NW_Massflow(1:IP70NWBreak),IP70NW_Pratio(1:IP70NWBreak),'-.b')
legend('90% NACA Whirl','90% NACA No Whirl','90% IP Whirl','90% IP No Whirl','location','eastoutside');
xlabel('Massflow (kg/s)')
ylabel('Pressure Ratio')
%title('Pressure Ratio Plot Comparison 90% Speed and 70% Speed ')
grid on


figure(8)
plot(T90W_Massflow(1:T90WBreak),T90W_E(1:T90WBreak), '-r')
hold on
plot(T85W_Massflow(1:T85WBreak),T85W_E(1:T85WBreak), '--r')
plot(T80W_Massflow(1:T80WBreak),T80W_E(1:T80WBreak), '-.r')
plot(T70W_Massflow(1:T70WBreak),T70W_E(1:T70WBreak), ':r')
plot(RO90W_Massflow(1:RO90WBreak),RO90W_E(1:RO90WBreak), '-b')
plot(RO85W_Massflow(1:RO85WBreak),RO85W_E(1:RO85WBreak), '--b')
plot(RO80W_Massflow(1:RO80WBreak),RO80W_E(1:RO80WBreak), '-.b')
plot(RO70W_Massflow(1:RO70WBreak),RO70W_E(1:RO70WBreak), ':b')
```

```
%legend('90% Whirl','90% No Whirl','85% Whirl','85% No Whirl','80% Whirl','80% No Whirl','70% Whirl','70% No Whirl')
xlabel('Massflow (kg/s)')
ylabel('Stage Efficiency Ratio')
%title('Isentropic Efficiency Plot')
grid on
text(4.3,.825,'70% W \rightarrow','Color','red')
text(5.7,.874,'80% W \downarrow','Color','red')
text(6.6,.88,'85% W \downarrow','Color','red')
text(7.7,.85,'\uparrow 90% W','Color','red')
text(5.5,.91,'70% W \downarrow','Color','blue')
text(6.2,.91,'80% W \downarrow','Color','blue')
text(7,.915,'85% W \downarrow','Color','blue')
text(8,.92,'\uparrow 90% W','Color','blue')


figure(9)
plot(RO90W_Massflow(1:RO90WBreak),RO90W_E(1:RO90WBreak), '-b')
hold on
plot(IGVRO90_Massflow(1:IGVRO90Break),IGVRO90_E(1:IGVRO90Break),'r')

figure(10)
plot(RO90W_Massflow(1:RO90WBreak),RO90W_Pratio(1:RO90WBreak), '-b')
hold on
plot(IGVRO90_Massflow(1:IGVRO90Break),IGVRO90_Pratio(1:IGVRO90Break),'r')
```

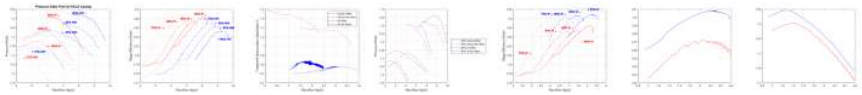

Thesis Presentation Plots

```
% much of this was cannabalized and put into 'thesis plots'

% Color coord, shapes for experimental
% experimental smooth Black
% experimental

% Rotor only, Black
% IP Red
% Naca Blue
% IGV Green
% IGVNACA cyan or magenta

% 90 -
% 85 --
% 80 -.
% 70 :


% mass recirculation
figure(15)
plot(T90W_Massflow(1:T90WBreak),100*T90W_TreatmentIn(1:T90WBreak)./T90W_Massflow(1:T90WBreak),'-b')
hold on
plot(IP90W_Massflow(1:IP90WBreak),100*IP90W_TreatmentIn(1:IP90WBreak)./IP90W_Massflow(1:IP90WBreak),'-r')
plot(T85W_Massflow(1:T85WBreak),100*T85W_TreatmentIn(1:T85WBreak)./T85W_Massflow(1:T85WBreak),'--b')
plot(IP85W_Massflow(1:IP85WBreak),100*IP85W_TreatmentIn(1:IP85WBreak)./IP85W_Massflow(1:IP85WBreak),'--r')
plot(T80W_Massflow(1:T80WBreak),100*T80W_TreatmentIn(1:T80WBreak)./T80W_Massflow(1:T80WBreak),'-.b')
plot(IP80W_Massflow(1:IP80WBreak),100*IP80W_TreatmentIn(1:IP80WBreak)./IP80W_Massflow(1:IP80WBreak),'-.r')
plot(T70W_Massflow(1:T70WBreak),100*T70W_TreatmentIn(1:T70WBreak)./T70W_Massflow(1:T70WBreak),':b')
plot(IP70W_Massflow(1:IP70WBreak),100*IP70W_TreatmentIn(1:IP70WBreak)./IP70W_Massflow(1:IP70WBreak),':r')
%legend('NACA Whirl','NACA No Whirl','IP Whirl','IP No Whirl')
text(6.5,2,'NACA','Color','blue')
text(7,.8,'IP','Color','red')
text(8,1.5,'\leftarrow 90%','Color','blue')
text(4,2.75,'\downarrow 70%','Color','blue')
text(8,.72,'\downarrow 90%','Color','red')
text(5,.78,'\downarrow 70%','Color','red')
xlabel('Massflow (kg/s)')
ylabel('Treatment Recirculation MassRatio %')
%title('Mass Recirculation')
grid on


figure(16)
plot(RO90W_Massflow(1:RO90WBreak),RO90W_E(1:RO90WBreak), '-k')
hold on
plot(IGVRO90_Massflow(1:IGVRO90Break),IGVRO90_E(1:IGVRO90Break),'g')
grid on
%title('IGV/ RO 90% Isentropic Efficiency Comparison')
ylabel('Stage Efficiency Ratio')
xlabel('Massflow (kg/s)')
text(8.2,.915,'\downarrow 90% Rotor Only','Color','black')
text(8,.875,'\downarrow 90% IGV','Color','green')

figure(17)
plot(RO90W_Massflow(1:RO90WBreak),RO90W_Pratio(1:RO90WBreak), '-k')
hold on
plot(IGVRO90_Massflow(1:IGVRO90Break),IGVRO90_Pratio(1:IGVRO90Break),'g')
```

```
%title('IGV/ RO Pressure Ratio Comparison')
ylabel('Pressure Ratio')
xlabel('Massflow (kg/s)')
text(7.75,1.51,'\leftarrow Rotor Only','Color','black')
text(6.5,1.48,'90% IGV \rightarrow','Color','green')
grid on




% Pressure Ratio NACA vs smooth casing
figure(19)
plot(Rex70_Massflow,Rex70_Pratio,':k')
hold on
plot(Rex80_Massflow,Rex80_Pratio,'-.ok')
plot(Rex85_Massflow,Rex85_Pratio,'--ok')
plot(Rex90_Massflow,Rex90_Pratio,'-ok')
plot(IPex85_Massflow,IPex85_Pratio,'-.^r')
plot(IPex80_Massflow,IPex80_Pratio,'--^r')
plot(IPex70_Massflow,IPex70_Pratio,'-^r')
text(7.4,1.15,'Smooth','Color','Black')
text(7.4,1.13,'IP','Color','Red')
%plot(RO90W_Massflow(1:RO90WBreak),RO90W_Pratio(1:RO90WBreak), '-b')
%plot(RO85W_Massflow(1:RO85WBreak),RO85W_Pratio(1:RO85WBreak), '--b')
%plot(RO80W_Massflow(1:RO80WBreak),RO80W_Pratio(1:RO80WBreak), '-.b')
%plot(RO70W_Massflow(1:RO70WBreak),RO70W_Pratio(1:RO70WBreak), ':b                ')
xlabel('Massflow (kg/s)')
ylabel('Pressure Ratio')
%title('Pressure Ratio Experimental Comparison')


figure(20)
plot(Rex70_Massflow,Rex70_E,':k')
hold on
plot(Rex80_Massflow,Rex80_E,'-.ok')
plot(Rex85_Massflow,Rex85_E,'--ok')
plot(Rex90_Massflow,Rex90_E,'-ok')
plot(IPex85_Massflow,IPex85_E,'-.^r')
plot(IPex80_Massflow,IPex80_E,'--^r')
plot(IPex70_Massflow,IPex70_E,'-^r')
text(7,0.65,'Smooth','Color','Black')
text(7,0.63,'IP','Color','Red')
%plot(RO90W_Massflow(1:RO90WBreak),RO90W_Pratio(1:RO90WBreak), '-b')
%plot(RO85W_Massflow(1:RO85WBreak),RO85W_Pratio(1:RO85WBreak), '--b')
%plot(RO80W_Massflow(1:RO80WBreak),RO80W_Pratio(1:RO80WBreak), '-.b')
%plot(RO70W_Massflow(1:RO70WBreak),RO70W_Pratio(1:RO70WBreak), ':b                ')
xlabel('Massflow (kg/s)')
ylabel('Stage Efficiency Ratio')
%title('Isentropic Efficiency Experimental Comparison')
```

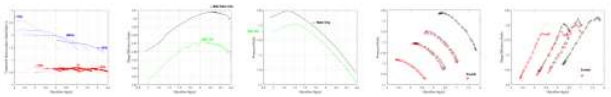

Refinement Plots

```
errorplotx=[1:40:2440];
for k=1:length(errorplotx)
errorplotPr(k)=Ref21M_Pratio(errorplotx(k));
errorplotE(k)=Ref21M_E(errorplotx(k));
end

figure(21)
plot(Ref800T_Massflow,Ref800T_Pratio,'-r')
hold on
plot(Ref7M_Massflow,Ref7M_Pratio,'-m')
plot(Ref21M_Massflow,Ref21M_Pratio,'-g')
plot(Ref38M_Massflow,Ref38M_Pratio,'-b')
errorbar(Ref21M_Massflow(errorplotx),errorplotPr,0.01*errorplotPr,'og')
grid on
xlabel('Massflow (kg/s)')
ylabel('Pressure Ratio')
%title('Pressure Ratio Refinement Data')
legend('800T','7M','21M','38M')

figure(22)
plot(Ref800T_Massflow,Ref800T_E,'-r')
hold on
plot(Ref7M_Massflow,Ref7M_E, '-m')
plot(Ref21M_Massflow,Ref21M_E,'-g')
plot(Ref38M_Massflow,Ref38M_E,'-b')
errorbar(Ref21M_Massflow(errorplotx),errorplotE,0.01*errorplotE,'og')
xlabel('Massflow (kg/s)')
ylabel('Stage Efficiency Ratio')
%title('Isentropic Efficiency Refinement Data')
legend('800T','7M','21M','38M','Location','northwest')
```

```
%%%%%%%%%%%%%%%%%%%%%%%%%%%%%%%%%%%%%%%%%%%%%%%%%%%%%%%%%%%%%%%%%%%%%%%%%%%%%%%%%%%%%%%%%%%%%%%%%%%%%%%%%%%%%%%%%%%%%%%%%%%%%%%%%%%%%
```

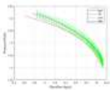
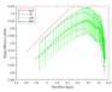

Thesis plots

```
%%%%%%%%%%%%%%%%%%%%%%%%%%%%%%%%%%%%%%%%%%%%%%%%%%%%%%%%%%%%%%%%%%%%%%%%%%%%%%%%%%%%%%%%%%%%%%%%%%%%%%%%%%%%%%%%%%%%%%%%%%%%%%%%%%%%%
% The big boi plots are below. I went for direct annotation using 'text()' instead of using 'legend()'
%  to add clarity, do this at your own peril



%   All Efficiencies Whirl
figure(23)
plot(IP90W_Massflow(1:IP90WBreak),IP90W_E(1:IP90WBreak), '-r')
hold on
plot(IP85W_Massflow(1:IP85WBreak),IP85W_E(1:IP85WBreak), '--r')
plot(IP80W_Massflow(1:IP80WBreak),IP80W_E(1:IP80WBreak), '-.r')
plot(IP70W_Massflow(1:IP70WBreak),IP70W_E(1:IP70WBreak), ':r')
plot(RO90W_Massflow(1:RO90WBreak),RO90W_E(1:RO90WBreak), '-k')
plot(RO85W_Massflow(1:RO85WBreak),RO85W_E(1:RO85WBreak), '--k')
plot(RO80W_Massflow(1:RO80WBreak),RO80W_E(1:RO80WBreak), '-.k')
plot(RO70W_Massflow(1:RO70WBreak),RO70W_E(1:RO70WBreak), ':k')
plot(T90W_Massflow(1:T90WBreak),T90W_E(1:T90WBreak), '-b')
plot(T85W_Massflow(1:T85WBreak),T85W_E(1:T85WBreak), '--b')
plot(T80W_Massflow(1:T80WBreak),T80W_E(1:T80WBreak), '-.b')
plot(T70W_Massflow(1:T70WBreak),T70W_E(1:T70WBreak), ':b')
plot(IGVRO90_Massflow(1:IGVRO90Break),IGVRO90_E(1:IGVRO90Break),'g')
plot(IGVNACA90_Massflow(1:IGVNACA90Break),IGVNACA90_E(1:IGVNACA90Break),'c')
xlabel('Massflow (kg/s)')
ylabel('Stage Efficiency Ratio')
%title('Isentropic Efficiency Plot for All Cases with Whirl')
legend('IP90','IP85','IP80','IP70','RO90','RO85','RO80','RO70','NACA90','NACA85','NACA80','NACA70','IGV90','IGV+NACA','Location','northeast')
grid on

% All Efficiencies No whirl
figure(24)
plot(IP90NW_Massflow(1:IP90NWBreak),IP90NW_E(1:IP90NWBreak), '-r')
hold on
plot(IP85NW_Massflow(1:IP85NWBreak),IP85NW_E(1:IP85NWBreak), '--r')
plot(IP80NW_Massflow(1:IP80NWBreak),IP80NW_E(1:IP80NWBreak), '-.r')
plot(IP70NW_Massflow(1:IP70NWBreak),IP70NW_E(1:IP70NWBreak), ':r')
plot(RO90NW_Massflow(1:RO90NWBreak),RO90NW_E(1:RO90NWBreak), '-k')
plot(RO85NW_Massflow(1:RO85NWBreak),RO85NW_E(1:RO85NWBreak), '--k')
plot(RO80NW_Massflow(1:RO80NWBreak),RO80NW_E(1:RO80NWBreak), '-.k')
plot(RO70NW_Massflow(1:RO70NWBreak),RO70NW_E(1:RO70NWBreak), ':k')
plot(T90NW_Massflow(1:T90NWBreak),T90NW_E(1:T90NWBreak), '-b')
plot(T85NW_Massflow(1:T85NWBreak),T85NW_E(1:T85NWBreak), '--b')
plot(T80NW_Massflow(1:T80NWBreak),T80NW_E(1:T80NWBreak), '-.b')
plot(T70NW_Massflow(1:T70NWBreak),T70NW_E(1:T70NWBreak), ':b')
xlabel('Massflow (kg/s)')
ylabel('Stage Efficiency Ratio')
%title('Isentropic Efficiency Plot for All Cases w/o Whirl')
legend('IP90','IP85','IP80','IP70','RO90','RO85','RO80','RO70','NACA90','NACA85','NACA80','NACA70','Location','northeast')
grid on


%   All Pratios Whirl
figure(25)
plot(IP90W_Massflow(1:IP90WBreak),IP90W_Pratio(1:IP90WBreak), '-r')
hold on
plot(IP85W_Massflow(1:IP85WBreak),IP85W_Pratio(1:IP85WBreak), '--r')
plot(IP80W_Massflow(1:IP80WBreak),IP80W_Pratio(1:IP80WBreak), '-.r')
plot(IP70W_Massflow(1:IP70WBreak),IP70W_Pratio(1:IP70WBreak), ':r')
plot(RO90W_Massflow(1:RO90WBreak),RO90W_Pratio(1:RO90WBreak), '-k')
plot(RO85W_Massflow(1:RO85WBreak),RO85W_Pratio(1:RO85WBreak), '--k')
plot(RO80W_Massflow(1:RO80WBreak),RO80W_Pratio(1:RO80WBreak), '-.k')
plot(RO70W_Massflow(1:RO70WBreak),RO70W_Pratio(1:RO70WBreak), ':k')
plot(T90W_Massflow(1:T90WBreak),T90W_Pratio(1:T90WBreak), '-b')
plot(T85W_Massflow(1:T85WBreak),T85W_Pratio(1:T85WBreak), '--b')
plot(T80W_Massflow(1:T80WBreak),T80W_Pratio(1:T80WBreak), '-.b')
plot(T70W_Massflow(1:T70WBreak),T70W_Pratio(1:T70WBreak), ':b')
plot(IGVRO90_Massflow(1:IGVRO90Break),IGVRO90_Pratio(1:IGVRO90Break),'g')
plot(IGVNACA90_Massflow(1:IGVNACA90Break),IGVNACA90_Pratio(1:IGVNACA90Break),'c')
xlabel('Massflow (kg/s)')
ylabel('Stage Total Pressure Ratio')
%title('Total Pressure Plot for All Cases with Whirl')
legend('IP90','IP85','IP80','IP70','RO90','RO85','RO80','RO70','NACA90','NACA85','NACA80','NACA70','IGV90','IGV+NACA','Location','northeast')
grid on

% All Pratios No whirl
figure(26)
plot(IP90NW_Massflow(1:IP90NWBreak),IP90NW_Pratio(1:IP90NWBreak), '-r')
hold on
```

```
plot(IP85NW_Massflow(1:IP85NWBreak),IP85NW_Pratio(1:IP85NWBreak), '--r')
plot(IP80NW_Massflow(1:IP80NWBreak),IP80NW_Pratio(1:IP80NWBreak), '-.r')
plot(IP70NW_Massflow(1:IP70NWBreak),IP70NW_Pratio(1:IP70NWBreak), ':r')
plot(RO90NW_Massflow(1:RO90NWBreak),RO90NW_Pratio(1:RO90NWBreak), '-k')
plot(RO85NW_Massflow(1:RO85NWBreak),RO85NW_Pratio(1:RO85NWBreak), '--k')
plot(RO80NW_Massflow(1:RO80NWBreak),RO80NW_Pratio(1:RO80NWBreak), '-.k')
plot(RO70NW_Massflow(1:RO70NWBreak),RO70NW_Pratio(1:RO70NWBreak), ':k')
plot(T90NW_Massflow(1:T90NWBreak),T90NW_Pratio(1:T90NWBreak), '-b')
plot(T85NW_Massflow(1:T85NWBreak),T85NW_Pratio(1:T85NWBreak), '--b')
plot(T80NW_Massflow(1:T80NWBreak),T80NW_Pratio(1:T80NWBreak), '-.b')
plot(T70NW_Massflow(1:T70NWBreak),T70NW_Pratio(1:T70NWBreak), ':b')
xlabel('Massflow (kg/s)')
ylabel('Stage Total Pressure Ratio')
%title('Total Pressure Plot for All Cases w/o Whirl')
legend('IP90','IP85','IP80','IP70','RO90','RO85','RO80','RO70','NACA90','NACA85','NACA80','NACA70','Location','northeast')
grid on




%(Ro whirl vs RO no whirl Pr & E)
figure(27)
plot(RO90NW_Massflow(1:RO90NWBreak),RO90NW_E(1:RO90NWBreak), '-k')
hold on
plot(RO85NW_Massflow(1:RO85NWBreak),RO85NW_E(1:RO85NWBreak), '--k')
plot(RO80NW_Massflow(1:RO80NWBreak),RO80NW_E(1:RO80NWBreak), '-.k')
plot(RO70NW_Massflow(1:RO70NWBreak),RO70NW_E(1:RO70NWBreak), ':k')
plot(RO90W_Massflow(1:RO90WBreak),RO90W_E(1:RO90WBreak), '-k')
plot(RO85W_Massflow(1:RO85WBreak),RO85W_E(1:RO85WBreak), '--k')
plot(RO80W_Massflow(1:RO80WBreak),RO80W_E(1:RO80WBreak), '-.k')
plot(RO70W_Massflow(1:RO70WBreak),RO70W_E(1:RO70WBreak), ':k')
text(9.5,.9,'No Whirl','color','black')
text(6,.9,'Whirl','color','black')
text(8.9,.87,'\leftarrow 90%','color','black')
text(8.2,.86,'\leftarrow 85%','color','black')
text(6.7,.82,'\leftarrow 80%','color','black')
text(6.05,.835,'\leftarrow 70%','color','black')
%title('Whirl vs No Whirl Effciency Comparison RO')
xlabel('Massflow (kg/s)')
ylabel('Stage Efficiency Ratio')
grid on

figure(28)
plot(RO90NW_Massflow(1:RO90NWBreak),RO90NW_Pratio(1:RO90NWBreak), '-k')
hold on
plot(RO85NW_Massflow(1:RO85NWBreak),RO85NW_Pratio(1:RO85NWBreak), '--k')
plot(RO80NW_Massflow(1:RO80NWBreak),RO80NW_Pratio(1:RO80NWBreak), '-.k')
plot(RO70NW_Massflow(1:RO70NWBreak),RO70NW_Pratio(1:RO70NWBreak), ':k')
plot(RO90W_Massflow(1:RO90WBreak),RO90W_Pratio(1:RO90WBreak), '-k')
plot(RO85W_Massflow(1:RO85WBreak),RO85W_Pratio(1:RO85WBreak), '--k')
plot(RO80W_Massflow(1:RO80WBreak),RO80W_Pratio(1:RO80WBreak), '-.k')
plot(RO70W_Massflow(1:RO70WBreak),RO70W_Pratio(1:RO70WBreak), ':k')
plot([RO90NW_Massflow(BEP_RO90NW),RO85NW_Massflow(BEP_RO85NW),RO80NW_Massflow(BEP_RO80NW),RO70NW_Massflow(BEP_RO70NW)], ...
    [RO90NW_Pratio(BEP_RO90NW),RO85NW_Pratio(BEP_RO85NW),RO80NW_Pratio(BEP_RO80NW),RO70NW_Pratio(BEP_RO70NW)],'-sk')
plot([RO90W_Massflow(BEP_RO90W),RO85W_Massflow(BEP_RO85W),RO80W_Massflow(BEP_RO80W),RO70W_Massflow(BEP_RO70W)], ...
    [RO90W_Pratio(BEP_RO90W),RO85W_Pratio(BEP_RO85W),RO80W_Pratio(BEP_RO80W),RO70W_Pratio(BEP_RO70W)],'-ok')
text(10,1.36,'No Whirl','color','black')
text(6.2,1.53,'Whirl','color','black')
text(10,1.5,'\leftarrow 90%','color','black')
text(9.6,1.4,'\leftarrow 85%','color','black')
text(9.2,1.325,'\leftarrow 80%','color','black')
text(8,1.25,'\leftarrow 70%','color','black')
xlabel('Massflow (kg/s)')
ylabel('Stage Total Pressure Ratio')
%title('Whirl vs No Whirl Pressure Ratio Comparison RO')
grid on




%(NACA Whirl vs NACA No whirl Pr & E)
figure(29)
plot(T90NW_Massflow(1:T90NWBreak),T90NW_E(1:T90NWBreak), '-b')
hold on
plot(T85NW_Massflow(1:T85NWBreak),T85NW_E(1:T85NWBreak), '--b')
plot(T80NW_Massflow(1:T80NWBreak),T80NW_E(1:T80NWBreak), '-.b')
plot(T70NW_Massflow(1:T70NWBreak),T70NW_E(1:T70NWBreak), ':b')
plot(T90W_Massflow(1:T90WBreak),T90W_E(1:T90WBreak), '-b')
plot(T85W_Massflow(1:T85WBreak),T85W_E(1:T85WBreak), '--b')
plot(T80W_Massflow(1:T80WBreak),T80W_E(1:T80WBreak), '-.b')
plot(T70W_Massflow(1:T70WBreak),T70W_E(1:T70WBreak), ':b')
text(9,.835,'No Whirl','color','blue')
text(6.4,0.88,'Whirl','color','blue')
text(7.7,0.89,'90% \downarrow','color','blue')
text(7,.88,'85% \downarrow','color','blue')
text(6.1,0.871,'80% \downarrow','color','blue')
text(5.5,.869,'70% \downarrow','color','blue')
xlabel('Massflow (kg/s)')
ylabel('Stage Efficiency Ratio')
%title('Whirl vs No Whirl Effiecncy Comparison NACA')
```

```
grid on

figure(30)
plot(T90NW_Massflow(1:T90NWBreak),T90NW_Pratio(1:T90NWBreak), '-b')
hold on
plot(T85NW_Massflow(1:T85NWBreak),T85NW_Pratio(1:T85NWBreak), '--b')
plot(T80NW_Massflow(1:T80NWBreak),T80NW_Pratio(1:T80NWBreak), '-.b')
plot(T70NW_Massflow(1:T70NWBreak),T70NW_Pratio(1:T70NWBreak), ':b')
plot(T90W_Massflow(1:T90WBreak),T90W_Pratio(1:T90WBreak), '-b')
plot(T85W_Massflow(1:T85WBreak),T85W_Pratio(1:T85WBreak), '--b')
plot(T80W_Massflow(1:T80WBreak),T80W_Pratio(1:T80WBreak), '-.b')
plot(T70W_Massflow(1:T70WBreak),T70W_Pratio(1:T70WBreak), ':b')
plot([T90NW_Massflow(BEP_T90NW),T85NW_Massflow(BEP_T85NW),T80NW_Massflow(BEP_T80NW),T70NW_Massflow(BEP_T70NW)], ...
    [T90NW_Pratio(BEP_T90NW),T85NW_Pratio(BEP_T85NW),T80NW_Pratio(BEP_T80NW),T70NW_Pratio(BEP_T70NW)],'-sb')
plot([T90W_Massflow(BEP_T90W),T85W_Massflow(BEP_T85W),T80W_Massflow(BEP_T80W),T70W_Massflow(BEP_T70W)], ...
    [T90W_Pratio(BEP_T90W),T85W_Pratio(BEP_T85W),T80W_Pratio(BEP_T80W),T70W_Pratio(BEP_T70W)],'-ob')


text(9,1.5,'No Whirl','color','blue')
text(6,1.52,'Whirl','color','blue')
text(9.2,1.375,'90% \uparrow','color','blue')
text(8.75,1.336,'85% \uparrow','color','blue')
text(8.4,1.28,'80% \uparrow','color','blue')
text(7.5,1.2,'70% \uparrow','color','blue')
xlabel('Massflow (kg/s)')
ylabel('Stage Total Pressure Ratio')
%title('Whirl vs No Whirl Pressure Ratio Comparison NACA')
grid on




% NACA vs RO whirl p-ratio
figure(31)
plot(T90W_Massflow(1:T90WBreak),T90W_Pratio(1:T90WBreak), '-b')
hold on
plot(T85W_Massflow(1:T85WBreak),T85W_Pratio(1:T85WBreak), '--b')
plot(T80W_Massflow(1:T80WBreak),T80W_Pratio(1:T80WBreak), '-.b')
plot(T70W_Massflow(1:T70WBreak),T70W_Pratio(1:T70WBreak), ':b')
plot(RO90W_Massflow(1:RO90WBreak),RO90W_Pratio(1:RO90WBreak), '-k')
plot(RO85W_Massflow(1:RO85WBreak),RO85W_Pratio(1:RO85WBreak), '--k')
plot(RO80W_Massflow(1:RO80WBreak),RO80W_Pratio(1:RO80WBreak), '-.k')
plot(RO70W_Massflow(1:RO70WBreak),RO70W_Pratio(1:RO70WBreak), ':k')
xlabel('Massflow (kg/s)')
ylabel('Pressure Ratio')
%title('Pressure Ratio Plot for NACA/ RO Casings with Whirl')
%text(7.6,1.53,'90% NW \downarrow','Color','blue')
%text(6,1.52,'90% W \downarrow','Color','red')
text(8,1.2,'Rotor Only','Color','black')
text(8,1.18,'NACA','Color','blue')
text(8.4,1.32,'\uparrow 90%','Color','black')
text(7.7,1.26,'\uparrow 85%','Color','black')
text(7.1,1.225,'\uparrow 80%','Color','black')
text(6.4,1.17,'\leftarrow 70%','Color','black')
%BEP line
plot([T90W_Massflow(BEP_T90W),T85W_Massflow(BEP_T85W),T80W_Massflow(BEP_T80W),T70W_Massflow(BEP_T70W)], ...
    [T90W_Pratio(BEP_T90W),T85W_Pratio(BEP_T85W),T80W_Pratio(BEP_T80W),T70W_Pratio(BEP_T70W)],'-ob')
plot([RO90W_Massflow(BEP_RO90W),RO85W_Massflow(BEP_RO85W),RO80W_Massflow(BEP_RO80W),RO70W_Massflow(BEP_RO70W)], ...
    [RO90W_Pratio(BEP_RO90W),RO85W_Pratio(BEP_RO85W),RO80W_Pratio(BEP_RO80W),RO70W_Pratio(BEP_RO70W)],'-ok')

%Stall Line
%plot([T90W_Massflow(T90WBreak),T85W_Massflow(T85WBreak),T80W_Massflow(T80WBreak),T70W_Massflow(T70WBreak)], ...
 %   [T90W_Pratio(T90WBreak),T85W_Pratio(T85WBreak),T80W_Pratio(T80WBreak),T70W_Pratio(T70WBreak)],'-ob')
%plot([RO90W_Massflow(RO90WBreak),RO85W_Massflow(RO85WBreak),RO80W_Massflow(RO80WBreak),RO70W_Massflow(RO70WBreak)], ...
%    [RO90W_Pratio(RO90WBreak),RO85W_Pratio(RO85WBreak),RO80W_Pratio(RO80WBreak),RO70W_Pratio(RO70WBreak)],'-ok')
grid on


% NACA vs RO whirl E
figure(32)
plot(T90W_Massflow(1:T90WBreak),T90W_E(1:T90WBreak), '-b')
hold on
plot(T85W_Massflow(1:T85WBreak),T85W_E(1:T85WBreak), '--b')
plot(T80W_Massflow(1:T80WBreak),T80W_E(1:T80WBreak), '-.b')
plot(T70W_Massflow(1:T70WBreak),T70W_E(1:T70WBreak), ':b')
plot(RO90W_Massflow(1:RO90WBreak),RO90W_E(1:RO90WBreak), '-k')
plot(RO85W_Massflow(1:RO85WBreak),RO85W_E(1:RO85WBreak), '--k')
plot(RO80W_Massflow(1:RO80WBreak),RO80W_E(1:RO80WBreak), '-.k')
plot(RO70W_Massflow(1:RO70WBreak),RO70W_E(1:RO70WBreak), ':k')
xlabel('Massflow (kg/s)')
ylabel('Stage Efficiency Ratio')
%title('Isentropic Efficiency Plot for NACA/ RO with Whirl')
grid on

text(7.8,0.915,'90% \downarrow','Color','black')
text(7,0.91,'85% \downarrow','Color','black')
text(6.2,0.905,'80% \downarrow','Color','black')
text(5.3,0.898,'70% \downarrow','Color','black')
text(7.5,0.85,'NACA','Color','blue')
text(4.2,0.875,'Rotor Only','Color','black')
```

```
%text(6,1.35,'\leftarrow 80% W','Color','red')
%text(5,1.32,'\uparrow 70% NW','Color','blue')
%text(4.5,1.29,'\downarrow 70% NW ','Color','red')


% IP vs RO
figure(33)
plot(IP90W_Massflow(1:IP90WBreak),IP90W_Pratio(1:IP90WBreak), '-r')
hold on
plot(IP85W_Massflow(1:IP85WBreak),IP85W_Pratio(1:IP85WBreak), '--r')
plot(IP80W_Massflow(1:IP80WBreak),IP80W_Pratio(1:IP80WBreak), '-.r')
plot(IP70W_Massflow(1:IP70WBreak),IP70W_Pratio(1:IP70WBreak), ':r')
plot(RO90W_Massflow(1:RO90WBreak),RO90W_Pratio(1:RO90WBreak), '-k')
plot(RO85W_Massflow(1:RO85WBreak),RO85W_Pratio(1:RO85WBreak), '--k')
plot(RO80W_Massflow(1:RO80WBreak),RO80W_Pratio(1:RO80WBreak), '-.k')
plot(RO70W_Massflow(1:RO70WBreak),RO70W_Pratio(1:RO70WBreak), ':k')
xlabel('Massflow (kg/s)')
ylabel('Pressure Ratio')
%title('Pressure Ratio Plot for IP/ RO Casings with Whirl')
text(8,1.2,'Rotor Only','Color','black')
text(8,1.18,'IP','Color','red')
text(8.4,1.32,'\uparrow 90%','Color','black')
text(7.7,1.26,'\uparrow 85%','Color','black')
text(7.1,1.225,'\uparrow 80%','Color','black')
text(6.4,1.17,'\leftarrow 70%','Color','black')
%BEP line
plot([IP90W_Massflow(BEP_IP90W),IP85W_Massflow(BEP_IP85W),IP80W_Massflow(BEP_IP80W),IP70W_Massflow(BEP_IP70W)], ...
    [IP90W_Pratio(BEP_IP90W),IP85W_Pratio(BEP_IP85W),IP80W_Pratio(BEP_IP80W),IP70W_Pratio(BEP_IP70W)],'-or')
plot([RO90W_Massflow(BEP_RO90W),RO85W_Massflow(BEP_RO85W),RO80W_Massflow(BEP_RO80W),RO70W_Massflow(BEP_RO70W)], ...
    [RO90W_Pratio(BEP_RO90W),RO85W_Pratio(BEP_RO85W),RO80W_Pratio(BEP_RO80W),RO70W_Pratio(BEP_RO70W)],'-ok')
grid on
%Stall Line
%plot([IP90W_Massflow(IP90WBreak),IP85W_Massflow(IP85WBreak),IP80W_Massflow(IP80WBreak),IP70W_Massflow(IP70WBreak)], ...
 %   [IP90W_Pratio(IP90WBreak),IP85W_Pratio(IP85WBreak),IP80W_Pratio(IP80WBreak),IP70W_Pratio(IP70WBreak)],'-ob')
%plot([RO90W_Massflow(RO90WBreak),RO85W_Massflow(RO85WBreak),RO80W_Massflow(RO80WBreak),RO70W_Massflow(RO70WBreak)], ...
%    [RO90W_Pratio(RO90WBreak),RO85W_Pratio(RO85WBreak),RO80W_Pratio(RO80WBreak),RO70W_Pratio(RO70WBreak)],'-ok')


% IP vs RO whirl eff
figure(34)
plot(IP90W_Massflow(1:IP90WBreak),IP90W_E(1:IP90WBreak), '-r')
hold on
plot(IP85W_Massflow(1:IP85WBreak),IP85W_E(1:IP85WBreak), '--r')
plot(IP80W_Massflow(1:IP80WBreak),IP80W_E(1:IP80WBreak), '-.r')
plot(IP70W_Massflow(1:IP70WBreak),IP70W_E(1:IP70WBreak), ':r')
plot(RO90W_Massflow(1:RO90WBreak),RO90W_E(1:RO90WBreak), '-k')
plot(RO85W_Massflow(1:RO85WBreak),RO85W_E(1:RO85WBreak), '--k')
plot(RO80W_Massflow(1:RO80WBreak),RO80W_E(1:RO80WBreak), '-.k')
plot(RO70W_Massflow(1:RO70WBreak),RO70W_E(1:RO70WBreak), ':k')
xlabel('Massflow (kg/s)')
ylabel('Stage Efficiency Ratio')
%title('Isentropic Efficiency Plot for IP/ RO with Whirl')
grid on

text(8.5,0.906,'\leftarrow 90%','Color','black')
text(7,0.908,'85% \downarrow','Color','black')
text(6.2,0.904,'80% \downarrow','Color','black')
text(5.3,0.897,'70% \downarrow','Color','black')
text(7.5,0.855,'IP','Color','red')
text(4.2,0.875,'Rotor Only','Color','black')



%(SM Bar plot for whirl)
SMplotx=[70 80 85 90];
SMploty=[SM_T_70W,SM_IP_70W,SM_RO_70W;
    SM_T_80W,SM_IP_80W,SM_RO_80W;
    SM_T_85W,SM_IP_85W,SM_RO_85W;
    SM_T_90W,SM_IP_90W,SM_RO_90W;];
figure(35)
bar(SMplotx,SMploty)
xlabel('Rotor Speed (%)')
ylabel('Stall Margin')
legend('NACA Whirl','IP Whirl','Rotor Only Whirl', 'Location','northeast')
%title('Stall Margin Improvement Comparison with Whirl')

SMplotx=[70 80 85 90];
SMploty=[SM_T_70NW,SM_IP_70NW,SM_RO_70NW;
    SM_T_80NW,SM_IP_80NW,SM_RO_80NW;
    SM_T_85NW,SM_IP_85NW,SM_RO_85NW;
    SM_T_90NW,SM_IP_90NW,SM_RO_90NW;];
figure(36)
bar(SMplotx,SMploty)
xlabel('Rotor Speed (%)')
ylabel('Stall Margin')
legend('NACA NWhirl','IP NWhirl','Rotor Only NWhirl', 'Location','northeast')
%title('Stall Margin Improvement Comparison w/o Whirl')
```

```
%(mass recirc for whirl NACA and IP)
figure(37)
plot(T90W_Massflow(1:T90WBreak),100*T90W_TreatmentIn(1:T90WBreak)./T90W_Massflow(1:T90WBreak),'-b')
hold on
plot(IP90W_Massflow(1:IP90WBreak),100*IP90W_TreatmentIn(1:IP90WBreak)./IP90W_Massflow(1:IP90WBreak),'-r')
plot(T85W_Massflow(1:T85WBreak),100*T85W_TreatmentIn(1:T85WBreak)./T85W_Massflow(1:T85WBreak),'--b')
plot(IP85W_Massflow(1:IP85WBreak),100*IP85W_TreatmentIn(1:IP85WBreak)./IP85W_Massflow(1:IP85WBreak),'--r')
plot(T80W_Massflow(1:T80WBreak),100*T80W_TreatmentIn(1:T80WBreak)./T80W_Massflow(1:T80WBreak),'-.b')
plot(IP80W_Massflow(1:IP80WBreak),100*IP80W_TreatmentIn(1:IP80WBreak)./IP80W_Massflow(1:IP80WBreak),'-.r')
plot(T70W_Massflow(1:T70WBreak),100*T70W_TreatmentIn(1:T70WBreak)./T70W_Massflow(1:T70WBreak),':b')
plot(IP70W_Massflow(1:IP70WBreak),100*IP70W_TreatmentIn(1:IP70WBreak)./IP70W_Massflow(1:IP70WBreak),':r')
text(6.5,2,'NACA','Color','blue')
text(7,.8,'IP','Color','red')
text(8,1.5,'\leftarrow 90%','Color','blue')
text(4,2.75,'\downarrow 70%','Color','blue')
text(8,.72,'\downarrow 90%','Color','red')
text(5,.78,'\downarrow 70%','Color','red')
xlabel('Massflow (kg/s)')
ylabel('Treatment Recirculation MassRatio %')
%title('Mass Recirculation with Whirl')
grid on




%(Mass recirc for no whirl NACA and IP)

figure(38)
plot(T90NW_Massflow(1:T90NWBreak),100*T90NW_TreatmentIn(1:T90NWBreak)./T90NW_Massflow(1:T90NWBreak),'-b')
hold on
plot(IP90NW_Massflow(1:IP90NWBreak),100*IP90NW_TreatmentIn(1:IP90NWBreak)./IP90NW_Massflow(1:IP90NWBreak),'-r')
plot(T85NW_Massflow(1:T85NWBreak),100*T85NW_TreatmentIn(1:T85NWBreak)./T85NW_Massflow(1:T85NWBreak),'--b')
plot(IP85NW_Massflow(1:IP85NWBreak),100*IP85NW_TreatmentIn(1:IP85NWBreak)./IP85NW_Massflow(1:IP85NWBreak),'--r')
plot(T80NW_Massflow(1:T80NWBreak),100*T80NW_TreatmentIn(1:T80NWBreak)./T80NW_Massflow(1:T80NWBreak),'-.b')
plot(IP80NW_Massflow(1:IP80NWBreak),100*IP80NW_TreatmentIn(1:IP80NWBreak)./IP80NW_Massflow(1:IP80NWBreak),'-.r')
plot(T70NW_Massflow(1:T70NWBreak),100*T70NW_TreatmentIn(1:T70NWBreak)./T70NW_Massflow(1:T70NWBreak),':b')
plot(IP70NW_Massflow(1:IP70NWBreak),100*IP70NW_TreatmentIn(1:IP70NWBreak)./IP70NW_Massflow(1:IP70NWBreak),':r')
text(6.5,2,'NACA','Color','blue')
text(7,.8,'IP','Color','red')
text(9,1.45,'\downarrow 90%','Color','blue')
text(5,2.28,'\leftarrow 70%','Color','blue')
text(9,.65,'90% \downarrow','Color','red')
text(5.2,.6,'70% \rightarrow','Color','red')
xlabel('Massflow (kg/s)')
ylabel('Treatment Recirculation MassRatio %')
%title('Mass Recirculation w/o Whirl')
grid on



%(RO and IGV PR&E)

figure(39)
plot(RO90W_Massflow(1:RO90WBreak),RO90W_E(1:RO90WBreak), '-k')
hold on
plot(IGVRO90_Massflow(1:IGVRO90Break),IGVRO90_E(1:IGVRO90Break),'g')
grid on
%title('IGV/ RO 90% Isentropic Efficiency Comparison')
ylabel('Stage Efficiency Ratio')
xlabel('Massflow (kg/s)')
text(8,.9,'90% Rotor Only \uparrow','Color','black')
text(8,.875,'\downarrow 90% IGV','Color','green')

figure(40)
plot(RO90W_Massflow(1:RO90WBreak),RO90W_Pratio(1:RO90WBreak), '-k')
hold on
plot(IGVRO90_Massflow(1:IGVRO90Break),IGVRO90_Pratio(1:IGVRO90Break),'g')
%title('IGV/ RO 90% Pressure Ratio Comparison')
ylabel('Pressure Ratio')
xlabel('Massflow (kg/s)')
text(7.75,1.51,'\leftarrow 90% Rotor Only','Color','black')
text(7.4,1.47,'90% IGV \rightarrow','Color','green')
grid on



%(NACA and IGV+NACA PR&E)
figure(41)
plot(IGVNACA90_Massflow(1:IGVNACA90Break),IGVNACA90_E(1:IGVNACA90Break),'c')
hold on
plot(T90W_Massflow(1:T90WBreak),T90W_E(1:T90WBreak), '-b')
grid on
%title('IGV+NACA/ NACA 90% Isentropic Efficiency Comparison')
ylabel('Stage Efficiency Ratio')
xlabel('Massflow (kg/s)')
text(6.3,.86,'90% NACA Whirl \rightarrow','Color','blue')
```

```
text(6.1,.79,'90% IGV+NACA \rightarrow','Color','cyan')


figure(42)
plot(IGVNACA90_Massflow(1:IGVNACA90Break),IGVNACA90_Pratio(1:IGVNACA90Break),'c')
hold on
plot(T90W_Massflow(1:T90WBreak),T90W_Pratio(1:T90WBreak), '-b')
%title('IGV+NACA/ NACA 90% Pressure Ratio Comparison')
ylabel('Pressure Ratio')
xlabel('Massflow (kg/s)')
text(6.5,1.52,'\downarrow 90% NACA Whirl','Color','blue')
text(6.4,1.44,'90% IGV+NACA \rightarrow','Color','cyan')
grid on




%(90\% SM Bar plot of RO NACA IP IGV IGVNACA)

SMplotx=[90];
SMploty=[SM_T_90W,SM_IGVNACA_90,SM_RO_90W,SM_IGVRO_90];
figure(43)
bar(SMplotx,SMploty)
xlabel('Rotor Speed (%)')
ylabel('Stall Margin')
legend('NACA Whirl','IGV+NACA','Rotor Only Whirl','IGV+Rotor', 'Location','northeast')
%title('Stall Margin Improvement Comparison between Whirl and IGV')
```

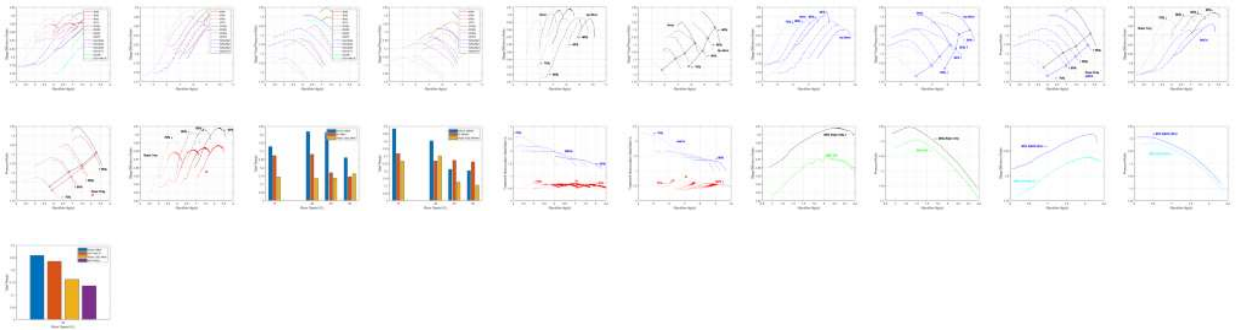

Experimental

```
% IP plots
figure(44)
plot(Rex70_Massflow,Rex70_E,':sk')
hold on
plot(Rex80_Massflow,Rex80_E,'-.sk')
plot(Rex85_Massflow,Rex85_E,'--sk')
plot(Rex90_Massflow,Rex90_E,'-sk')
plot(IPex85_Massflow,IPex85_E,'-.^r')
plot(IPex80_Massflow,IPex80_E,'--^r')
plot(IPex70_Massflow,IPex70_E,'-^r')
text(7,0.64,'Smooth','Color','Black')
text(7,0.63,'IP','Color','Red')
text(7.4,0.84,'90% \downarrow','Color','Black')
text(6.55,.83,'85% \downarrow','Color','Black')
text(5.9,.82,'80% \downarrow','Color','Black')
text(5.2,.82,'70% \downarrow','Color','Black')
xlabel('Massflow (kg/s)')
ylabel('Stage Efficiency Ratio')
%title('RO-IP, Isentropic Efficiency Experimental Data Comparison')
grid on


figure(45)
plot(Rex70_Massflow,Rex70_Pratio,':sk')
hold on
plot(Rex80_Massflow,Rex80_Pratio,'-.sk')
plot(Rex85_Massflow,Rex85_Pratio,'--sk')
plot(Rex90_Massflow,Rex90_Pratio,'-sk')
plot(IPex85_Massflow,IPex85_Pratio,'-.^r')
plot(IPex80_Massflow,IPex80_Pratio,'--^r')
plot(IPex70_Massflow,IPex70_Pratio,'-^r')
text(7,1.14,'Smooth','Color','Black')
text(7,1.12,'IP','Color','Red')
text(5.7,1.435,'90% \rightarrow','Color','Black')
text(5,1.35,'85% \rightarrow','Color','Black')
text(4.5,1.3,'80% \rightarrow','Color','Black')
text(4.3,1.24,'70% \downarrow','Color','Black')
xlabel('Massflow (kg/s)')
ylabel('Pressure Ratio')
%title('RO-IP, Pressure Ratio Experimental Data Comparison')
grid on
%plot(RO90W_Massflow(1:RO90WBreak),RO90W_Pratio(1:RO90WBreak), '-b')
```

```
%plot(RO85W_Massflow(1:RO85WBreak),RO85W_Pratio(1:RO85WBreak), '--b')
%plot(RO80W_Massflow(1:RO80WBreak),RO80W_Pratio(1:RO80WBreak), '-.b')
%plot(RO70W_Massflow(1:RO70WBreak),RO70W_Pratio(1:RO70WBreak), ':b


SMplotx=[70 80 85];
SMploty=[SM_Rexp_70,SM_IPexp_70;SM_Rexp_80,SM_IPexp_80;SM_Rexp_85,SM_IPexp_85];
figure(46)
bar(SMplotx,SMploty)
xlabel('Rotor Speed (%)')
ylabel('Stall Margin')
legend('Rotor Only Experimental','IP Experimental', 'Location','northeast')
%title('Stall Margin Improvement Comparison with Whirl')



% NACA plots
figure(47)
%plot(Rex85_Massflow,Rex85_E,'--ok')

plot(NACAex85NW_Massflow,NACAex85NW_E,'--vb')
hold on
plot(ROex85NW_Massflow,ROex85NW_E,'--sk')
text(8,.8,'\leftarrow 85% Smooth','Color','Black')
text(8.5,.75,'\leftarrow 85% NACA','Color','Blue')
xlabel('Massflow (kg/s)')
ylabel('Stage Efficiency Ratio')
%title('RO-IP, Isentropic Efficiency Experimental Data Comparison')
grid on




figure(48)
%plot(Rex85_Massflow,Rex85_Pratio,'--ok')
plot(NACAex85NW_Massflow,NACAex85NW_Pratio,'--vb')
hold on
plot(ROex85NW_Massflow,ROex85NW_Pratio,'--sk')
text(8.4,1.5,'\downarrow 85% Smooth','Color','Black')
text(7.5,1.45,'\downarrow 85% NACA','Color','Blue')
xlabel('Massflow (kg/s)')
ylabel('Pressure Ratio')
%title('RO-IP, Pressure Ratio Experimental Data Comparison')
grid on
%plot(RO90W_Massflow(1:RO90WBreak),RO90W_Pratio(1:RO90WBreak), '-b')







SMplotx=[85];
SMploty=[SM_Rexp85NW,SM_NACAexp85NW];
figure(50)
bar(SMplotx,SMploty)
xlabel('Rotor Speed (%)')
ylabel('Stall Margin')
legend('Rotor Only Experimental','NACA Experimental', 'Location','northeast')
%title('Stall Margin Improvement Comparison with Whirl')
```

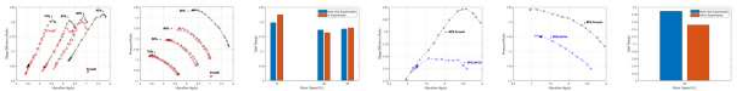

Comp Plots

```
figure(52)
plot(Rex70_Massflow,Rex70_E,':sk')
hold on
plot(Rex80_Massflow,Rex80_E,'-.sk')
plot(Rex85_Massflow,Rex85_E,'--sk')
plot(Rex90_Massflow,Rex90_E,'-sk')
plot(IPex85_Massflow,IPex85_E,'-.^r')
plot(IPex80_Massflow,IPex80_E,'--^r')
plot(IPex70_Massflow,IPex70_E,'-^r')
plot(IP90W_Massflow(1:IP90WBreak),IP90W_E(1:IP90WBreak), '-r')
hold on
plot(IP85W_Massflow(1:IP85WBreak),IP85W_E(1:IP85WBreak), '--r')
plot(IP80W_Massflow(1:IP80WBreak),IP80W_E(1:IP80WBreak), '-.r')
plot(IP70W_Massflow(1:IP70WBreak),IP70W_E(1:IP70WBreak), ':r')
%plot(RO90W_Massflow(1:RO90WBreak),RO90W_E(1:RO90WBreak), '-k')
plot(RO85W_Massflow(1:RO85WBreak),RO85W_E(1:RO85WBreak), '--k')
plot(RO80W_Massflow(1:RO80WBreak),RO80W_E(1:RO80WBreak), '-.k')
plot(RO70W_Massflow(1:RO70WBreak),RO70W_E(1:RO70WBreak), ':k')
text(7.5,0.855,'\uparrow 90% IP CFD','Color','red')
```

```
text(7.3,0.925,'\downarrow 90% Rotor Only CFD','Color','black')
text(6.6,0.675,'\leftarrow 90% Smooth Experimental','Color','Black')
text(6,0.65,'\leftarrow 85% IP Experiemntal','Color','Red')
text(4,0.855,' 70% IP CFD \rightarrow','Color','red')
text(4.3,0.91,'70% Rotor Only CFD \downarrow','Color','black')

xlabel('Massflow (kg/s)')
ylabel('Stage Efficiency Ratio')
grid on

figure(54)
plot(Rex70_Massflow,Rex70_Pratio,':sk')
hold on
plot(Rex80_Massflow,Rex80_Pratio,'-.sk')
plot(Rex85_Massflow,Rex85_Pratio,'--sk')
plot(Rex90_Massflow,Rex90_Pratio,'-sk')
plot(IPex85_Massflow,IPex85_Pratio,'-.^r')
plot(IPex80_Massflow,IPex80_Pratio,'--^r')
plot(IPex70_Massflow,IPex70_Pratio,'-^r')
plot(IP90W_Massflow(1:IP90WBreak),IP90W_Pratio(1:IP90WBreak), '-r')
plot(IP85W_Massflow(1:IP85WBreak),IP85W_Pratio(1:IP85WBreak), '--r')
plot(IP80W_Massflow(1:IP80WBreak),IP80W_Pratio(1:IP80WBreak), '-.r')
plot(IP70W_Massflow(1:IP70WBreak),IP70W_Pratio(1:IP70WBreak), ':r')
plot(RO90W_Massflow(1:RO90WBreak),RO90W_Pratio(1:RO90WBreak), '-k')
plot(RO85W_Massflow(1:RO85WBreak),RO85W_Pratio(1:RO85WBreak), '--k')
plot(RO80W_Massflow(1:RO80WBreak),RO80W_Pratio(1:RO80WBreak), '-.k')
plot(RO70W_Massflow(1:RO70WBreak),RO70W_Pratio(1:RO70WBreak), ':k')
%plot(IGVRO90_Massflow(1:IGVRO90Break),IGVRO90_Pratio(1:IGVRO90Break),'g')
%text(8,1.2,'Rotor Only','Color','black')
text(4,1.29,'70% CFD \downarrow','Color','black')
text(8.1,1.45,'\leftarrow 90% CFD','Color','black')
text(7.8,1.25,'\uparrow 90% Exp.','Color','black')
text(4.5,1.15,'70% Exp. \rightarrow','Color','black')
%text(6.4,1.17,'\leftarrow 70%','Color','black')
text(7,1.14,'Smooth','Color','Black')
text(7,1.12,'IP','Color','Red')
xlabel('Massflow (kg/s)')
ylabel('Pressure Ratio')
grid on


figure(55)
plot(NACAex85NW_Massflow,NACAex85NW_Pratio,'--vb')
hold on
plot(ROex85NW_Massflow,ROex85NW_Pratio,'--sk')
plot(RO85NW_Massflow(1:RO85NWBreak),RO85NW_Pratio(1:RO85NWBreak), '--k')
plot(T85NW_Massflow(1:T85NWBreak),T85NW_Pratio(1:T85NWBreak), '--b')
text(7.1,1.5,'85% Smooth Exp. \rightarrow','Color','Black')
text(7,1.4,'85% NACA Exp. \rightarrow','Color','Blue')
text(9,1.485,'\downarrow 85% Rotor Only CFD','Color','Black')
text(9.2,1.33,'\uparrow 85% NACA CFD','Color','Blue')
xlabel('Massflow (kg/s)')
ylabel('Pressure Ratio')
%title('RO-IP, Pressure Ratio CFD-Experimental Data Comparison')
grid on

figure(56)
plot(NACAex85NW_Massflow,NACAex85NW_E,'--vb')
hold on
plot(ROex85NW_Massflow,ROex85NW_E,'--sk')
plot(RO85NW_Massflow(1:RO85NWBreak),RO85NW_E(1:RO85NWBreak), '--k')
plot(T85NW_Massflow(1:T85NWBreak),T85NW_E(1:T85NWBreak), '--b')
text(8.95,.81,'\uparrow 85% Smooth Exp.','Color','Black')
text(8.7,.75,'\leftarrow 85% NACA Exp.','Color','Blue')
text(7.6,.89,'85% Rotor Only CFD \rightarrow','Color','Black')
text(6.7,.833,'85% NACA CFD \rightarrow','Color','Blue')
xlabel('Massflow (kg/s)')
ylabel('Stage Efficiecny')
%title('RO-IP, Efficiecny CFD-Experimental Data Comparison')
grid on


figure(57)
plot(Rex90_Massflow,Rex90_E,'-sk')
hold on
plot(IGVRO90_Massflow(1:IGVRO90Break),IGVRO90_E(1:IGVRO90Break),'-g')
plot(RO90W_Massflow(1:RO90WBreak),RO90W_E(1:RO90WBreak), '-k')
text(7.5,0.92,'90% Rotor Only Whirl \downarrow','Color','Black')
text(7.6,.85,'90% IGV \uparrow','Color','Green')
text(7.35,.78,'\leftarrow 90% Rotor Only Exp.','Color','Black')
xlabel('Massflow (kg/s)')
ylabel('Stage Efficiency Ratio')
grid on


figure(58)
plot(Rex90_Massflow,Rex90_Pratio,'--sk')
hold on
plot(RO90W_Massflow(1:RO90WBreak),RO90W_Pratio(1:RO90WBreak), '--k')
plot(IGVRO90_Massflow(1:IGVRO90Break),IGVRO90_Pratio(1:IGVRO90Break), '--g')
text(8,1.5,'\leftarrow 90% Rotor Only','Color','Black')
```

```
text(7.5,1.43,'90% IGV \rightarrow','Color','Green')
text(7.5,1.35,'\leftarrow 90% Smooth Exp')
xlabel('Massflow (kg/s)')
ylabel('Pressure Ratio')
%title('85% NW, Pressure Ratio CFD-Experimental Data Comparison')
grid on
```

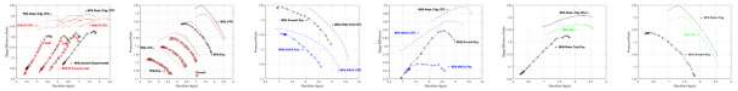

Published with MATLAB® R2022a

THIS PAGE INTENTIONALLY LEFT BLANK

List of References

[1] M. D. Hathaway, "Passive endwall treatments for enhancing stability," U.S. Army Research Laboratory, Glenn Research Center,, Cleveland, Ohio, Tech. Rep. 214409, 2007 [Online]. Available: https://ntrs.nasa.gov/api/citations/20070025023/downloads/20070025023.pdf

[2] Aeolus, "Intake & compression," Accessed Apr. 18, 2023 [Online]. Available: https://www.jet-x.org/a3.html#3

[3] M. F. et al., "Aerodynamic optimization and mechanism investigation on performance improvements in a transonic compressor cascade," *Machines*, vol. 244, no. 1, 2023 [Online]. https://doi.org/10.3390/machines11020244.

[4] W. H. J. et al., "1997 best paper award—controls and diagnostics committee: Active stabilization of rotating stall and surge in a transonic single-stage axial compressor," *ASME. J. Turbomach.*, vol. 120, no. 4, October 1998 [Online]. doi: https://doi.org/10.1115/1.2841772.

[5] M. B. Jones, "Experimental and computaional analysis of advanced casing treatments in a transonic compressor," M.S. thesis, Department of Mechanical and Aerospace Engineering, Naval Postgraduate School, Monterey, CA, USA, 2022 [Online].

[6] G. E. M. et al., "A fundamental criterion for the application of rotor casing treatment." *ASME. J. Fluids Eng.*, vol. 101, no. 2, June 1979 [Online]. doi: https://doi.org/10.1115/1.3448945.

[7] B. L. Meinster, "Stall characteristic prediction in a single passage of a transonic axial compressor rotor," M.S. thesis, Department of Mechanical and Aerospace Engineering, Naval Postgraduate School, Monterey, CA, USA, 2021 [Online].

[8] W. R. Holmes, "Cfd modeling of an axial transonic compressor with inlet guide vanes for military applications," M.S. thesis, Department of Mechanical and Aerospace Engineering, Naval Postgraduate School, Monterey, CA, USA, 2012 [Online].

[9] J. C. Green, "A manufacturing process to implement transonic compressor endwall casing treatments," M.S. thesis, Department of Mechanical and Aerospace Engineering, Naval Postgraduate School, Monterey, CA, USA, 2021 [Online].

[10] P. Giambruno, "Upstream instrumentation and inlet flow analysis of a transonic compressor," M.S. thesis, Department of Mechanical and Aerospace Engineering, Naval Postgraduate School, Monterey, CA, USA, 2023 [Online].

[11] N. P. School, "Turbopropulsion laboratory and gas dynamics laboratory," Accessed Apr. 18, 2023 [Online]. Available: https://nps.edu/web/mae/turbo

[12] T. M. Adams, "Optimization of a transonic compressor stator casing temperature and pressure instrumentation," M.S. thesis, Department of Mechanical and Aerospace Engineering, Naval Postgraduate School, Monterey, CA, USA, 2023 [Online].

[13] D. J. McNab, "Experimental testing and CFD modeling of an advanced transonic compressor for military applications," M.S. thesis, Department of Mechanical and Aerospace Engineering, Naval Postgraduate School, Monterey, CA, USA, 2011.

[14] Stratasys, "Fortus 450mc industrial FDM 3D printer," May. 1, 2023 [Online]. Available: https://www.stratasys.com/en/3d-printers/printer-catalog/fdm-printers/fortus-450mc/

[15] MatWeb, *Overview of materials for Polycarbonate, Extruded*, O3101, 2023 [Online]. Available: https://www.matweb.com/search/DataSheet.aspx?MatGUID=501acbb63cbc4f748faa7490884cdbca&ckck=1

[16] Protolabs, "Aluminum 3D printing service," May. 2, 2023 [Online]. Available: https://www.protolabs.com/services/3d-printing/direct-metal-laser-sintering/aluminum/

[17] MatWeb, *Overview of materials for 3000 Series Aluminum Alloy*, M01042, 2023 [Online]. Available: https://www.matweb.com/search/DataSheet.aspx?MatGUID=82c8a6ba80e641d9b872e7a62af33093

[18] ANSYS, *ANSYS Meshing User's Guide*, ANSYS, Inc., Canonsburg, PA, Nov. 2010 [Online]. Available: https://www.researchgate.net/profile/Mohamed-Mourad-Lafifi/post/How_to_remove_warpage_angle_and_violation_of_heuristic_criterion_warning_in_LS-Dyna/attachment/5d0c0713cfe4a7968dacddf1/AS%3A771994878496770%401561069330997/download/Meshing_Tutorial_Ans.sys.pdf

[19] Xerox, *Xerox ElemX 3D Printer*, BR34670, 2022 [Online]. Available: https://www.a3d-project.com/index.php?controller=attachment&id_attachment=41

Initial Distribution List

1. Defense Technical Information Center
   Ft. Belvoir, Virginia

2. Dudley Knox Library
   Naval Postgraduate School
   Monterey, California